Customer	**:**	**ESRIN**	**Document Ref**	**:**	**SST_CCI_D5.1_CAR_V1.1**
Contract No	**:**	**ESA/AO/1-9322/18/I-NB**	**Issue Date**	**:**	**30 November 2023**
WP No	**:**		**Issue**	**:**	**1.1**

Project : **ESA CCI Phase 3 Sea Surface Temperature (SST)**

Title : **Climate Assessment Report D5.1 v1.1**

Abstract : This document presents a climate assessment of the European Space Agency Sea Surface Temperature Climate Change Initiative (ESA SST CCI) Phase 3 products, Release version CDR3.0.

Author :

Chris Atkinson, Nick Rayner, John Kennedy, Thomas Sikorski, Giulia Bonino, Raven Quilestino-Olario, Raj P. Roshin, James Carton and Luisa Lamas

Checked :

Owen Embury, Chris Merchant

Accepted by ESA :

Digitally signed by Sarah Connors
Date: 2023.12.12 13:37:42 Z

Distribution :

EUROPEAN SPACE AGENCY
CONTRACT REPORT

The work described in this report was done under ESA contract. Responsibility for the contents resides in the author or organisation that prepared it.

AMENDMENT RECORD

This document shall be amended by releasing a new edition of the document in its entirety. The Amendment Record Sheet below records the history and issue status of this document.

AMENDMENT RECORD SHEET

ISSUE	DATE	REASON FOR CHANGE
1	06/11/2023	Version for review
1.1	30/11/2023	Final version

TABLE OF CONTENTS

1. INTRODUCTION

1.1 Purpose and Scope

This document presents a climate assessment of the European Space Agency Sea Surface Temperature Climate Change Initiative (ESA SST CCI) Phase 3 products, Release version CDR3.0. It includes comparison of the products to other climate data sets of SST as well as to Release version CDR2.1 to provide a link to previous Climate Assessment Reports.

We assess the following CDR3.0 products:

- AVHRR (v3.0). SSTs from Advanced Very High Resolution Radiometer (AVHRR) instruments in L2P format at Global Area Coverage (GAC) resolution (4km at nadir) for AVHRR instruments aboard NOAA satellites or Full Resolution Area Coverage (FRAC) resolution (1.1 km at nadir) for AVHRR instruments aboard EUMETSAT Metop satellites, covering July 1979 – December 2021. (Shortened to SST CCI AVHRR)

- SLSTR (v3.0). SSTs from Sea and Land Surface Temperature Radiometer (SLSTR) instruments in L3C format at 0.05° latitude by 0.05° longitude resolution covering May 2016 – December 2021. (Shortened to SST CCI SLSTR)

- AMSR (v3.0). SSTs from Advanced Scanning Microwave Radiometer (AMSR) instruments in L2P format at 75 x 43 km resolution covering June 2002 – October 2011 (AMSR-E) and 62 x 35 km resolution covering July 2012 – October 2017 (AMSR2). (Shortened to SST CCI AMSR)

- Analysis (v3.0). A satellite-only SST-depth (20 cm) L4 daily analysis created by the Operational Sea surface Temperature and sea Ice Analysis (OSTIA) system from the SST CCI AVHRR, SST CCI SLSTR, SST CCI AMSR and SST CCI ATSR products at 0.05° latitude by 0.05° longitude resolution covering 1980 – 2021. (Shortened to SST CCI Analysis)

We also assess the CDR2.1 ATSR product alongside the CDR3.0 data. The ATSR product was not updated for CDR3.0. An earlier assessment of the ATSR product was also made in the CDR2.0 Climate Assessment Report [SST CCI CAR, 2019].

- ATSR (v2.1). SSTs from Along Track Scanning Radiometer (ATSR) instruments in L3U format at 0.05° latitude by 0.05° longitude resolution covering November 1991 – April 2012. (Shortened to SST CCI ATSR)

In addition, this document also presents reports received from users of the SST CCI v3.0 products and any recommendations they have made for future SST CCI products.

1.2 Structure of the Document

After this introduction, the document is divided into sections that are briefly described below:

Section 2 gives an Executive Summary of the key scientific results.

Section 3 presents an assessment of variability and trends in the CDR3.0 products and comparison to other SST products. To assess the multi-annual and decadal behaviour of the long-term products, comparisons are made to existing SST data sets used in high profile monitoring reports. Differences between the SST CCI products and the

comparison datasets are highlighted. The SST CCI products are also assessed against their CDR2.1 counterparts to determine what progress has been achieved.

Section 4 presents a user case study that describes a new version of the Met Office Hadley Centre sea Ice and Sea-Surface Temperature (HadISST.2.4.0.0) and compares it to SST CCI v3 over the common data period 1980-2021.

Section 5 details voluntary reports received from registered users of the SST CCI v3.0 products, describing their application and what they have discovered from using the products.

Section 6 lists any further reported issues identified by registered users and any other recommendations they have made for future SST CCI products.

1.3 Referenced Documents

The following is a list of documents with a direct bearing on the assessments made in this report.

Atkinson, C.P., N.A. Rayner, J. Roberts-Jones and R.O. Smith (2013): Assessing the quality of sea surface temperature observations from drifting buoys and ships on a platform-by-platform basis, J. Geophys. Res. Oceans, 118, 3507–3529, doi:10.1002/jgrc.20257.

Atkinson, C.P., N.A. Rayner, J.J. Kennedy and S.A. Good (2014): An Integrated Database of Ocean Temperature and Salinity Observations, J. Geophys. Res., 119, 7139-7163, doi:10.1002/2014JC010053.

Banzon, V., T.M. Smith, T.M. Chin, C. Liu and W. Hankins (2016): A long-term record of blended satellite and in situ sea-surface temperature for climate monitoring, modeling and environmental studies, Earth Syst. Sci. Data, 8, doi:10.5194/essd-8-165-2016.

Brasnett, B. (2008): The impact of satellite retrievals in a global sea-surface-temperature analysis, Q. J. R. Meteorol. Soc., 134, doi:10.1002/qj.319.

Fiedler, E.K., A. McLaren, V. Banzon, B. Brasnett, S. Ishizaki, J. Kennedy, N. Rayner, J. Roberts-Jones, G. Corlett, C.J. Merchant and C. Donlon (2019): Intercomparison of long-term sea surface temperature analyses using the GHRSST Multi-Product Ensemble (GMPE) system, Remote Sens. Environ., 222, doi:10.1016/j.rse.2018.12.015.

Global Climate Observing System (GCOS). 2022. The 2022 GCOS ECV Requirements (GCOS 245). World Meteorological Organisation: Geneva, Switzerland. https://gcos.wmo.int/en/essential-climate-variables/sst.

Good, S.A., M.J. Martin and N.A. Rayner (2013): EN4: Quality controlled ocean temperature and salinity profiles and monthly objective analyses with uncertainty estimates, J. Geophys. Res. Oceans, doi:10.1002/2013JC009067.

Gulev, S.K., P.W. Thorne, J. Ahn, F.J. Dentener, C.M. Domingues, S. Gerland, D. Gong, D.S. Kaufman, H.C. Nnamchi, J. Quaas, J.A. Rivera, S. Sathyendranath, S.L. Smith, B. Trewin, K. von Schuckmann, and R.S. Vose, 2021: Changing State of the Climate System. In Climate Change 2021: The Physical Science Basis. Contribution of Working Group I to the Sixth Assessment Report of the Intergovernmental Panel on Climate Change [Masson-Delmotte, V., P. Zhai, A. Pirani, S.L. Connors, C. Péan, S. Berger, N. Caud, Y. Chen, L. Goldfarb, M.I. Gomis, M. Huang, K. Leitzell, E. Lonnoy, J.B.R. Matthews, T.K. Maycock, T. Waterfield, O. Yelekçi, R. Yu, and B. Zhou (eds.)]. Cambridge University Press, Cambridge, United Kingdom and New York, NY, USA, pp. 287–422, doi:10.1017/9781009157896.004.

Hirahara, S., M. Ishii and Y. Fukuda (2014): Centennial-scale sea surface temperature analysis and its uncertainty, J. Climate, 27, doi:10.1175/JCLI-D-12-00837.1.

Huang, B., P.W. Thorne, V.F. Banzon, T.B. Boyer, G. Chepurin, J.H. Lawrimore, M.J. Menne, T.M. Smith, R.S. Vose and H.M. Zhang (2017): Extended Reconstructed Sea Surface Temperatures Version 5 (ERSSTv5): Upgrades, Validations, and Intercomparisons, J. Climate, 30, doi:10.1175/JCLI-D-16-0836.1.

Huang, B., C. Liu, V. Banzon, E. Freeman, G. Graham, B. Hankins, T. Smith and H.-M. Zhang (2021): Improvements of the Daily Optimum Interpolation Sea Surface Temperature (DOISST) Version 2.1, J. Climate, 34, doi:10.1175/JCLI-D-20-0166.1.

Ishii, M., A. Shouji, S. Sugimoto and T. Matsumoto (2005): Objective analyses of sea-surface temperature and marine meteorological variables for the 20th century using ICOADS and the Kobe Collection, Int. J. Climatol., 25, 865–879, doi:10.1002/joc.1169.

Johnson, G. C. and R. Lumpkin, Eds., 2023: Global Oceans [in "State of the Climate in 2022"]. Bull. Amer. Meteor. Soc., 104 (9), S146–S206, https://doi.org/10.1175/BAMS-D-23-0076.2

Kaplan, A., Y. Kushnir, M. Cane and M. Blumenthal (1997): Reduced space optimal analysis for historical data sets: 136 years of Atlantic sea surface temperatures, J. Geophys. Res. Oceans, 102, 27,835– 27,860, doi:10.1029/97JC01734.

Kennedy, J.J., N.A. Rayner, C.P. Atkinson and R.E. Killick (2019): An ensemble data set of sea-surface temperature change from 1850: the Met Office Hadley Centre HadSST.4.0.0.0 data set, J. Geophys. Res., 124, doi:10.1029/2018JD029867.

Lanzante, J.R. (1996): Resistant, robust and non-parametric techniques for the analysis of climate data: theory and examples, including applications to historical radiosonde station data, Int. J. Climatol., 16: 1197–1226, doi:10.1002/(SICI)1097-0088(199611)16:11<1197::AID-JOC89>3.0.CO;2-L.

Merchant, C.J., O. Embury, N.A. Rayner, D.I. Berry, G.K. Corlett, K. Lean, K.L. Veal, E.C. Kent, D.T. Llewellyn-Jones, J.J. Remedios and R. Saunders (2012): A 20 year independent record of sea surface temperature for climate from Along-Track Scanning Radiometers, J. Geophys. Res., 117, C12013, doi:10.1029/2012JC008400.

Merchant, C.J. and O. Embury (2020): Adjusting for desert-dust-related biases in a climate data record of sea surface temperature, Remote Sens., 12(16), 2554, doi:10.3390/rs12162554.

Rayner, N.A., D.E Parker, E.B. Horton, C.K. Folland, L.V. Alexander, D.P. Rowell, E.C. Kent and A. Kaplan (2003): Global analyses of sea surface temperature, sea ice, and night marine air temperature since the late nineteenth century, J. Geophys. Res., Vol. 108, No. D14, 4407, doi:10.1029/2002JD002670.

Reynolds, R.W., N.A. Rayner, T.M. Smith, D.C. Stokes and W. Wang (2002): An improved in situ and satellite SST analysis for climate, J. Climate, 15, 1609-1625, doi:10.1175/1520-0442(2002)015<1609:AIISAS>2.0.CO;2.

Reynolds, R.W., T.M. Smith, C. Liu, D.B. Chelton, K.S. Casey and M.G. Schlax (2007): Daily High-Resolution-Blended Analyses for Sea Surface Temperature, J. Climate, 20, 5473–5496, doi:/10.1175/2007JCLI1824.1.

SST CCI Climate Assessment Report (CAR), SST_CCI-CAR-UKMO-201, Issue 1, 16 June 2019, https://climate.esa.int/en/projects/sea-surface-temperature/SST-key-documents/.

SST CCI Product Validation and Intercomparison Report (PVIR), SST_CCI_D4.1_PVIR_v2.1, 20 January 2023.

WMO-No. 1316, 2023. State of the Global Climate 2022. World Meteorological Organisation: Geneva, Switzerland. https://library.wmo.int/records/item/66214-state-of-the-global-climate-2022.

Woodruff, S.D., S.J. Worley, S.J. Lubker, Z. Ji, J.E. Freeman, D.I. Berry, P. Brohan, E.C. Kent, R.W. Reynolds, S.R. Smith and C. Wilkinson (2011): ICOADS Release 2.5: Extensions and enhancements to the surface marine meteorological archive. Int. J. Climatol. (CLIMAR-III Special Issue), 31, 951-967, doi:10.1002/joc.2103.

1.4 Definitions of Terms

The following terms have been used in this report with the meanings shown.

Term	Definition
AATSR	Advanced Along-Track Scanning Radiometer
AMSR	Advanced Microwave Scanning Radiometer
ATSR	Along-Track Scanning Radiometer
ATSR-1	First ATSR instrument
ATSR-2	Second ATSR instrument
AVHRR	Advanced Very High Resolution Radiometer
CAR	Climate Assessment Report
CCI	Climate Change Initiative
CDR	Climate Data Record
COBE SST	Centennial in situ Observation-Based Estimates of variability of SSTs
CMC	Canadian Meteorological Centre
DailyOI	Reynolds Daily Optimal Interpolation analysis
DMI	Dipole Mode Index
EN4	Met Office Hadley Centre subsurface profile observations dataset
ENSO	El Niño Southern Oscillation
ERSSTv5	Extended Reconstruction SST V5
ESA	European Space Agency
EUMETSAT	European Organisation for the Exploitation of Meteorological Satellites
FRAC	Full Resolution Area Coverage
GAC	Global Area Coverage
GCOS	Global Climate Observing System
HadIOD	Hadley Centre Integrated Ocean Database
HadISST	Met Office Hadley Centre Sea-ice and SST dataset
HadSST	Hadley Centre Sea Surface Temperature dataset
ICOADS	International Comprehensive Ocean-Atmosphere Data Set
K	Kelvin
L2P	Level 2 (Pre-processed)
L3U	Level 3 uncollated
L3C	Level 3 collated
L4	Level 4
Metop	A series of polar-orbiting satellites operated by EUMETSAT
NOAA	National Oceanic and Atmospheric Administration (USA)
OI	Optimum interpolation

Term	Definition
OI.v2	Reynolds et al (2002) Optimal Interpolation analysis
OSTIA	Operational Sea surface Temperature and sea Ice Analysis
RD	Reference Document
SIRDS	SST CCI Independent Reference Data Set
SLSTR	Sea and Land Surface Temperature Radiometer
SST	Sea Surface Temperature
TAMG	Tropical Atlantic Meridional SST Gradient

2. EXECUTIVE SUMMARY

Here we provide a bullet point summary of the key points from this Climate Assessment Report. The ESA SST CCI Release version CDR3.0 products assessed are:

- AVHRR (v3.0). SSTs from AVHRR instruments in L2P format at Global Area Coverage (GAC) resolution (4km at nadir) for AVHRR instruments aboard NOAA satellites or Full Resolution Area Coverage (FRAC) resolution (1.1 km at nadir) for AVHRR instruments aboard EUMETSAT Metop satellites, covering July 1979 – December 2021. (Hereafter, SST CCI v3.0 AVHRR)

- SLSTR (v3.0). SSTs from SLSTR instruments in L3C format at 0.05° latitude by 0.05° longitude resolution covering May 2016 – December 2021. (Hereafter, SST CCI v3.0 SLSTR)

- AMSR (v3.0). SSTs from AMSR instruments in L2P format at 75 x 43 km resolution covering June 2002 – October 2011 (AMSR-E) and 62 x 35 km resolution covering July 2012 – October 2017 (AMSR2). (Hereafter, SST CCI v3.0 AMSR)

- Analysis (v3.0). Satellite-only SST-depth (20 cm) L4 daily analysis created by the Operational Sea surface Temperature and sea Ice Analysis (OSTIA) system from the SST CCI v3.0 AVHRR, SST CCI v3.0 SLSTR, SST CCI v3.0 AMSR and SST CCI v2.1 ATSR products at 0.05° latitude by 0.05° longitude resolution covering 1980 – 2021. (Hereafter, SST CCI v3.0 Analysis)

We also assess the CDR2.1 ATSR product alongside the CDR3.0 data. The ATSR product was not updated for CDR3.0. An earlier assessment of the ATSR product was also made in the CDR2.0 Climate Assessment Report [SST CCI CAR, 2019].

- ATSR (v2.1). SSTs from ATSR instruments in L3U format at 0.05° latitude by 0.05° longitude resolution covering November 1991 – April 2012. (Hereafter, SST CCI v2.1 ATSR)

These are utilised over the full period 1979-2021.

In addition, we summarise key findings arising from use of the SST CCI v3.0 products by users and any feedback and recommendations they have for the SST CCI products.

Assessment of variability and trends in the SST CCI v3.0 products and comparison of products to other climate SST data sets and SST CCI v2.1 products (Section 3):

- The comparison datasets are in good agreement in terms of resolving global climate variability, though larger disagreements can occur in some regions and for some time periods (e.g., the Southern Ocean, prior to the mid-to-late 2000s).
- In global and hemispheric averages, the spread of the comparison datasets is wider in the 1980s and 1990s than later decades. At multi-annual to decadal timescales the spread can exceed a tenth kelvin whilst from the late-1990s onwards it is generally within a tenth kelvin.
- The DailyOIv2.1 dataset is a cool outlier prior to the mid-2000s of order a few tenths of a kelvin in the global average.
- Seasonal differences of order several tenths of a kelvin peak-to-peak magnitude are evident between the SST CCI v3.0 products and some of the comparison datasets in the Northern and Southern hemispheres, particularly in the 1980s and diminishing (but not entirely) in later decades. This may be partly attributable to

the differing representations of SST; however, this may not fully explain the change in seasonality seen only in the comparison data prior to the mid-1990s.

- The SST CCI v3.0 data are in good agreement with the comparison data and each other (i.e. internally between data streams) to order a few tenths of a kelvin in terms of resolving global and hemispheric climate variability. This includes the newly added NOAA-AVHRR (NOAA 6, 8 and 10), Metop-AVHRR, AMSR and SLSTR data as well as the Analysis.
- For all assessed regions and indices, the SST CCI v3.0 data are generally consistent with each other and the comparison data in terms of the observed interannual-to-decadal climate variability. Relatively greater disagreements can occur in some regions and times (e.g., in the Southern Ocean).
- For global and hemispheric climate variability the SST CCI v2.1 ATSR and SST CCI v3.0 SLSTR and Analysis tend to lie toward the cooler end of the comparison data ensemble, whilst the SST CCI v3.0 AMSR tends to be relatively warmer. The spread of individual SST CCI v3.0 AVHRR sensors can encompass the comparison data.
- On decadal timescales a coolness in the mid-high latitudes relative to the comparison data of order a tenth kelvin or more is a general feature of all SST CCI v3.0 data except AMSR (and except AVHRR in the 1980s in the southern hemisphere which is in better agreement with the comparison data). In the 1990s the SST CCI v2.1 ATSR is cooler in these regions than the SST CCI v3.0 AVHRR, with the SST CCI v3.0 AVHRR in closer agreement with the comparison data (this seems due to errors in individual AVHRR instruments tending to cancel in the average).
- SST CCI v3.0 AVHRR has been improved versus v2.1, with fewer spikes, better stability, and better agreement with other SST CCI v3.0 and comparison datasets. Periods of note include 1982-1983 when previous large warm spikes have been removed and during the 2000s where a cool bias relative to SST CCI v2.1 AATSR has been removed.
- A major improvement in the SST CCI v3.0 AVHRR and Analysis is in the northern tropical Atlantic and Indian Oceans where the handling of dust aerosol impact on the retrievals has been significantly improved and cool biases have been removed.
- Individual SST CCI v3.0 AVHRR sensors are generally in good agreement where they overlap, notably in the 2010s for AVHRR18, AVHRR19, MetopA and MetopB. A divergence of sensors is seen in the 2000s, particularly in the northern North Pacific and North Atlantic and the Southern Ocean. The Southern Ocean is particularly problematic with divergences approaching several tenths of a kelvin in both the 1990s and 2000s.
- The composite (average) of all SST CCI v3.0 AVHRR sensors generally outperforms the individual sensors in terms of stability and noise.
- Newly added SST CCI v3.0 SLSTR and Metop-AVHRR data are in good agreement with each other. In global and hemispheric averages, the SLSTR is generally slightly cooler than Metop-AVHRR and sits towards the cool end of the comparison data ensemble.
- There is some evidence of seasonal biases of order a tenth kelvin for both SST CCI v3.0 Metop-AVHRRs in the tropics.
- From 2008-2021, trends for AATSR-MetopA-SLSTR, Metop-AVHRR and the comparison data are in good agreement, the AATSR-MetopA-SLSTR trends are generally slightly lower than Metop-AVHRR by order a few millikelvin per year.
- Newly added SST CCI v3.0 AMSR data show good agreement with the other SST CCI v3.0 data and the comparison data in terms of broad climate variability. Regionally the agreement can be more variable with AMSR data both warmer and cooler than the other SST CCI data by several tenths of a kelvin or more. In

some regions this can bring AMSR into better agreement with the comparison data than the other SST CCI v3.0 data (e.g., in the mid-latitudes) but in other regions the agreement can be worse.

- The SST CCI v3.0 AMSR data display seasonal anomalies relative to the other SST CCI v3.0 data which can approach several tenths of a kelvin peak-to-peak magnitude in higher latitudes.
- Some climate indices have been improved in the SST CCI v3.0 AVHRR and Analysis data due to better handling of aerosols effects on the AVHRR retrievals, notably for Nino 1+2 and TAMG indices.
- Trends for the SST CCI v3.0 data and the comparison data are in general in good agreement, including over the full 1980-2021 period where for most regions the spread of trends is within 0.01 K per year (equivalent to 0.1 K per decade), comparable to the GCOS stability requirement of 0.1 K per decade [GCOS, 2022].
- Relatively warmer SST CCI v3.0 AVHRR data in the southern hemisphere in the 1980s leads to trends at the lower end of the comparison ensemble over 1982-2016 (and vice versa in the northern hemisphere). Relatively cooler SST CCI v2.1 ATSR data in the 1990s leads to trends at the higher end of the comparison ensemble in the southern hemisphere over the 1992-2021 period.

Key points arising from User Case Study (HadISST.2.4.0.0, Section 4):

- The Met Office Hadley Centre sea Ice and Sea-Surface Temperature (HadISST) data set provides a global picture of sea-surface temperature (SST) and sea ice conditions since the mid-nineteenth century. In order to achieve this global view back to the mid-nineteenth century, statistical interpolation techniques have been employed to fill in an estimate of variability between and consistent with the available measurements made in situ. High quality satellite data are essential to provide an improved understanding of variability globally within this process.
- In this User Case Study, HadISST version 2.4.0.0 has used SST CCI v3 data for AVHRR, ATSR and SLSTR to produce a new reconstruction back to January 1850. The incorporation of SST CCI v3 data has brought with it a number of advantages. HadISST.2.4.0.0 and the SST CCI v3 analysis are very close in terms of their SST anomaly time series over most analysis regions and in terms of their decadal average SST anomaly and variability, particularly relative to other commonly-used SST data sets. This means that these data sets could be used together with confidence in linked activities that require SST data sets at different spatiotemporal resolution, but that need as little discontinuity as possible between the data sets used in each case. For example, they could be used as lower-boundary forcing for atmosphere-only climate model simulations, or reanalyses, at different times or with different resolution models. No previous pair of data sets has been created with this as an ambition, or with this as the outcome.

Key points arising from use of the SST CCI v3.0 products by registered users (Section 5):

Six sets of volunteer trail-blazer users tested the pre-release SST CCI v3 products in the context of their applications. The following points were their observations on the utility of the data.

- The team at Deutscher Wetterdienst reported the successful reproduction of the EUMETSAT CM SAF HOAPS 4.0 dataset (Andersson et al., 2017) using the ESA SST CCI Analysis product version 3.0. Also, that ESA SST CCI Analysis product version 3.0 is a viable alternative to the NOAA 0.25° daily Optimum Interpolation Sea Surface Temperature dataset in the HOAPS processing framework. In addition, ESA SST CCI Analysis product version 3.0 seemingly leads to

improvements of individual EUMETSAT CM SAF HOAPS parameters; further analysis is needed.

- The team at the Nansen and Bjerknes Centers found that, in general, there is a gradual increase in SST of the Nordic Seas and the Barents Sea shown by the SST CCI v3 data. A major exception is in the region of the inflow of Atlantic Water (AW) in the eastern Nordic Seas which indicates the increasing role of atmospheric impact on the SST of the region in comparison to the inflowing AW. The new SST data will be used to study the relative importance of AW inflow and the atmospheric forcing on the SST of the Nordic Seas and the Barents Sea. In addition, the data will be used for a contribution on marine heat waves (MHW) in the region is planned for the next Ocean Science Report (OSR8).
- The team at the University of the Philippines considered that the SST CCI analysis v3 dataset provides a balanced resolution wherein the 0.05-degree resolution can address the concerns of missing SST data of coarser SST datasets especially towards the coast. At the same time, it fits the recommended length (i.e., 30 years) needed to calculate the baseline climatology for MHW detection. In terms of scientific usage, the SST CCI analysis v3 is a promising SST product that can provide a more in-depth analysis on temperature-related changes globally since it goes way back (1979-1980) than other available SSTs. The scope of the SST information is also rich given that it is global.
- The team at CMCC found that the SST CCI Analysis version 3 provides a spatial and temporal coverage of the sea surface temperature field that is essential for studies with the aim to improve SST predictability over the Mediterranean Sea and is perfectly suitable to be used as a train and test dataset for deep machine learning approach.
- The work of the team at the Instituto Hidrográfico in Portugal showed that the SST CCI v3 is consistent with in-situ SST, with most RMSE spanning between 0.2°C and 0.6°C. The data also reproduced the general seasonal and inter-annual variability and magnitude of the surface temperature measured by the moored buoys, with seasonal MSE rarely exceeding the 0.2°C. For most buoy locations, however, there was a tendency for SST CCI v3 to show warmer summers and cooler winters. The SST CCI v3 is of particular interest to analyse the spatial and temporal variability of the sea surface at the Eastern Atlantic Ocean for the past 30 years. This product provides an important source of information, especially for the open ocean, where surface temperature measurements are scarce and sporadic.

Feedback on ease of use of the products (Section 6):

All trail blazer users' feedback noted that the CCI SST v3 dataset is very easy to use. The below are quotes from their feedback.

- Very easy to use.
- The SST CCI analysis v3 product is actually easy to use. R environment loads the .nc file easily and it can be prepared well due to the proper organization and stacking of data. Initially, we opt to test it in detecting MHW events. However, limitations in computer capacity inhibited us from processing since we cannot combine 40 years of data which is needed before we can filter for the Philippine seas boundary. But nevertheless, product- and documentation-wise, the SST CCI analysis v3 is easy to wrangle.
- The SST CCI Analysis product version 3 is easy to download and the documentation is complete.
- Daily global datasets are readily accessible and easy to work with. The processing and analysis of the data during this work was performed using Python 3.8 and no relevant problems were encountered.
- The documentation was clear and sufficient to understand the data and use it.

- More information on the uncertainty of each SST CCI v3 measurement would be beneficial for this analysis. (Note: Three uncertainty components are provided with each CCI SST value at level 2 and 3.)

Further recommendations for the future by registered users (Section 6):

Trail blazer users were asked for further feedback and their recommendations for future development.

- Downloading the global dataset is easy to me (as I am sitting in Norway), however may not be easy for someone sitting in an African nation. Instead of downloading the global data, it may be helpful if one can select and download the data for their region of interest. (Note: This is addressed through surftemp.net.)
- A subset tool is requested for future downloads to aid researchers focusing on smaller boundaries in not downloading the whole 40-year global files. Aside from recommending updates to 2022 or 2023, we do hope that the SST CCI be also made available with data access forms or filters so that students like us with no high-powered computers can subset it before downloading.
- Continuous validation with in-situ data should be undertaken in order to improve the product by minimizing the bias and error from interpolations.

3. ASSESSMENT OF VARIABILITY AND TRENDS IN SST CCI V3.0 PRODUCTS AND COMPARISON TO OTHER PRODUCTS

This section assesses the variability and trends in the ESA SST CCI v3.0 products and compares them to other SST products to determine to what extent the new SST CCI products are credible Climate Data Records. The SST CCI v3.0 products are also assessed against precursor SST CCI v2.1 products to determine what progress has been achieved.

3.1 Introduction

To assess the multi-annual and decadal behaviour of the SST CCI v3.0 products, comparisons are made to other SST data sets and SST CCI v2.1. The data sets selected include those used as part of high profile reports including the IPCC Sixth Assessment Report [AR6; Gulev et al., 2021], WMO State of the Global Climate 2022 [WMO-No. 1316, 2023] and BAMS State of the Climate 2022 [Johnson and Lumpkin, 2023]. Differences between the SST CCI products and the comparison datasets are highlighted.

3.2 Data sets

The SST CCI v3.0 products assessed are:

- AVHRR (v3.0). SSTs from AVHRR instruments in L2P format at Global Area Coverage (GAC) resolution (4km at nadir) for AVHRR instruments aboard NOAA satellites or Full Resolution Area Coverage (FRAC) resolution (1.1 km at nadir) for AVHRR instruments aboard EUMETSAT Metop satellites, covering July 1979 – December 2021. (Hereafter, SST CCI v3.0 AVHRR).

- SLSTR (v3.0). SSTs from SLSTR instruments in L3C format at 0.05° latitude by 0.05° longitude resolution covering May 2016 – December 2021. (Hereafter, SST CCI v3.0 SLSTR.)

- AMSR (v3.0). SSTs from AMSR instruments in L2P format at 75 x 43 km resolution covering June 2002 – October 2011 (AMSR-E) and 62 x 35 km resolution covering July 2012 – October 2017 (AMSR2). (Hereafter, SST CCI v3.0 AMSR).

- Analysis (v3.0). Satellite-only SST-depth (20 cm) L4 daily analysis created by the Operational Sea surface Temperature and sea Ice Analysis (OSTIA) system from the SST CCI v3.0 AVHRR, SST CCI v3.0 SLSTR, SST CCI v3.0 AMSR and SST CCI v2.1 ATSR products at 0.05° latitude by 0.05° longitude resolution covering 1980 – 2021. (Hereafter, SST CCI v3.0 Analysis.)

We also assess the SST CCI v2.1 ATSR product alongside the SST CCI v3.0 data. The ATSR product was not updated for v3.0. An earlier assessment of the ATSR product was also made in the CDR2.0 Climate Assessment Report [SST CCI CAR, 2019].

- ATSR (v2.1). SSTs from ATSR instruments in L3U format at 0.05° latitude by 0.05° longitude resolution covering November 1991 – April 2012. (Hereafter, SST CCI v2.1 ATSR.)

These are compared to the following data sets over the period 1979-2021.

3.2.1 SIRDS (DRIFTING BUOY AND ARGO)

The SST CCI Independent Reference Data Set (SIRDS) comprises in situ observations of SST from various surface-only and profiling platform types. It was initially created for the ESA SST CCI Phase 2 project for use in validating satellite SST products and its time coverage was subsequently extended for the European Union Copernicus Climate Change Service (C3S, https://climate.copernicus.eu/, C3S_312a Lot 3). The SIRDS data are extracted from the Hadley Centre Integrated Ocean Database version 1.2.0.0 (HadIOD, Atkinson et al. 2014, https://www.metoffice.gov.uk/hadobs/hadiod/sirds.html) and cover 1978-present with separate monthly files for different observation types. Each file contains the observed SST data plus additional HadIOD metadata for each observation (where available) such as bias corrections, measurement uncertainties and quality control decisions.

In this assessment we make use of SIRDS data from drifting buoys and Argo floats to create two instrumentally-homogenous records of global in situ SST. These observation types are generally considered un-biased and stable over time which is helpful for climate studies and they are often used as a benchmark for assessing other SST data. The drifting buoy and Argo networks have grown over time and in their earlier periods, when less widespread, regional averages of SST can become noisy due to a lack of coverage. For this assessment we therefore focus on drifting buoys from 1990-onwards and Argo from 2005-onwards.

The HadIOD drifting buoy data are taken from ICOADS.2.5.1 [Woodruff et al., 2011] and the Copernicus Marine Environmental Monitoring Service (CMEMS; product INSITU_GLO_NRT_OBSERVATIONS_013_030, http://marine.copernicus.eu/). In the SIRDS, CMEMS data are used from June 2016 onwards due to a drop in the number of ICOADS drifting buoy observations at this time. All drifting buoy data are quality checked using Met Office Hadley Centre QC checks, with further checks applied to the ICOADS data from 1986-2015 based on an updated version of the QC checks described in Atkinson et al. (2013).

The HadIOD Argo data are taken from EN4 [Good et al., 2013] and have been quality checked by the EN4 suite of QC checks. For each Argo profile the shallowest temperature observation passing quality control in the depth range 4-6m is selected for inclusion in the SIRDS.

The SIRDS drifting buoy and Argo data are gridded to get SST anomalies at 5-degree monthly resolution. These data sets will simply be referred to as ‘drifter’ and ‘Argo’.

The SIRDS data are provided by the Met Office Hadley Centre, https://www.metoffice.gov.uk/hadobs.

3.2.2 HADSST4

HadSST.4.0.1.0 (the Met Office Hadley Centre Sea-Surface Temperature data set version 4.0.1.0, Kennedy et al., 2019) is a gridded data set of SST anomalies (relative to a 1961-1990 average) from 1850 to present. The monthly grids have a resolution of 5° latitude by 5° longitude. HadSST.4.0.1.0 is based on quality-controlled in situ measurements of SST from the International Comprehensive Ocean Atmosphere Data Set (ICOADS) release 3.0 (1850-2014). It is updated using data from ICOADS release 3.0.1 (2015-onwards) supplemented with drifting buoy data provided by CMEMS (2016-onwards). In situ measurements are those made at the surface by ships, drifting buoys and moored buoys. Ship measurements are made using a variety of methods and bias adjustments have been applied to the data to minimise the impact of artificial variability caused by changes in instrumentation. In the period examined here, the principal changes are: (1) A switch from mostly ship-based observations in the 1980s to a mixture of ship and buoy observations by the late 2000s; (2) A switch from a mixture of bucket

and Engine Room Intake (ERI) ship measurements in the 1980s to predominantly ERI ship measurements by the late 2000s.

The uncertainties associated with bias adjustments, measurement errors and sampling error have been estimated and we make use of these. The bias adjustment uncertainties are presented as an ensemble of 200 interchangeable data sets, where parameters used in the statistical modelling of the biases are varied within their likely ranges to produce the ensemble.

In addition to gridded SST anomalies, HadSST.4.0.1.0 provides gridded actual SSTs. We make use of these SST actuals to calculate SST anomalies relative to the same climatology used for all datasets in this assessment.

The dataset is not infilled and gridded SSTs are only estimated in those grid boxes that contain observations. Consequently, the data set is not globally complete.

The HadSST.4.0.1.0 data are provided by the Met Office Hadley Centre, https://www.metoffice.gov.uk/hadobs.

3.2.3 HADISST

Met Office Hadley Centre sea Ice and SST (HadISST) is a globally complete analysis of sea-surface temperature and sea-ice concentrations from 1870-present. It is based on in situ and satellite (AVHRR) measurements of SST. Gaps in the data coverage are filled using a statistical technique known as Reduced Space Optimal Interpolation [Kaplan et al. 1997]. In areas of the ocean where there is an estimated non-zero sea ice concentration, the SST is inferred from the sea ice concentration. HadISST1.1 [Rayner et al. 2003] is presented on a 1 degree latitude by 1 degree longitude monthly grid, although the anomaly analysis is performed on a 2 degree latitude by 2 degree longitude grid (and then added to a 1 degree latitude by longitude climatology) in the modern period (1949 onwards) including the whole period covered in this report.

The HadISST data are provided by the Met Office Hadley Centre, https://www.metoffice.gov.uk/hadobs.

3.2.4 ERSSTV5

The Extended Reconstructed Sea Surface Temperature version 5 (ERSSTv5, Huang et al. 2017 provides a monthly quasi-global spatially-complete SST record on a 2 degree latitude by 2 degree longitude grid from 1854 through present. The grid is offset slightly such that the equator passes through the centre of one of the grid boxes rather than forming the boundary of one of the grid boxes. It is based on in situ measurements of SST and uses a combination of Empirical Orthogonal Teleconnections (derived from an analysis of in situ and satellite SSTs) and a low-frequency smoothing to reconstruct SSTs globally. ERSSTv5 incorporates ship and buoy observations from the ICOADS database release 3.0 and near-surface data from Argo floats. Sea ice concentrations from HadISST2 are used to relax reconstructed SSTs in partial ice-covered areas toward the freezing point (−1.8°C).

ERSSTv5 builds upon developments made in ERSSTv4, which included the use of Night-time Marine Air Temperatures (NMAT) in addition to ship metadata to detect and correct for biases associated with changes in measurement practice over time, corrections for the transition from ship-based to buoy-based measurements over the past few decades, and greater weight given to more reliable buoy-based measurements. ERSSTv5 features improved bias correction to ship observations, using more homogeneous buoy observations as a baseline after 2010 and as reference for NMAT-based corrections prior to this. It also improves the spatial interpolation approaches used to estimate temperatures in data-sparse regions. This results in a better representation of high

latitude SSTs and more realistic spatio-temporal variations including e.g., El Niño and La Niña events.

The NOAA Extended Reconstructed Sea Surface Temperature (ERSST) data are provided by the NOAA National Centers for Environmental Information (NCEI), https://www.ncei.noaa.gov/products/extended-reconstructed-sst.

3.2.5 COBE-SST2

The Centennial in situ Observation-Based Estimates of the Variability of SST, version 2 (COBE-SST2, Hirahara et al. 2014) provides a monthly, global spatially-complete SST record on a 1-degree latitude by 1-degree longitude grid from 1850 through present. A "Multi-Time-Scale" (MTA) analysis method is used to reconstruct daily SST fields as a sum of a trend, interannual variations and daily changes, from quality checked in situ SST observations. Interannual-to-decadal changes are reconstructed using EOFs based on satellite and in situ SST data. This SST analysis method is an improvement over that of its predecessor COBE-SST (Ishii et al. 2005). In situ SST observations are taken from the ICOADS database release 2.5 with operational (GTS) JMA data used after 2008. In sea ice regions, sea ice concentrations are used to estimate SSTs using an updated empirical equation representing the ice-SST relationship.

Prior to analysis, biases of individual SST measurement types are estimated to help correct for biases associated with the changes in measurement practice over time (e.g., since the 1980s, a gradual reduction in the proportion of ship observations made by buckets versus ERI and an increase in the coverage of buoy observations). Bias adjustments are made relative to buoy-based measurements as a baseline. For historical observations with missing measurement type metadata, bias adjustments are applied that ensure consistency with other SST and NMAT observations.

COBE-SST 2 and Sea Ice data are provided by the NOAA PSL, Boulder, Colorado, USA, from their website at https://psl.noaa.gov. Data are updated irregularly, at the time of download data were available from 1850-2019.

3.2.6 OI.V2

The Reynolds et al. (2002) weekly and monthly OI.v2 is based on in situ and satellite data. The satellite SST retrievals come from the AVHRR series of instruments and biases in the satellite data are adjusted to more closely match the in situ data. In sea ice regions SSTs are inferred from sea ice concentrations based on equations representing the observed ice-SST relationship and using an updated method from OI.v1. The resulting fields are interpolated using optimal interpolation and the data are presented on a 1 degree latitude by 1 degree longitude weekly and monthly grid from October 1981-present. The monthly grids are used herein.

NOAA Optimum Interpolation (OI) monthly SST V2 data are provided by the NOAA PSL, Boulder, Colorado, USA, from their website at https://psl.noaa.gov. Note, since January 2023 this product has now ceased updating and users are directed to Daily OI V2.1 for weekly and monthly resolutions.

3.2.7 DAILY OI V2.1

The Daily optimum interpolation (OI) version 2.1 [Huang et al. 2021] is based on in situ and satellite data. The satellite SST retrievals come from the AVHRR series of instruments and biases in the satellite data are adjusted to more closely match the in situ data. Satellite and ship observations are referenced to buoys to compensate for platform differences and sensor biases. In sea ice regions SSTs are inferred from sea ice concentrations. The dataset is interpolated using optimal interpolation to fill gaps on the grid and create spatially complete maps of sea surface temperature. The data are

presented on a 0.25 degree latitude by 0.25 degree longitude daily grid from September 1981-present.

From 1981-2015 the OI version 2.1 data are the same as for OI version 2.0 [Reynolds et al. 2007; Banzon et al. 2016] but using an updated file format. From 2016-onwards several improvements were implemented, in part to address an emerging cool bias in OI version 2.0 [Huang et al. 2021]. These improvements include: (1) switching the real time in situ data source to ICOADS-D R.3.0.2; (2) adding near-surface Argo data; (3) updating the ship-buoy SST corrections; (4) switching from Metop-A and NOAA-19 to Metop-A and Metop-B to replace degraded AVHRR data; (5) revising the sea ice concentration to SST conversion method (removing warm biases in the Arctic). In Autumn 2021 a switch was made to using VIIRS and Metop-B.

NOAA 1/4degree Daily OI SST V2.1 data from 09/1981-present were downloaded from https://www.ncei.noaa.gov/products/optimum-interpolation-sst.

3.2.8 CMC V2.0 AND V3.0

The Canadian Meteorological Centre (CMC) global SST analysis [Brasnett 2008] is based on in situ and satellite data. The satellite SST retrievals come from both infrared and microwave instruments. Biases in the satellite data are adjusted separately by instrument and by day and night to match the in-situ ship and buoy data more closely. No particular method is applied to adjust data to a specified depth, the ship and buoy data that the satellite data are referenced to are assumed to have a typical depth of one metre. In sea ice regions SSTs are inferred based on sea ice concentrations. The dataset is interpolated using optimal interpolation to create spatially complete maps of sea surface temperature.

CMC version 2.0 is presented on a 0.2 degree latitude by 0.2 degree longitude daily grid from September 1991-March 2017. Satellite infrared SST retrievals are from the ATSR-series of instruments (ATSR1, ATSR2, AATSR) and AVHRR (NOAA 16,17,18 and 19 and MetOp-A) and microwave SST retrievals are from AMSR-E, TMI and WindSat.

CMC version 3.0 is presented on a 0.1 degree latitude by 0.1 degree longitude daily grid from January 2016-present. Satellite infrared SST retrievals are from AVHRR (NOAA 18 and 19 and MetOp-A and B) and microwave SST retrievals are from AMSR2.

Fiedler et al. (2019) found the CMC version 2.0 SST analysis to perform well versus other long term daily high-resolution infilled analyses available at the time (including DailyOI V2.0 and the SST CCI Analysis version 1) in terms of differences from Argo data, temporal and spatial homogeneity and feature resolution.

Canada Meteorological Center. 2012. CMC 0.2 deg global sea surface temperature analysis. Ver. 2.0. PO.DAAC, CA, USA. Dataset accessed 2022-11-29 at https://doi.org/10.5067/GHCMC-4FM02.

Canada Meteorological Center. 2016. GHRSST Level 4 CMC 0.1 deg global sea surface temperature analysis. Ver. 3.0. PO.DAAC, CA, USA. Dataset accessed 2022-11-29 at https://doi.org/10.5067/GHCMC-4FM03.

3.3 Methods

3.3.1 GRIDDING

The SST CCI v3.0 products and the comparison data sets are presented on a range of different grids. To make a direct comparison, the data were first converted into SST anomalies relative to a common climatology. The SST CCI v3.0 climatology was used which is derived from the SST CCI v3.0 Analysis for the period 1991-2020. Where required the climatology was re-gridded from its daily 0.05-degree latitude by 0.05-degree longitude grid to accommodate the spatial and temporal resolution of the different datasets being processed. In effect this step also applies a common land mask to the data as anomalies cannot be calculated over land where climatology values are not defined. All anomalies were then aggregated onto 1-degree and 5-degree monthly grids (except for the SIRDS and HadSST4 datasets which were 5-degree only) ready for use in the assessment.

When processing the SST CCI v3.0 products, the 20cm depth SST was used which also provides an estimate of the daily mean. For the L2 and L3 SST CCI products only observations with quality flag=5 were used, except for the v3.0 AMSR (quality flag>=4) and v3.0 AVHRR (quality flag>=4, except AVHRR15 where quality flag=5).

To facilitate assessment of the L2 and L3 SST CCI v3.0 products over longer periods, the 1-degree anomalies from some sensors were combined to create composite datasets. Each composite is a simple average of all available gridded data each month for a particular series of instruments. Composites were created separately for the NOAA-AVHRRs, Metop-AVHRRs, (A)ATSRs and SLSTRs. In addition, a composite of AATSR-MetopA-SLSTR data was created with MetopA data only used from April 2012-April 2016 to fill the gap in the series. The first month of SLSTR-A data (May 2016) was subsequently segregated for the final release as it is data from the satellite commissioning phase with very low data volume (its inclusion here will not materially affect the assessment results).

3.3.2 TIME SERIES AND LINEAR TRENDS

Time series of area-averaged SST anomalies were calculated using the 5-degree monthly gridded data for each dataset for the regions shown in Figure 3-1 and Table 3-1. These provide a useful means for assessing the relative biases and variability in the different data sets considered. Area averages were calculated as a weighted average of all non-missing grid box values within the area. The weights were proportional to the area of ocean within a grid box. In 5-degree coastal grid boxes which were not entirely covered by ocean, the area of ocean was estimated using the climatology (grid boxes in the 0.05-degree climatology with an assigned SST were assumed to be 100% ocean).

Area averages were calculated for each data set using their native coverage and also after reducing their coverage to that of HadSST4. This facilitates a more like-for-like comparison with the HadSST4 dataset which is based on gridded (non-infilled) in situ data and thus is representative of the coverage of the in-situ observation network.

A further set of area averages were also calculated with a sea ice mask applied. Sea temperatures from within the ice pack are provided for spatially complete products such as the SST CCI Analysis and some of the comparison datasets and these are otherwise included in the regional averages. By omitting sea ice regions, a more like-for-like comparison can be made with the SST CCI L2 and L3 products and non-infilled comparison datasets whose coverage stops at the ice edge. A 5-degree monthly sea ice mask was used which was created from the SST CCI v3.0 Analysis daily sea ice fields (a 5-degree box is masked if its average sea ice fraction is > 0 for that month). The exact position of the ice edge will vary between products dependent on methodology, however

to first order this approach should omit the bulk of the unwanted ice pack regions in each product. The resulting masked time series should broadly represent areas of open ocean.

For each area averaged timeseries an SST-coverage timeseries was also calculated. For each month the SST-coverage was calculated as the percent of the area sampled by the 5-degree gridded data. For spatially complete datasets the SST-coverage will always be near 100%. For the SST CCI L2 and L3 products, drops in coverage can be used to help identify apparently erroneous features that are caused by low data volumes versus those caused by errors in the retrievals.

Timeseries of differences relative to the SST CCI Analysis were also calculated. To first order this removes the climate signal and allows relative biases between the datasets to be more easily distinguished. Similar plots but with a 12-month moving average applied were also created, which smooths over differences at seasonal or shorter timescales and helps to distinguish more persistent biases.

Linear trends in the area-average timeseries were calculated from all non-missing monthly values using the ordinary least squares method. A resistant method for estimating the trends – median of pairwise slopes [Lanzante 1996] - was also used (not shown) to check that outliers did not have a strong effect on the results. The long-term warming during this period is comparable in magnitude to the year-to-year variability, therefore, linear trends are not an ideal 'model' for temperature change over this period. Nonetheless they can highlight differences such as relative biases between the data sets. Because of the differing time coverage of the SST CCI v3.0 and comparison datasets, trends were calculated over various periods so the different products could be assessed:

- 1980-2021 (the total time range of the SST CCI v3.0 data; the HadSST4, ERSSTv5 and HadISST comparison data also cover this period).
- 1982-2016 (assesses the NOAA-AVHRR composite and adds the DailyOI, OI.v2 and COBE-SST2 comparison data, also facilitates comparison with the precursor SST CCI v2.1 release).
- 1992-2021 (assesses the (A)ATSR-MetopA-SLSTR composite and adds the CMC comparison data).
- 2008-2021 (assesses the Metop-AVHRR composite and adds the drifter-only and Argo-only SIRDS comparison data).

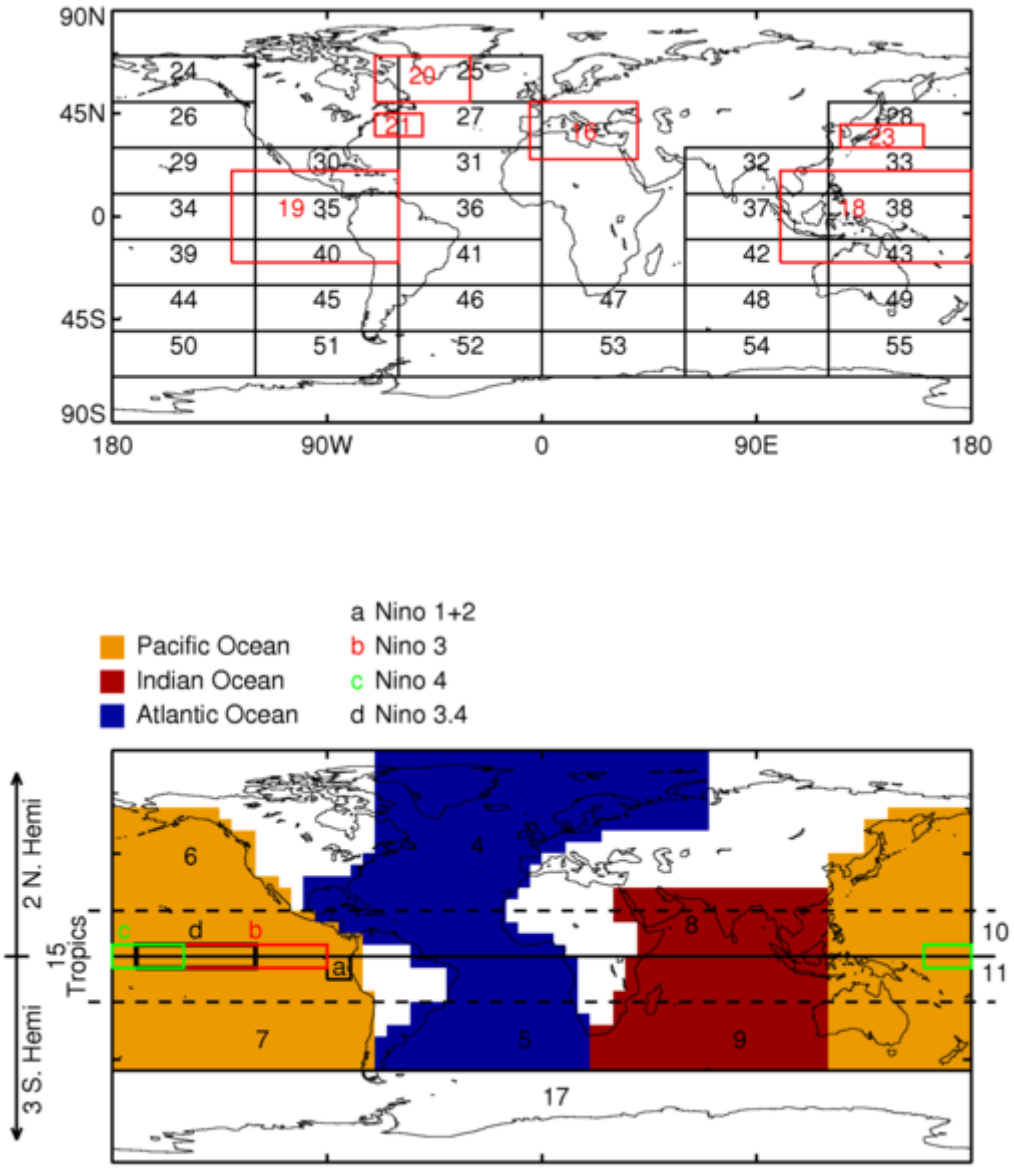

Figure 3-1. Maps showing the regions used in the calculation of area averages. The regions are also described in Table 3-1.

Table 3-1. List of regions used for the calculation of area averages. The regions are also shown in Figure 3-1.

Region Number	Region Name	Region Number	Region Name
1	Globe	28	Area 30°-50°N, 120°-180°E
2	Northern Hemisphere	29	Area 10°-30°N, 180°-120°W
3	Southern Hemisphere	30	Area 10°-30°N, 120°-60°W
4	North Atlantic Ocean	31	Area 10°-30°N, 60°-0°W
5	South Atlantic to 50°S5	32	Area 10°-30°N, 60°-120°E
6	North Pacific Ocean	33	Area 10°-30°N, 120°-180°E
7	South Pacific to 50°S	34	Area 10°N-10°S, 180°-120°W
8	North Indian Ocean	35	Area 10°N-10°S, 120°-60°W
9	South Indian Ocean to 50°S	36	Area 10°N-10°S, 60°-0°W
10	Northern Tropics	37	Area 10°N-10°S, 60°-120°E
11	Southern Tropics	38	Area 10°N-10°S, 120°-180°E
12	Atlantic Ocean to 50°S	39	Area 10°-30°S, 180°-120°W
13	Pacific Ocean to 50°S	40	Area 10°-30°S, 120°-60°W
14	Indian Ocean to 50°S	41	Area 10°-30°S, 60°-0°W
15	Tropics 20°N-20°S	42	Area 10°-30°S, 60°-120°E
16	Mediterranean	43	Area 10°-30°S, 120°-180°E
17	Southern Ocean, 50°S Southwards	44	Area 30°-50°S, 180°-120°W
18	Western Tropical Pacific	45	Area 30°-50°S, 120°-60°W
19	Eastern Tropical Pacific	46	Area 30°-50°S, 60°-0°W
20	Greenland 50°-70°N, 30°-70°W	47	Area 30°-50°S, 0°-60°E
21	Gulfstream 35°-45°N 50°-70°W	48	Area 30°-50°S, 60°-120°E
22	Southern Hemisphere and Northern Indian Ocean minus rest of NH	49	Area 30°-50°S, 120°-180°E
23	Kuroshio 30°-40°N, 125°-160°E	50	Area 50°-70°S, 180°-120°W

24	Area 50°-70°N, 180-120W	51	Area 50°-70°S, 120°-60°W
25	Area 50°-70°N, 60°-0°W	52	Area 50°-70°S, 60°-0°W
26	Area 30°-50°N, 180°-120°W	53	Area 50°-70°S, 0°-60°E
27	Area 30°-50°N, 60°-0°W	54	Area 50°-70°S, 60°-120°E
		55	Area 50°-70°S, 120°-180°E

3.3.3 INDICES

In addition to the time series for the regions described in Figure 3-1 and Table 3-1, indices for certain standard modes of variability were also calculated. The Niño indices are standard regions used to help characterise the nature of El Niño and La Niña events. These were:

1. Niño 1+2 [0°-10°S, 90°-80°W]
2. Niño 3 [5°N-5°S, 150°W-90°W]
3. Niño 4 [5°N-5°S, 160°E-150°W]
4. Niño 3.4 [5°N-5°S, 170°W-120°W]
5. Dipole Mode Index (DMI) calculated as the difference between the area-average SST anomalies for the regions [50°-70°E, 10°S-10°N] and [90°-110°E, 10°S-10°N]
6. Tropical Atlantic Meridional SST gradient (TAMG) calculated as the difference between the area-average SST anomalies for the regions [60°W-African Coast, 5°-28°N] and [60°W-20°E, 20°S-5°N]

These six indices are all based on area-averages which were calculated in the same way as for the area averages in Section 3.3.2.

3.3.4 MULTI-ANNUAL AND DECADAL AVERAGES

Decadal averages were calculated using the gridded 1-degree monthly SST anomalies (except for SIRDS and HadSST4 datasets which used the 5-degree data) for the periods 1982-1991, 1992-2001, 2002-2011 and 2012-2021. For each grid cell, an average was only calculated where a dataset entirely covered the averaging period and where at least 30% of monthly values were non-missing (e.g., if the averaging period was 1982-1991 and a dataset began in 1983 then no average would be calculated, even if 90% of monthly values were potentially present). 1982 is a convenient starting year for the decadal averages as it allows more comparison datasets to be included in the earlier periods (DailyOI and OI.v2 in the 1980s and CMC in the 1990s), 1992 is also the first full year of ATSR1 data. (Note that the SST CCI data for 1979-1981 are still assessed using timeseries and linear trends, see Section 3.3.2).

Multi-annual averages were also calculated for the periods 2017-2021 (for assessing the SST CCI v3.0 SLSTR data), 2008-2017 (the period over which the SST CCI v3.0 NOAA-AVHRR and Metop-AVHRR composites overlap), 2003-2010 (for assessing SST CCI v3.0 AMSR-E) and 2013-2016 (for assessing SST CCI v3.0 AMSR-2).

These averages are presented as maps which help to assess spatially the relative biases and multi-annual variability in the different data sets. To aid inter-comparison of the decadal averages for the SST CCI v3.0 and comparison datasets, plots of zonal averages were also made. To help identify differences between the decadal averages, differences relative to the SST CCI v3.0 Analysis were calculated, which to first order removes the

climate signal and allows relative biases between the datasets to be more easily distinguished (the differences use the 5-degree data which is common to all datasets). Decadal average maps for all datasets are shown in Section 3.4.8, whilst other averages are presented throughout the Results to facilitate the assessment.

3.4 Results

Note that all the timeseries and linear trend plots shown in this section are with sea ice masking applied and without colocation to HadSST4 (see Section 3.3.2) unless stated otherwise. For SIRDS drifter and Argo data, SST timeseries are only used from 1990 and 2005 onwards respectively as prior to this a lack of observational coverage can introduce significant noise into the globally averaged anomalies. Only a subset of the area-average timeseries (Table 3-1, Figure 3-1) have been selected for interest and presented in this section.

In terms of climate variability over the 1980-2021 period of interest, several well-known phenomena are observed in the global-average SST anomalies (e.g., Figure 3-9). In particular:

- a cooling and subsequent recovery of SSTs over several years following the eruptions of El Chichón in 1982 and Mount Pinatubo in 1991;
- a sharp warming and subsequent cooling caused by strong El Niño events in 1982/1983, 1997/1998 and 2015/2016;
- cooler La Niña events during 1983-1985, 1988-1989, 1998-2001, 2007-2009, 2010-2012, 2016-2018 and 2020-2023; and
- enhanced interannual variability related to a sequence of La Niña–El Niño–La Niña events over the period 2007-2012.

And there has been an overall warming of global SST over this period, as seen in global and hemispheric trends (e.g., Figure 3-38).

3.4.1 COMPARISON DATA

Figure 3-2 shows the globally averaged SST anomalies for all the comparison data. In general, the comparison data are in good agreement in terms of interannual variability and the warming trend over time, though in the 1980s and 1990s the spread of the datasets widens (both with and without co-location to common coverage). The DailyOIv2.1 dataset is noticeably cooler than the other comparison data prior to the mid-2000s by order a few tenths of a kelvin. Prior to 2006 the DailyOIv2.1 makes use of Pathfinder AVHRR data which Reynolds et al. (2007) found has a residual cool bias in the night-time SST retrievals, particularly in the tropics. This feature is apparent in zonal averages of the comparison data (Figure 3-3) where a tropical cool bias is seen for DailyOIv2.1 prior to the mid-2000s. As such, when comparing the SST CCI products to the comparison data, the DailyOIv2.1 product is not shown in time series or zonal average plots and on trend plots is distinguished with a separate symbol. It is however still helpful to include the DailyOIv2.1 product as a comparison dataset as at the time of writing this dataset is actively updating. Aside from DailyOIv2.1, the decadal zonal averages for the comparison datasets shown in Figure 3-3 are generally in agreement at most latitudes over time to within a few tenths of a kelvin and good agreement is seen in terms of the observed widespread warming (noting that no obvious warming is observed in the Southern Ocean) and also the decadal variability in narrower latitude bands. Of note are the relative coolness of HadSST4 and COBE-SST2 in the tropics and subtropics in the 1980s; the relative lack of latitudinal variability in CMC v2.0 in the Southern Hemisphere in the 1990s; a tendency for HadISST variability to occasionally be outlying e.g., in the 2010s in the Southern Hemisphere; and larger anomalies in the gridded (non-infilled) in situ datasets (HadSST4 and drifter) in the Arctic due to lack of coverage. Zonal averages for drifting buoys are not shown in the 1980s due to a lack of observations and coverage.

Figure 3-4 and Figure 3-5 show SST anomalies for the Northern Hemisphere and Southern Hemisphere for the comparison data. As for the global average, there is good agreement in terms of interannual variability and the warming trend with the spread of the datasets tending to increase in the 1980s and 1990s (both with and without co-location to common coverage, though in the Southern Hemisphere co-location does have a modest impact on reducing the spread owing to lower in situ coverage). One feature of interest, particularly evident in Figure 3-4 for the Northern Hemisphere, is a seasonal cycle in the 1980s and early-to-mid 1990s for several of the comparison datasets. This is less evident in the global average (Figure 3-2) because the hemispheric cycles are out of phase. Because these are SST anomalies relative to a climatology created from the SST CCI v3.0 Analysis (albeit for 1991-2020), this suggests possible differences between the seasonal cycles of the comparison data and the SST CCI v3.0 data. Plots of comparison data and SST CCI v3.0 data SST anomalies (Figure 3-6 and Figure 3-7, bottom panels) show that this seasonality in the 1980s is not evident in the SST CCI v3.0 Analysis (implying that the seasonal cycle in the 1980s SST CCI data is comparable to that of the 1991-2020 climatology period) and only occurs in the comparison data (this is particularly evident in the Northern hemisphere).

To investigate these seasonal differences further, Figure 3-6 and Figure 3-7 (top panels) show SST anomalies for the comparison data in the Northern Hemisphere and Southern Hemisphere relative to the SST CCI v3.0 Analysis. In the 1980s, seasonal differences of order several tenths of a kelvin peak-to-peak magnitude are seen for all available comparison datasets, particularly in the Northern Hemisphere. In the Northern Hemisphere these seasonal differences then diminish in magnitude (though are still evident) from the early 1990s onwards, whilst in the Southern Hemisphere the seasonal differences gradually disappear for all comparison datasets during the 1990s before reappearing again more weakly in the 2000s onwards for the HadSST4, ERSSTv5 and COBE-SST2 datasets. Also, if differences are plotted relative to the HadSST4 product (not shown) the HadISST seasonality is more clearly seen to be out of phase with the other datasets in the Northern Hemisphere. The CMC and drifter datasets (which begin in the 1990s) show little evidence of comparable seasonal differences, whilst Argo (which begins in the 2000s) shows clear seasonal differences as well.

The seasonal differences in the comparison data relative to the SST CCI v3.0 Analysis are likely due, at least in part, to the differing representation of SST amongst the products and the seasonal and depth dependency of diurnal SST variations. The SST CCI Analysis provides an estimate of the daily average SST at 20 cm depth. The drifter data will also approximate a daily average 20 cm SST due to regular sampling at approximately this depth, and thus the lack of seasonal difference relative to the SST CCI v3.0 Analysis is reassuring. The SIRDS Argo data, which subsample the depth range 4-6 metres and approximate a foundation SST (a depth free of diurnal variability) display a seasonal difference of peak-to-peak magnitude order a few tenths of a kelvin and are cooler relative to SST CCI v3.0 Analysis data in the summer hemisphere. In the 1980s, ship observations are the predominant method of in situ SST measurement and comprise a mix of shallower bucket measurements and deeper (order metres) engine room intake measurements. Thus, in situ SSTs at that time represent (on average) depths deeper than 20 cm.

The precise SST represented in the 1980s for the different comparison datasets is complicated and will vary by dataset method. For example, the comparison datasets that use satellite data (DailyOI v2.1, OI.v2, HadISST and CMC) bias adjust the satellite data using in situ ship and buoy data as a reference, such that the interpolated SST fields will represent a depth typical of in situ observations over time. Furthermore, the DailyOI v2.1 adjusts ships relative to buoys assuming a constant warm offset (0.14 K pre-2016, 0.01 K from 2016-onwards) such that the product is considered to represent SST at the nominal 0.2 metre drifting buoy depth (moored buoys are generally considered unbiased on average relative to drifting buoys, though a 1 metre sampling depth is typically assumed). CMC also gives more weight to buoys in its bias correction, so will tend to this depth when drifting buoy data are available. The in situ based datasets (HadSST4, ERSSTv5

and COBE-SST2) go further in making adjustments to minimise the effects of changes in instrumentation over time, with buoys used as a baseline. However, as for DailyOI v2.1, these adjustments are typically made in some multi-annual to decadal mean sense (though each dataset takes its own approach[1]) due to a focus on accurately resolving longer-term climate trends and variability (and sometimes also data limitations), such that shorter term relative biases between different in situ types may not be corrected. In the case of HadSST4, oceanic profile data down to 10 metre depth are also used as a reference, further complicating the situation.

Some SST CCI v3.0 data are also adjusted to in situ observations through a process of satellite calibration. The NOAA-AVHRR brightness temperature are corrected for calibration errors using buoy and near-surface oceanic profile data in the 1980s (NOAA 6-10), and drifting buoy data from the 1990s-onwards (NOAA 11-19). (Metop-AVHRRs are adjusted to AATSR/SLSTR, acting as an independent satellite reference.) The bias-aware optimal-estimation scheme used to correct the calibration of NOAA-AVHRR uses piece-wise linear fits over various explanatory variables for brightness temperature bias (e.g., atmospheric moisture, time), which should ensure corrections are appropriate for ocean regions for which no in situ are available (significant during the 1980s) and avoid overfitting to the in situ data that are available. The SST CCI v3.0 Analysis also has a post-hoc calibration-spike adjustment which harmonises the statistical distribution of differences relative to HadSST4 before 1997 to those after, using the method in Merchant and Embury (2020). However, this is a global daily adjustment which should not be affected by seasonal differences of opposite phase in the Northern and Southern hemispheres, as seen in Figure 3-6 and Figure 3-7.

The upshot here is that, for all comparison datasets, seasonal comparisons to the SST CCI v3.0 Analysis will likely and to varying degrees reflect the changes in in situ instrumentation over time. Given the prevalence of deeper (order metres) engine room intake ship observations in the 1980s, seasonal differences to the SST CCI v3.0 Analysis more like Argo might thus be expected for that period. However, in the 1980s the magnitudes of the seasonal differences are greater than seen for Argo which implies other effects may also be important. Given that ship data are known to suffer from various biases, residual (uncorrected) seasonal ship biases are a possible cause, though as we are only considering differences here, effects in the retrievals (or other factors) cannot be ruled out. As time goes on the buoys make a growing contribution to the measurement of in situ SST and this probably explains the diminishing seasonal differences by the mid-1990s onwards; this might also imply issues with the comparison data are the more likely source of unexplained seasonal bias in the 1980s. The relative lack of seasonal differences in the CMC comparison dataset is curious but may be due to the greater weight given to buoys in the satellite bias adjustment. In part these results emphasise the need to carefully consider the differing representations of bulk SST when choosing and comparing datasets, particularly prior to buoy data becoming widespread, however this does not appear to fully explain some of the seasonal differences seen between the comparison data and SST CCI v3.0 products, notably in the 1980s.

---

[1] *For the period 1980-onwards: ERSSTv5 applies spatially, seasonally and temporally variable adjustments to ship data pre-2010 based on differences between SSTs and night-time marine air temperatures with an additional constant adjustment to buoy data, post-2010 a temporally variable direct adjustment to buoy data is made, a low-pass 16-year temporal smoothing is also applied to the adjustments; COBE-SST2 applies separate constant adjustments to ship Engine Room Intake (ERI) and insulated bucket data relative to drifting buoys; HadSST4 applies a spatially and temporally variable adjustment to ERI data relative to drifting buoy and near-surface oceanic profile data with a 5-year temporal smoothing, for insulated bucket data a spatially and seasonally variable adjustment is applied relative to near-surface oceanic profile data. COBE-SST2 and HadSST4 take differing approaches to ship metadata recovery that enable the separate ERI and bucket corrections to be applied. Note that pre-1980, separate ship adjustments addressing uninsulated bucket data are increasingly important.*

Figure 3-8 shows SST anomalies for the comparison datasets relative to the SST CCI v3.0 Analysis with a 12-month moving average applied for the Northern Hemisphere and Southern Hemisphere. This highlights the persistent biases between the datasets at multi-annual to decadal timescales. As noted for Figure 3-4 and Figure 3-5, but clearer in Figure 3-8, the spread of the datasets tends to increase in the 1980s and 1990s (both with and without co-location to common coverage, though in the Southern Hemisphere co-location does make a modest impact on reducing the spread). In the 1980s (if excluding DailyOIv2.1) the increase in spread is mainly due to the relative coolness of the HadSST4 and COBE-SST2 datasets compared with the other datasets available at this time (and is consistent with their relative coolness in the tropics and subtropics in the 1980s as noted in Figure 3-3). Broadly the products agree to within a tenth kelvin from the mid-1990s onwards, and to within a few tenths of a kelvin in the 1980s and early-1990s (excepting DailyOIv2.1, as discussed above). The spread of regional linear trends over this period is generally within 0.01 K per year or less (equivalent to 0.1 K per decade, see Section 3.4.7 and e.g., Figure 3-39), which is comparable to the GCOS stability requirement of 0.1 K per decade [GCOS, 2022]. As noted in Section 3.4.7, this is not a formal validation of product stability, however the spread of multiple products to within GCOS requirements is reassuring.

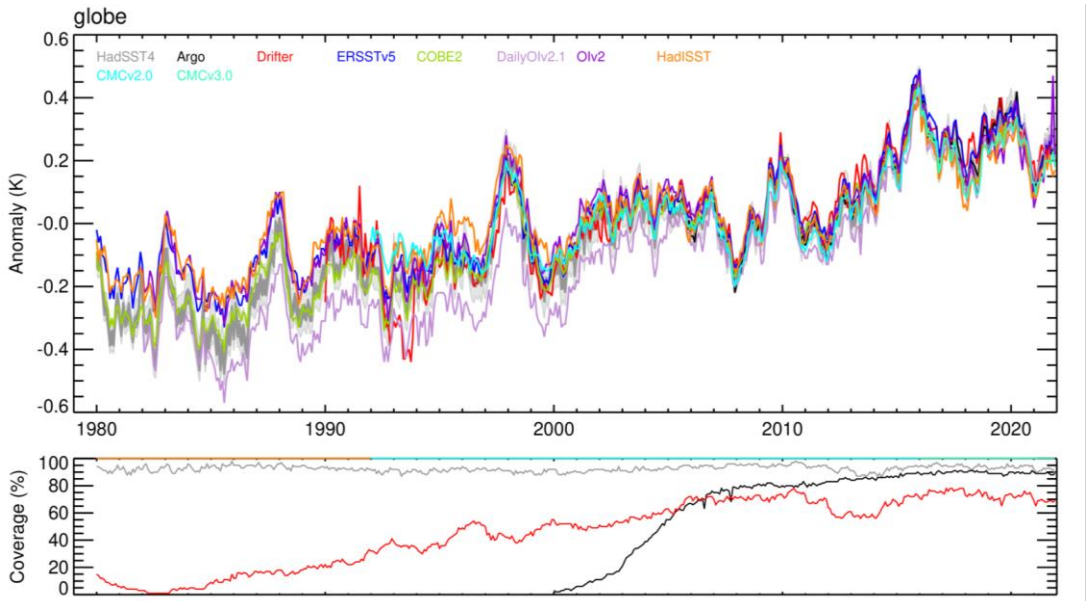

Figure 3-2. (Top) Global average SST anomalies (K, relative to the SST CCI v3.0 climatology 1991-2020) for each of the comparison datasets; (Bottom) % spatial coverage of each data set (colours as per the top panel).

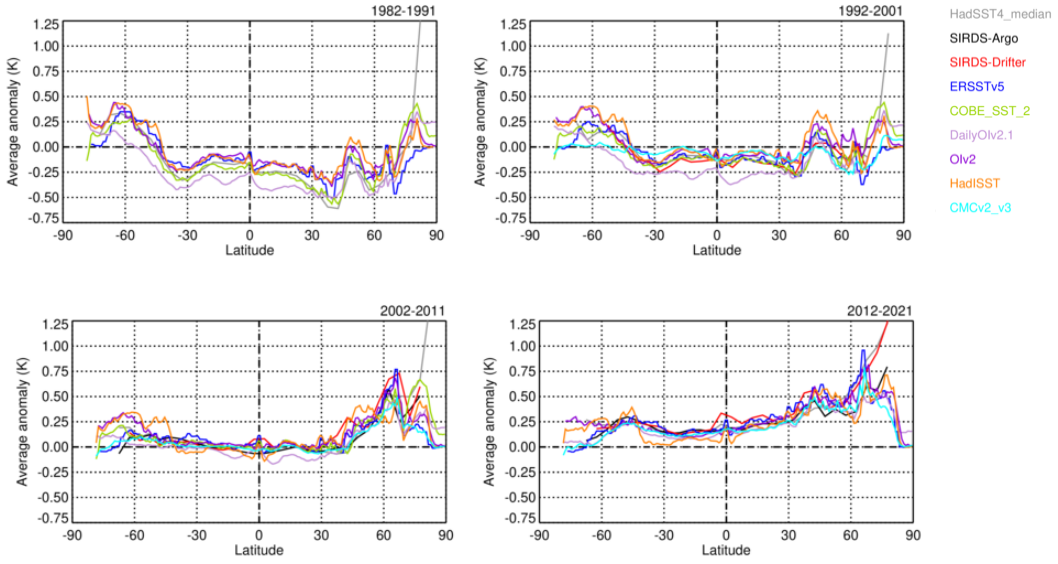

Figure 3-3. Decadal and then zonally averaged SST anomalies (K, relative to the SST CCI v3.0 climatology 1991-2020) for each of the comparison datasets.

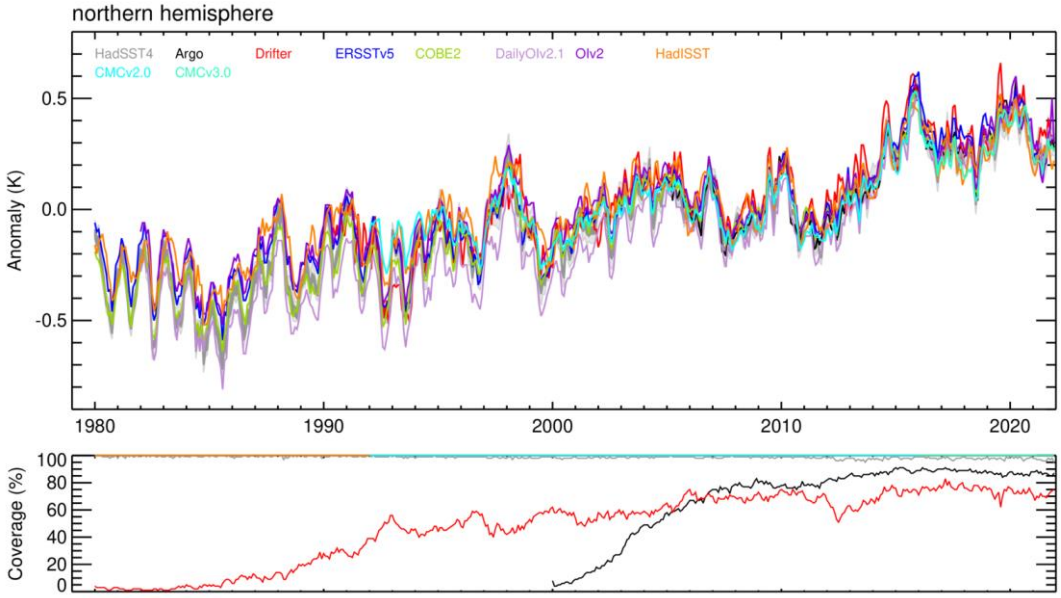

Figure 3-4. (Top) Northern Hemisphere SST anomalies (K, relative to the SST CCI v3.0 climatology 1991-2020) for each of the comparison datasets; (Bottom) % spatial coverage of each data set (colours as per the top panel).

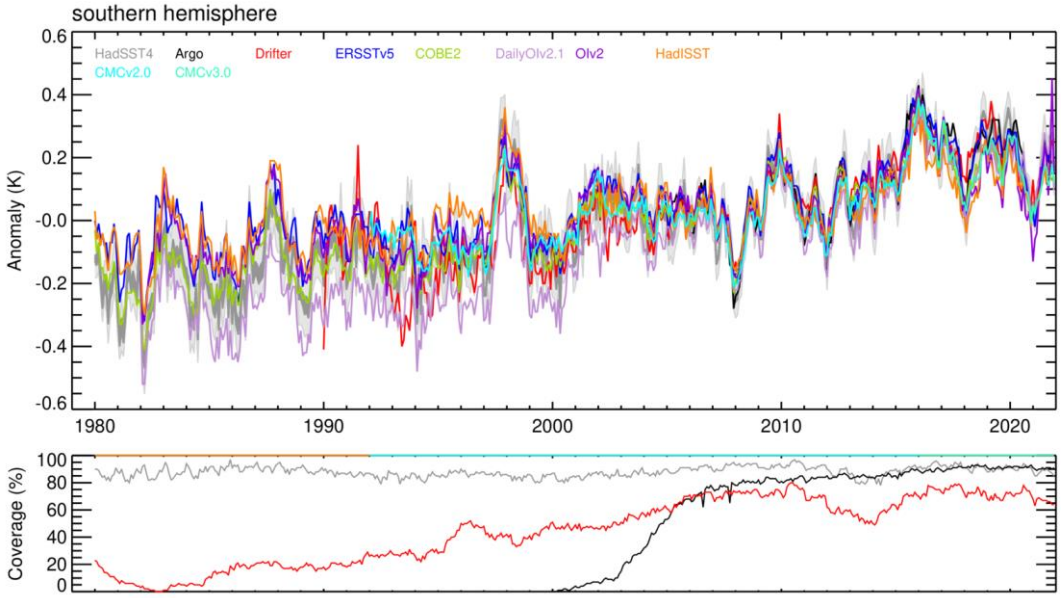

Figure 3-5. (Top) Southern Hemisphere SST anomalies (K, relative to the SST CCI v3.0 climatology 1991-2020) for each of the comparison datasets; (Bottom) % spatial coverage of each data set (colours as per the top panel).

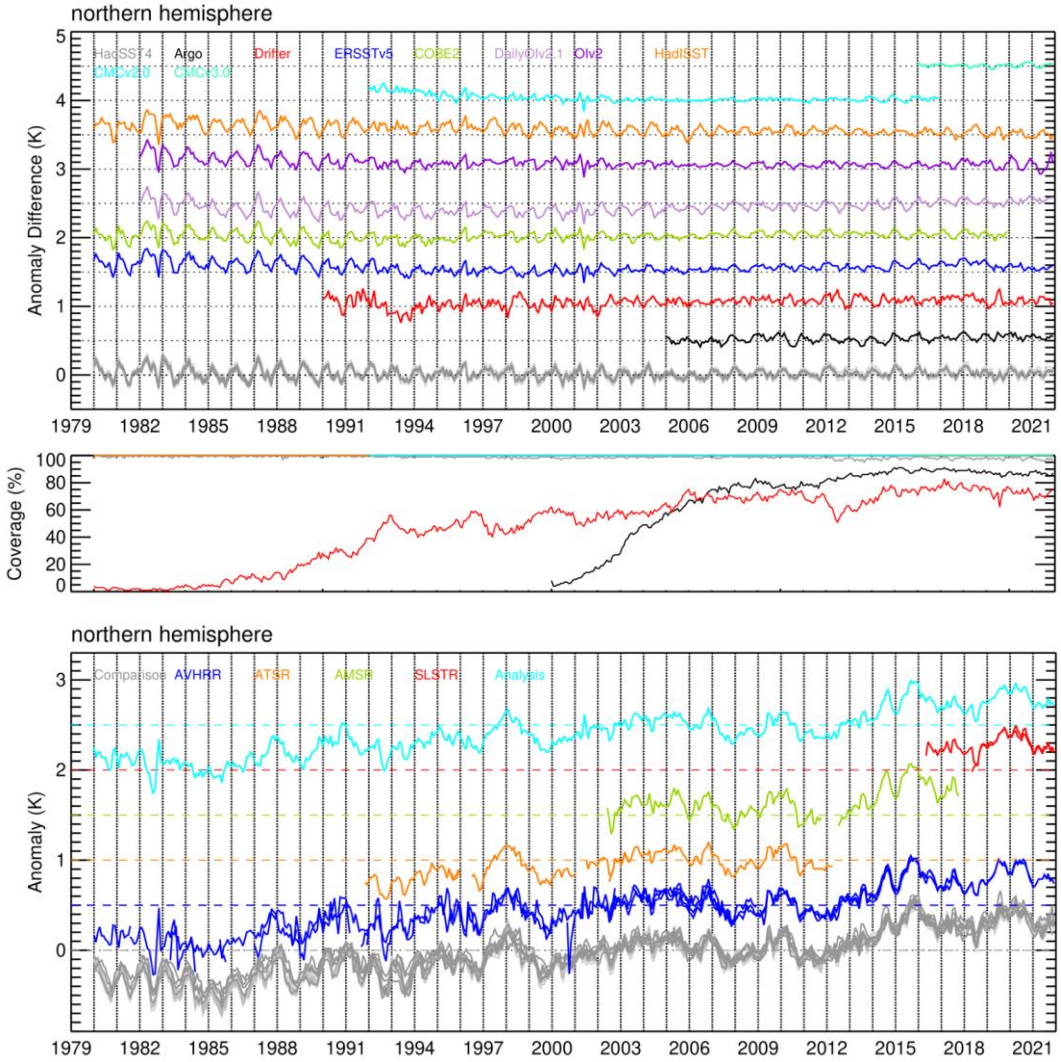

Figure 3-6. Northern hemisphere SST anomalies (K, relative to the SST CCI v3.0 climatology 1991-2020); (Top) the comparison data minus the SST CCI v3.0 Analysis (K); (Bottom) anomalies for the SST CCI v3.0 products and the comparison data. Timeseries are spaced by 0.5 K in both panels. Coloured horizontal dashed lines (bottom plot) denote the zero anomaly line for each dataset (colour as per plot legend).

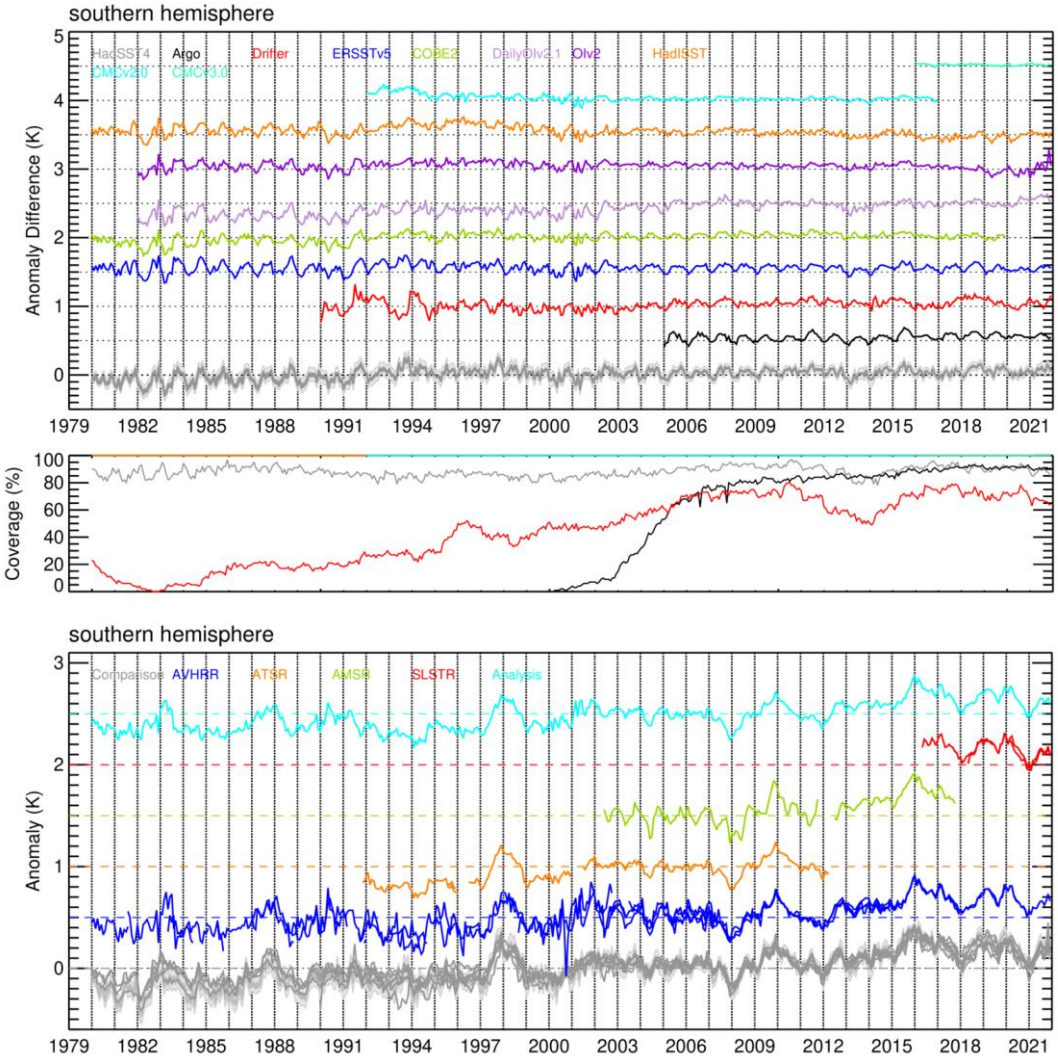

Figure 3-7. Southern hemisphere SST anomalies (K, relative to the SST CCI v3.0 climatology 1991-2020); (Top) the comparison data minus the SST CCI v3.0 Analysis (K); (Bottom) anomalies for the SST CCI v3.0 products and the comparison data. Timeseries are spaced by 0.5 K in both panels. Coloured horizontal dashed lines (bottom plot) denote the zero anomaly line for each dataset (colour as per plot legend).

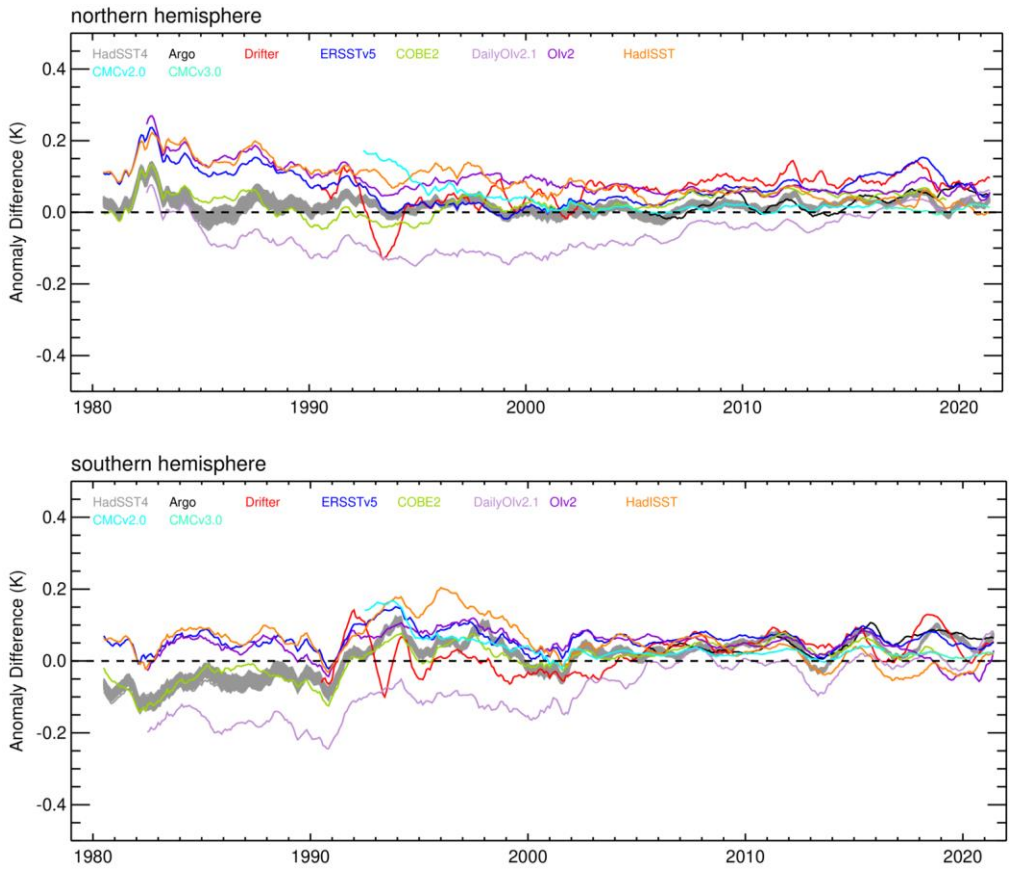

Figure 3-8. Northern and Southern hemisphere SST anomalies (K, relative to the SST CCI v3.0 climatology 1991-2020): the comparison data minus the SST CCI v3.0 Analysis (K) with a 12-month moving average applied.

3.4.2 SST CCI DATA – OVERVIEW

Figure 3-9 shows globally averaged SST anomaly timeseries for the SST CCI v3.0 data and the comparison data. In general, the SST CCI v3.0 data are consistent with each other (i.e. internally between data streams) and with the comparison data in terms of the observed climate variability. This includes the NOAA-AVHRR (NOAA 6, 8 and 10), Metop-AVHRR, AMSR and SLSTR data which are newly added for v3.0 (Metop-A was included in v2.1 but at lower GAC resolution). The large cool spike seen for the AVHRR data in 2000 is caused by low data volumes and coverage at this time. A smaller cool spike seen for the SLSTR-B data in May 2018 is because the data begin on 30/05/18, which results in low coverage for this month. The first month of the SLSTR-A data (May 2016) is also cooler than subsequent months by around a tenth kelvin, this is data from the satellite commissioning phase with very low data volume and has subsequently been segregated for the final product release (its inclusion here will not materially affect the assessment results).

To highlight differences between the datasets, Figure 3-10 shows differences relative to the SST CCI v3.0 Analysis. Monthly anomalies for the SST CCI v3.0 products and the comparison data generally agree to within 0.2 K, and to within 0.1 K from 2003 onwards (Figure 3-10, upper panel). Prior to the early 2000s, the AVHRR and ATSR retrievals are relatively noisy and there is greater disagreement amongst the comparison data. With a 12-month moving average applied to highlight persistent biases, we generally see agreement amongst the SST CCI v3.0 products to within 0.1 K (Figure 3-10, lower panel). The ATSRs and SLSTRs tend to lie at the cooler end of the comparison data ensemble, whilst the AMSR data tends to be relatively warm. The spread of individual AVHRR sensors can at times encompass the comparison data ensemble and on occasions exceed it (e.g., relatively cool AVHRR data in the 2000s). The Analysis tends to track towards the cooler sensor data and at times can also be slightly cooler than the SST CCI data that it is assimilating (notably during the 1980s-1990s and at times in the 2010s). The pre-1997 Analysis data has a post-hoc calibration-spike adjustment applied which includes a mean cooling adjustment of around 0.02 K which likely explains the relative coolness at this time, though the optimal interpolation performed by the Analysis could also be a factor.

Figure 3-11 and Figure 3-12 show SST anomaly timeseries and differences relative to the SST CCI v3.0 Analysis for the Northern and Southern hemispheres. As for the globally averaged timeseries, in general the SST CCI v3.0 data are consistent with each other and the comparison data in terms of the observed climate variability, with the Analysis, ATSRs and SLSTRs generally towards the cooler end of the comparison data ensemble, the AMSR relatively warmer and the AVHRRs more variable. In the 1980s the comparison data ensemble spread increases and in the Southern hemisphere the AVHRR data lie toward the warmer end of the ensemble whereas in the northern hemisphere the AVHRR data are cool relative to most of the ensemble. As for the global average the Analysis tends to track towards the cooler sensor data and can at times be slightly cooler than the data it is assimilating.

The SST anomaly timeseries for all the assessed regions (Section 3.3.2) and indices (Section 3.3.3) broadly show that the SST CCI v3.0 data are consistent with each other and the comparison data in terms of the observed interannual-to-decadal climate variability. A few example regions are shown in Figure 3-13. Differences amongst the SST CCI v3.0 and comparison datasets can be larger than that seen for the global and hemispheric averages discussed above, though generally are smaller than the climate signal. The Southern Ocean and the Mediterranean Sea are examples of regions with particularly large differences and are highlighted in Section 3.4.6.

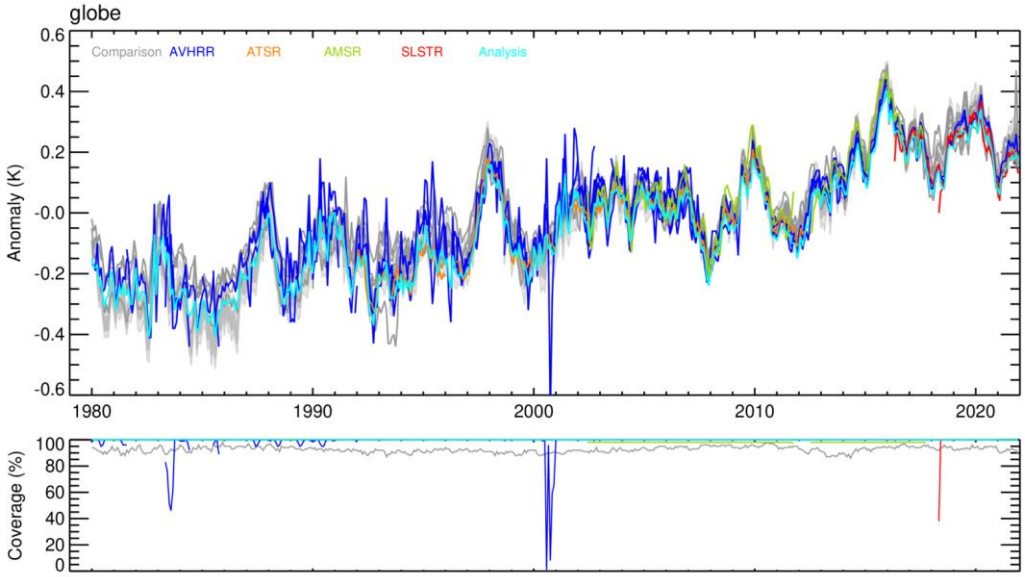

Figure 3-9. Global average SST anomalies (K, relative to the SST CCI v3.0 climatology 1991-2020) for the SST CCI v3.0 datasets and the comparison data. Only % spatial coverage (bottom) for the HadSST4 comparison dataset (grey) is shown (which approximates the coverage of the in situ network). A small amount of AVHRR data from 1979 is not shown as the ice mask applied to the data is based on the SST CCI v3.0 Analysis which begins in 1980.

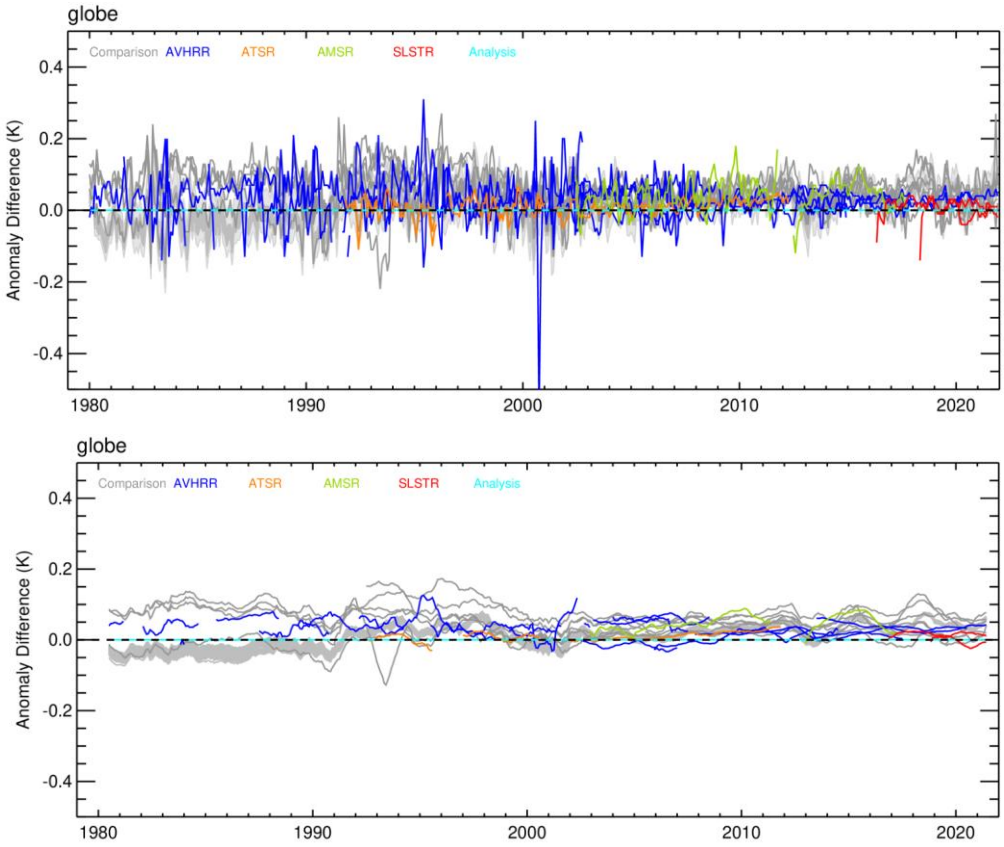

Figure 3-10. Global average SST anomalies (K, relative to the SST CCI v3.0 climatology 1991-2020): comparison data and SST CCI v3.0 data minus the SST CCI v3.0 Analysis (K, top) and with a 12-month moving average applied (bottom). Note

that 12-month averages are not calculated if there are missing data in the averaging window.

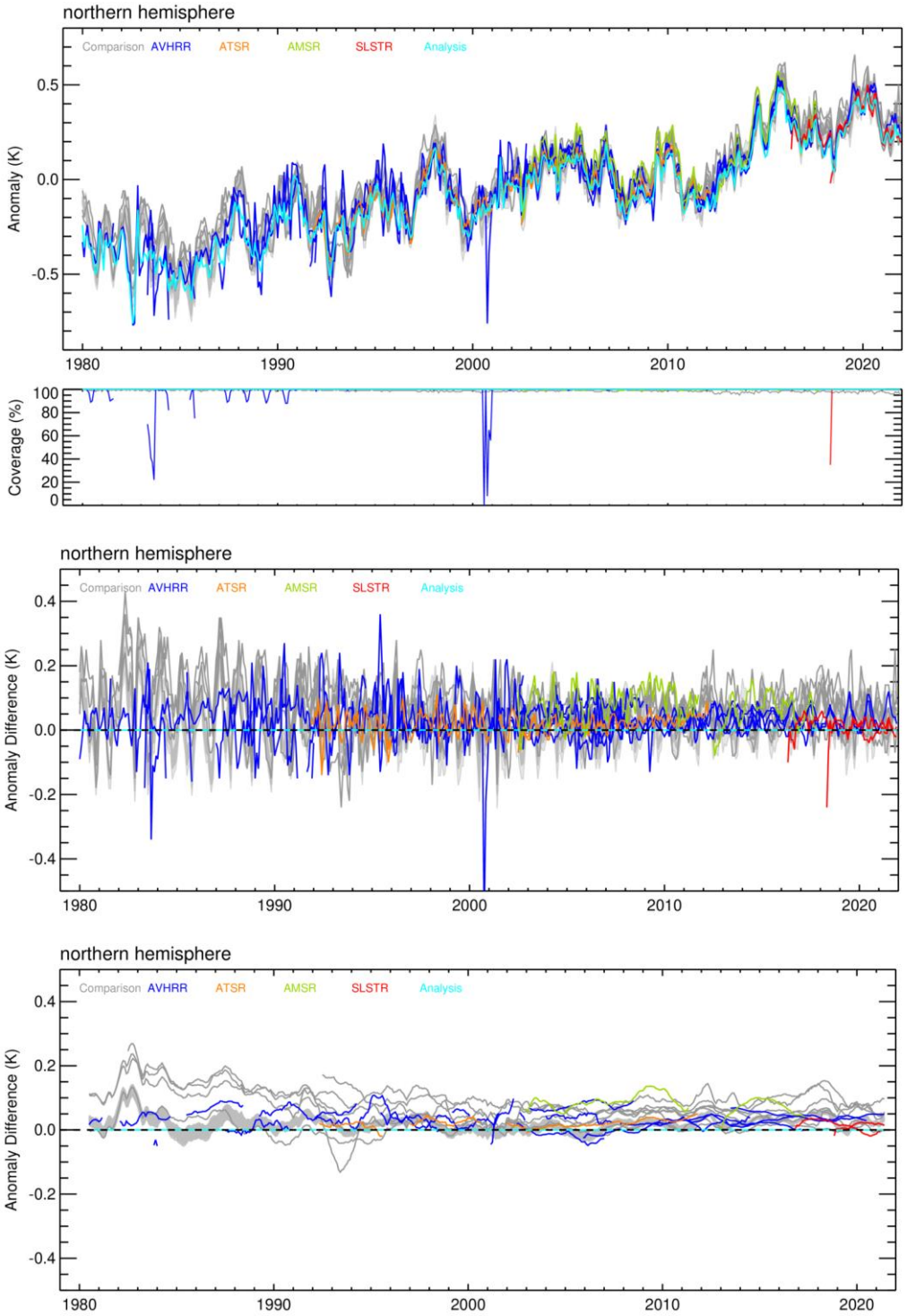

Figure 3-11. Northern hemisphere SST anomalies (K, relative to the SST CCI v3.0 climatology 1991-2020) for the SST CCI v3.0 and comparison data (top), the comparison data and SST CCI v3.0 data minus the SST CCI v3.0 Analysis (K, middle) and with a 12-month moving average applied (bottom).

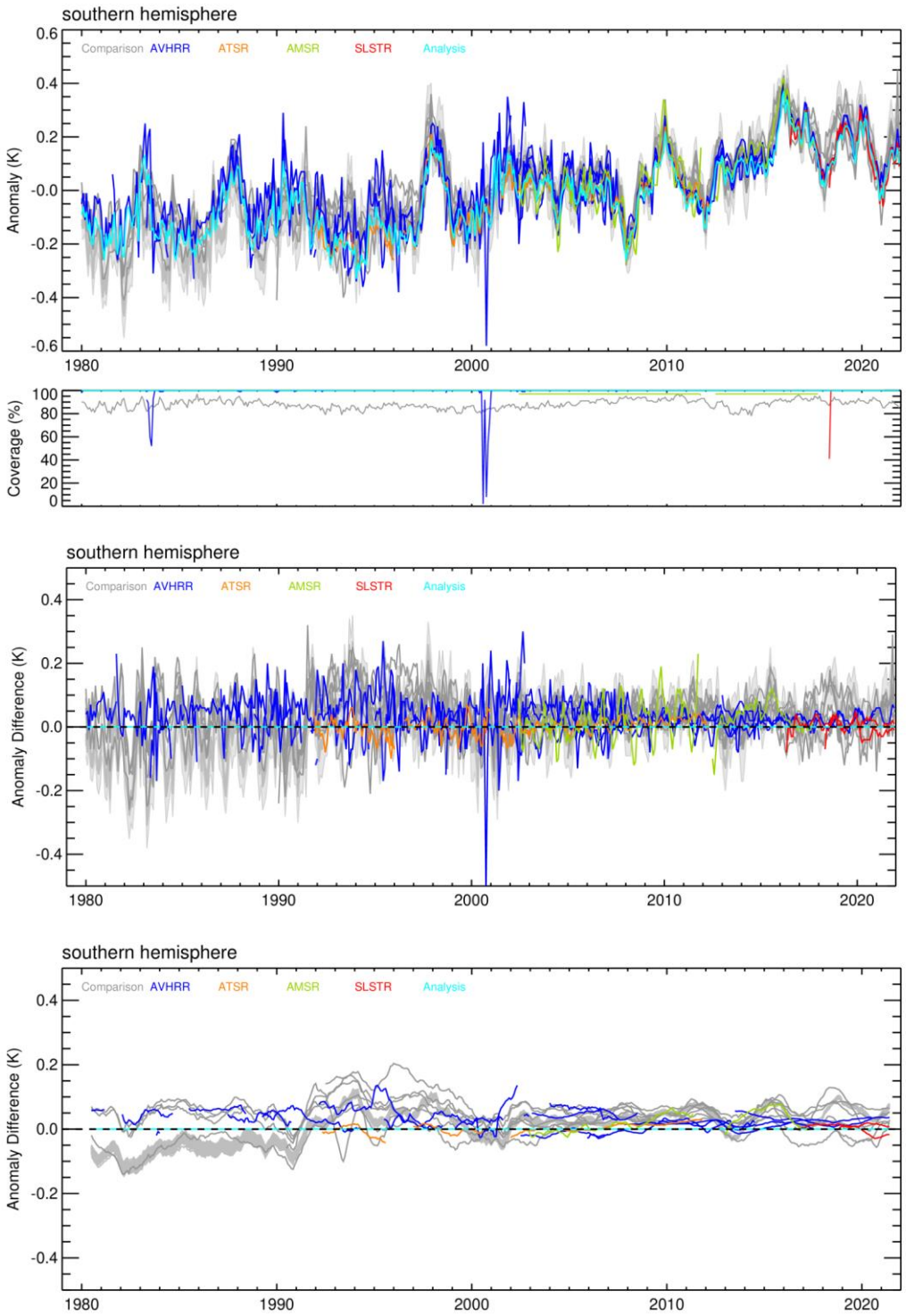

Figure 3-12. Southern hemisphere SST anomalies (K, relative to the SST CCI v3.0 climatology 1991-2020) for the SST CCI v3.0 and the comparison data (top), the comparison data and SST CCI v3.0 data minus the SST CCI v3.0 Analysis (K, middle) and with a 12-month moving average applied (bottom).

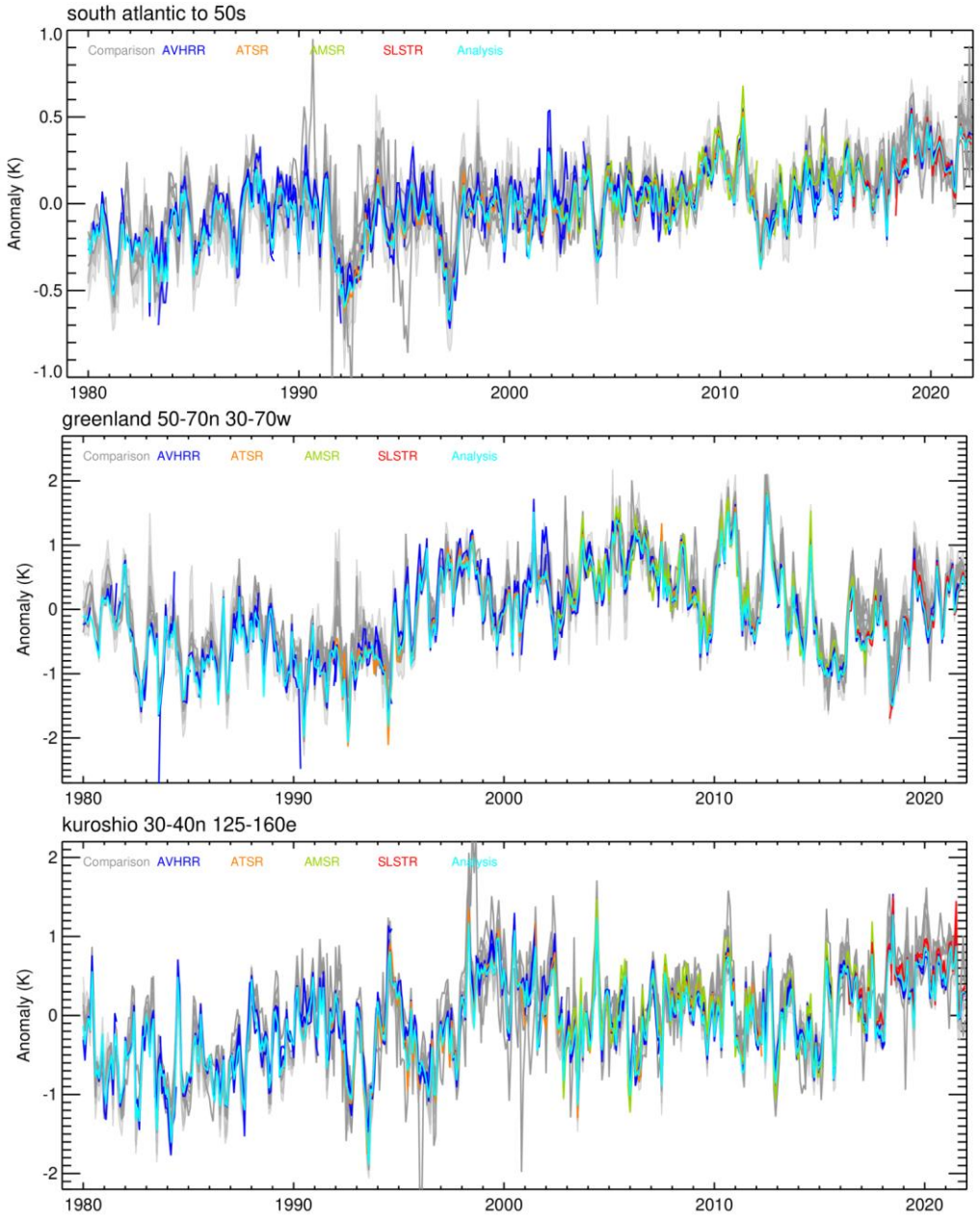

Figure 3-13. SST anomalies (K, relative to the SST CCI v3.0 climatology 1991-2020) for the SST CCI v3.0 and comparison data for (top) the South Atlantic; (middle) around Greenland; (bottom) the Kuroshio region.

To assess the progress made for the v3.0 SST CCI products, we now include the SST CCI v2.1 data in the comparisons. Figure 3-14 shows globally averaged timeseries with the v2.1 data included (noting that only the AVHRR and Analysis have changed between versions) and differences relative to the SST CCI v3.0 Analysis. The improvement in the SST CCI AVHRR (and the Analysis which assimilates the AVHRR) from v2.1 to v3.0 is clear, with better stability, fewer spikes and better general agreement with the other SST CCI and comparison datasets over time. Of note is an improvement from 1982-1983 with considerably reduced warm spikes in the v3.0 data (it is noted that the El Chichón eruption occurred from March-September 1982, causing an increase in atmospheric sulphate aerosols for many months afterward and difficulties for the accurate retrieval of SSTs from infrared instruments, however these spikes are not localised to regions with elevated aerosol and are instead caused by AVHRR instrument issues). Also evident is the improvement in agreement between the SST CCI v2.1 AATSR (not updated for v3.0) and the SST CCI v3.0 AVHRR during the 2000s, with the AVHRR data generally becoming warmer by order a few tenths of a kelvin from v2.1 to v3.0 and coming into better agreement with the comparison data. Similar improvements are also seen at other times e.g., 1994-1996, 1998-1999 and 2013-2015.

Figure 3-15 shows zonal averages of the SST CCI v3.0, v2.1 data and comparison data for different decades, which broadly assesses the spatial consistency of the SST CCI data over time. The SST CCI v3.0 data are broadly in alignment with the comparison data across decades and latitudes, however a persistent coolness of the SST CCI v3.0 products relative to the comparison data of up to a few tenths of a kelvin is evident in the northern and southern midlatitudes for most decades (exceptions are AVHRR data in the southern hemisphere in the 1980s, and somewhat for AVHRR and AATSR in the northern hemisphere in the 2000s). This presumably is why, for the global averages (Figure 3-10) the SST CCI v3.0 products (excluding AMSR) generally lie towards the cooler end of the comparison data ensemble. The AVHRR v3.0 bias-aware optimal-estimation scheme may play a role in any cool bias, with in situ data and AATSR/SLSTR data acting as reference for the NOAA-AVHRRs and Metop-AVHRRs respectively. Whilst the AATSR and also SLSTR (Figure 3-23, left panel) show similar mid-latitude cool biases, drifting buoy data (used for tuning NOAA 11-19 from the 1990s onwards) do not (Figure 3-3), implying that, for the NOAA-AVHRRs at least, the reference data are not a cause of this problem. Figure 3-15 (top left panel) shows that the relative warmth of the SST CCI v3.0 AVHRR data seen in the 1980s Southern Hemisphere timeseries (Figure 3-12) occurs due to a warmth in the southern sub-tropics coupled with a lack of coolness (as compared with later decades) in the Southern Ocean (the switch to using buoy and near-surface oceanic profile data as a reference for NOAA 6-10 in the 1980s could be a factor here). Figure 3-15 (top right panel) also shows that the agreement between SST CCI v2.1 ATSR (and the SST CCI v3.0 Analysis which tends to follow the ATSR) and the comparison data is worse than for AVHRR in the 1990s, with ATSR having a larger relative cool bias in the mid to high latitudes, though as discussed in Section 3.4.3 this may be due to larger errors in individual AVHRR instruments tending to cancel out in their average at this time. Figure 3-15 shows that the improvements in the AVHRR and Analysis from SST CCI v2.1 to v3.0 have largely occurred in the northern tropics during the 1980s-2000s with v3.0 relatively warmer and now in alignment with the comparison data (though improvements can be seen at other locations and times e.g., in the Southern Ocean during the 1990s and the southern tropics during the 2000s). Figure 3-16 shows the difference between the v2.1 and v3.0 SST CCI Analyses as decadal maps which highlights where the SST CCI products have changed between versions. In general, the changes seen in the zonal average plots (Figure 3-15) are reasonably consistent zonally, although the improvements made in the northern tropics are centred on the Atlantic and Indian Oceans where the handling of aerosol impact on the retrievals has been improved (see Section 3.4.3).

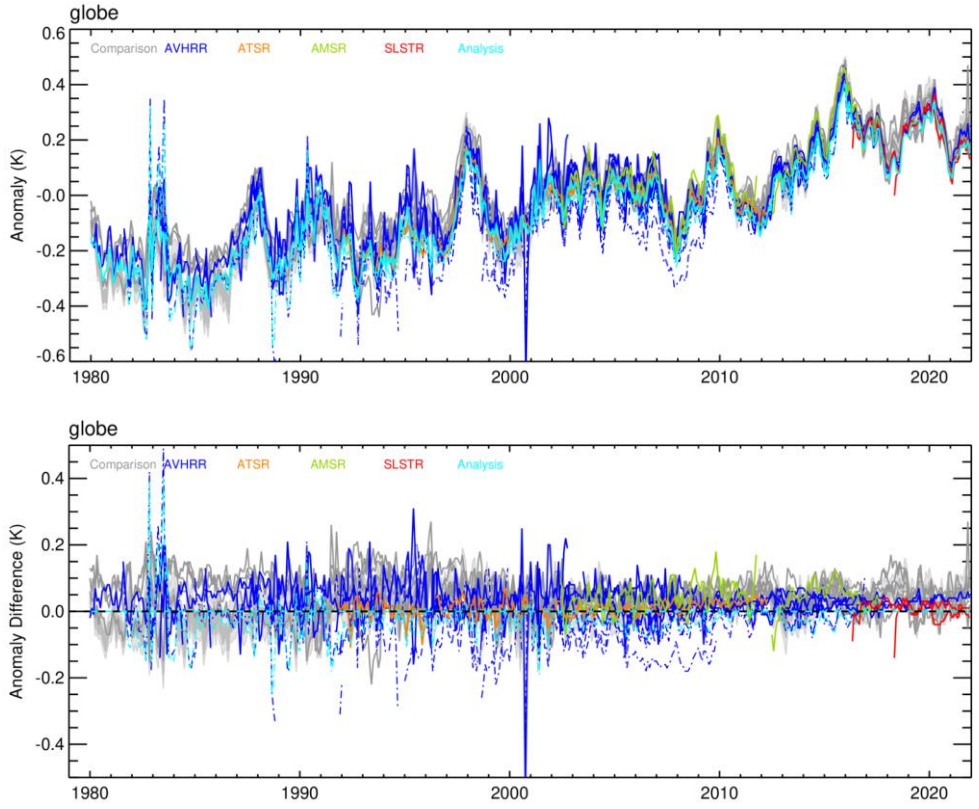

Figure 3-14. Global average SST anomalies (K, relative to the SST CCI v3.0 climatology 1991-2020) for the SST CCI v3.0 data, the SST CCI v2.1 data (dashed lines) and the comparison data (top) and the SST CCI v3.0, SST CCI v2.1 and comparison data minus the SST CCI v3.0 Analysis (K, bottom). Note that the ATSR data was not updated from v2.1 to v3.0.

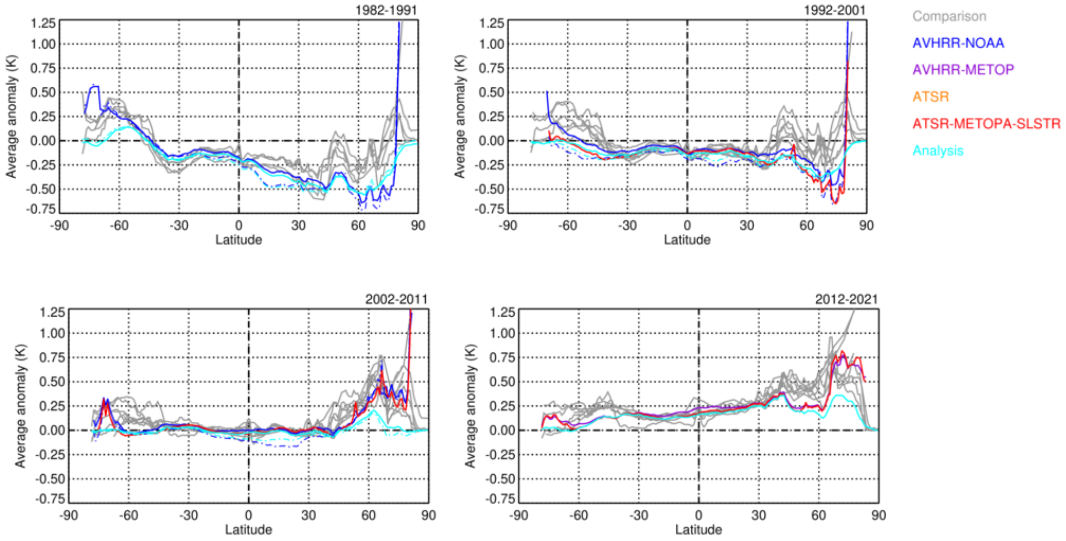

Figure 3-15. Decadal and then zonally averaged SST anomalies (K, relative to the SST CCI v3.0 climatology 1991-2020) for the SST CCI v3.0, SST CCI v2.1 (dashed lines) and comparison datasets.

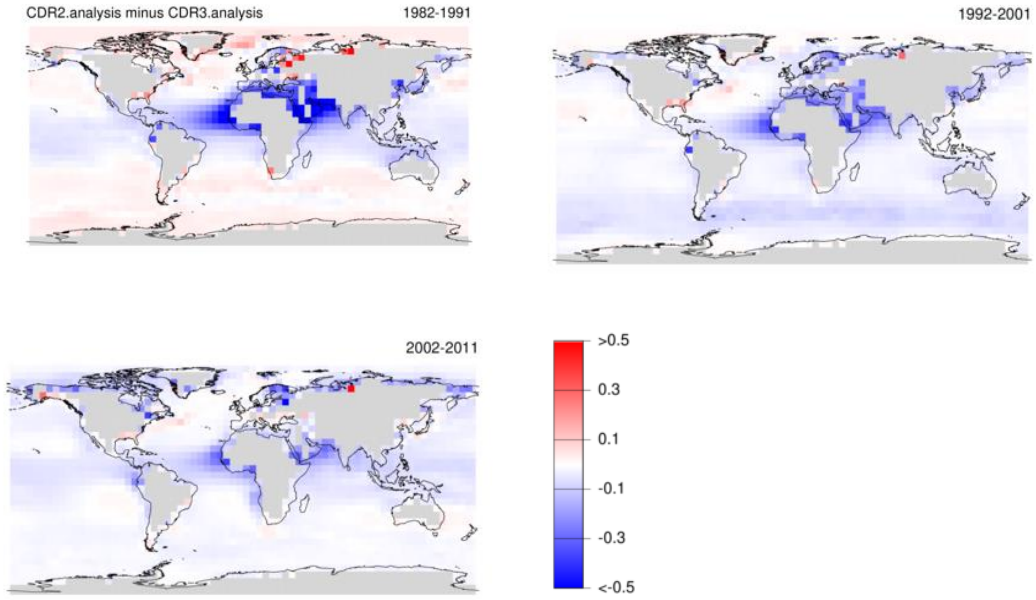

Figure 3-16. Maps of decadal average SST anomalies (K, relative to the SST CCI v3.0 climatology 1991-2020) showing the SST CCI v2.1 Analysis minus the SST CCI v3.0 Analysis (K).

3.4.3 SST CCI DATA - AVHRR

Figure 3-17 (top panel) shows globally averaged SST anomalies for the individual SST CCI v3.0 AVHRR sensors. In general, the different sensors show good agreement in terms of the observed climate variability and stability over time. The larger discrepancies observed for AVHRR15 in 2000 correspond to a drop in data volume and coverage. Data for the AVHRR 06, 08 and 10 sensors, which are newly added for SST CCI v3.0, also show fluctuations in coverage that are larger than for other AVHRR sensors and which may explain some of the noise in their timeseries relative to other AVHRR data and also the comparison data (Figure 3-10), however issues with the retrievals are also likely to be a factor. The AVHRR 06, 08 and 10 sensors are AVHRR/1 instruments which is an older 2-channel design that can only retrieve SST at night (which means the poleward extent of coverage will diminish in polar latitudes during Summer). The AVHRR 08 and 10 sensors also appear slightly cooler than other coincident AVHRR sensors (albeit the fluctuating coverage again makes this tricky to assess with confidence) which may explain the slight coolness seen for the AVHRR v3.0 composite (Figure 3-22) and SST CCI v3.0 Analysis (Figure 3-16) compared with v2.1 in the 1980s away from the tropics. Not all discrepancies between sensors are associated with drops in coverage and for individual months from the 1980s to late-2000s we see differences (noise) in the global average approaching a few tenths of a kelvin or more between sensors (from AVHRR06 to AVHRR18) where they overlap in time (Figure 3-17, bottom panel). This is less evident in the 2010s for AVHRRs 18 and 19 and Metops A and B which generally agree to within a tenth kelvin or better.

In the 2000s we see a divergence of the AVHRR data with AVHRRs 15 and 17 warmer than AVHRRs 16 and 18 by about a tenth kelvin (from 2007-onwards Metop A is somewhat in-between). AVHRRs 15 and 17 are in morning orbits which might be expected to produce better data because the diurnal variability adjustment to 10:30 local time will be smaller than that required for AVHRRs 16 and 18 which are in afternoon orbits (this applies to other AVHRR instruments too, however other factors such as instrument performance and retrieval tuning will also be important). However the divergence of the AVHRR data in the 2000s tends to be within the spread of the comparison data ensemble in global and hemispheric timeseries (see Figure 3-10, Figure 3-11 and Figure 3-12, bottom panels) making it difficult to judge the relative performance of the different sensors. Regional timeseries indicate that the divergence in the 2000s appears greatest in the extra-tropical North Pacific (Figure 3-18, top panel), the extra-topical North Atlantic, and particularly the Southern Ocean (Figure 3-18, bottom panel), with discrepancies approaching several tenths of a kelvin in the latter. In the Southern Ocean different AVHRR sensors also diverge in earlier periods e.g., AVHRRs 11, 12 and 14 during the 1990s, and this region is particularly problematic. AVHRRs 12 and 14 (and 15) suffer from orbital drift towards a twilight orbit which causes difficulties for SST retrieval as well as a loss of coverage (increasingly only observing northerly latitudes at day and southerly latitudes at night) and is a likely contributor to the observed divergence.

It is worth noting that the composite of all SST CCI v3.0 AVHRR sensors generally outperforms the individual AVHRR sensors in terms of stability and comparison with the SST CCI v2.1 ATSR data. The AVHRR sensors are tuned individually so this is likely the effect of errors in individual instruments tending to cancel out. Figure 3-19 (top and middle panels) shows that the composite AVHRR data agrees with the composite ATSR data in the 1990s and 2000s to generally within a tenth of a degree kelvin in the Northern hemisphere and approaching a few tenths of a kelvin in the Southern hemisphere, which is less than the spreads of the individual AVHRR sensors at that time. During the 2000s, when the individual AVHRR sensors diverge (Figure 3-17), the AVHRR composite itself remains stable and in alignment with the AATSR data. Figure 3-19 (bottom panel) shows the AVHRR and ATSR composites in the Southern Ocean, where agreement with the ATSR composite is considerably better than is obtained for individual sensors (contrast this with Figure 3-18, bottom). During the ATSR1 period (1991-1996) the ATSR and AVHRR composite diverge, with the AVHRR relatively warmer but also in better

agreement with the comparison data (with and without co-location to HadSST4, albeit a lack of coverage of in situ data in this region makes it harder to assess), consistent with zonal average anomalies for the 1990s (Figure 3-15). Although designed for accuracy, the ATSR retrievals can still suffer from biases and the relatively cooler ATSR data seen in Figure 3-19 in the early-mid 1990s in the Southern hemisphere (and to a lesser extent the Northern hemisphere) coincides with known issues with the ATSR1 instrument (failure of the 3.7 micron channel and problems with the detector cooler resulting in higher levels of radiometric noise). Separate validation [PVIR, 2023] shows that the ATSR1 instrument is still 'better' than individual AVHRR instruments at the same time in terms of smaller retrieval biases (albeit with slightly greater retrieval noise) and so better stability of the AVHRR composite is again likely due to errors in individual instruments tending to cancel out. In the Southern Ocean a shorter-lived divergence of ATSR2 and the AVHRR composite is also seen from 2000-2002, with ATSR2 relatively cool and in some months in worse agreement with the comparison data than is AVHRR. AVHRR 14 and 15 are known to have problems around this time but were retained to fill the gap in ATSR2 in the first half of 2001 when no other sensors are available, so any superior agreement of the AVHRR composite with the comparison data at this time is likely fortuitous.

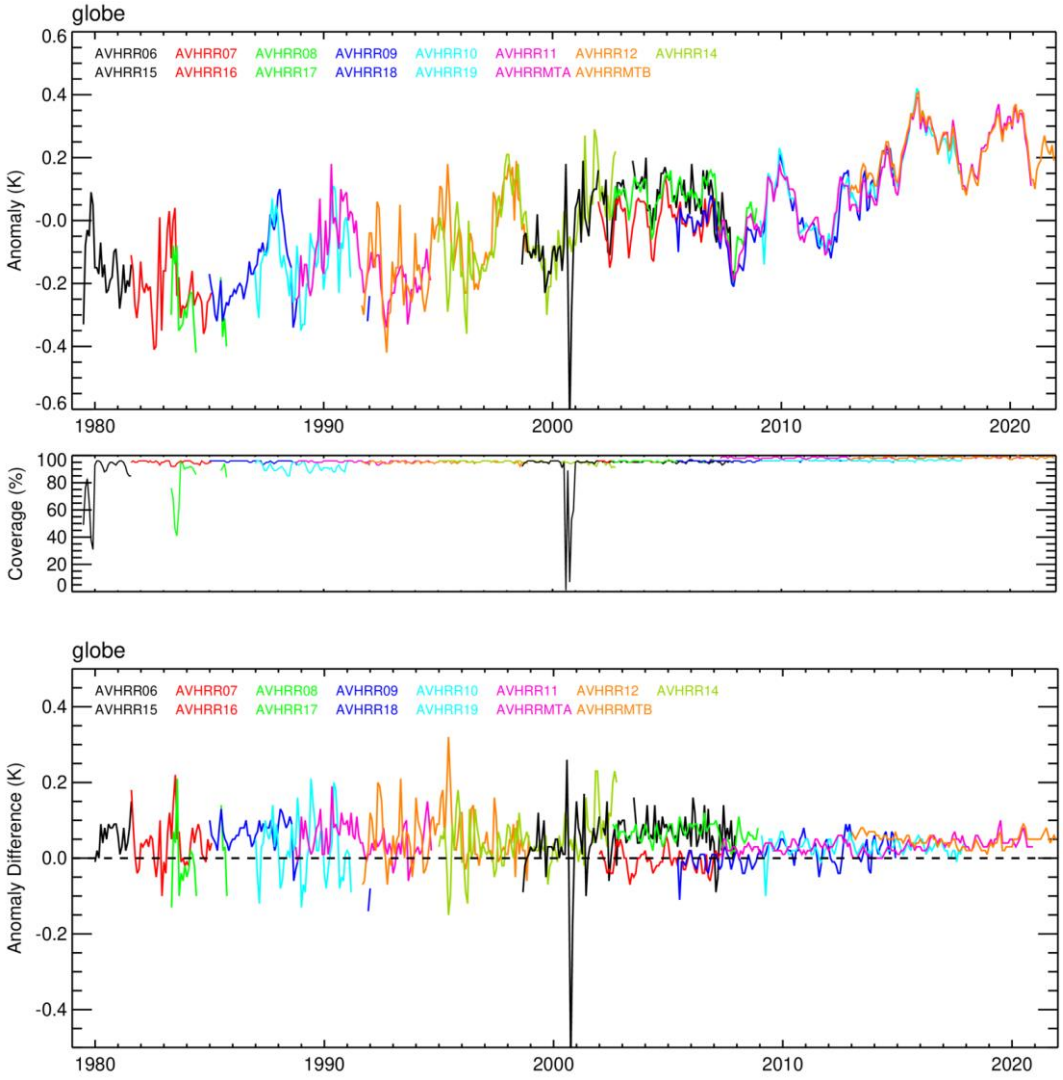

Figure 3-17. Global average SST anomalies (K, relative to the SST CCI v3.0 climatology 1991-2020) for all SST CCI v3.0 AVHRR sensors (top) and the SST CCI v3.0 AVHRR data minus the SST CCI v3.0 Analysis (K, bottom). No ice masking is applied (top) as the L2p AVHRR data are already masked.

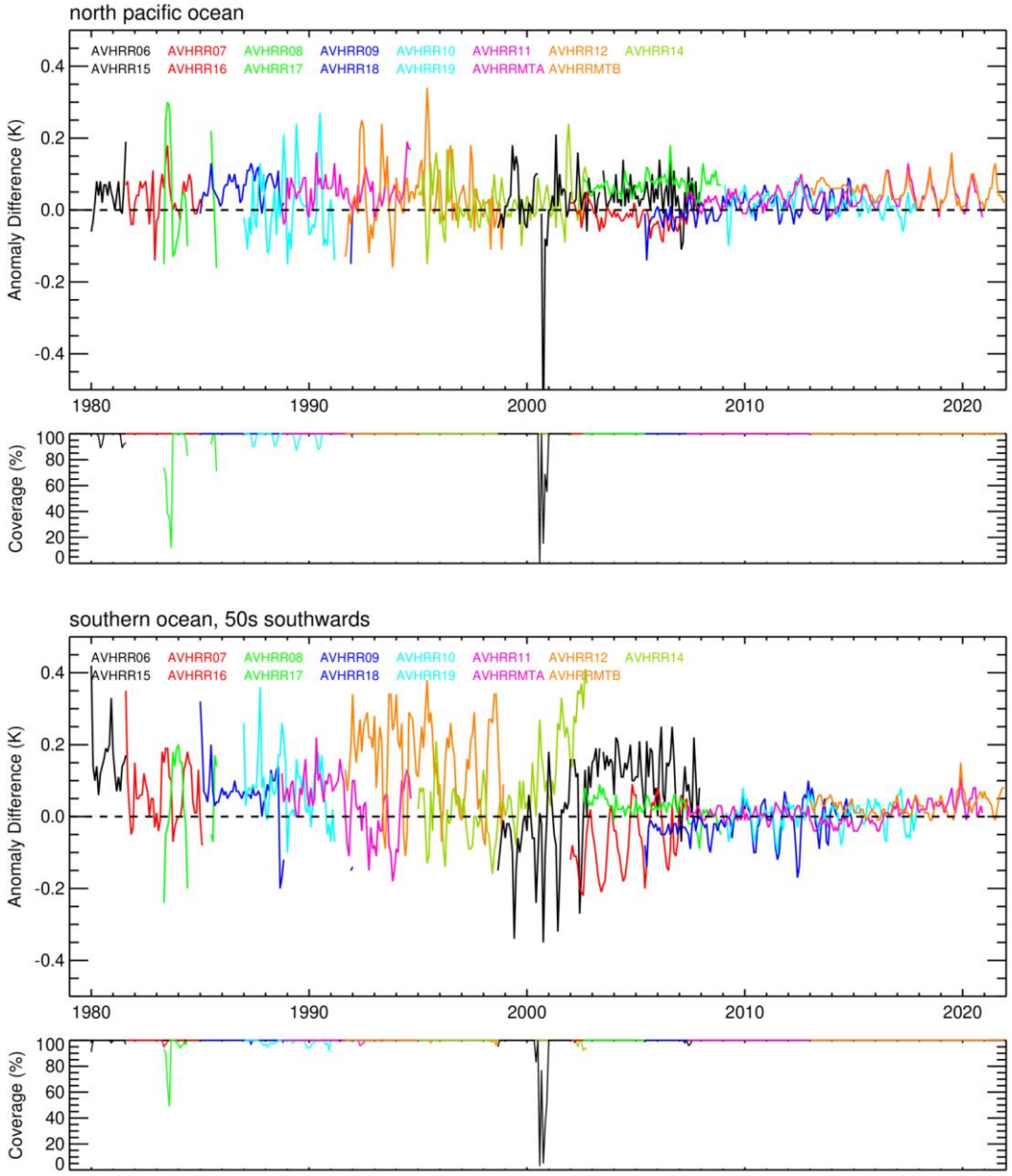

Figure 3-18. Regionally averaged SST anomalies (K, relative to the SST CCI v3.0 climatology 1991-2020): the SST CCI v3.0 AVHRR data minus the SST CCI v3.0 Analysis (K) in the North Pacific Ocean (top) and the Southern Ocean (bottom).

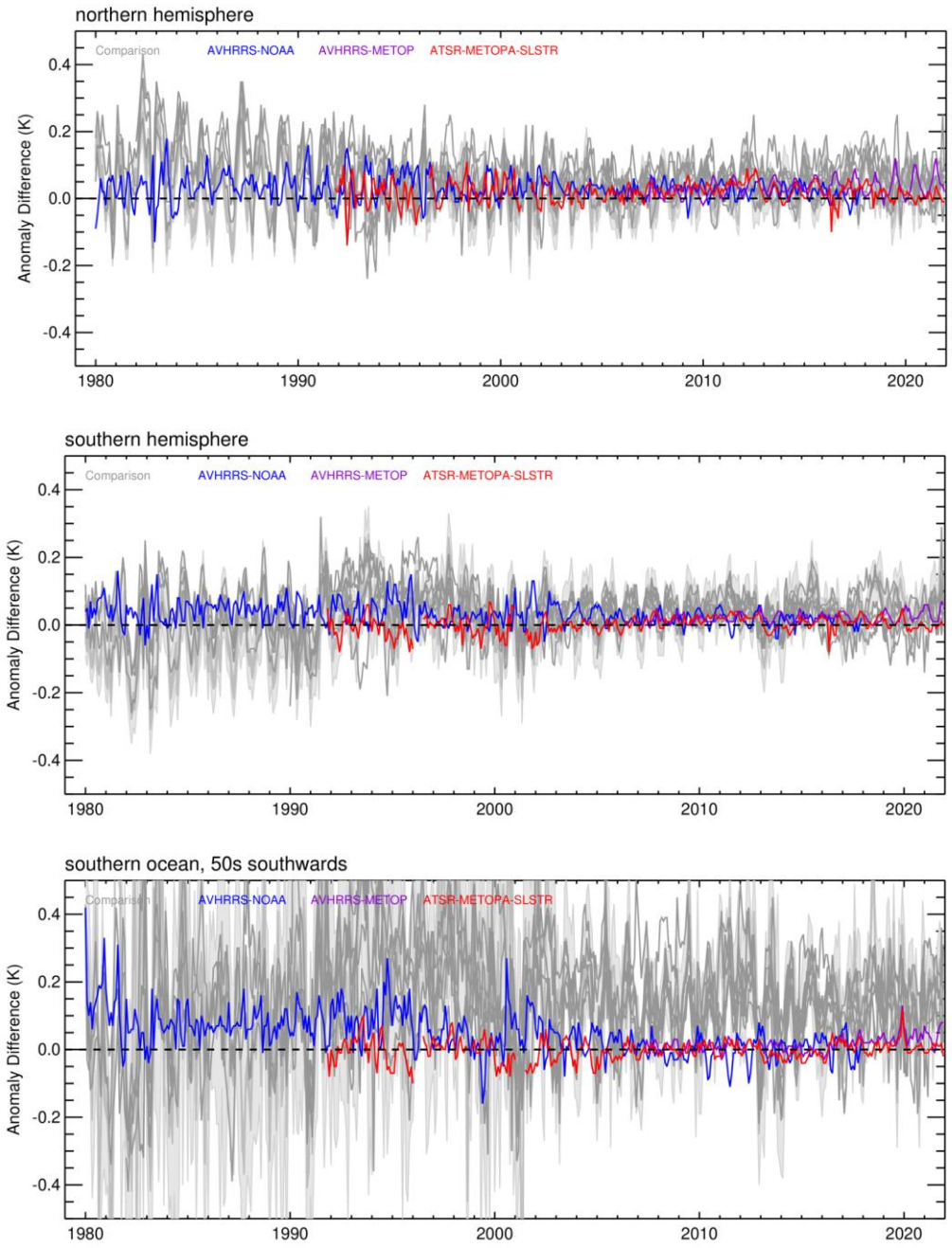

Figure 3-19. Regionally averaged SST anomalies (K, relative to the SST CCI v3.0 climatology 1991-2020): composites of the SST CCI v3.0 AVHRR, ATSR and SLSTR data minus the SST CCI v3.0 Analysis (K) in the Northern Hemisphere (top), the Southern Hemisphere (middle) and the Southern Ocean (bottom). For the ATSR-MetopA-SLSTR composite, MetopA data is only used from April 2012-April 2016 to fill the gap in the series between AATSR and SLSTR-A.

To assess the progress made for the SST CCI v3.0 AVHRR products, we now include the SST CCI v2.1 AVHRR products in the comparisons. Figure 3-20 shows the globally averaged SST anomalies for all individual AVHRR sensors for SST CCI v3.0 and v2.1. The SST CCI v3.0 data are more stable and less noisy than the SST CCI v2.1 products and thus better resolve global climate variability. An improvement in the AVHRR07 data from 1982-1983 is particularly evident. Improvements from SST CCI v2.1 to SST CCI v3.0 are seen in the AVHRR timeseries for most regions (not shown) with improvements particularly evident in regions known to be affected by aerosols. This is illustrated in Figure 3-21 for the north Indian Ocean and eastern tropical Atlantic where frequent cool anomalies of order several tenths of a kelvin caused by atmospheric dust blown from the Sahara Desert are no longer evident in the SST CCI v3.0 AVHRR products. This aerosol effect is frequent and large enough to be visible in the decadal average anomalies for these regions. Figure 3-22 (upper panels) shows decadal averages for the SST CCI v3.0 and v2.1 AVHRR products, where a relative coolness of the SST CCI v2.1 AVHRR product is evident in the eastern tropical Atlantic, Mediterranean Sea, Red Sea, Persian Gulf and Arabian Sea. This change from v2.1 to v3.0 is particularly evident when viewed as differences relative to the SST CCI v3.0 Analysis (Figure 3-22, lower panels) with the relative coolness in these regions now clearly reduced in the v3.0 data. As already highlighted in Section 3.4.2, this improvement is also evident in decadal zonal averages (Figure 3-15) where in the tropical northern hemisphere the zonal averages for SST CCI v3.0 AVHRR are relatively warmer than for SST CCI v2.1 AVHRR and in better agreement with the comparison data. The SST CCI v3.0 Analysis is similarly improved in these latitudes (Figure 3-15), including during the 1990s and 2000s when ATSR data were also available for assimilation. As noted in Section 3.4.2, improvements in the SST CCI v3.0 AVHRR are seen also in other locations, including a relative warming of the AVHRR in the Southern Ocean (and to a lesser extent the northern mid-latitudes) in the 1990s and the tropics as a whole in the 2000s (Figure 3-22, lower panels), which improves the agreement with the comparison data (Figure 3-15). These regional changes contribute to the improvements in the globally averaged SSTs at these times (Figure 3-14).

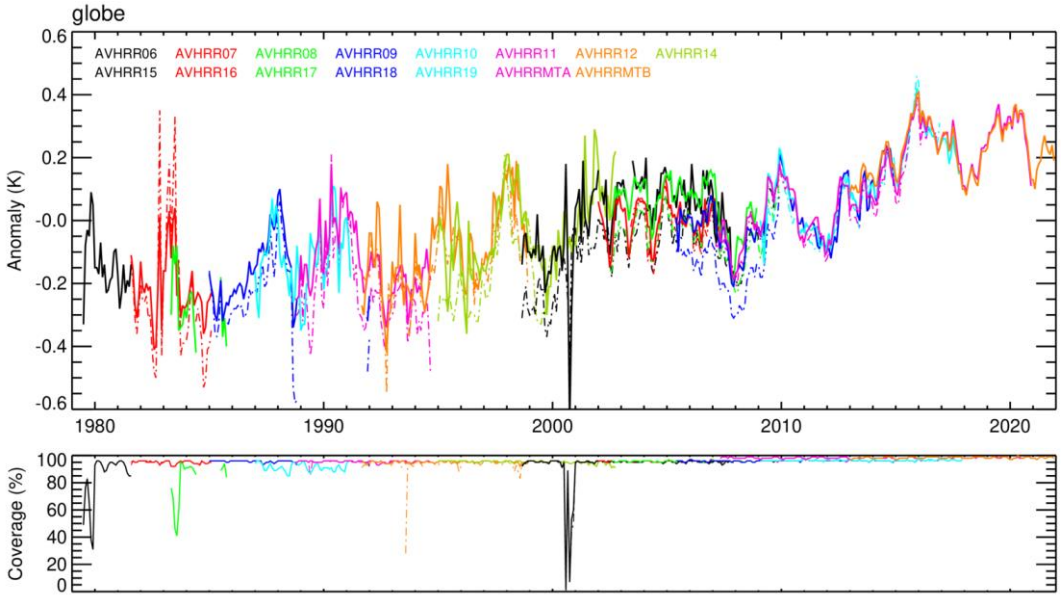

Figure 3-20. Global average SST anomalies (K, relative to the SST CCI v3.0 climatology 1991-2020) for all SST CCI AVHRR sensors for SST CCI v3.0 and SST CCI v2.1 (dashed). No ice masking is applied as the L2p AVHRR data are already masked.

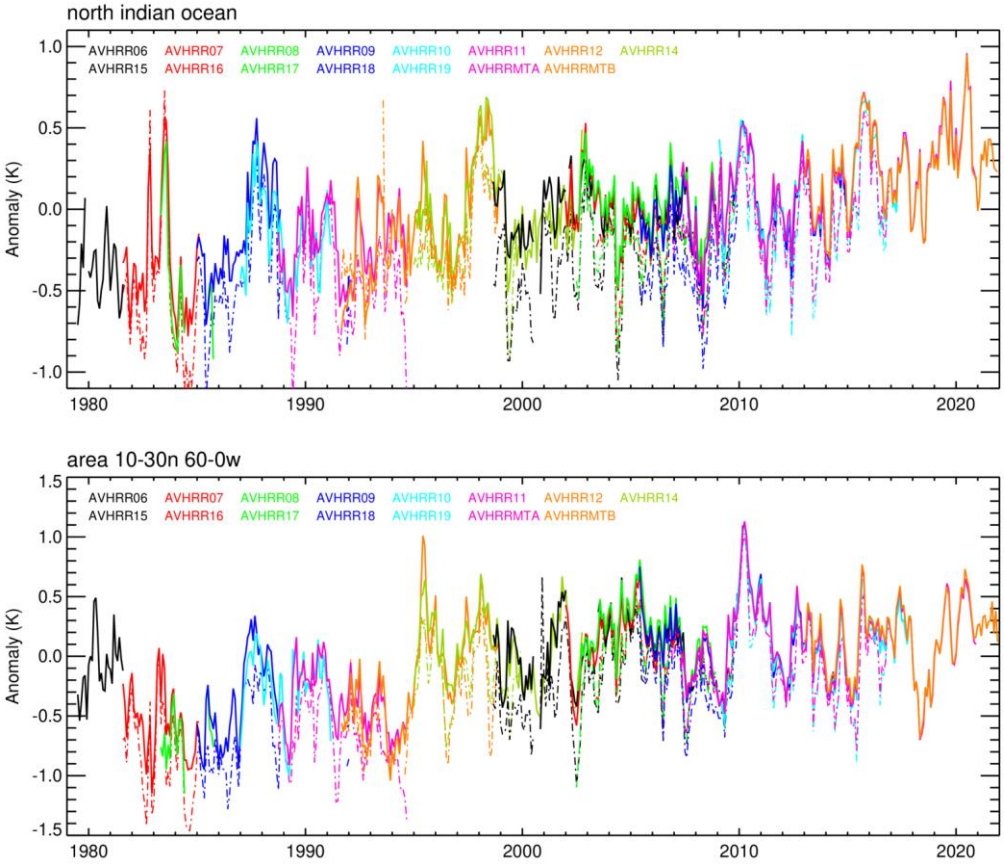

Figure 3-21. Regionally averaged SST anomalies (K, relative to the SST CCI v3.0 climatology 1991-2020) for the North Indian Ocean (top) and the eastern tropical

Atlantic (bottom) for all SST CCI AVHRR sensors for SST CCI v3.0 and SST CCI v2.1 (dashed).

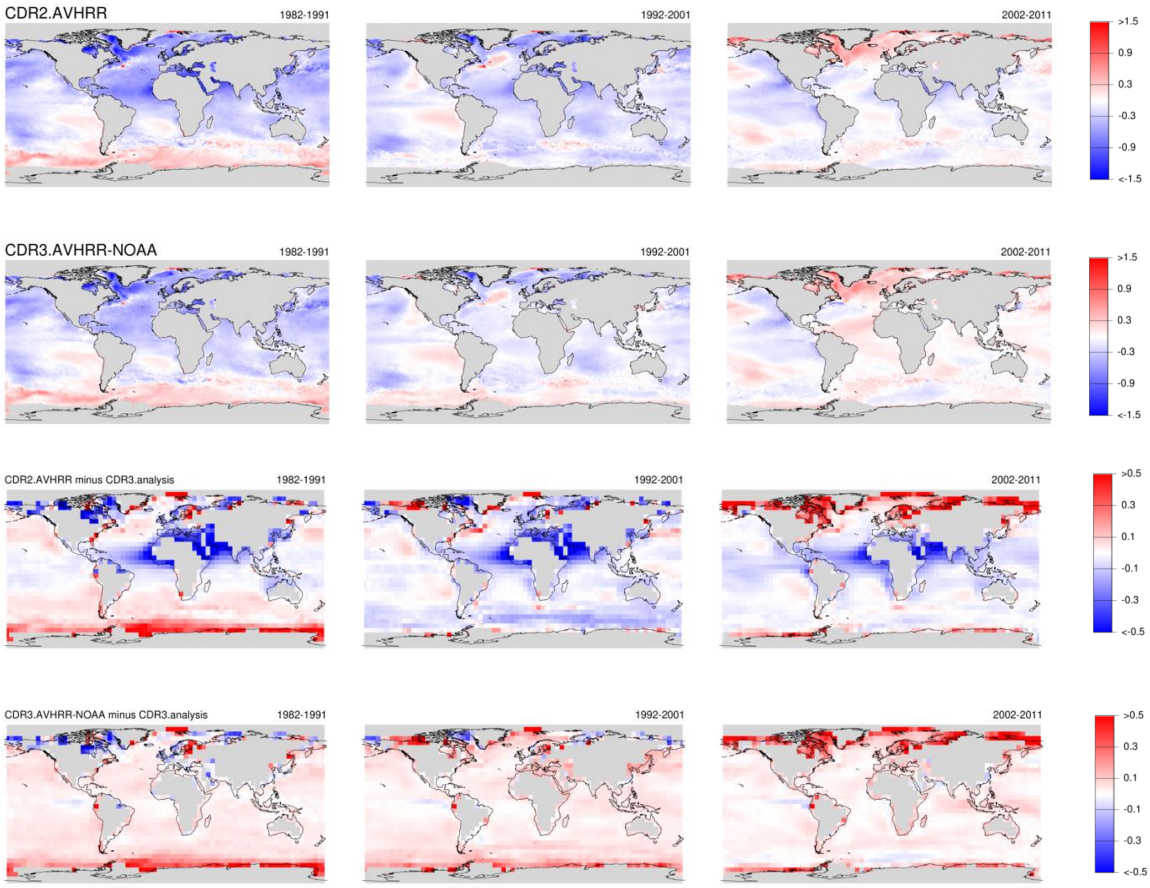

Figure 3-22. Decadal average SST anomalies (K, relative to the SST CCI v3.0 climatology 1991-2020) for 1982-1991, 1992-2001 and 2002-2011 of the AVHRR composites for SST CCI v2.1 and SST CCI v3.0 (top and upper middle rows) and the SST CCI v2.1 and SST CCI v3.0 data minus the SST CCI v3.0 Analysis (K, lower middle and bottom rows).

3.4.4 SST CCI DATA – SLSTR AND METOP-AVHRR

SLSTR and Metop-B data have been newly added for the SST CCI v3.0 release to help extend coverage from 2016 to 2021. Data from Metop-A and AVHRR19 have also been extended beyond 2016. Metop-A data are processed in v3.0 at full resolution (instead of GAC until v2.1) and all v3.0 AVHRR data benefit from revised processing including new bias-aware optimal-estimation (with Metop AVHRRs harmonised at brightness temperature level to ATSR and SLSTR). Figure 3-9 shows that for globally averaged SST anomalies these new data are in good agreement with each other in terms of resolving global climate variability. Figure 3-10, Figure 3-11 and Figure 3-12 emphasise this agreement between data from these sensors and with the comparison data in both global and hemispheric averages to order a tenth kelvin. For globally averaged SST anomalies, Metop-B appears warmer than Metop-A by order 0.05 K circa 2013-2015 (Figure 3-17, bottom panel) and SLSTR-B appears slightly cooler than SLSTR-A by order 0.05 K or less, particularly from 2020-2021 (Figure 3-10, bottom panel). The SLSTR data sit towards the cooler end of the comparison data ensemble in both northern and southern hemisphere averages and are generally slightly cooler than the Metop data (Figure 3-11 and Figure 3-12, bottom panels).

To further assess the spatial consistency of the SLSTR and Metop-AVHRR data, Figure 3-23 (left panel) shows zonal averages of the SLSTR and Metop-AVHRR composite data for the period 2017-2021. The SLSTR and Metop-AVHRR composites agree with the comparison data in the tropics and subtropics, however in the mid-latitudes we see that they are both cooler than the comparison data by up to a few tenths of a kelvin (particularly in the northern mid-latitudes). As discussed in Section 3.4.2, this relative coolness in the mid-to-high latitudes seems to be a general feature of all SST CCI v3.0 data (except AMSR, Section 3.4.5). The SLSTR is cooler than Metop-AVHRR in the tropics and the Southern Ocean by around a tenth kelvin or less (regional timeseries in the Southern Ocean, not shown, indicate this chiefly occurs in the Atlantic and Indian Ocean sectors). The SST CCI v3.0 Analysis, which is largely based on Metop-AVHRR and SLSTR data in this period, is similarly affected (Figure 3-23), tracking closer to the SLSTR where it deviates from Metop-AVHRR.

Figure 3-19, which shows SST anomalies for the northern and southern hemispheres (top and middle panels) relative to the SST CCI v3.0 Analysis for the SLSTR (May 2016 onwards) and AVHRR composites, suggests that the relative coolness of SLSTR versus Metop-AVHRR has a seasonal element, being particularly pronounced in the hemispheric Summer (it is especially evident in the northern hemisphere timeseries from 2019 onwards). Regional timeseries suggest that this effect seems to mainly arise in the tropics and particularly the western tropical Pacific. Figure 3-24 shows SST anomalies for the northern and southern tropics (top and middle panels) relative to the SST CCI v3.0 Analysis for the SLSTR and AVHRR composites. In the SLSTR period (May 2016 onwards) we see that SLSTR is generally cooler than Metop-AVHRR with the latter showing a greater relative warmth of order a tenth kelvin in the summer hemisphere. To assess whether this seasonality is a feature of the SLSTR or Metop-AVHRR, Figure 3-25 shows SST anomalies in the northern tropics for the comparison data relative to the SST CCI v3.0 Analysis. Of particular interest is the drifter data, which in terms of the SST represented is the most directly comparable to the SST CCI v3.0 data. The drifter data shows no evidence of a Metop-like seasonal warmth in the Summer at this time (this is also seen for the other comparison data), however noise in the timeseries makes detection of a seasonal signal of order a tenth kelvin challenging; a similar result is seen in the southern tropics (not shown). Separate validation [PVIR, 2023] shows that Metop-AVHRR generally displays greater seasonal differences versus drifting buoy data than SLSTR. Furthermore single-view sensors such as Metop-AVHRR would expect to suffer more from high atmospheric water vapor levels in the tropics. Overall, this would suggest that the Metop-AVHRR retrievals likely suffer from seasonal biases relative to SLSTR and in situ data in the tropics.

To investigate this further, Figure 3-26 shows SST anomalies for the northern and southern tropics for individual SST CCI v3.0 AVHRR sensors relative to the SST CCI v3.0 Analysis. This suggests that the seasonal fluctuations are a robust feature of all MetOp-AVHRR data and are also seen prior to the SLSTR period. In the northern tropics there is evidence of a seasonal difference between Metop-A and AATSR where they overlap (May 2007-April 2012, Figure 3-24 upper panel) though this is less clear than for comparisons to SLSTR. In addition, zonal average SST anomalies for the 2008-2017 period (when the NOAA-AVHRR and Metop-AVHRR composites overlap) show a slight relative warmth of Metop-AVHRR versus NOAA-AVHRR in the tropics (Figure 3-23, right panel), as was seen for Metop-AVHHR versus SLSTR from 2017 onwards (left panel).

It is noted that seasonal fluctuations are also evident for some NOAA AVHRR sensors, e.g., AVHRRs 12, 15 and 17 in the southern tropics show a similar seasonality to Metop-A (Figure 3-26, bottom panel) and in the case of AVHRRs 12 and 15 with a greater magnitude. Validation of AVHRR data [PVIR, 2023] shows that Metop-AVHRR generally has less seasonal variation versus in situ data than NOAA-AVHRR and it may be that other instrumental issues with the NOAA AVHRRs are obscuring these effects here.

Figure 3-27 shows trends for the Metop-AVHRR and ATSR-MetopA-SLSTR composites for the period 2008-2021. In general, the trends agree well with each other and the comparison data although the trends for the ATSR-MetopA-SLSTR composite are generally slightly lower than for Metop-AVHRR by order a few millikelvin per year. This in part is consistent with the relative coolness described above for Metop-A versus Metop-B and SLSTR versus Metop-AVHRR. However, in some regions the difference between AATSR and Metop-AVHRR is also a factor. Away from the tropics a relatively warm AATSR contributes to the lower trends, particularly in the North Atlantic and North Pacific, whereas in the tropics (and less so parts of the Southern Ocean) a relatively cool AATSR can act to increase the trends and counteract the tendency of Metop-A and SLSTR towards lower trends. This is most evident in the west tropical Pacific (Figure 3-24, bottom panel) where the relative coolness of both the AATSR and SLSTR lead to a trend that is comparable to Metop-AVHRR (see Figure 3-27).

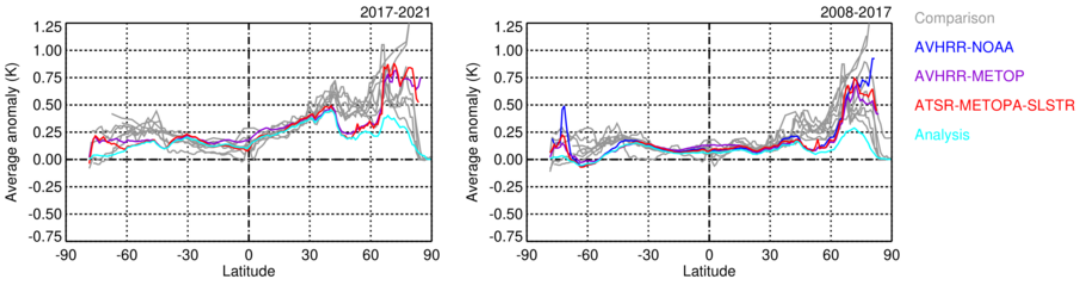

Figure 3-23. Zonally averaged SST anomalies (K, relative to the SST CCI v3.0 climatology 1991-2020) for the SST CCI v3.0 composite data averaged over the periods 2017-2021 (left) and 2008-2017 (right).

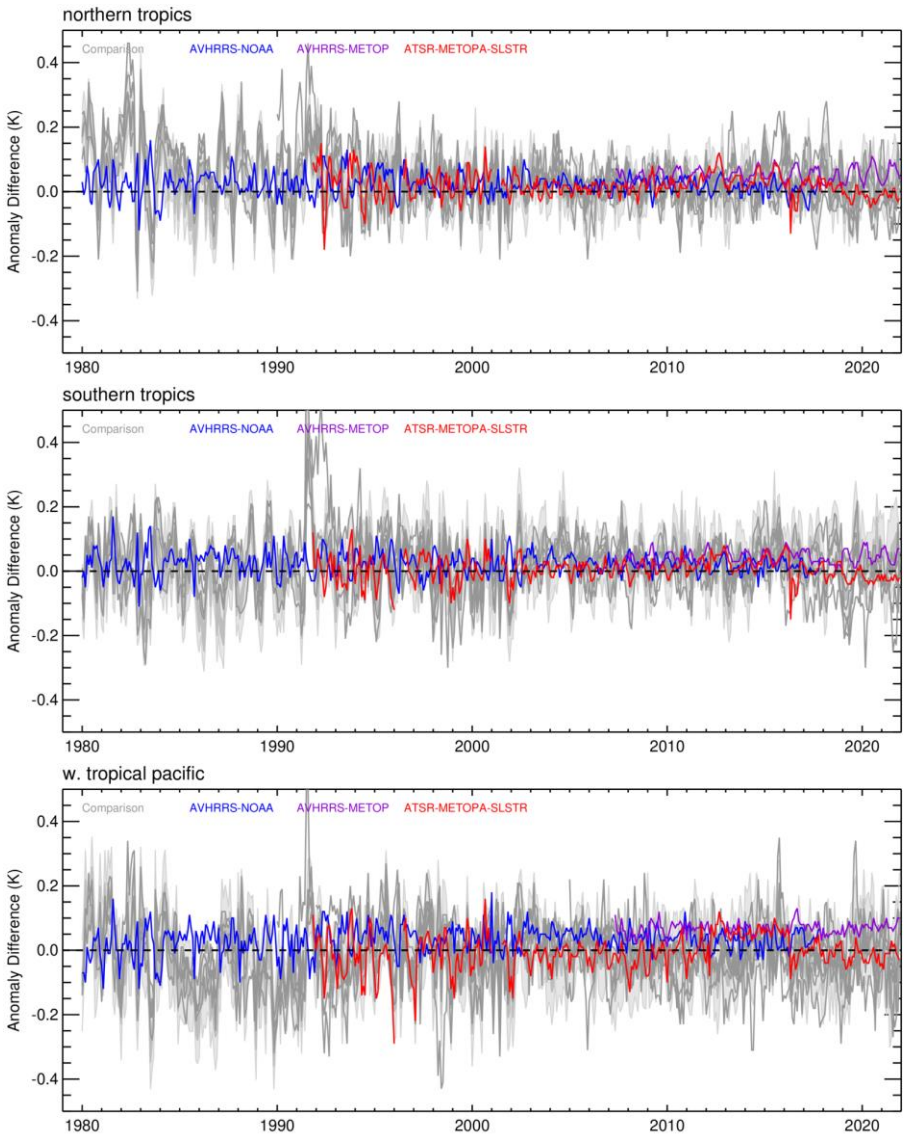

Figure 3-24. Regionally averaged SST anomalies (K, relative to the SST CCI v3.0 climatology 1991-2020): composites of the SST CCI v3.0 AVHRR, ATSR and SLSTR data minus the SST CCI v3.0 Analysis (K) in the northern tropics (top), the southern tropics (middle) and the western tropical Pacific (bottom). For the ATSR-MetopA-SLSTR composite, MetopA data is only used from April 2012-April 2016 to fill the gap in the series between AATSR and SLSTR-A.

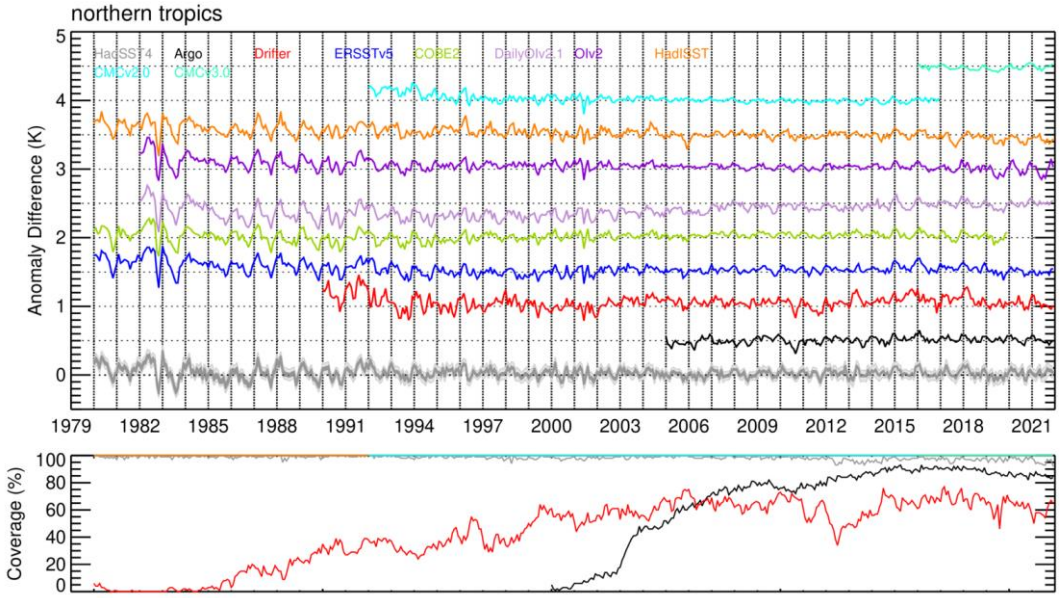

Figure 3-25. Regionally averaged SST anomalies (K, relative to the SST CCI v3.0 climatology 1991-2020) in the northern tropics, comparison data minus the SST CCI v3.0 Analysis (K). Difference timeseries are spaced by 0.5 K.

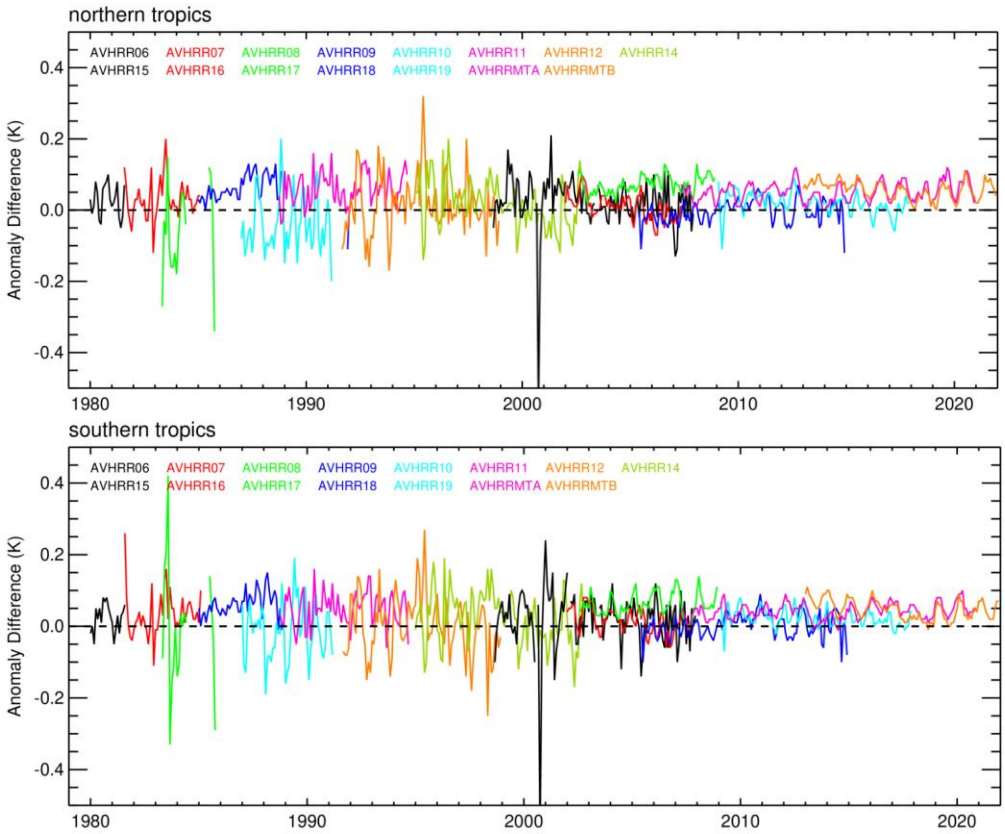

Figure 3-26. Regionally averaged SST anomalies (K, relative to the SST CCI v3.0 climatology 1991-2020): SST CCI v3.0 AVHRR data minus the SST CCI v3.0 Analysis (K) in the northern tropics (top) and the southern tropics (bottom).

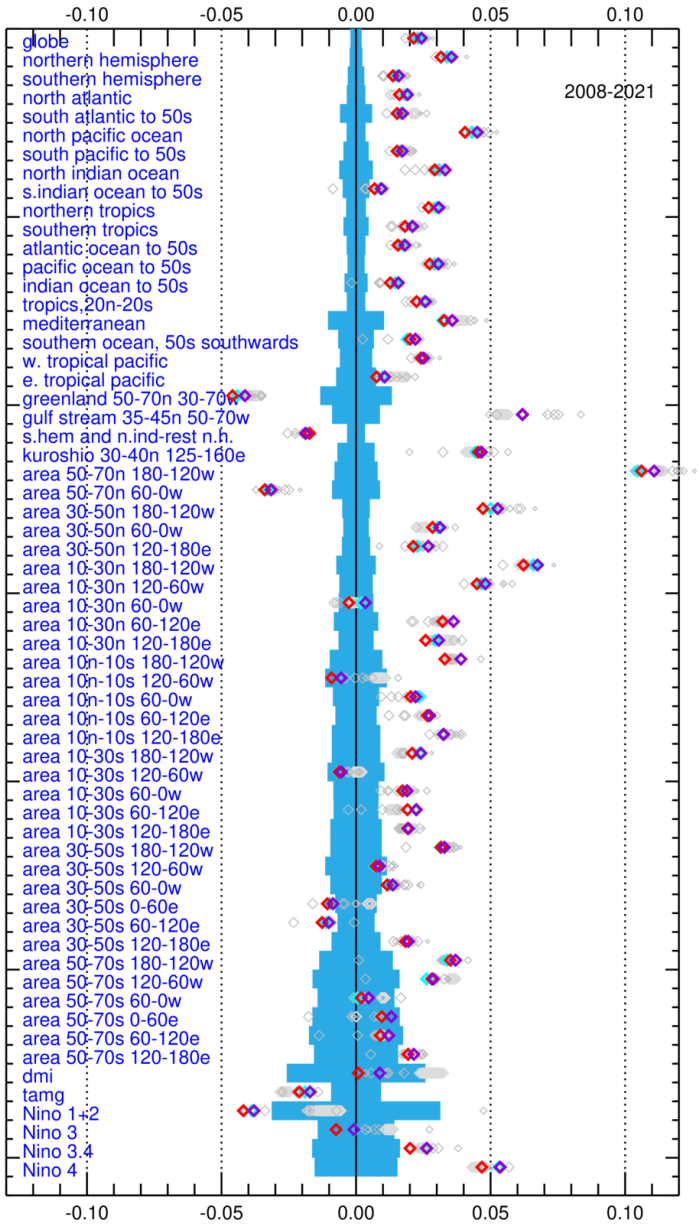

Figure 3-27. Linear trends (K/year) for the period 2008-2021 for all regions and indices used in the assessment for (red) the ATSR-MetopA-SLSTR composite, (purple) the Metop-AVHRR composite, (cyan) the SST CCI v3.0 Analysis and (grey) the available comparison data (DailyOI uses a smaller symbol, the HadSST4 100-member ensemble is lighter grey). The pale blue area is an estimate of the uncertainty in the trend arising from measurment and sampling errors in the HadSST4 dataset (which is based only on in situ observations), the spread is generally small for large area averages (e.g., global and hemispheric averages) or for well-sampled regions such as the North Atlantic.

3.4.5 SST CCI DATA - AMSR

Figure 3-9 shows that for globally averaged SST anomalies the SST CCI v3.0 AMSR data are in good agreement with the other SST CCI v3.0 datasets and the comparison data. Figure 3-10 highlights that AMSR can at times be warmer than the other SST CCI data in the global average by up to around a tenth kelvin, although still in agreement with the comparison data ensemble. This warmth is evident in both northern and southern hemispheres (Figure 3-11 and Figure 3-12), particularly for AMSR-E in the northern hemisphere which also lies outside the comparison data ensemble from around 2009-2010. For zonal average anomalies over the AMSR-E and AMSR2 periods (Figure 3-28) we see a similar pattern for both AMSR sensors, with generally good agreement with the comparison data and other SST CCI v3.0 data in the tropics and subtropics, and a relative warmth of the AMSR data versus the other SST CCI v3.0 data in the mid to high latitudes that brings the AMSR data into better agreement with the comparison data. This may reflect that the AMSR retrievals are a more direct regression to in situ data than for other SST CCI v3.0 sensors, such that closer broad agreement with the comparison data may be expected. However, these zonal averages can mask more interesting regional differences. Figure 3-29 and Figure 3-30 show maps of SST anomalies for AMSR-E and AMSR2 and the SST CCI v3.0 Analysis, and maps of differences between AMSR and other datasets relative to the Analysis, averaged over the AMSR-E and AMSR2 periods. (Note the missing data areas in AMSR-E and AMSR2 arising from data being masked to remove the impact of Radio Frequency Interference, in particular in the South Atlantic.) In terms of the large-scale patterns of climate variability, both AMSR-E and AMSR2 are broadly in agreement with the Analysis (Figure 3-29 and Figure 3-30, top rows). However, when considering differences from the Analysis we see similar patterns for both AMSR-E and AMSR2 (Figure 3-29 and Figure 3-30, middle row, left panels). In general, we see warmer AMSR anomalies in the high northern latitudes, parts of the extra-tropical North Pacific, the eastern tropical Pacific and Atlantic, the southeast Pacific, the eastern subtropical Atlantic, the southeast Indian Ocean, the Southern Ocean, in marginal seas (e.g., the Mediterranean region and the Labrador Sea and Hudson Bay regions) and at various near-coastal locations. We see cooler AMSR anomalies in the subtropical and mid-latitude North Atlantic and Gulf Stream, the tropical Indian Ocean, the western and central tropical Pacific, parts of the western subtropical South Atlantic and Indian Oceans and around the Agulhas Current. Regionally, the differences between AMSR and the Analysis can approach several tenths of a kelvin or more.

The differences seen between the SST CCI v2.1 ATSR and SST CCI v3.0 AVHRR data and the Analysis are much smaller in magnitude than for AMSR (Figure 3-29 and Figure 3-30, middle row, right panels) which is consistent with the zonal averages where we see the Analysis tending to track the ATSR and AVHRR data at these times (Figure 3-28). If we look at differences between in situ comparison data and the Analysis (Figure 3-29 and Figure 3-30, bottom row) we see that their agreement with the AMSR differences are mixed. Regions with better agreement include e.g., warm anomalies in the northern North Pacific, the eastern tropical Atlantic and parts of the Southern Ocean. Regions with worse agreement include e.g., cool anomalies in the tropics and North Atlantic. Also of note is worse agreement in many near-coastal regions where AMSR tends to be warmer by up to several tenths of a kelvin e.g., in the Mediterranean (particularly AMSR-E), along the western US coastline and along the western coastline of southern Africa. AMSR also tends to be warmer in the sea ice regions of the Southern Ocean, however a lack of in situ comparison data in these regions makes this difficult to assess. Sampling may be an issue in some locations because of the large (order 70 x 40 km) pixel size of microwave data relative to climatology when calculating AMSR anomalies, and because the microwave cannot be retrieved within approximately 75 km of coastline or sea ice. To address this, Figure 3-31 shows additional maps made of differences between AMSR and the SST CCI v3.0 Analysis at 1-degree resolution. These show that the 5-degree difference patterns (Figure 3-29 and Figure 3-30, middle left panels) are still fairly robust at 1-degree resolution which, although not ruling out sampling effects altogether,

highlights that these patterns are not strongly concentrated at smaller scales (see e.g., the western coastline of southern Africa) which might be expected for sampling artefacts.

Overall, this implies that, at multi-annual timescales, AMSR may perform better than the other SST CCI v3.0 data in certain problematic regions (notably the mid-latitudes), however this is not the case in all locations.

Another feature of interest in the SST CCI v3.0 AMSR data are seasonal anomalies relative to the other SST CCI v3.0 data. Figure 3-32 shows differences between the various SST CCI v3.0 data and the SST CCI v3.0 Analysis for the Northern and Southern hemispheres. The AMSR data display a broad annual cycle with a relative warmth in Spring / Summer and a relative coolness in Autumn / Winter of order a few tenths of a kelvin peak-to-peak magnitude. In Figure 3-32, differences are also apparent between the seasonal variability for AMSR-E and AMSR-2. In the Northern hemisphere AMSR-E has a less clearly defined annual variability than for AMSR-2, with AMSR-E showing a broader warm peak and perhaps evidence of a bi-annual cycle superimposed on the annual cycle. In the Southern hemisphere the AMSR-E annual cycle seems to grow over time whereas no annual cycle is apparent in the AMSR-2 data. When looking at equivalent regional timeseries for AMSR there is a general pattern of greater magnitude seasonal variability in the higher latitudes (though less apparent for AMSR2 in the Southern hemisphere, and with seasonal variability generally harder to discern in the Southern Ocean) and some evidence of bi-annual variability in the tropical regions. A few regional timeseries are shown in Figure 3-33. The top panel shows timeseries for the SST CCI v3.0 data relative to the SST CCI v3.0 Analysis in the mid-latitude North Atlantic. This shows results like that seen for the Northern hemisphere (Figure 3-32, top panel) but with a larger peak-to-peak magnitude of several tenths of a kelvin of the AMSR seasonal variability. The middle panel shows the same North Atlantic region but for the comparison data. Looking at the drifting buoy timeseries we see no evidence of seasonal variability comparable to AMSR which implies that this is a feature of the AMSR data. The bottom panel of Figure 3-33 shows regional timeseries for the SST CCI v3.0 data relative to the SST CCI v3.0 Analysis in the monsoon regions of the northern-most Indian Ocean and surrounds (the in situ data are not shown as the drifting buoy data are too noisy to resolve the AMSR seasonal variability). The AMSR shows a clear bi-annual cycle with relatively warmer peaks in Spring and Autumn when the ITCZ is passing overhead. The cause of this relative seasonal variability in AMSR is uncertain and may vary regionally. Possible factors are the impact of atmospheric contamination (e.g., precipitation and cloud) on the satellite retrievals and their coverage or seasonal changes in surface roughness (which affects surface emissivity).

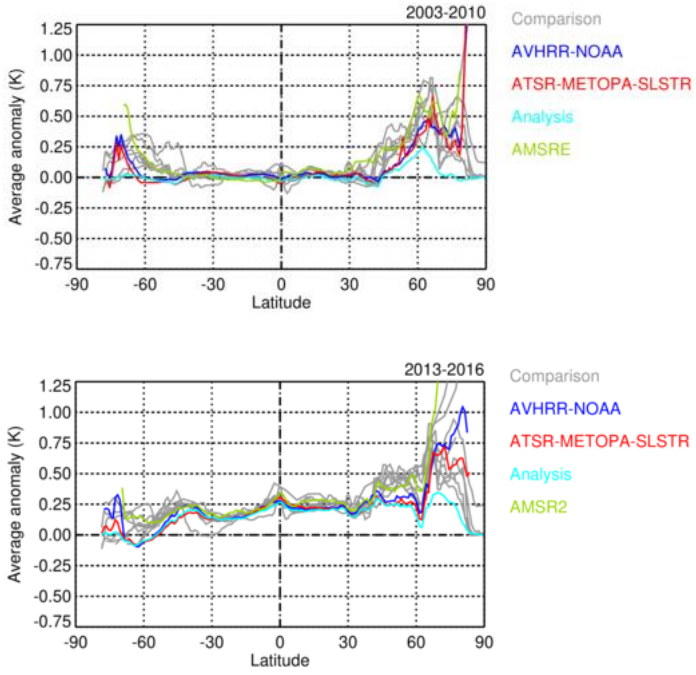

Figure 3-28. Zonally averaged SST anomalies (K, relative to the SST CCI v3.0 climatology 1991-2020) for SST CCI v3.0 composite data, Analysis and AMSR averaged over the periods 2003-2010 (for assessing AMSR-E) and 2013-2016 (for assessing AMSR-2).

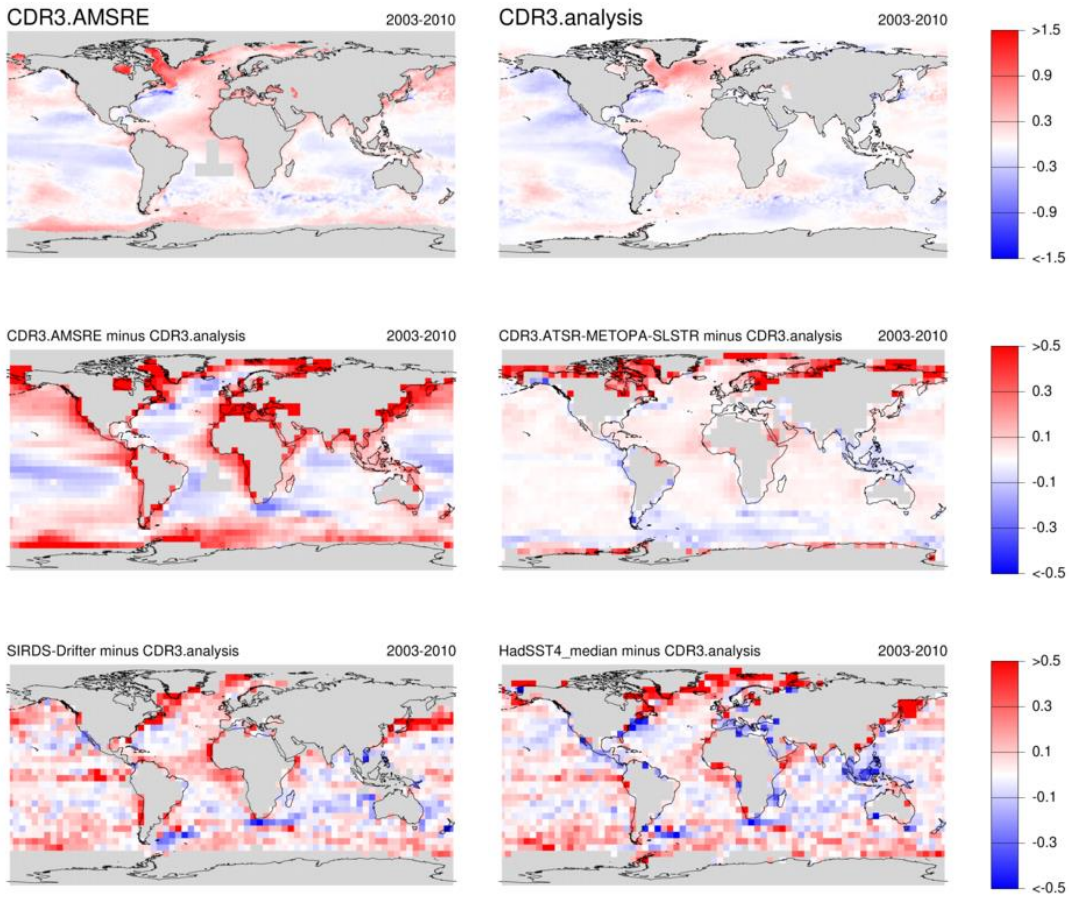

Figure 3-29. Maps of SST anomalies (K, relative to the SST CCI v3.0 climatology 1991-2020) averaged over 2003-2010 (for assessing AMSR-E). Global SST anomalies for SST CCI v3.0 AMSR-E and the SST CCI v3.0 Analysis (top row); AMSR-E, the ATSR-MetopA-SLSTR composite, drifting buoys and HadSST4 minus the SST CCI v3.0 Analysis (K) (middle and bottom rows). Missing data areas in AMSR-E arise from data being masked to remove the impact of Radio Frequency Interference (in particular the South Atlantic).

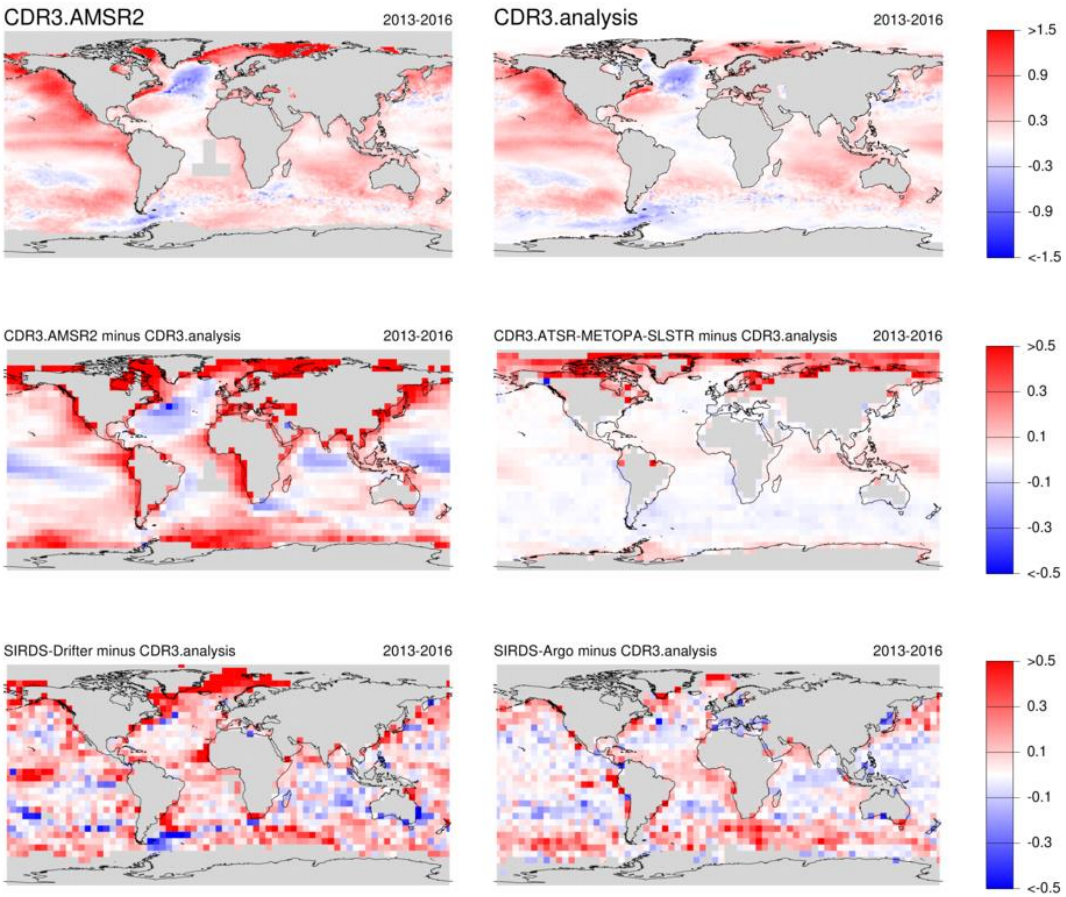

Figure 3-30. Maps of SST anomalies (K, relative to the SST CCI v3.0 climatology 1991-2020) averaged over 2013-2016 (for assessing AMSR-2). Global SST anomalies for SST CCI v3.0 AMSR-2 and the SST CCI v3.0 Analysis (top row); AMSR-2, the ATSR-MetopA-SLSTR composite, drifting buoys and Argo minus the SST CCI v3.0 Analysis (K) (middle and bottom rows). Missing data areas in AMSR-2 arise from data being masked to remove the impact of Radio Frequency Interference (in particular the South Atlantic).

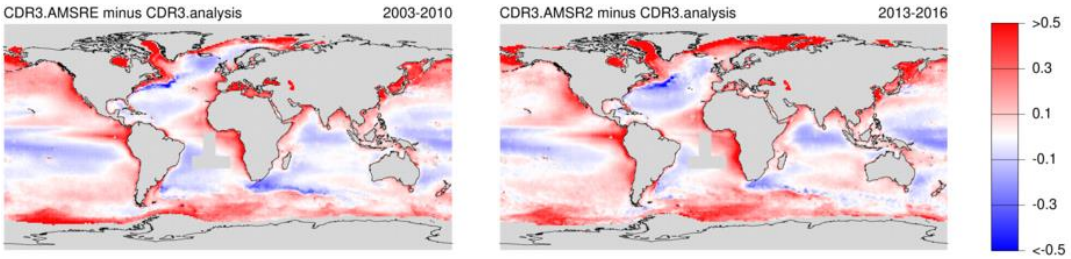

Figure 3-31. Maps of SST anomalies (K, relative to the SST CCI v3.0 climatology 1991-2020) averaged over 2003-2010 (for assessing AMSR-E) and 2013-2016 (for assessing AMSR-2) minus the SST CCI v3.0 Analysis (K) for data gridded at 1x1 degrees. Missing data areas in AMSR-E and AMSR-2 arise from data being masked to remove the impact of Radio Frequency Interference (in particular the South Atlantic).

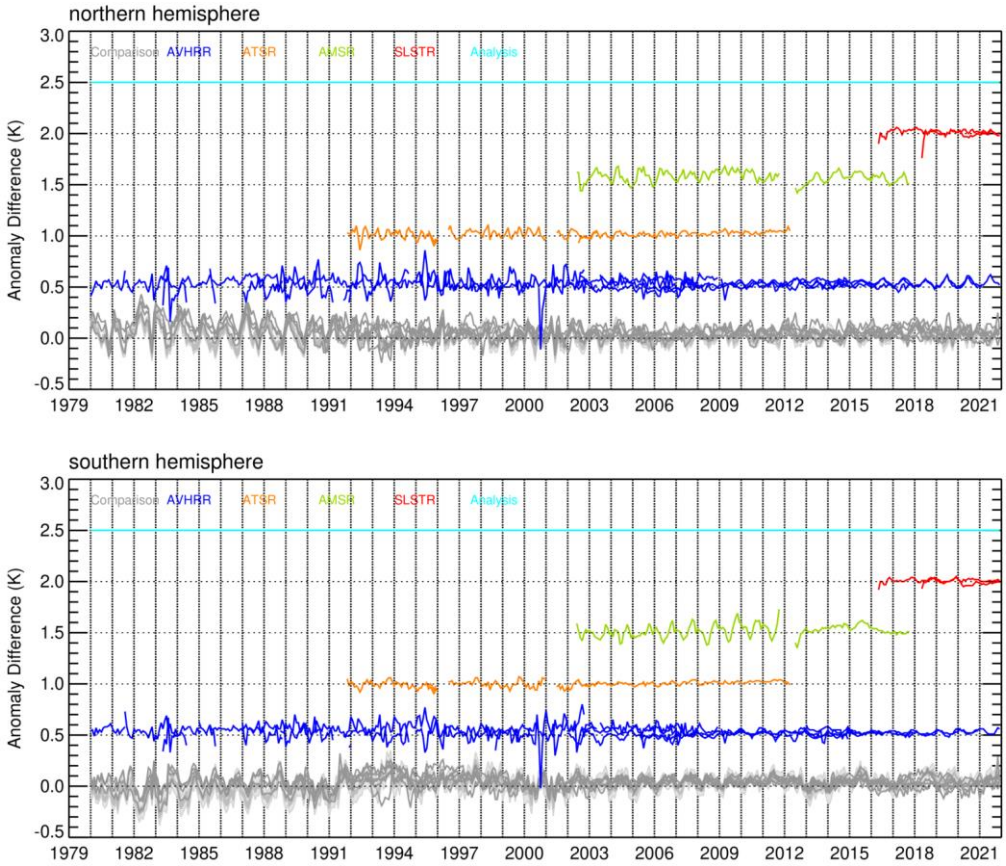

Figure 3-32. Regionally averaged SST anomalies (K, relative to the SST CCI v3.0 climatology 1991-2020): the SST CCI v3.0 data minus the SST CCI v3.0 Analysis (K) for the Northern Hemisphere (top) and Southern Hemisphere (bottom). Difference timeseries are spaced by 0.5 K.

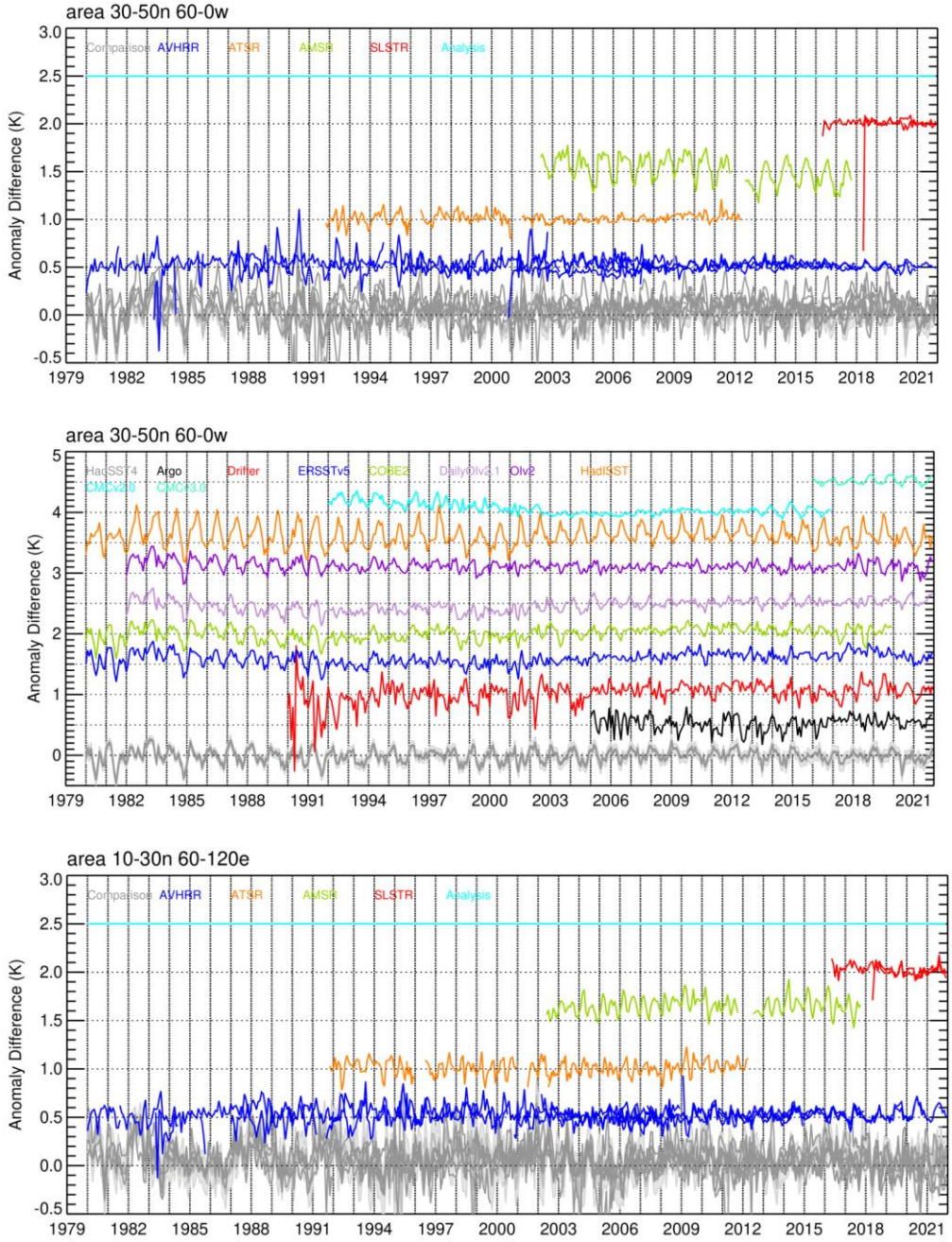

Figure 3-33. Regionally averaged SST anomalies (K, relative to the SST CCI v3.0 climatology 1991-2020): the SST CCI v3.0 data minus the SST CCI v3.0 Analysis (K) for the mid-latitude North Atlantic (top) and northern-most North Indian Ocean (bottom). The middle plot is equivalent to the top plot except showing the comparison data minus the SST CCI v3.0 Analysis. Difference timeseries are spaced by 0.5 K.

3.4.6 OTHER SST FEATURES OF INTEREST

We first consider agreement between the SST CCI v3.0 datasets and the comparison data for the climate indices presented in Section 3.3.3. For the Niño indices timeseries good agreement is seen between the SST CCI v3.0 datasets and the comparison data. Agreement between the AVHRR data and the Analysis and the comparison data is improved in the Niño regions for SST CCI version 3.0 versus version 2.1 due to better stability of the AVHRR data and fewer erroneous spikes (Figure 3-34, top), however these improvements are generally small relative to index variability. One notable exception is for the Niño 1+2 index in 1982-1983, where the version 3.0 SST anomalies are now in noticeably better agreement with the comparison data (Figure 3-34, middle). For Niño indices trends from 2008-2021 (Figure 3-27) we see that the Niño 1+2 and Niño 3 indices trends for the SST CCI v3.0 data appear lower than for many of the comparison data (both with and without colocation). A similar result is seen in other regions located in the eastern tropical Pacific (e.g., 10°N-10°S, 120°W-60°W). This is caused by a relative coolness of the SST CCI products beginning from around the mid-2010s and which gradually increases up to 2021 (this is evident in Figure 3-34 (middle) for the Niño 1+2 timeseries). However, the uncertainty in the in situ trends due to measurement and sampling errors is comparable to the differences seen with the SST CCI data (Figure 3-27, blue bars), and closer inspection of the comparison data timeseries (not shown) suggest that the Argo data timeseries (although noisy) tend to more closely track the SST CCI data, together implying that the difference in SST CCI trends may in part be due to errors in the comparison data. Some evidence of lower SST CCI trends in these regions is also seen from 1991-2021 (Figure 3-40), albeit less so due to the longer assessment period and (on inspection) a tendency for SST CCI products to be slightly relatively cooler at times in the 1990s and 2000s as well. For the Tropical Atlantic Meridional SST Gradient index (TAMG), agreement with the comparison data is also improved for SST CCI v3.0 due to the removal of periodic cool biases in the AVHRR data caused by aerosols in the index's northern pole (Figure 3-34, bottom). The Dipole Mode Index (DMI) also shows modest improvement for version 3.0 (not shown) due to fewer erroneous spikes in the SST CCI v3.0 AVHRR data. As for the Niño indices the improvements in DMI are modest relative to index variability, though the improvements in the TAMG are more noticeable, particularly in the mid-late 1990s.

Figure 3-35 (top) shows SST anomalies in the tropics for the SST CCI v3.0 and v2.1 products and the comparison data. As already noted in Section 3.4.2 and Section 3.4.3, the SST CCI v3.0 AVHRR and Analysis data show improved stability and fewer spikes versus v2.1, notably from 1982-1983. Of additional note in the tropics is a relative coolness in the SST CCI products for several months following the eruption of Mt. Pinatubo in June 1991. The SST CCI AVHRR and Analysis products appear biased cool at this time due to the effects of volcanic atmospheric aerosols on the retrievals. Although this bias has been reduced for the SST CCI v3.0 products, a residual cool bias of a few tenths of a kelvin still remains in the tropics for the latter half of 1991.

In the precursor assessment of the SST CCI v2.1 products [SST CCI CAR, 2019], it was observed that in the Gulf Stream region the products displayed a warmth relative to the comparison data prior to the early 2000s. This still appears to be the case for the v3.0 products and the latest comparison data (Figure 3-35, bottom), though the CMC comparison data are warmest in the 1990s.

This earlier assessment also noted that in the Southern Ocean the SST CCI v2.1 products lay at the cool end of the comparison data ensemble from around 1992-onwards. Figure 3-36 shows that for the version 3.0 data some improvements have been made in this region with some AVHRR sensors (notably AVHRR12 and 14 in the 1990s) becoming warmer (upper middle panel), however a relative coolness is still apparent (lower middle panel) and seems to occur in most sectors of the Southern Ocean (bottom panel). Uncertainty and lack of coverage in the comparison datasets make this a difficult region to assess although these results are seen with and without co-location to the

HadSST4 data. This coolness in the Southern Ocean from around 1992-onwards (and the better agreement of AVHRR in the 1980s) is consistent with the decadal zonal average patterns discussed earlier in Section 3.4.2. In the decadal zonal average for 1982-1991 (Figure 3-15) we also see that the Analysis diverges from the AVHRR and the comparison data in the Southern Ocean, becoming relatively cooler by a tenth kelvin or more. This is not evident in Figure 3-36 (lower middle panel), however it is clearly seen in the equivalent plot without sea ice masking applied (not shown), implying that the Analysis SSTs in its sea ice regions are notably cooler than the other comparison products at this time.

One further region of interest is the Mediterranean, which trends show is one of the fastest warming analysed regions from 1980-2021 (Figure 3-38), but which has also seen some of the largest changes in trends from v2.1 to v3.0 for the Analysis and AVHRR products (Figure 3-39) and also has a relatively large difference in trends for the v3.0 Analysis versus the ATSR-MetopA-SLSTR composite as compared with other regions (Figure 3-40) (robust trends, not shown, display similar results). Figure 3-37 (top) emphasises that SST anomalies for the SST CCI v3.0 and comparison data are broadly in agreement in terms of the climate variability observed in the Mediterranean over time. However, if we consider differences relative to the SST CCI v3.0 Analysis (Figure 3-37, middle) we see that monthly differences with the comparison data can be several tenths of a kelvin, monthly differences with the ATSR v2.1 and AVHRR v3.0 data can be a few tenths of a kelvin or more (particularly prior to the mid-2000s), and that AMSR v3.0 data is persistently warm by several tenths of a kelvin in this region (particularly AMSR-E). Of note is the relative warming of the AVHRR and Analysis data from v2.1 to v3.0 by a few tenths of a kelvin or more (particularly prior to the mid-2000s) due to the improved handling of dust aerosol effects in v3.0 (Figure 3-16) which results in the lower trend seen for the v3.0 products. For 12-month moving averages (Figure 3-37, bottom) we see that several comparison datasets (HadSST4, ERSSTv5, COBE-SST2 and DailyOIv2.1) are persistently and increasingly cool in earlier decades relative to the SST CCI v3.0 products, resulting in greater warming trends in these comparison data, whilst a relative coolness of the ATSR1 and ATSR2 data versus AVHRR (and also a slight warmth of SLSTR-A versus AVHRR) results in the greater warming trends seen for the ATSR-MetopA-SLSTR composite versus the Analysis (which tends to lie between the ATSR and AVHRR data). The Analysis stability is relatively unaffected by the introduction of warm AMSR data, likely due to the relatively low volumes of AMSR data versus other sensors.

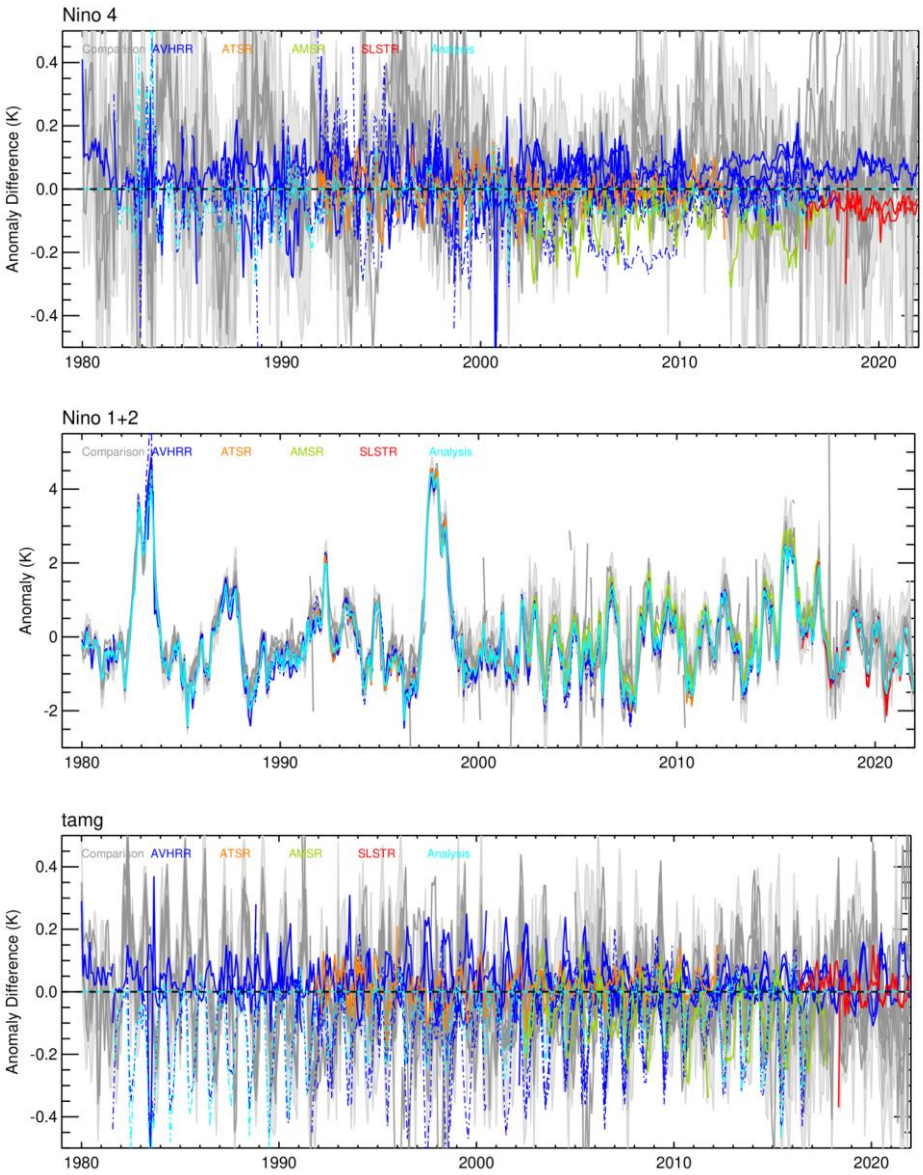

Figure 3-34. Regionally averaged SST anomaly timeseries (K, relative to the SST CCI v3.0 climatology 1991-2020) of interest: (top) SST CCI v3.0 data, SST CCI v2.1 data and the comparison data minus the SST CCI v3.0 Analysis for the Niño 4 index; (middle) SST CCI v3.0 data and comparison data anomaly timeseries for the Niño 1+2 index; (bottom) as for top except for the TAMG index.

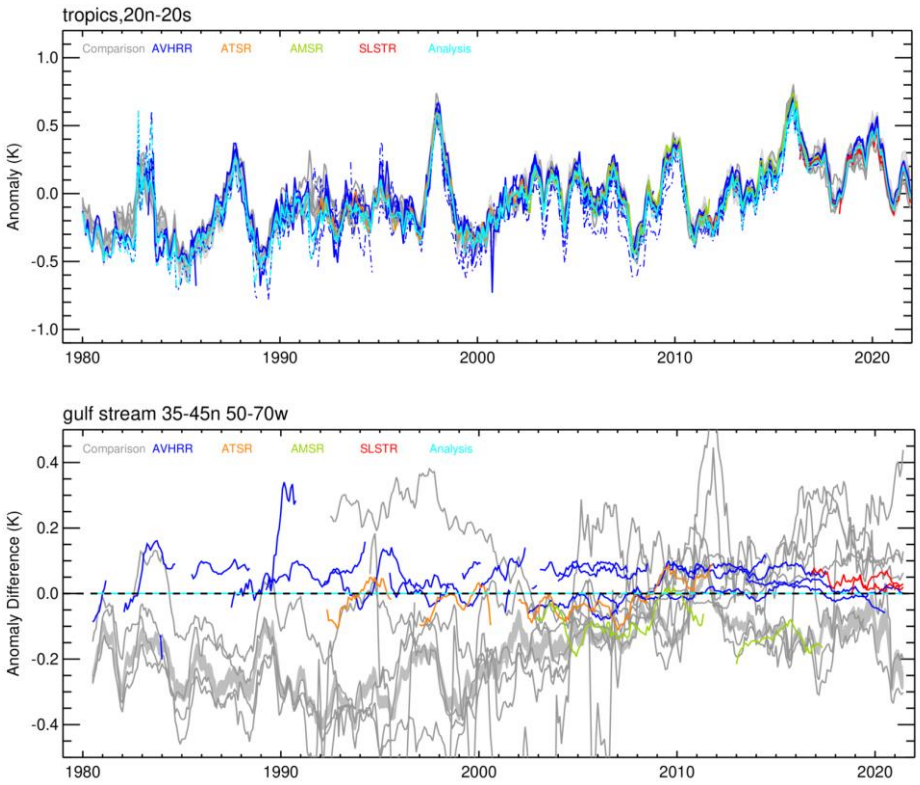

Figure 3-35. Regionally averaged SST anomaly timeseries (K, relative to the SST CCI v3.0 climatology 1991-2020) of interest: (top) SST CCI v3.0 data, SST CCI v2.1 data (dashed) and comparison data timeseries for the tropics; (bottom) SST CCI v3.0 data and comparison data minus the SST CCI v3.0 Analysis with a 12-month moving average applied for the Gulf Stream region.

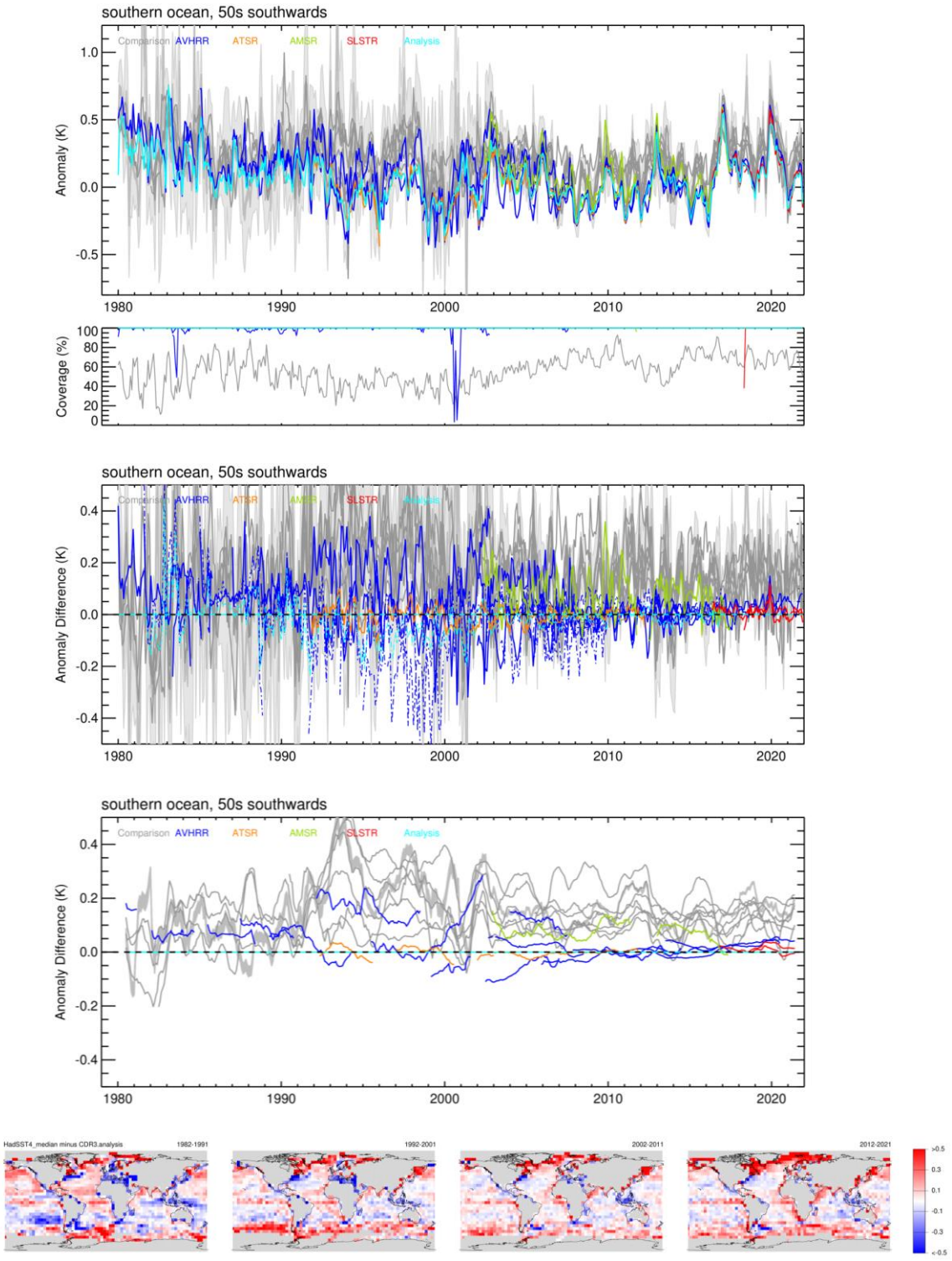

Figure 3-36. Southern Ocean SST anomalies (K, relative to the SST CCI v3.0 climatology 1991-2020): (top) SST anomalies for the SST CCI v3.0 and comparison data; (upper middle) the SST CCI v3.0 data, SST CCI v2.1 data (dashed) and comparison data minus the SST CCI v3.0 Analysis (K); (lower middle) the SST CCI v3.0 data and comparison data minus the SST CCI v3.0 Analysis (K) with a 12-month moving average applied; (bottom) Maps of decadal average SST anomalies: HadSST4 minus the SST CCI v3.0 Analysis (K).

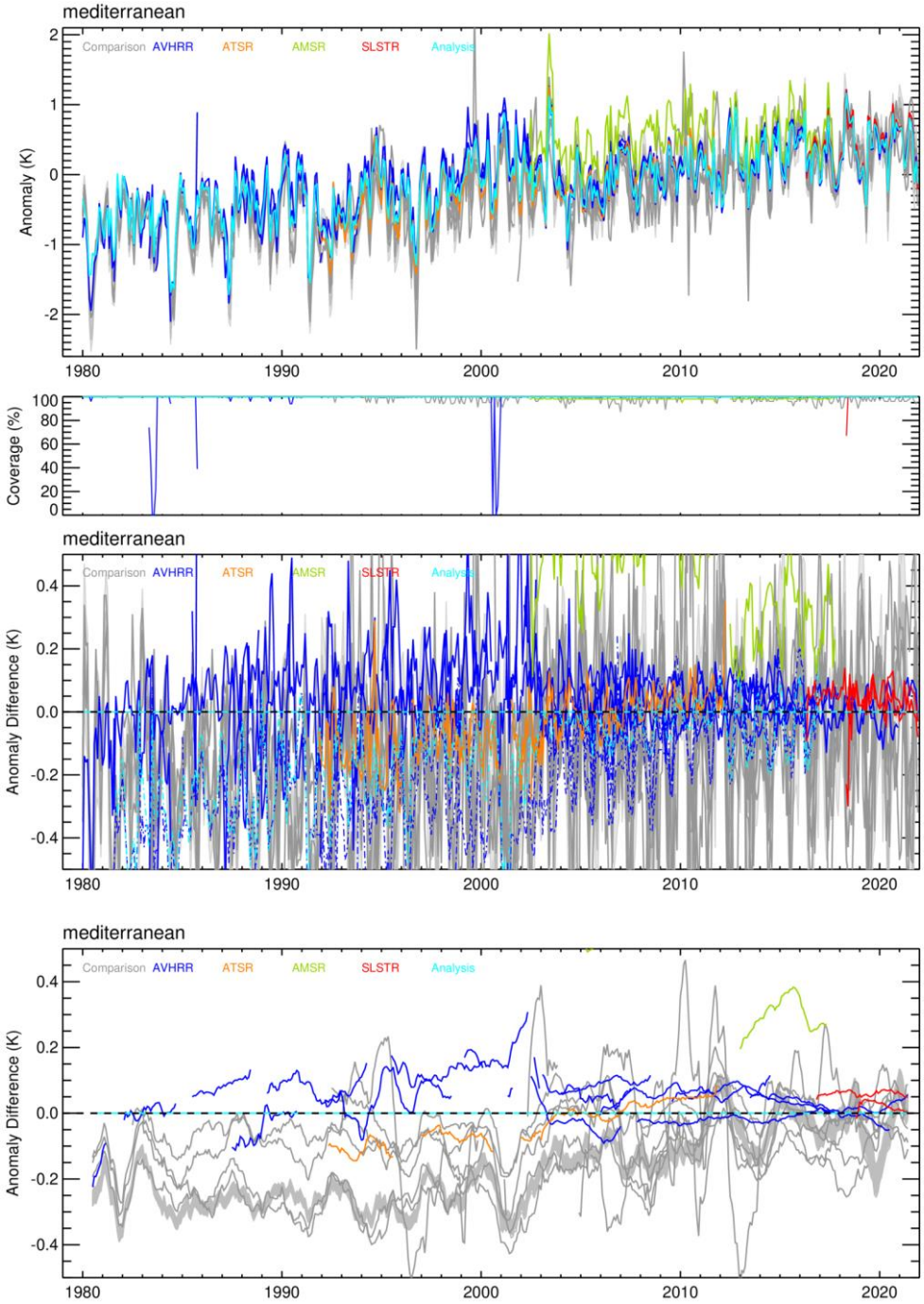

Figure 3-37. Mediterranean SST anomaly timeseries (K, relative to the SST CCI v3.0 climatology 1991-2020): (top) SST anomalies for the SST CCI v3.0 and comparison data; (middle) the SST CCI v3.0 data, SST CCI v2.1 data (dashed) and comparison data minus the SST CCI v3.0 Analysis (K); (bottom) the SST CCI v3.0 and comparison data minus the SST CCI v3.0 Analysis (K) with a 12-month moving average applied (the noisy comparison data from 1995-onwards is from drifters which have low coverage in this region).

3.4.7 TRENDS

Figure 3-38 shows trends for 1980-2021, which covers the full period of the SST CCI v3.0 data (except for a small amount of AVHRR data in 1979). Only the SST CCI v3.0 Analysis can be assessed over this period (as separate composites are used for NOAA-AVHRR and Metop-AVHRR) and it is compared with all available comparison datasets. In general, the trends for 1980-2021 for the SST CCI v3.0 Analysis are in good agreement with the comparison datasets in most regions and as expected show a general warming over time (the Southern Ocean is a notable exception showing no clear trend over this period). In most regions the spread of trends is within 0.01 K per year (equivalent to 0.1 K per decade) which is comparable to the GCOS stability requirement of 0.1 K per decade [GCOS, 2022]. It is emphasised that this is an intercomparison and not a formal validation of dataset stability. The lack of long-term stable reference data away from the tropical moored buoy arrays makes the assessment of global stability challenging (e.g., Merchant et al. 2012; Fiedler et al. 2019). However, the spread of the various products to within GCOS requirements is reassuring given the varying methods and combinations of satellite and in situ data used in their construction. One area of note is the Gulf Stream where trends are lower than the comparison datasets; this is attributable to the relative warmth of the SST CCI v3.0 products prior to the early 2000s in this region (Figure 3-34, bottom). Trends in the Mediterranean, which also show interesting differences, are discussed in more detail in Section 3.4.6.

Figure 3-39 shows trends for 1982-2016 which covers the period of the SST CCI v2.1 data and allows the version 3.0 and version 2.1 Analysis and AVHRR data to be compared. As seen for the 1980-2021 period, the trends for the SST CCI v3.0 data and the available comparison data compare well, showing the expected general warming over time. Again, the spread of trends is broadly comparable to the GCOS stability requirement. The trend for the southern hemisphere lies towards the lower end of the comparison data and the trend for the northern hemisphere lies towards the upper end, which is consistent with relatively cooler AVHRR data in the 1980s in the northern hemisphere (Figure 3-11) and relatively warmer AVHRR data in the 1980s in the southern hemisphere (Figure 3-12), coupled with a slight relative coolness of the SST CCI v3.0 products in both hemispheres in later decades. There is generally little difference between the trends for the version 3.0 and 2.1 data, which is unsurprising given the main decadal change from version 2.1 to 3.0 over this period is the removal of cool biases in the AVHRR data in the tropical North Atlantic which occurs for all decades (Figure 3-16) (also noting that the ATSR has not been updated for v3.0 and that the Analysis is not seen to adjust towards the newly added AMSR data). Warming of the AVHRR data in the Southern Ocean in the mid-late 1990s for v3.0 (Figure 3-15) has not discernibly affected the trends relative to v2.0, presumably because this lies towards the centre of the 1982-2016 trend period. Also of note for the 1982-2016 period is an increase of the version 3.0 trend in the Niño 1+2 index, which likely is in part due to the removal of large warm spikes during 1982-1983 (and consequently is less evident in robust trends, not shown).

Figure 3-40 shows trends for 1992-2021 which covers the ATSR1-SLSTR period. Again, we see that the trends compare well with the available comparison data and show the expected general warming trend over time. The trends for the SST CCI v3.0 ATSR-MetopA-SLSTR composite and the Analysis tend towards the upper end of the comparison data in the southern hemisphere (notably in the Southern Ocean) which is perhaps surprising given this was not evident for the AATSR-MetopA-SLSTR composite trends over the period 2008-2021 (Figure 3-27) and which tended to be lower than equivalent trends for Metop-AVHRR (see Section 3.4.4). This increase in trends over the longer 1992-2021 period is likely attributable to a coolness of the ATSR data in these regions in the 1990s as discussed in Section 3.4.2 (see also Figure 3-15) and in Section 3.4.3 (see also Figure 3-19, middle and bottom panels).

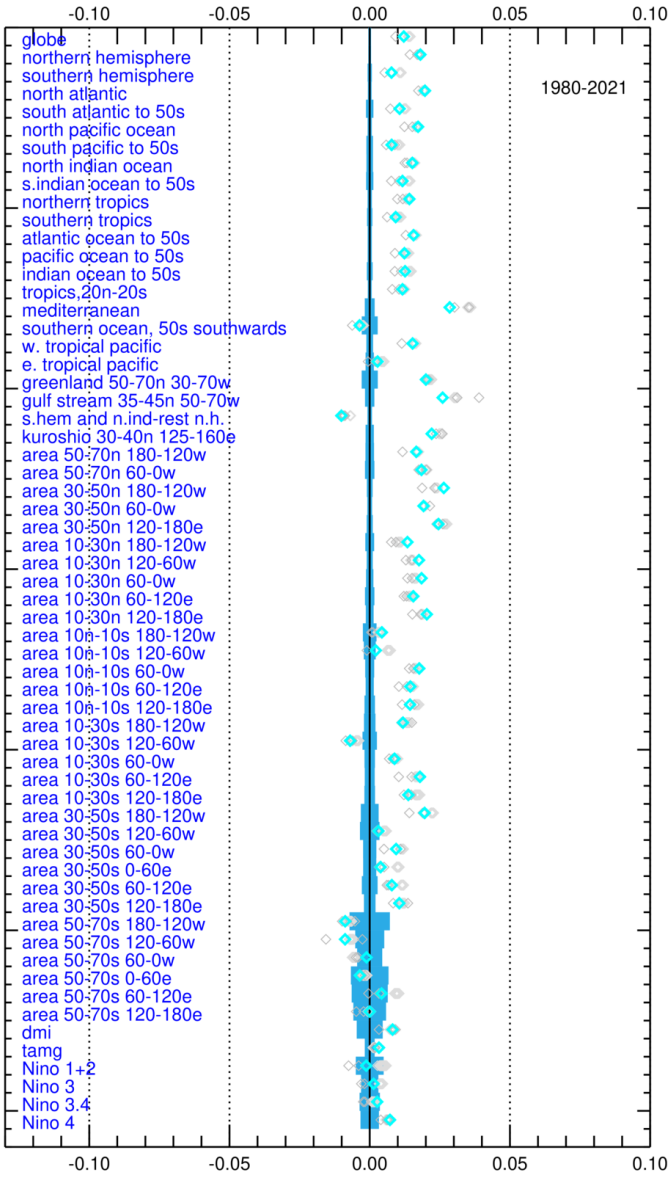

Figure 3-38. Linear trends (K/year) for the period 1980-2021 for all regions and indices used in the assessment for (cyan) the SST CCI v3.0 Analysis and (grey) the available comparison data (the HadSST4 100-member ensemble is lighter grey). The pale blue area is an estimate of the uncertainty in the trend arising from measurement and sampling errors in the HadSST4 dataset (which is based only on in situ observations), the spread is generally small for large area averages (e.g., global and hemispheric averages) or for well-sampled regions such as the North Atlantic.

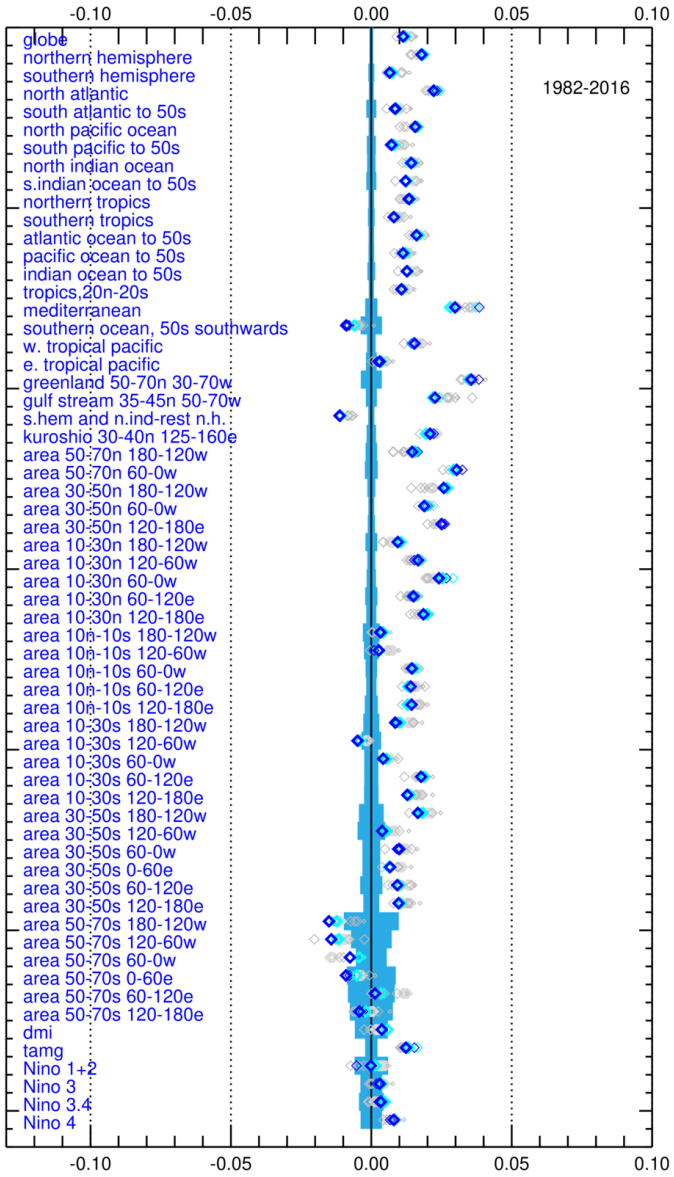

Figure 3-39. Linear trends (K/year) for the period 1982-2016 for all regions and indices used in the assessment for (blue) the SST CCI v3.0 NOAA-AVHRR composite, (cyan) the SST CCI v3.0 Analysis and (grey) the available comparison data (DailyOI uses a smaller symbol, the HadSST4 100-member ensemble is lighter grey). Trends for the SST CCI v2.1 data are also plotted as smaller coloured symbols. The pale blue area is an estimate of the uncertainty in the trend arising from measurement and sampling errors in the HadSST4 dataset (which is based only on in situ observations), the spread is generally small for large area averages (e.g., global and hemispheric averages) or for well-sampled regions such as the North Atlantic.

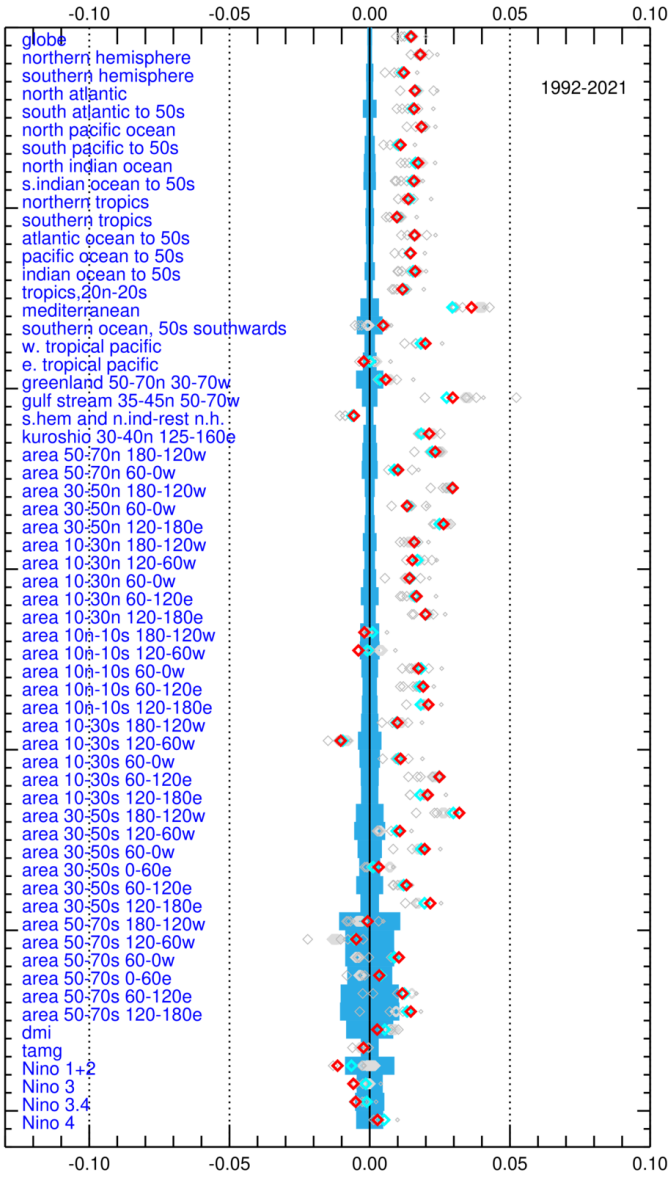

Figure 3-40. Linear trends (K/year) for the period 1992-2021 for all regions and indices used in the assessment for (red) the ATSR-MetopA-SLSTR composite, (cyan) the SST CCI v3.0 Analysis and (grey) the available comparison data (DailyOI uses a smaller symbol, the HadSST4 100-member ensemble is lighter grey). The pale blue area is an estimate of the uncertainty in the trend arising from measurement and sampling errors in the HadSST4 dataset (which is based only on in situ observations), the spread is generally small for large area averages (e.g., global and hemispheric averages) or for well-sampled regions such as the North Atlantic.

3.4.8 DECADAL AVERAGES

Figure 3-41 shows decadal average anomalies for the SST CCI v3.0 data and the comparison data. This shows that the patterns of interannual-to-decadal climate variability captured by the decadal averages are in broad agreement for all datasets (as also evident in the zonal average anomalies shown in Figure 3-15). It emphasises that the climate variability at these timescales is well resolved and that the relative differences between the datasets that have been discussed in previous sections are generally smaller than the climate signal itself. The most striking differences between the datasets shown in Figure 3-41 are at the mesoscales due to the differing methods used for assimilating and interpolating observations and representing SST gradients, and in the Arctic where different approaches to estimating sea ice concentration and in-ice SSTs can lead to large anomalies where warm water is exposed as the sea ice fluctuates and retreats over time.

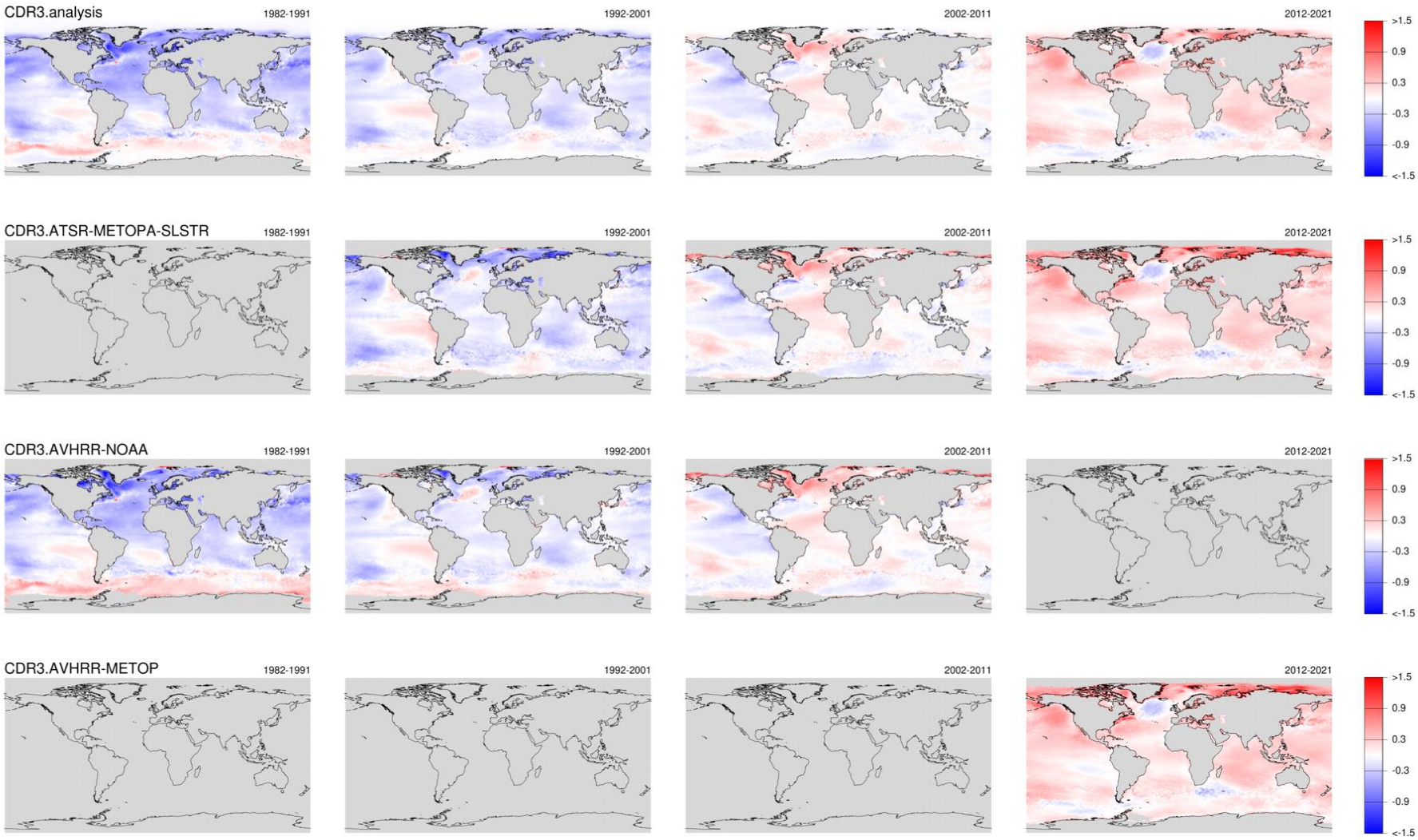
CDR3.analysis
1982-1991
1992-2001
2002-2011
2012-2021
CDR3.ATSR-METOPA-SLSTR
1982-1991
1992-2001
2002-2011
2012-2021
CDR3.AVHRR-NOAA
1982-1991
1992-2001
2002-2011
2012-2021
CDR3.AVHRR-METOP
1982-1991
1992-2001
2002-2011
2012-2021
>1.5
0.9
0.3
-0.3
-0.9
<-1.5

sst cci

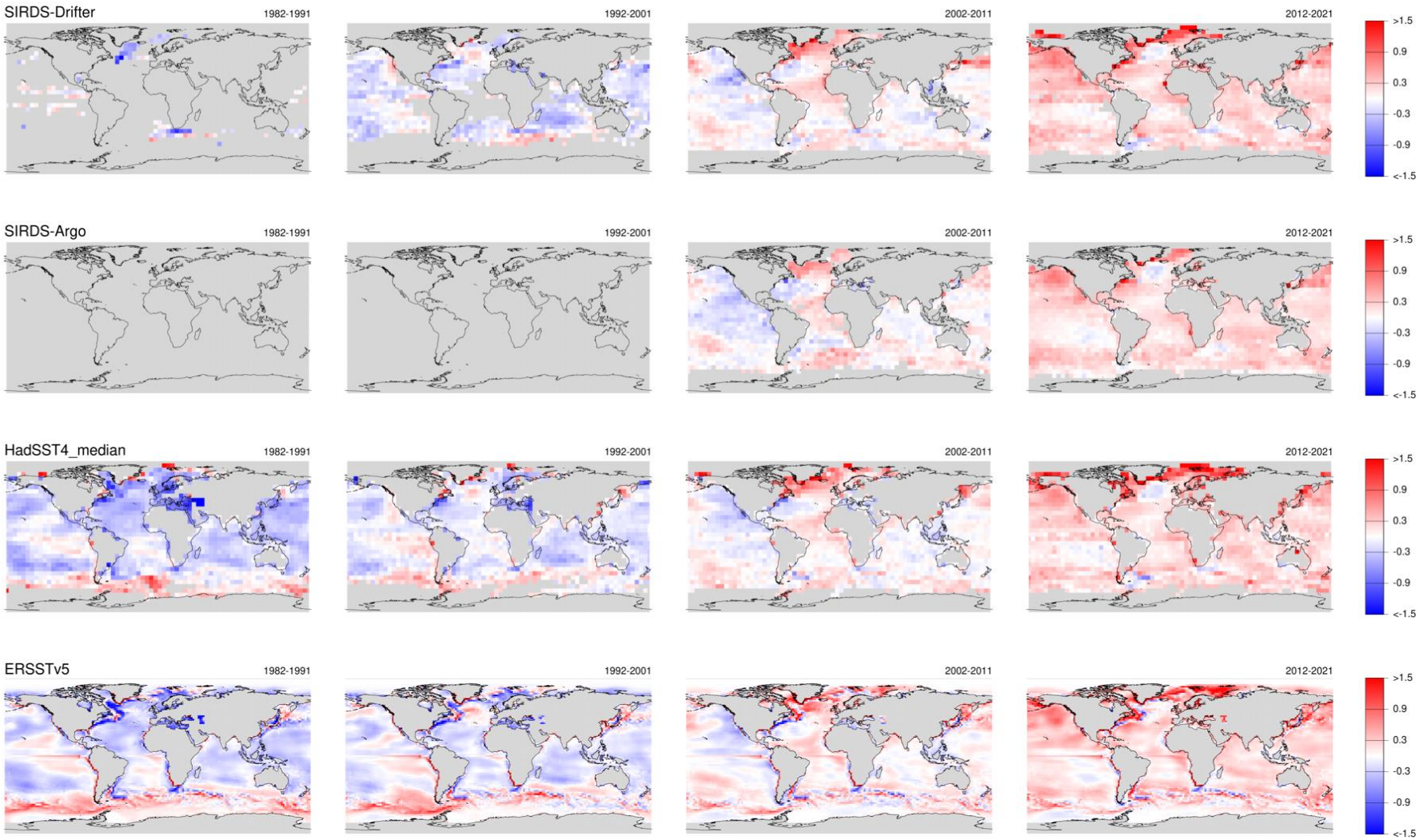
SIRDS-Drifter
1982-1991
1992-2001
2002-2011
2012-2021
SIRDS-Argo
1982-1991
1992-2001
2002-2011
2012-2021
HadSST4_median
1982-1991
1992-2001
2002-2011
2012-2021
ERSSTv5
1982-1991
1992-2001
2002-2011
2012-2021
>1.5
0.9
0.3
-0.3
-0.9
<-1.5

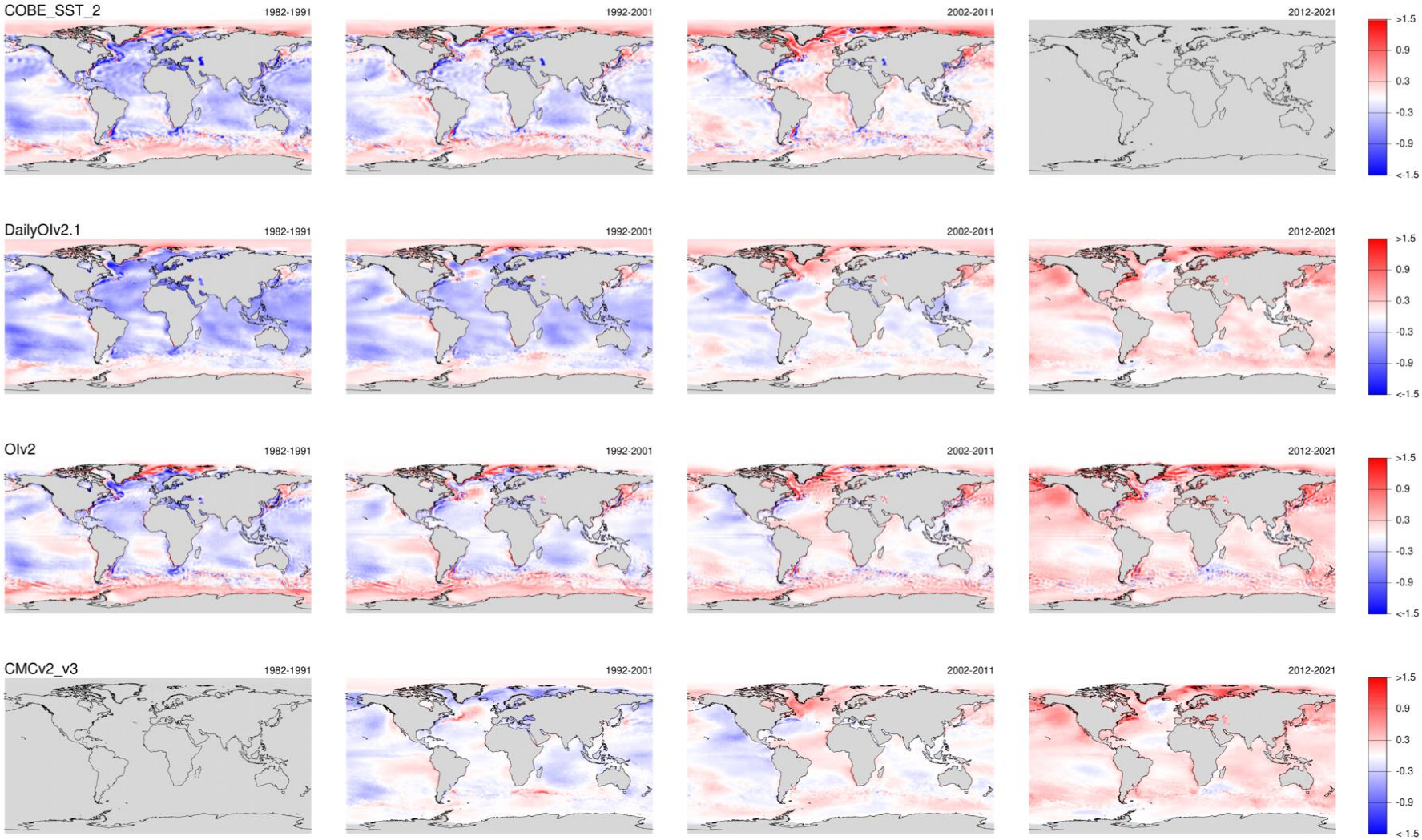
COBE_SST_2
1982-1991
1992-2001
2002-2011
2012-2021
DailyOIv2.1
1982-1991
1992-2001
2002-2011
2012-2021
OIv2
1982-1991
1992-2001
2002-2011
2012-2021
CMCv2_v3
1982-1991
1992-2001
2002-2011
2012-2021
>1.5
0.9
0.3
-0.3
-0.9
<-1.5

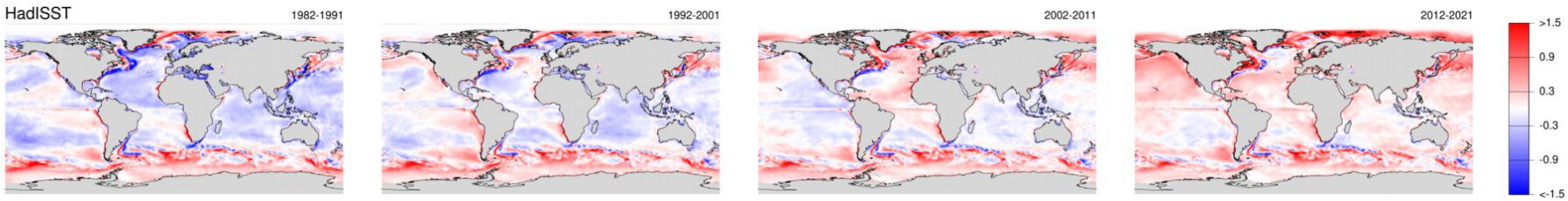

Figure 3-41. Decadal average SST anomalies (K, relative to the SST CCI v3.0 climatology 1991-2020) for the SST CCI v3.0 data and comparison data. Anomalies are only calculated where a dataset has complete time coverage over a decade and at each grid cell where at least 30% of months have a valid SST. All datasets are gridded to 1 degree except for drifter, Argo and HadSST4 which are gridded to 5 degrees.

This Page Is Intentionally Blank

4. USER CASE STUDY: PRODUCTION AND ANALYSIS OF HADISST.2.4.0.0

4.1 Background

The Met Office Hadley Centre sea Ice and Sea-Surface Temperature (HadISST) data set has been extensively used in climate science over many years. This is in large part because it provides a global picture of sea-surface temperature (SST) and sea ice conditions since the mid-nineteenth century. In order to achieve this global view back to the mid-nineteenth century, statistical interpolation techniques have been employed to fill in an estimate of variability between and consistent with the available measurements made *in situ*, largely by Voluntary Observing Ships. HadISST2.1 and 2.2, used in ERA5, ERA-20C and CERA20C used Phase 1 SST CCI AVHRR retrievals for the period 1996-2010.

High quality satellite data are essential to provide an improved understanding of variability globally to:

i. better inform interpolation of early data;
ii. reduce uncertainty in appropriate bias corrections to apply to ship measurements; and
iii. better explain currently unexplained differences between key century-scale analyses used in many applications in climate science.

In HadISST version 2.4.0.0 produced in this User Case Study, SST CCI v3.0 data for AVHRR, ATSR and SLSTR have been used to produce a new reconstruction back to January 1850.

4.2 Brief overview of the method

Kennedy et al. (2024, in prep) documents the data set construction process. We provide a brief overview here. The available measurements are used in a multi-step ensemble reconstruction which builds up a complete picture of SST variability in every month since 1850.

The multi-step reconstruction allows the different components of the observing system to be used according to their strengths and provides more consistent variability through time. The SST CCI data with its relatively small biases and high resolution extending over 40 years is an excellent complement to the longer but sparser *in situ* record.

HadISST.2.4.0.0 is presented as a 20-member ensemble. This allows exploration of the combined uncertainty arising from both bias correction of the *in situ* data, and the reconstruction. The *in situ* data are first drawn from the 200-member HadSST.4.0.1.0 ensemble (Kennedy et al., 2019). Satellite data are then adjusted to align them fully with HadSST.4.0.1.0 before *in situ* and satellite data are combined on a monthly, 1 degree latitude by 1 degree longitude grid to create an *in situ*/satellite observations blend. In practice, the v3.0 SST CCI data require very little, if any, adjustment.

An initial reconstruction was performed at low resolution (monthly average, 5 degree latitude by 5 degree longitude) using only the *in situ* data. This gives an initial estimate of the covariance patterns used in the large-scale reconstruction and the full uncertainty model is used to estimate the principal component series. These are then regressed against the combined *in situ* and satellite data to produce higher-resolution covariance patterns.

The large-scale reconstruction is subtracted from the gridded 1 degree latitude by 1 degree longitude observations before the local optimal interpolation is performed. The SST CCI v3.0 data are used to estimate a non-stationary covariance kernel for the second step of the reconstruction which uses a local optimal interpolation scheme to reconstruct mid-scale variability (features down to 1° resolution). Samples are drawn from this mid-scale reconstruction. This ensures realistic variability in regions that are sparsely observed or completely unobserved. The mid-scale sample is combined with the large and best-guess mid-scale reconstructions and the marginal ice zone temperature is added.

This multi-step approach results in consistent autocorrelation throughout almost the whole record. This indicates that the fields are neither overly smooth nor overly noisy.

4.3 Results

Here we focus on comparisons between HadISST.2.4.0.0 and SST CCI v3.0, together with the other comparison data sets used in Section 3 of this Climate Assessment Report, over the common data period 1980-2021.

Kennedy et al. (2024, in prep) explores HadISST.2.4.0.0 further over the full period, 1850-2021, but the global mean SST anomaly is compared to HadSST.4.0.1.0 in Figure 4-1. This comparison is undertaken with and without colocation, which illustrates the effect of geographical sampling of the available *in situ* measurements on the resultant global average. All 20 ensemble members are shown in each case.

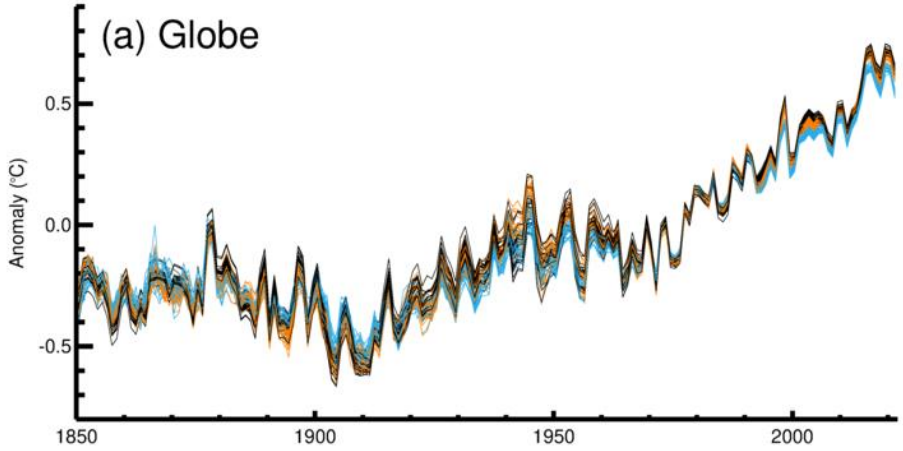

Figure 4-1. Global annual average SST anomaly (°C, relative to 1961-90) in HadISST.2.4.0.0 (full global average, blue), HadISST.2.4.0.0 (average of data colocated with HadSST.4.0.1.0, orange) and HadSST.4.0.1.0 (black). Taken from Kennedy et al. (2024, in prep).

It is clear that, despite the addition of the SST CCI v3.0 data in HadISST.2.4.0.0, the collocated global average still aligns well with the HadSST.4.0.1.0 average. The ensemble spreads identify times when either the bias corrections applied to the *in situ* data and/or the HadISST.2.4.0.0 reconstruction are less certain.

Focusing now on the period 1980-2021, we explore the global and hemispheric averages in more detail. Figure 4-2 compares the full monthly global average SST anomalies in HadISST.2.4.0.0, the SST CCI v3.0 Analysis and the other comparison data used in Section 3 of this report. We choose to explore the non-colocated, non-sea-ice-masked comparison because this is the truest test of the similarity of HadISST.2.4.0.0 and the SST CCI v3.0 Analysis, but this will affect the comparison with other data sets compared to the other sections in this report. The two anomaly time series align very closely and the bottom panel of Figure 4-2 (red curve) demonstrates that they lie within 0.05 K of each other in nearly every month.

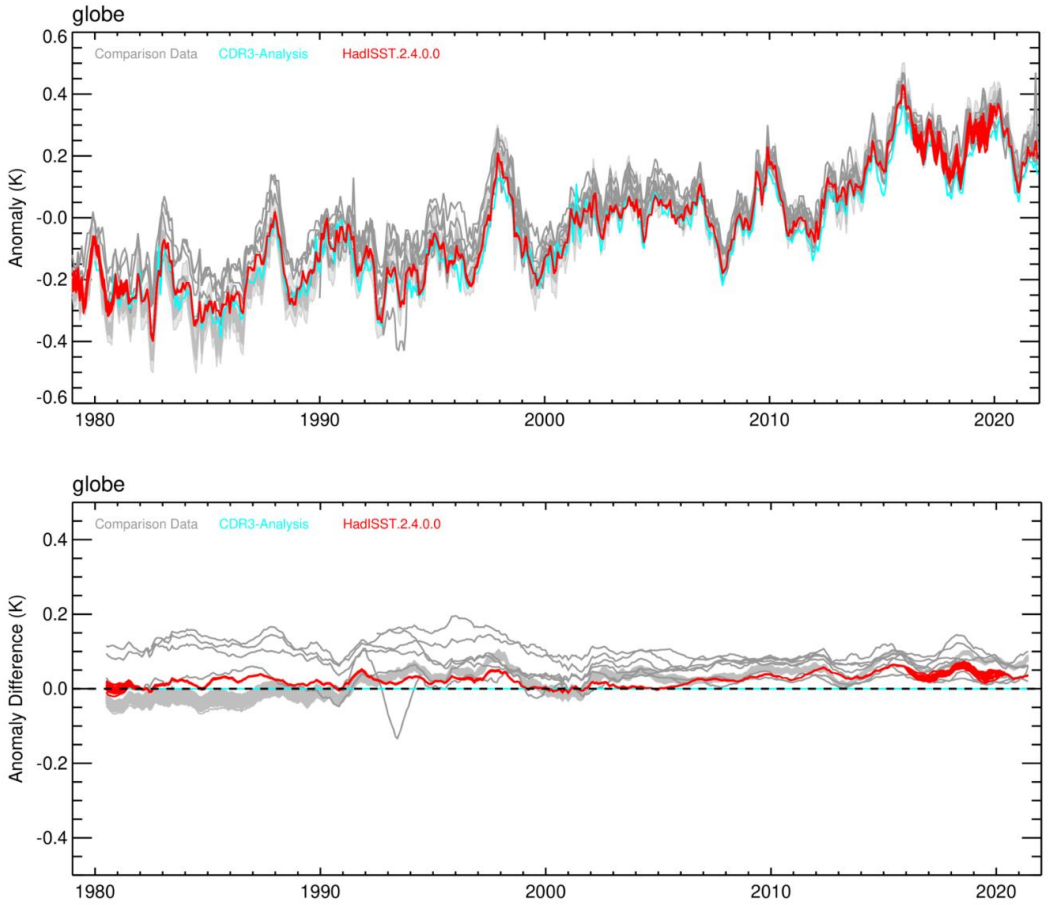

Figure 4-2. Upper panel: Global average monthly SST anomaly (K, relative to SST CCI v3.0 climatology 1991-2020). Time series are not colocated and have not had sea ice areas masked. Bottom panel: Moving average differences of monthly averages (K, comparison data set minus SST CCI v3.0 Analysis).

The Northern Hemisphere monthly average time series in Figure 4-3 shows a greater difference in the 1980s between HadISST.2.4.0.0 and SST CCI v3.0 and there is a pronounced seasonal cycle in HadISST.2.4.0.0 in this period, but this is more in phase with the comparison data than the seasonal cycle in HadISST1. Here we have masked regions which contain sea ice to remove the effect of the different sea ice specifications in the two analyses. The temporal evolution of the Northern Hemisphere difference suggests that there is likely some small residual relative cool bias in the SST CCI v3.0 Analysis after the eruptions of El Chichòn and Mount Pinatubo, with an additional small offset also in 1987 (but less than 0.1 K). Outside of these periods, the two analyses again lie within 0.05 K of each other on a monthly hemispheric average.

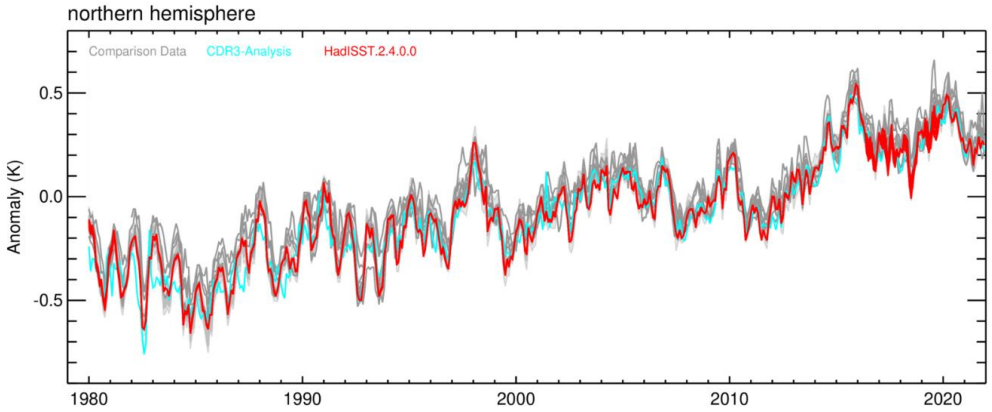

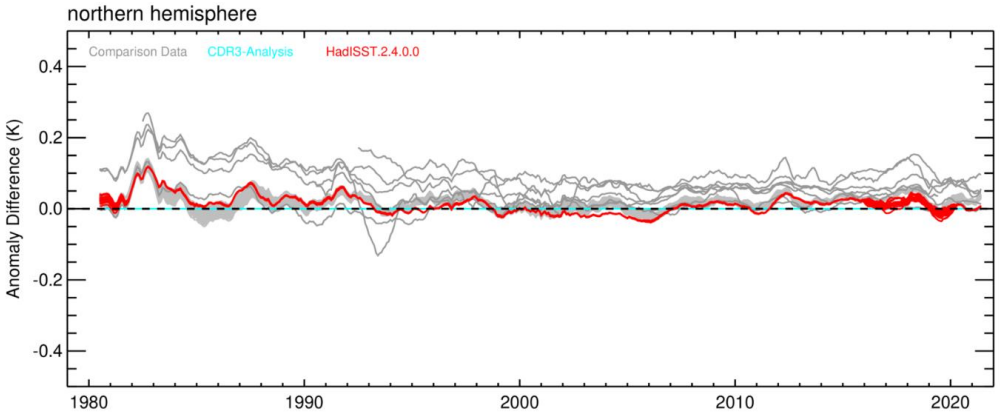

Figure 4-3. Upper panel: Northern Hemisphere average monthly SST anomaly (K, relative to SST CCI v3.0 climatology 1991-2020). Time series are not colocated but have had sea ice areas masked. Bottom panel: Moving average differences of monthly averages (K, comparison data set minus SST CCI v3.0 Analysis).

Figure 4-4 shows greater similarity between HadISST.2.4.0.0 and SST CCI v3.0 Analysis than with the comparison data in the Southern Hemisphere, in particular in the mid-1990s. In this region, HadISST.2.4.0.0 and SST CCI v3.0 Analysis lie within 0.1 K of each other on the hemispheric average in each month. There is a suggestion of an increasing difference between them towards the end of the period with HadISST.2.4.0.0 appearing progressively warmer than SST CCI v3.0. It is clear here that geographical sampling plays a large part in the reported SST anomaly (and confirmed when comparing with co-located plots, not shown) – compare the thick grey HadSST.4.0.1.0 ensemble in the lower panel of Figure 4-4 to the red curve of HadISST.2.4.0.0 in the 1980s when ship measurements in the Southern Hemisphere are sparse relative to the well-sampled SST CCI v3.0 AVHRR data.

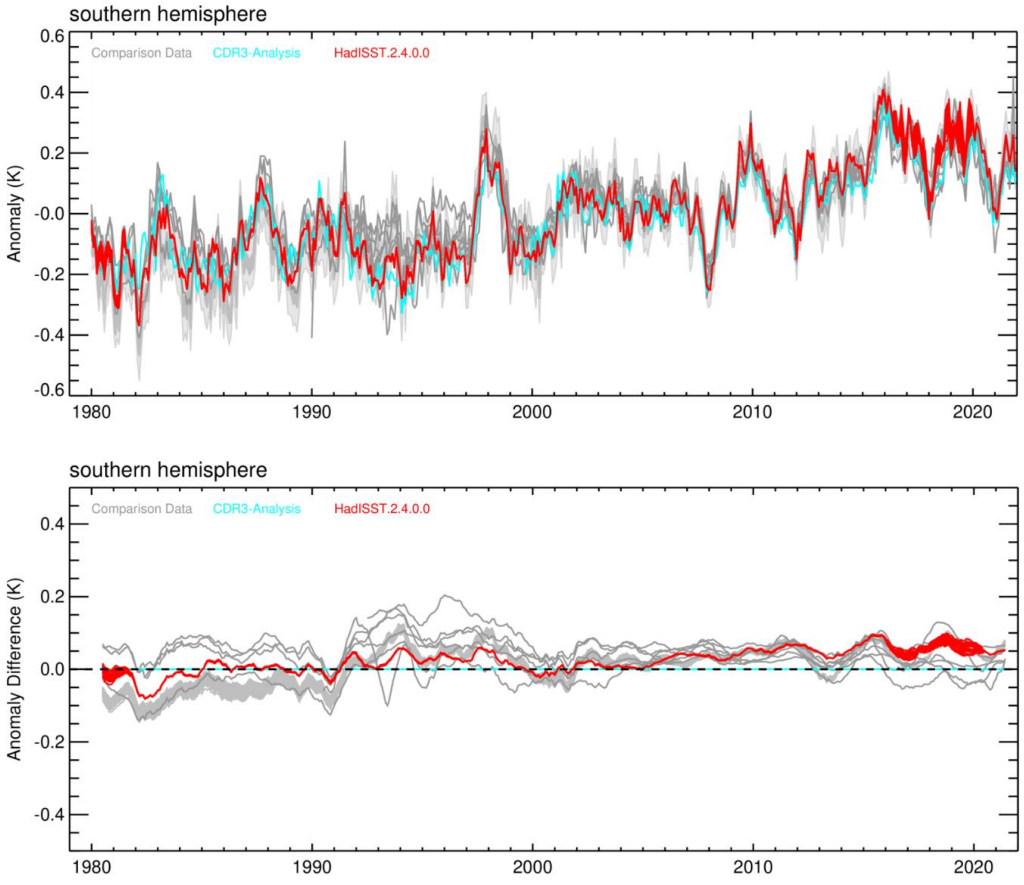

Figure 4-4. Upper panel: Southern Hemisphere average monthly SST anomaly (K, relative to SST CCI v3.0 climatology 1991-2020). Time series are not colocated but have had sea ice areas masked. Bottom panel: Moving average differences of monthly averages (K, comparison data set minus SST CCI v3.0 Analysis).

Exploring maps of decadal average SST anomaly in Figure 4-5, we see mostly similarities but some subtle differences in the geographical patterns in each decade in (the first ensemble member of) HadISST.2.4.0.0 and in SST CCI v3.0. Difference maps are presented in Figure 4-6.

Clearly, ERSSTv5, HadISST1 and OI.v2 are warmer globally in 2012-2021 (confirmed by Figure 4-2) and in the Southern Ocean throughout the whole period (see also Figure 4-7).

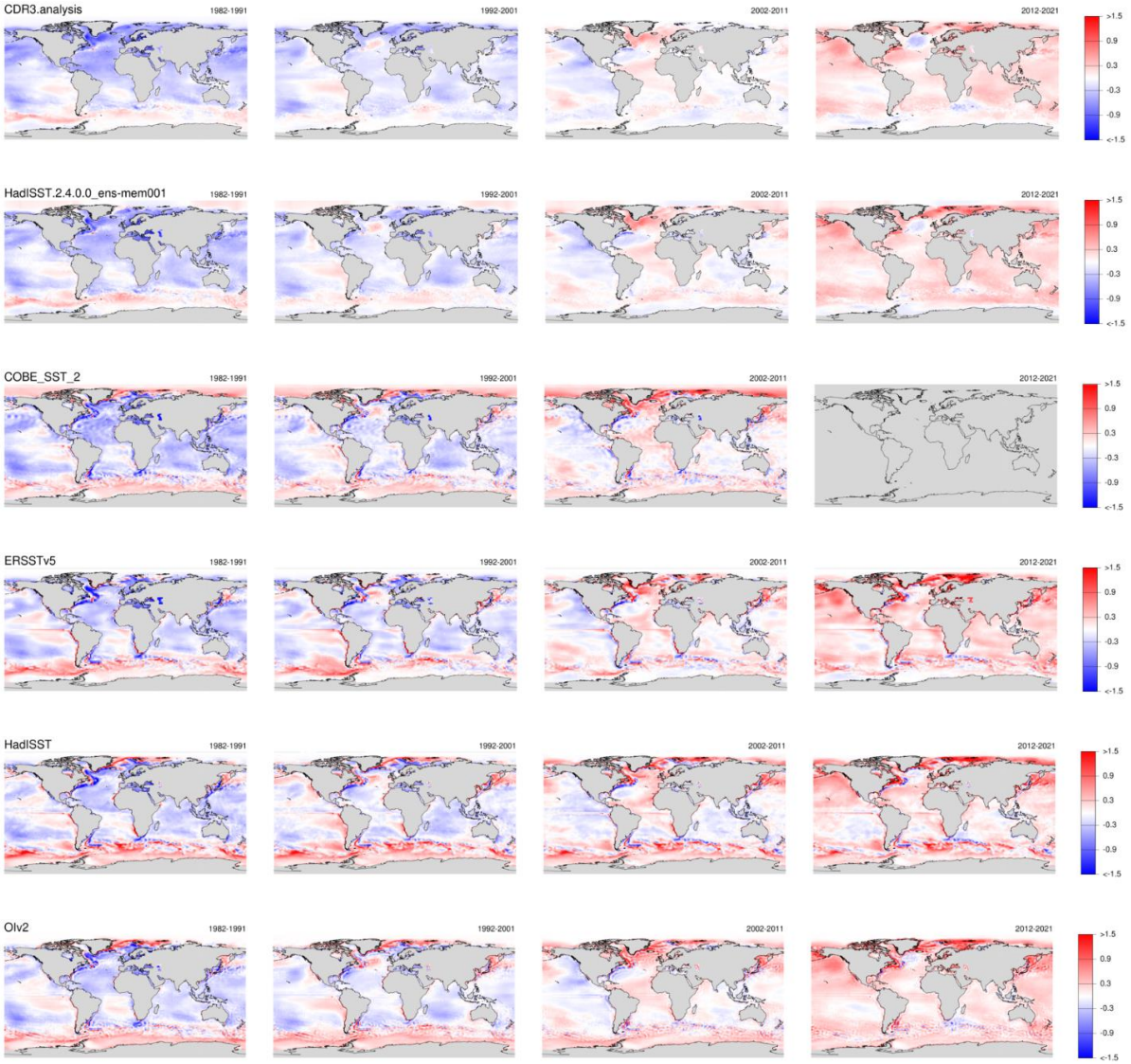

Figure 4-5. Decadal average SST anomalies (K, relative to SST CCI v3.0 climatology 1991-2020). Decades, left to right are: 1982-1991; 1992-2001; 2002-2011; and 2012-2021. First row: SST CCI v3.0 Analysis. Second row: HadISST.2.4.0.0. Third row: COBE-2 SST. Fourth row: ERSSTv5. Fifth row: HadISST1. Sixth row: OI.v2.

Figure 4-6 also demonstrates that HadISST1 and OI.v2 are cooler than the other analyses in the Indian Ocean in 2012-2021, with HadISST1 being coolest. These decadal difference maps highlight hemispheric differences in the 1980s in COBE-2 (and also, but less so, in other data sets, including HadISST.2.4.0.0) from SST CCI v3.0.

HadISST.2.4.0.0 is however, clearly cooler than the SST CCI v3.0 Analysis in the Mediterranean throughout the period (see also Figure 4-8). Areas in the SST CCI v3.0 Analysis where infrared satellite retrievals are still slightly affected by dust (north-west Indian Ocean, off the western coast of Africa), are warmer in HadISST.2.4.0.0 by ~0.2 K (Figure 4-6), but this is now of the same magnitude as differences in other regions.

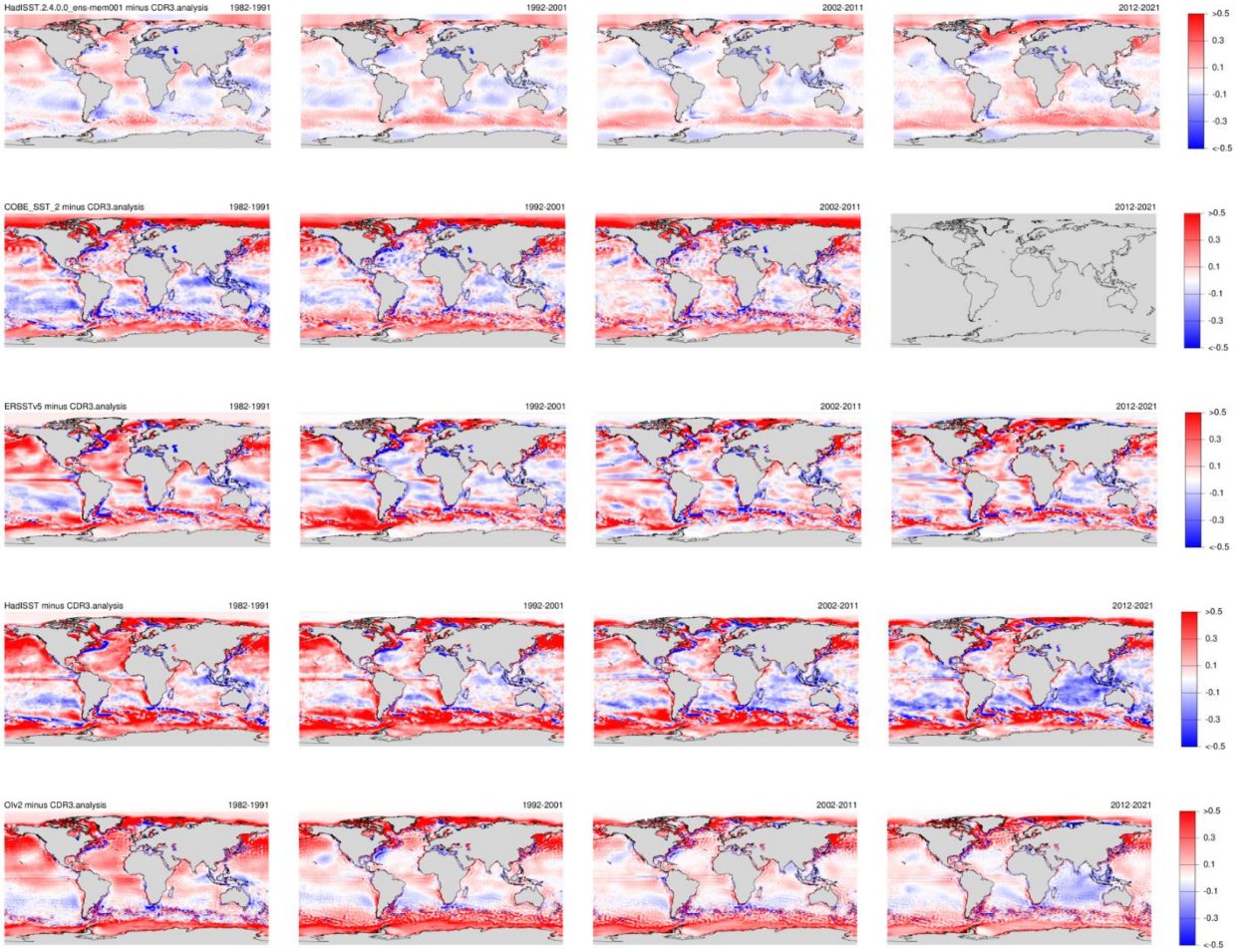

Figure 4-6. Decadal average SST differences from SST CCI v3.0 Analysis (K). Decades, left to right are: 1982-1991; 1992-2001; 2002-2011; and 2012-2021. First row: HadISST.2.4.0.0. Second row: COBE-2 SST. Third row: ERSSTv5. Fourth row: HadISST1. Fifth row: OI.v2.

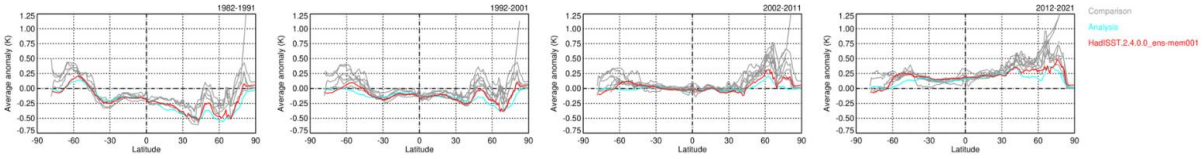

Figure 4-7. Latitudinal decadal average SST anomalies (K, relative to SST CCI v3.0 climatology 1991-2020). Decades are (left to right): 1982-1991; 1992-2001; 2002-2011; 2012-2021. Shown are SST CCI v3.0 Analysis (cyan), HadISST.2.4.0.0 ensemble member 1 (red) and other comparison data sets (grey, see earlier text for details).

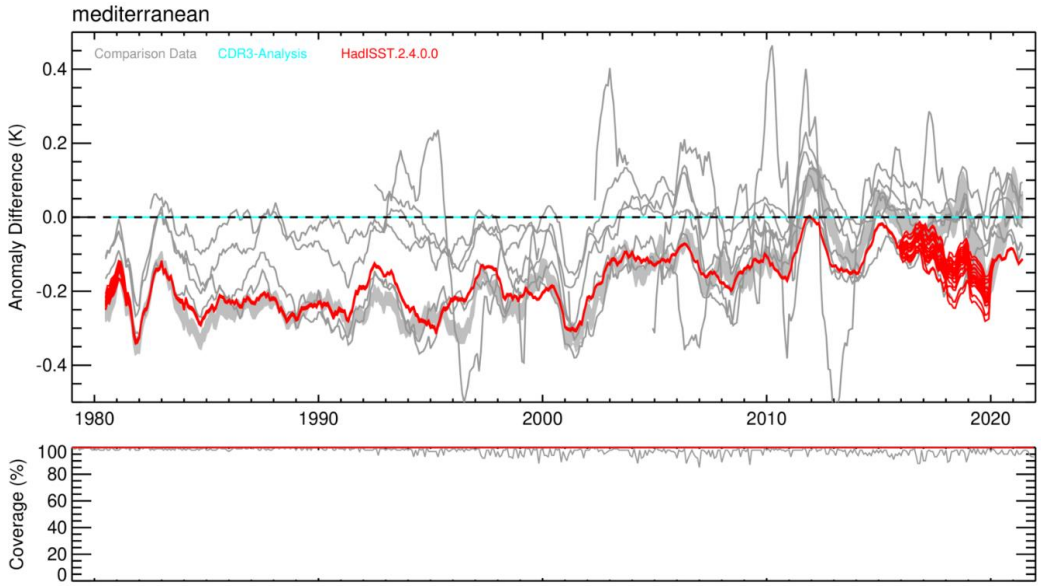

Figure 4-8. Upper panel: Moving average differences of monthly Mediterranean SST anomaly averages (K, comparison data set minus SST CCI v3.0 Analysis). Bottom panel: Percentage coverage of the region in HadISST.2.4.0.0 (red) and HadSST.4.0.1.0 (grey).

In general, HadISST.2.4.0.0 and SST CCI v3.0 agree well averaged both over latitudinal and longitudinal bands (Figure 4-7 and Figure 4-9 respectively) and tend to be, to varying degrees, on average cooler than the comparison data sets 1980-2021.

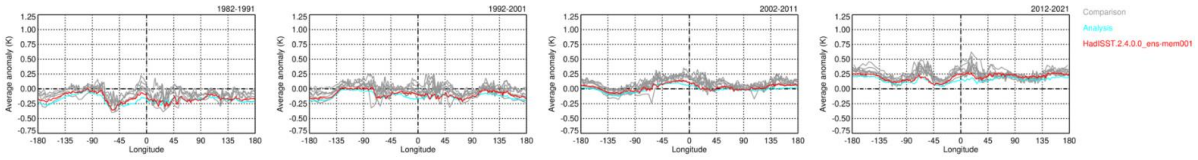

Figure 4-9. Longitudinal decadal average SST anomalies (K, relative to SST CCI v3.0 climatology 1991-2020). Decades are (left to right): 1982-1991; 1992-2001; 2002-2011; 2012-2021. Shown are SST CCI v3.0 Analysis (cyan), HadISST.2.4.0.0 ensemble member 1 (red) and other comparison data sets (grey, see earlier text for details).

Maps of SST anomaly standard deviation (Figure 4-10) enable comparison of the variability in the SST anomaly fields in each data set. This is a good test of HadISST.2.4.0.0 which was created on a monthly 1 degree latitude by 1 degree longitude grid. Does it capture the same variability when compared on that spatiotemporal resolution to a data set like the SST CCI v3.0 Analysis which was produced on a 0.05 degree latitude by 0.05 degree longitude daily grid? Figure 4-10 shows that HadISST.2.4.0.0 and SST CCI v3.0 Analysis are in generally good agreement, but Figure 4-11 shows relatively more variability in HadISST.2.4.0.0 in the high gradient regions. This likely results from a difference in background climatology between the two data sets in these regions, but it is interesting that this is not also seen in HadISST1, which looks relatively more consistent with the SST CCI v3.0 Analysis here.

HadISST.2.4.0.0 is also relatively more variable than the SST CCI v3.0 Analysis in sea ice regions in both hemispheres.

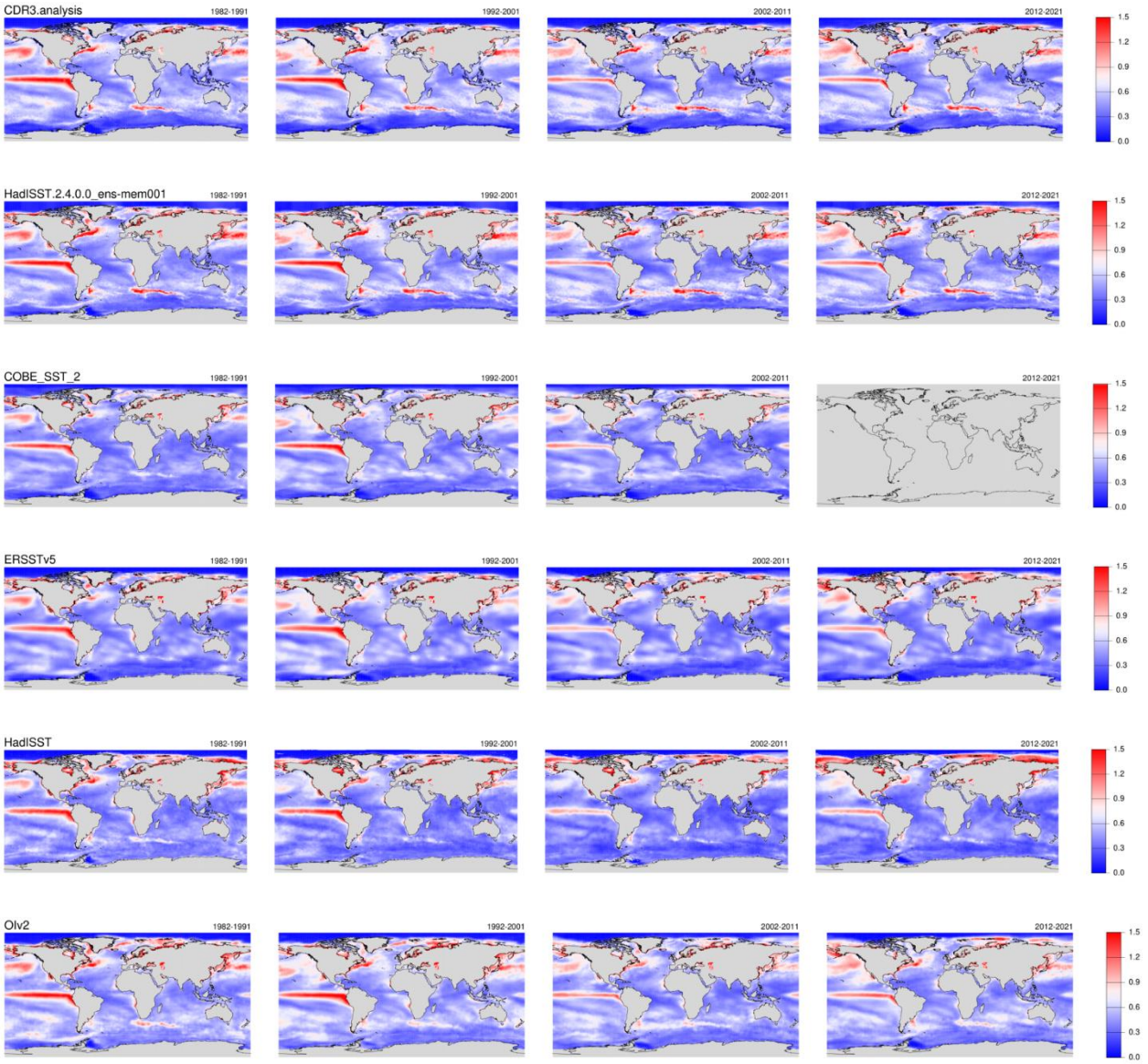

Figure 4-10. Decadal average SST monthly anomaly standard deviation (K). Decades, left to right are: 1982-1991; 1992-2001; 2002-2011; and 2012-2021. First row: SST CCI v3.0 Analysis. Second row: HadISST.2.4.0.0. Third row: COBE-2 SST. Fourth row: ERSSTv5. Fifth row: HadISST1. Sixth row: OI.v2.

However, compared to HadISST1, HadISST.2.4.0.0 is more consistent with the SST CCI v3.0 Analysis in open ocean areas with HadISST1 containing much less variability than SST CCI v3.0 here. This demonstrates the added information included through the HadISST.2.4.0.0 multi-step reconstruction method. Comparing the difference map between HadISST.2.4.0.0 and SST CCI v3.0 and that between the OI.v2 and SST CCI v3.0, the former is more consistent in open ocean areas, with the OI.v2 map being relatively patchy. This is likely a consequence of the spatially-homogeneous approach used in HadISST.2.4.0.0 with a large-scale reconstruction used everywhere, followed by a mid-scale analysis also performed consistently everywhere. The OI.v2 uses a local OI method only and so its variability will be perhaps more affected by local data availability.

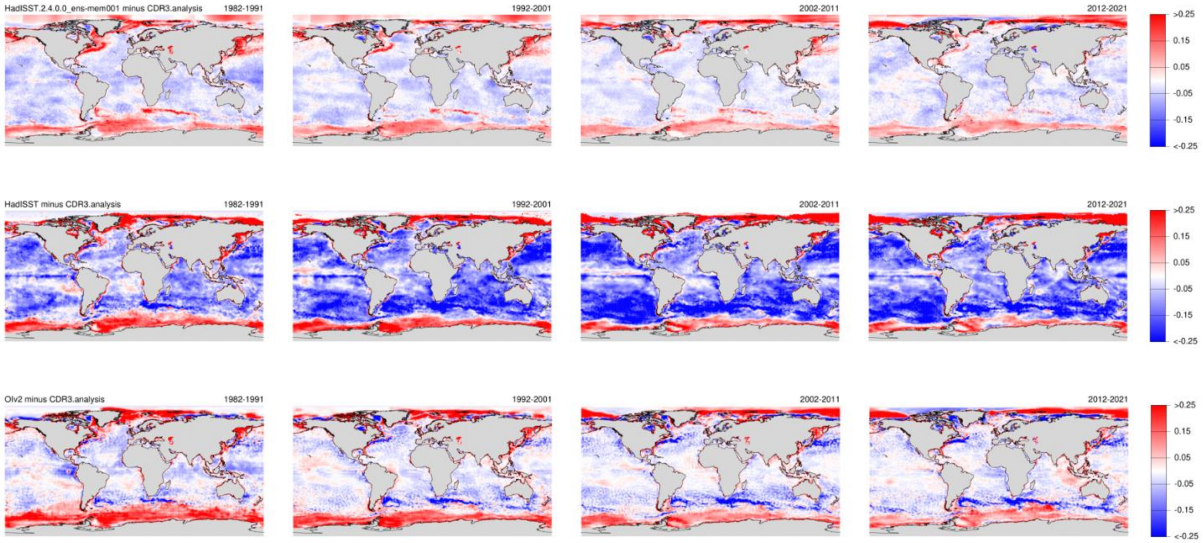

Figure 4-11. Decadal average standard deviation differences from SST CCI v3.0 Analysis (K). Decades, left to right are: 1982-1991; 1992-2001; 2002-2011; and 2012-2021. First row: HadISST.2.4.0.0. Second row: HadISST1. Third row: OI.v2. Where map is red, SST CCI v3.0 has a lower standard deviation. Where map is blue, the comparison data set has a lower standard deviation.

As suggested by Figure 4-10, variability in the different SST analyses is fairly consistent when averaged over latitude (Figure 4-12) or longitude (Figure 4-13) bands, with some notable exceptions (the surface *in situ*, non-infilled data sets whose standard deviation is affected by sampling in southern and high northern latitudes).

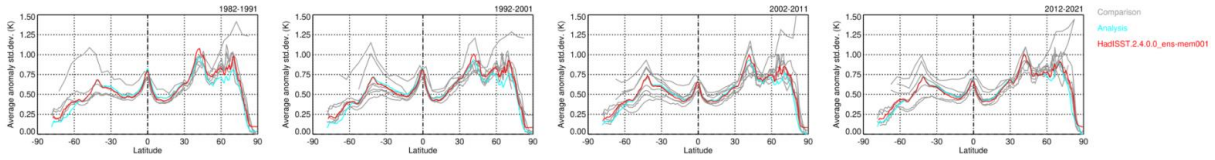

Figure 4-12. Latitudinal decadal average SST anomaly standard deviation (K). Decades are (left to right): 1982-1991; 1992-2001; 2002-2011; 2012-2021. Shown are SST CCI v3.0 Analysis (cyan), HadISST.2.4.0.0 ensemble member 1 (red) and other comparison data sets (grey, see earlier text for details).

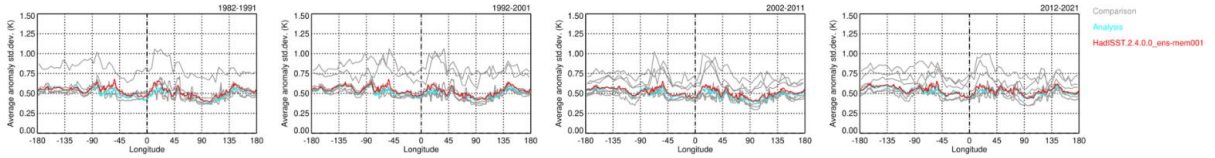

Figure 4-13. Longitudinal decadal average SST anomaly standard deviation (K). Decades are (left to right): 1982-1991; 1992-2001; 2002-2011; 2012-2021. Shown are SST CCI v3.0 analysis (cyan), HadISST.2.4.0.0 ensemble member 1 (red) and other comparison data sets (grey, see earlier text for details).

On the whole, linear trends in HadISST.2.4.0.0 agree well with those in SST CCI v3.0 (Figure 4-14). Larger differences in trend can be seen in the Mediterranean (as previously discussed, SST CCI v3.0 seems to be an outlier here) and in the Southern Ocean (see also Figure 4-15).

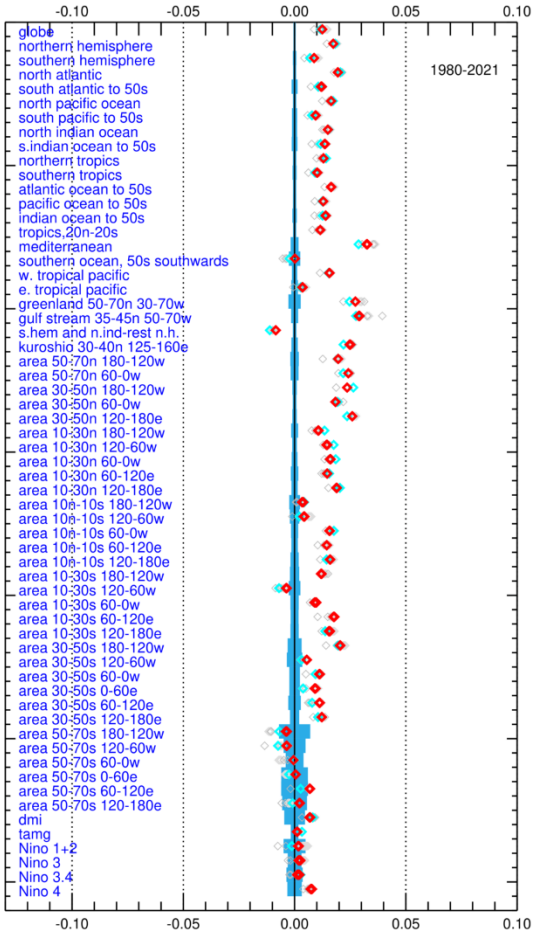

Figure 4-14. Linear trends in SST anomaly (K/year) in each analysis region. Shown are SST CCI v3.0 Analysis (cyan), HadISST.2.4.0.0 ensemble (red) and other comparison data sets (grey, see earlier text for details).

The different linear trend in the Southern Ocean seems to arise from a change in the 1980s. It isn't clear whether this shift (Figure 4-15) is a feature of HadISST.2.4.0.0 or of the SST CCI v3.0 Analysis.

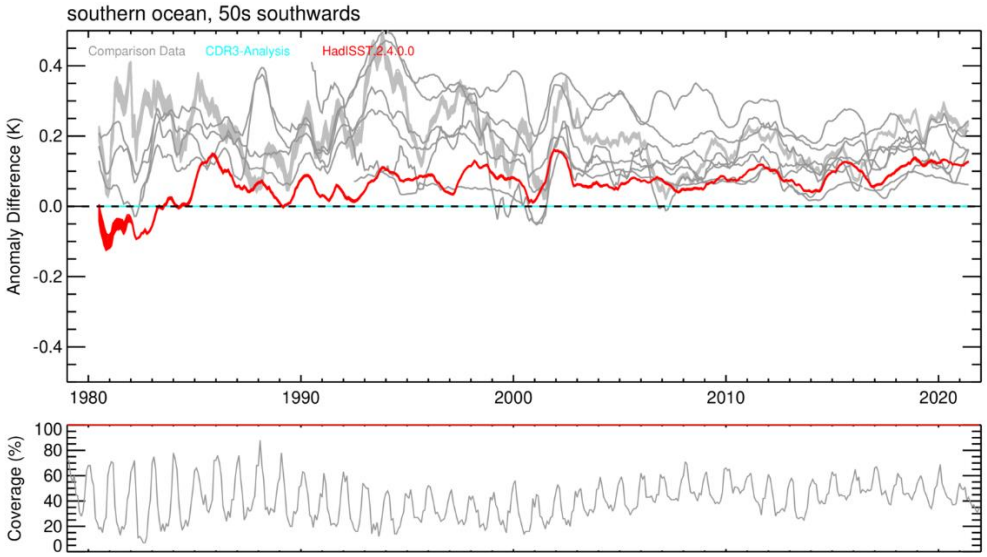

Figure 4-15. Upper panel: Moving average differences of monthly Southern Ocean (south of 50S) SST anomaly averages (K, comparison data set minus SST CCI v3.0 Analysis). Bottom panel: Percentage coverage of the region in HadISST.2.4.0.0 (red) and HadSST.4.0.1.0 (grey).

One final area of interest to explore is the Niño 3.4 region, often used to describe ENSO variability (Figure 4-16). We see relatively good agreement here between HadISST.2.4.0.0 and the SST CCI v3.0 Analysis (relative to that with the other comparison data sets), with agreement often (but not always) within 0.1 K. An interesting feature of HadISST.2.4.0.0 here is the large ensemble spread at the end of the timeseries. This arises from uncertainty in bias corrections applied to ship measurements from 2016 onwards.

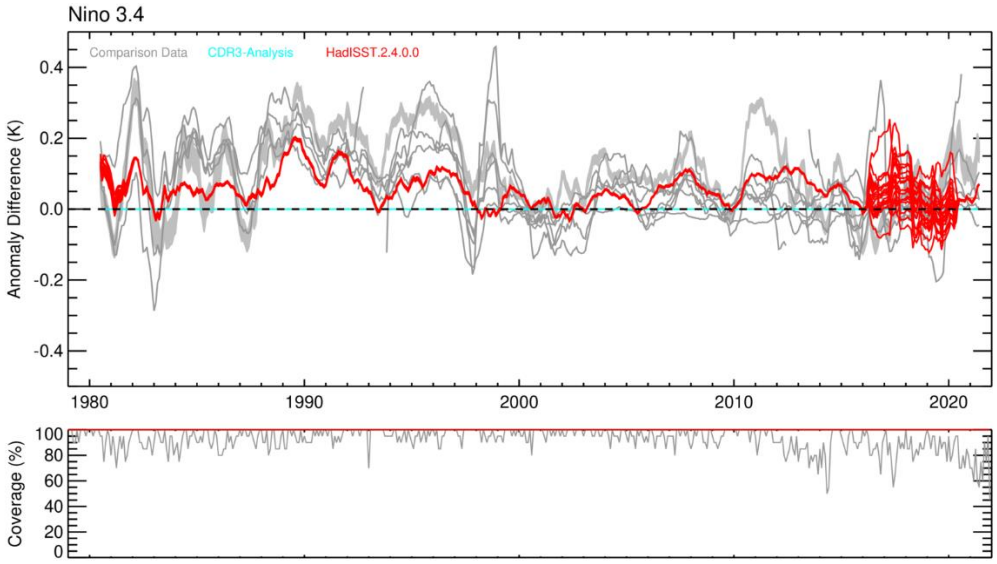

Figure 4-16. Upper panel: Moving average differences of monthly Niño 3.4 SST anomaly averages (K, comparison data set minus SST CCI v3.0 Analysis). Bottom panel: Percentage coverage of the region in HadISST.2.4.0.0 (red) and HadSST.4.0.1.0 (grey).

4.4 Discussion

We have seen that the incorporation of SST CCI v3.0 data into a new version of HadISST, HadISST.2.4.0.0, has brought with it a number of advantages. HadISST.2.4.0.0 and the SST CCI v3.0 Analysis are very close in terms of their SST anomaly time series over most analysis regions and in terms of their decadal average SST anomaly and variability, particularly relative to other commonly-used SST data sets.

This means that these data sets could be used together with confidence in linked activities that require SST data sets at different spatiotemporal resolution, but that need as little discontinuity as possible between the data sets used in each case. For example, they could be used as lower-boundary forcing for atmosphere-only climate model simulations, or reanalyses, at different times or with different resolution models. This is new – no previous pair of data sets has been created with this as an ambition, or with this as the outcome. It is testament to the multi-year investment in the quality of the satellite data sets that has been made within the ESA CCI project.

5. VOLUNTARY REPORTS BY REGISTERED USERS

It has been very valuable in all three phases of the SST CCI project to release new product versions to voluntary "trail blazer" users ahead of general data release. The SST CCI team benefit from their feedback and the test users' application of the data provides a variety of examples of ways in which the data can be used. In this phase, we were fortunate to have six teams assess the pre-release data and this section contains their assessments of the utility of the SST CCI v3 products in the context of their applications.

In the following sub-sections, teams from six countries (Germany, Italy, Norway, Portugal, the Philippines and the US) provide reports of their experiences. The SST CCI v3 products are used in (i) development of a new version of a satellite record of variables relevant to the water cycle (HOAPS); (ii) development of a machine-learning approach to prediction of Mediterranean SST; (iii) a study of marine heatwaves in the vicinity of the Philippines; (iv) an investigation of the 'Atlantification' and the occurrence of 'Marine heat waves' in the Nordic Seas and the Barents Sea; (v) assessing their utility for ocean and climate studies over the Portuguese marine and coastal waters; and (vi) assessing their relative bias in the 1980s.

5.1 T. Sikorski, A. Niedorf, H. Konrad, K. Fennig, M. Schröder (DWD)

5.1.1 KEY MESSAGES

- Successful reproduction of the EUMETSAT CM SAF HOAPS 4.0 dataset (Andersson et al., 2017) using the ESA SST CCI Analysis product version 3.0
- ESA SST CCI Analysis product version 3.0 is a viable alternative to the NOAA 0.25° daily Optimum Interpolation Sea Surface Temperature dataset in the HOAPS processing framework
- ESA SST CCI Analysis product version 3.0 seemingly leads to improvements of individual EUMETSAT CM SAF HOAPS parameters; further analysis is needed.

5.1.2 SCIENTIFIC ANALYSIS

In the scope of this study, we address the Hamburg Ocean Atmosphere Parameters and Fluxes from Satellite data record (HOAPS) from the EUMETSAT Satellite Application Facility on Climate Monitoring (CM SAF). As the name suggests, the HOAPS dataset provides global estimates for multiple atmospheric and oceanic parameters over the ice-free ocean. Published parameters in the scope of HOAPS 4.0 (Andersson et al., 2017) are evaporation, freshwater budget, latent heat flux, near surface specific humidity, near surface wind speed, precipitation, and total column water vapour. The estimates are based mostly on observations made by the passive microwave radiometers Special Sensor Microwave/Imager (SSM/I) and its successor Special Sensor Microwave Imager/Sounder (SSMIS). The HOAPS 4.0 data is available from EUMETSAT CM SAF via https://wui.cmsaf.eu or https://doi.org/10.5676/EUM_SAF_CM/HOAPS/V002.

Sea surface temperature (SST) is an important a priori information in the algorithm. It is taken from external sources. At present, SST in HOAPS is not based on microwave observations.

5.1.3 AIMS OF THE STUDY

The EUMETSAT CM SAF HOAPS algorithm and dataset are developed continuously. The latest, published version is HOAPS 4.0 (Andersson et al., 2017). HOAPS 4.0 uses the NOAA 0.25° daily Optimum Interpolation Sea Surface Temperature dataset (OISST; Reynolds et al., 2007; Reynolds, 2009) as one of its input sources (Andersson et al., 2016).

Using a different sea surface temperature (SST) dataset will affect the upcoming new version of the HOAPS dataset. In this study, we will examine the effects of switching from OISST to the

ESA SST CCI Analysis product in HOAPS. The analysis will rely on evaporation and related latent heat flux as well as near surface wind speed. This includes the following questions:

- How will these parameters change?
- What are the advantages/disadvantages of the SST CCI dataset in the scope of the HOAPS processing?

These questions are answered with future developments of the HOAPS dataset in mind.

5.1.4 METHOD

5.1.4.1 HOAPS 4.X VS. HOAPS 4.0

As previously described, the HOAPS algorithm for the upcoming new version is still under development. The HOAPS 4.0 dataset was released in 2017. The recently available algorithm has been adapted for some improvements and bug fixes in the meantime. Since effects on future HOAPS versions play also an important role in this study, we will use here a non-official, newer HOAPS algorithm version. We label this newer version with HOAPS 4.x. The official algorithm and dataset version (from 2017, using OISST data) will be denoted as HOAPS 4.0.

HOAPS 4.0 data is available in monthly means and 6-hourly composites. Its spatial resolution is 0.5 × 0.5 degree. We generated the new, non-official, monthly HOAPS 4.x dataset at the same spatial resolution using the SST CCI analysis v3.0 dataset. Hence, these two HOAPS datasets (4.0 and 4.x) differ in the input SST data. An overview of the used datasets and their respective SST data is given in Table 5-1.

Table 5-1: Summary of HOAPS datasets and their corresponding SST dataset

HOAPS dataset	SST dataset	
HOAPS 4.0	OISST – NOAA 0.25° daily Optimum Interpolation Sea Surface Temperature	The dataset is available at a 0.25 × 0.25 degree daily spatiotemporal resolution. It is based on satellite observations (originating e.g., from the AVHRR instrument) as well as in situ observations by ships and buoys. The covered period reaches from 1981 until present.
HOAPS 4.x	SST CCI analysis v3.0 – ESA SST CCI Analysis product version 3.0	This L4 product contains SST derived from SST CCI ATSR, SST CCI AVHRR, SST CCI AMSR and SST CCI SLSTR products. The satellite-only SST-depth analysis was created by OSTIA system. The dataset's spatial resolution is 0.05 × 0.05 degree. It covers the period from 1980 until 2021 on a daily time scale.

Both SST datasets feature a finer spatial grid than 0.5 × 0.5 degree, which is the spatial resolution of the official HOAPS data. Since this spatial resolution is required for SST input data, we adjust each SST dataset to the coarser resolution of HOAPS in a first step. In a second step, the HOAPS algorithm applies an internal correction to the SST data. The HOAPS algorithm then uses these corrected SST data when processing the microwave observations. We use the same correction for both SST dataset (SST CCI analysis v3.0 and OISST). We use the corrected SST values in our direct comparison of the SST datasets (Section R).

In this study, we focus on the period January 1987 until December 1998. This period is covered by the SSM/I instrument. We do not use its successor SSMIS since the fundamental climate data record (FCDR) for SSMIS has been modified in the meantime, too. It should be noted that this period includes the El Niño event from winter 1997/98 as well as the Mt. Pinatubo eruption from

1991. The HOAPS dataset has been found sensitive to the occurrence of El Niño (Masunaga et al., 2019, Robertson et al., 2020).

Our interest in this study lies in the spatial differences caused by swapping the SST datasets and the respective temporal evolution. For investigating spatial features, we compute maps of the 12-year average as well as zonal and global means. Time series of global means provide a first guess of temporal features.

5.1.4.2 HOAPS VS. NOCS

The comparison of HOAPS 4.x and HOAPS 4.0 outlined above will indicate how the SST datasets affect HOAPS output differently. For an additional independent assessment of each HOAPS version's quality, we compare the produced HOAPS 4.0 and 4.x output to a reference dataset. Our reference in this study is the National Oceanographic Centre Southampton (NOCS) Flux dataset version 2.0 (NOCS 2.0, Taylor et al., 2009). We apply this comparison to the HOAPS 4.x (SST CCI analysis v3.0) and HOAPS 4.0 (OISST) data.

The NOCS 2.0 dataset provides estimates for the following parameters: 10m-air-temperature, cloud cover, 10m-specific-humidity, latent heat flux, net longwave radiation, net shortwave radiation, sea level pressure, sea surface temperature, sensible heat flux and 10m-wind-speed. All NOCS 2.0 parameters are monthly averages. They are available on a 1° × 1° spatial grid and cover the period 1973 until 2014. In this study, we will use latent heat flux, sea surface temperature and wind speed for our comparison.

The NOCS 2.0 dataset bases amongst others on ship and buoy measurements (Berry and Kent, 2009, 2011). Due to the lesser ship traffic in the southern hemispheric oceans, we expect a bias within the NOCS 2.0 observations (Berry and Kent, 2009). In order to remove such a bias, the NOCS 2.0 dataset provides a quality mask. In our comparison approach, we will filter the HOAPS and the NOCS 2.0 datasets for grid cells/times that the datasets have in common and are marked to be of good quality.

5.1.5 RESULTS

5.1.5.1 SEA SURFACE TEMPERATURE INPUT DATA

5.1.5.1.1 SST CCI analysis v3.0 vs. OISST

Here, we will have look at the differences between internally corrected SST from both datasets at HOAPS final gridded resolution (0.5°, monthly). Both datasets show similar SST patterns (top and middle row of Figure 5-1) with a maximum in the tropics and two minima at the poles. The minima originating from the upwelling areas at the eastern coastlines of the Pacific and Atlantic are clearly visible too, as well as the minimum of the ITCZ. The global mean difference between the two datasets (SST CCI analysis v3.0 minus OISST) is about 0.1 K. The difference plot (last row of Figure 5-1) reveals that local extremes are more pronounced in the SST CCI analysis v3.0 data than in the OISST data, e.g., in the colder regions of the ITCZ and mid-latitude Pacific (blueish colour marks lower values compared to OISST). Other examples are the warmer areas in the sub-/tropics, especially the Indic and western Pacific.

There is a distinct annual cycle visible in the time series of global mean values for both datasets (Figure 5-2). On this time scale both datasets show a similar behaviour. On monthly time scales, the difference between both datasets fluctuates by up to 0.25 K, but remains positive most of the time (i.e., SST CCI analysis v3.0 exceeds OISST). Only one month in the first half of 1996 shows a negative value, close to zero.

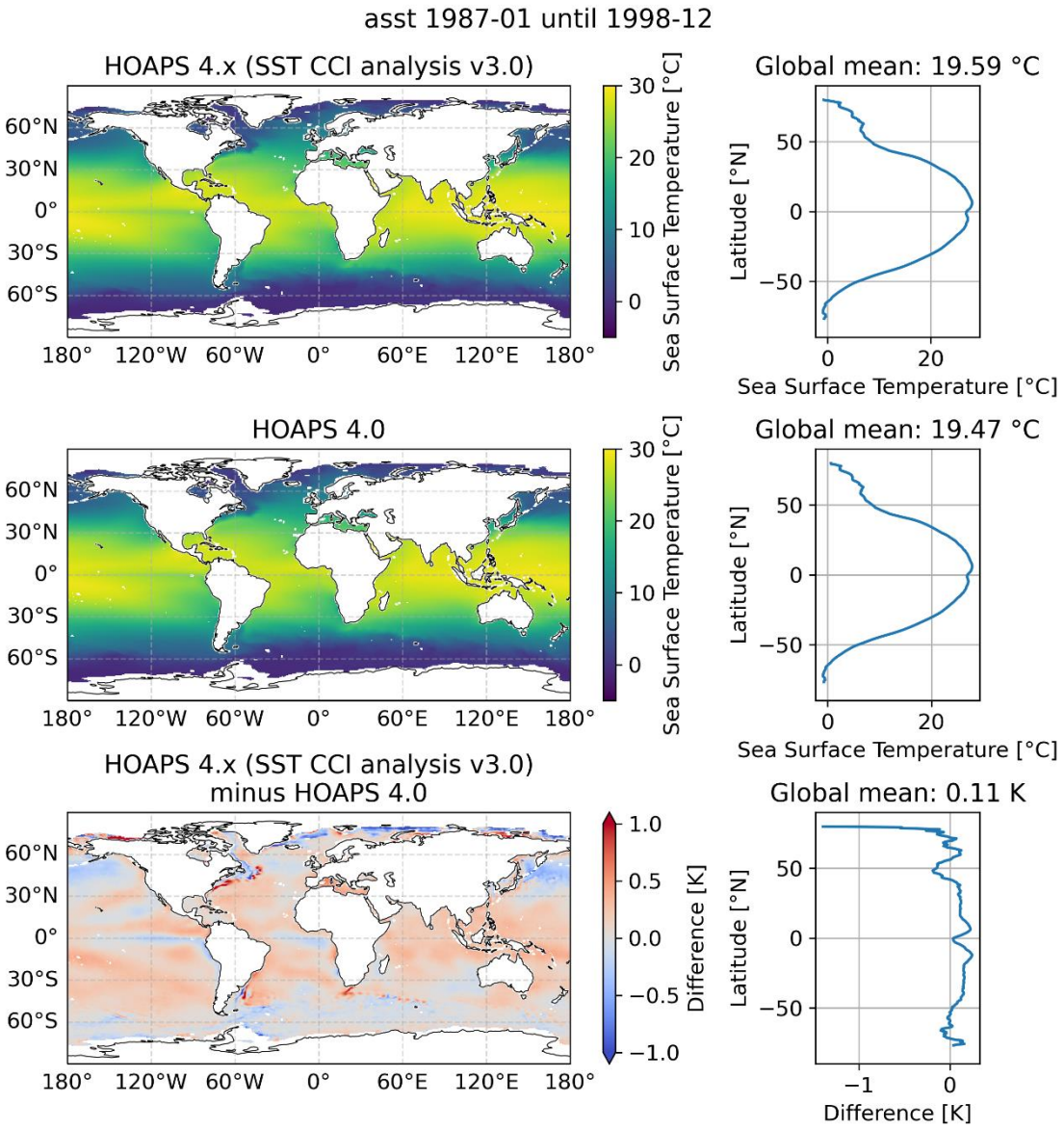

Figure 5-1: Mean sea surface temperature for the years 1987 until 1998. The top row shows the spatial variations of the ESA SST CCI analysis v3.0 data. The panels in the middle illustrate the OISST dataset. The bottom row shows the difference ESA SST CCI analysis v3.0 minus OISST. Respective two-dimensional SST fields are plotted on the left side. The right column shows the corresponding zonal means (global means in the titles).

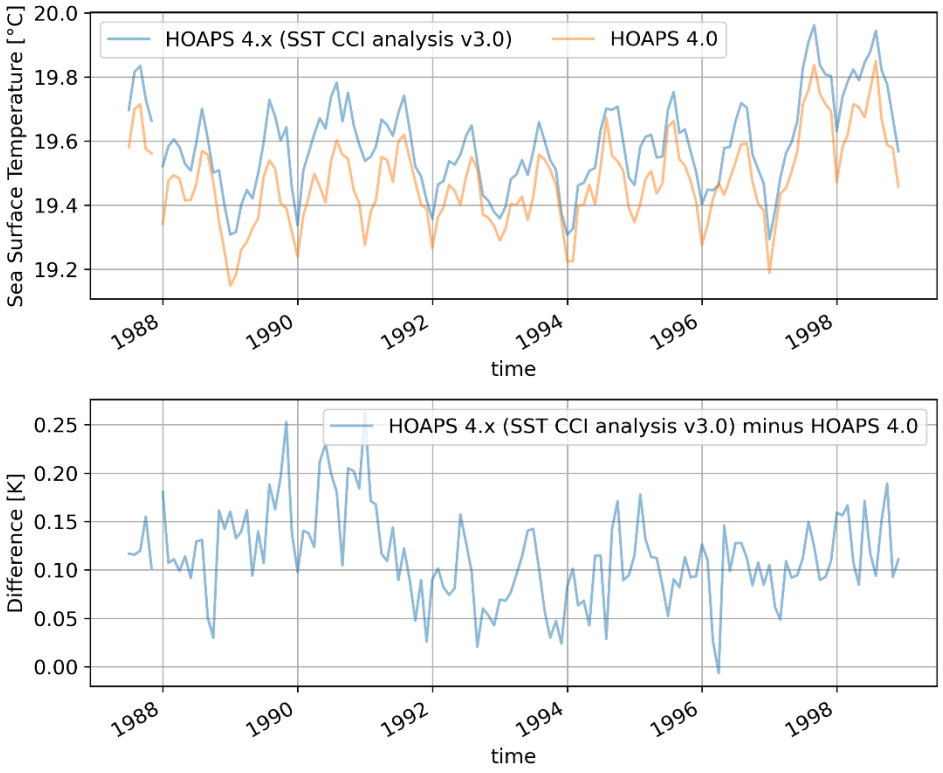

Figure 5-2: Global mean SST time series. The upper panel shows the time series of monthly global means of the SST CCI analysis v3.0 (blue) and OISST (orange) datasets for the years 1987 until 1998. The time series of their monthly difference is given in the lower panel.

5.1.5.1.2 HOAPS v4.x (SST CCI analysis v3.0) vs. NOCS 2.0 SST

Comparable mean global fields for sea surface temperatures originating from SST CCI analysis v3.0 and NOCS 2.0 datasets are presented in Figure 5-3. The map of NOCS 2.0 SST (Figure 5-3, middle left panel) shows a similar global pattern, as we would expect from the upper both maps of Figure 5-1. The zonal averages at the right side of Figure 5-3 are also similar to those of Figure 5-1. The global mean presented in Figure 5-3 are about 1.1 K higher than their respective analogues in Figure 5-1. This higher values result from the filtering of unreliable data as per NOCS 2.0 quality mask which usually affects the mainly unobserved, cold Southern Ocean most (dark shading in the maps of Figure 5-3).

As visible in the bottom panel of Figure 5-3, the NOCS SST exceeds the values in HOAPS 4.x (SST CCI analysis v3.0). On global average, NOCS SST is 0.28 K larger, which is about 1.3% of the global mean. Note that NOCS bulk SST was compared with T_{skin} as output from HOAPS processing. The global difference map (Figure 5-3, bottom left) displays a uniform distribution in space, with the negative values fluctuating around the global average with a few exceptions. These exceptional locations can be found at the Atlantic coasts of North and South America, the tip of South Africa and the northern Pacific coast of Asia. In these areas, the difference of HOAPS 4.x (SST CCI analysis v3.0) minus NOCS 2.0 SSTs is positive.

A similar picture result from the comparison of OISST (HOAPS 4.0) with NOCS 2.0. Hence, we do not show a corresponding figure here.

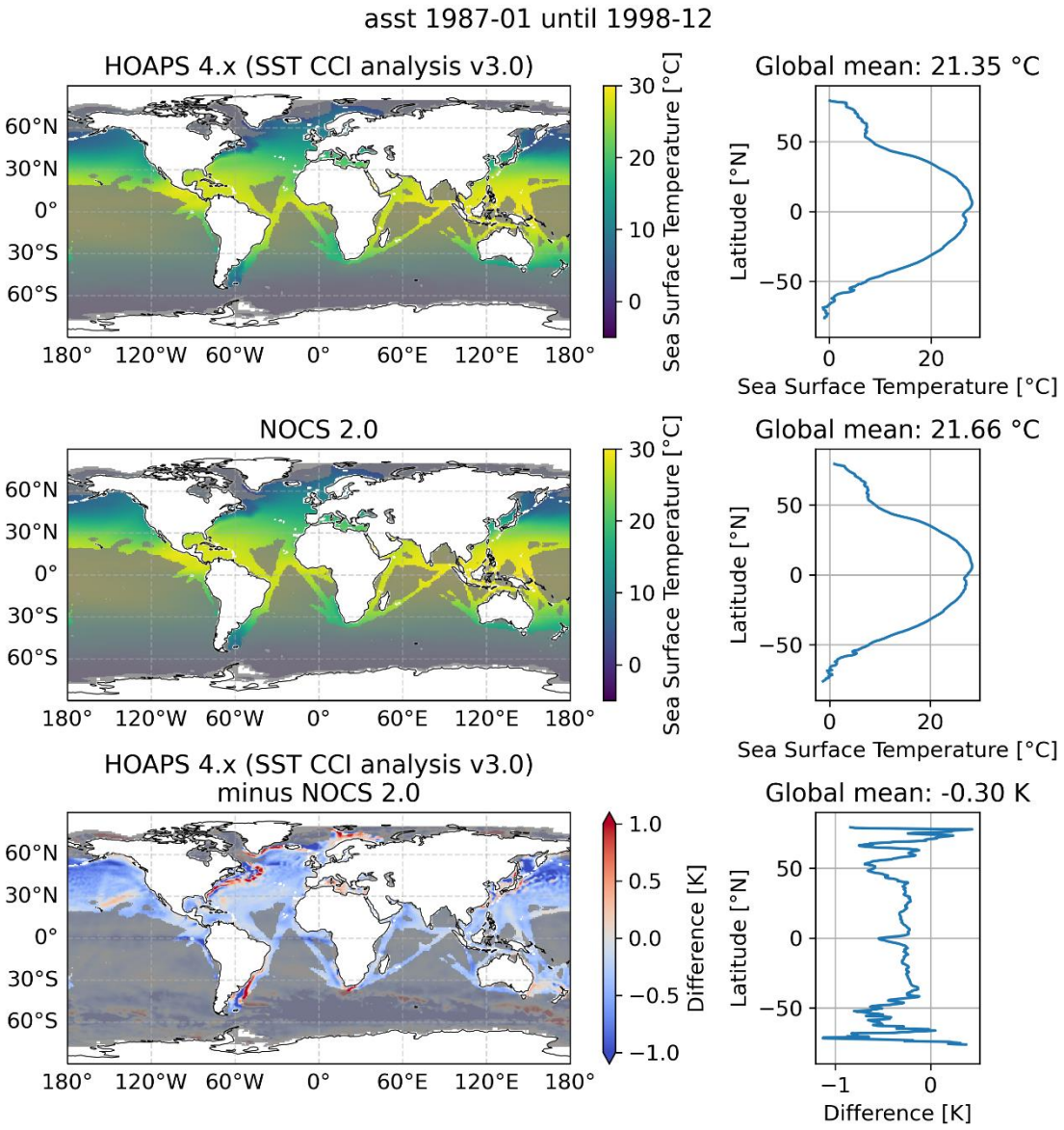

Figure 5-3: Mean sea surface temperature from HOAPS 4.x (SST CCI analysis v3.0) and NOCS 2.0 for the years 1987 until 1998. The top row shows the spatial variations of the SST CCI analysis v3.0 data. The panels in the middle illustrate the NOCS 2.0 dataset. The bottom row shows the difference between both datasets. Respective two-dimensional fields are plotted on the left side. The right column shows the corresponding zonal means (global means in the titles). The grey shading marks areas of unreliable NOCS 2.0 data, i.e. less than 60% of all months from January 1987 until December 1998 are used for the average. Please note: Global and zonal means in the right column are based only on all grid cells/times for which high quality NOCS data is available. In case of global and zonal means, we do not filter for a minimum amount of available months. Note that SST from NOCS is a bulk SST.

We present time series of global mean differences for both SST datasets used in HOAPS (SST CCI analysis v3.0 and OISST) vs. NOCS 2.0 SST in Figure 5-4. Both times series have negative values all the time, which vary around the global temporal and spatial averages of -0.30 K (SST CCI analysis v3.0) and -0.41 K (OISST) respectively. From Figure 5-4 we see, the variability in the HOAPS 4.x (SST CCI analysis v3.0) minus NOCS 2.0 time series is larger compared to HOAPS 4.0 (OISST) minus NOCS 2.0.

Furthermore, there is an offset between the two difference time series. Apart from March/April 1996, the differences with respect to SST CCI analysis v3.0 are larger, i.e., the SST CCI analysis v3.0 dataset is closer to the NOCS 2.0 dataset.

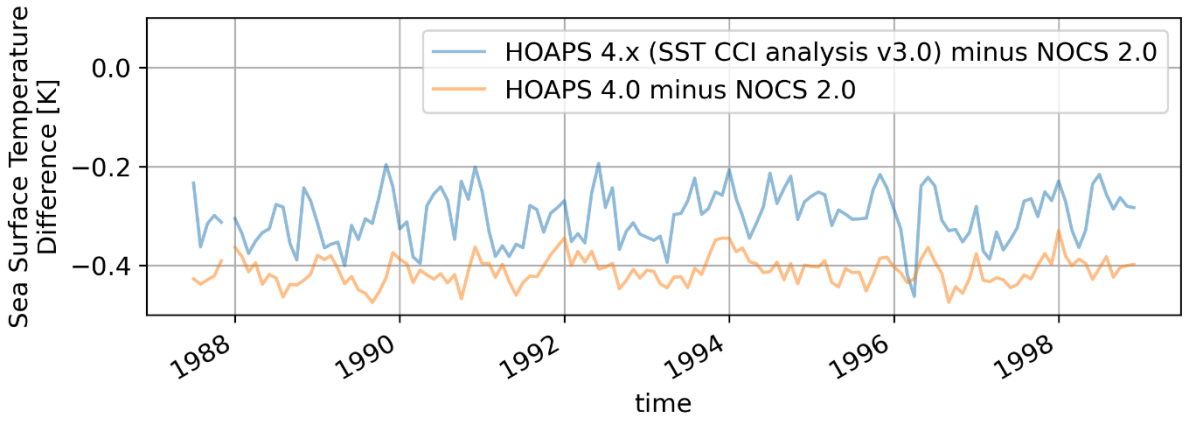

Figure 5-4: Global mean SST time series of HOAPS SSTs minus NOCS 2.0 SST. The figure shows the time series of monthly global mean SST differences. The blue line illustrates the data for SST CCI analysis v3.0 minus NOCS 2.0 difference. The orange line displays the HOAPS 4.0 minus NOCS 2.0 data. Both time series cover the period 1987 until 1998. Please note: Both time series have been computed by using only grid cells that contain high quality NOCS data. Note that SST from NOCS is a bulk SST.

5.1.5.2 WIND SPEED

5.1.5.2.1 SST CCI analysis v3.0 vs. OISST

Wind speed at 10 m height in HOAPS is inverted from MW observations via optimization of the atmospheric state via the 1D-Var retrieval and utilizing the RTTOV radiative transfer model as forward model (Andersson et al., 2011). SST serves as one component of the atmospheric state and for defining the initial guess of the optimization procedure. The expected large-scale wind patterns present in HOAPS 4.0 can be reproduced with SST CCI analysis v3.0 data (Figure 5-5). Globally, there is a difference in 10m-wind-speed between the HOAPS 4.x (SST CCI analysis v3.0) and HOAPS 4.0 data of -0.04 m/s, which corresponds to a decrease of about 0.5%. This decrease results from lower wind speeds in the subtropical upwelling regions and sub-/polar areas at the sea ice edges. Although the areas of all western boundary currents show an increase of wind speed in HOAPS 4.x (SST CCI analysis v3.0) compared HOAPS 4.0, the previously described decrease is dominating on a global scale.

The month-to-month differences between global mean values (Figure 5-6) vary within the entire period from about -0.15 m/s up to 0.10 m/s. These differences correspond to about 2% lower wind speed up to 1.3% higher wind speeds in HOAPS 4.x (SST CCI analysis v3.0) compared to HOAPS 4.0. These variations are not homogeneously distributed over the entire period, but occur in three distinct phases:

- 1988–1992, with larger fluctuations between -0.15m/s and 0 m/s;
- 1992–1997, with less strong variations (-0.05 m/s until about 0.02 m/s);
- 1997–1998, again with larger fluctuations but from -0.05 m/s up to 0.1 m/s.

The first phase of the differences also differs from the other two phases in its mean. The difference of both datasets HOAPS 4.x (SST CCI analysis v3.0) minus HOAPS 4.0 is in the first phase about -0.08 m/s. It increases in the years 1991 until 1993 to a new value at about -0.02 m/s, which is the inter-annual mean level during the last two phases. A similar transition can be observed for the analysed SST (Figure 5-2, lower panel). However, further analysis is needed.

The closer agreement of global mean wind speed from 1992–1998 can also be found, to a lesser degree, in the respective time series of the SST datasets (Figure 5-2). It indicates a direct relationship to the SST input.

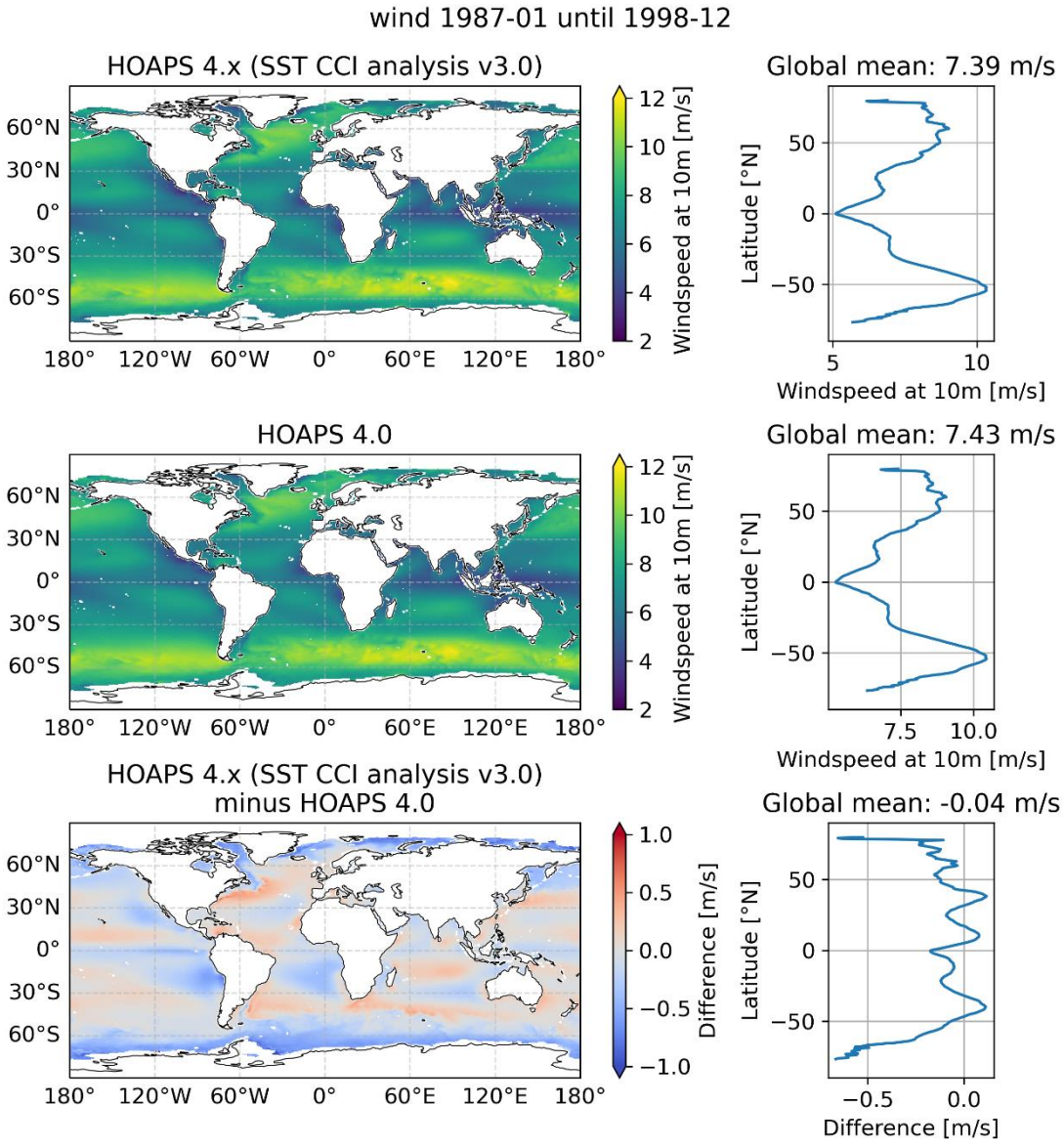

Figure 5-5: Mean 10 m wind speed for the years 1987 until 1998. The top row shows the spatial variations of the HOAPS 4.x (SST CCI analysis v3.0) data. The panels in the middle illustrate the HOAPS 4.0 dataset. The bottom row shows the difference between both datasets. Respective two-dimensional fields are plotted on the left side. The right column shows the corresponding zonal means (global means in the titles).

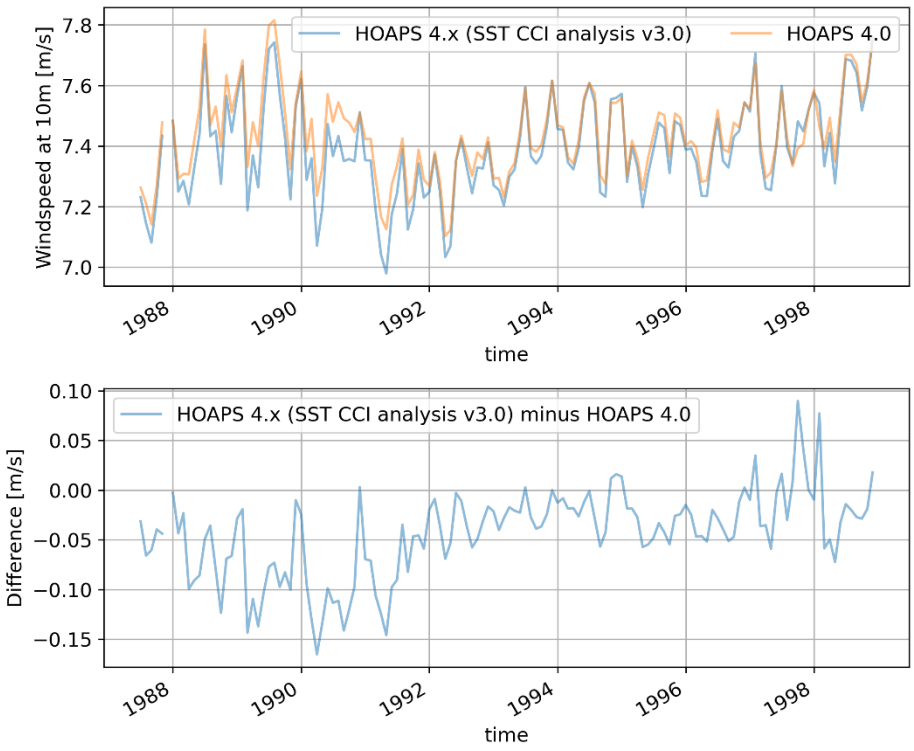

Figure 5-6: Monthly time series of 10m-wind-speed. The upper panel shows the time series of monthly global means for HOAPS 4.x (SST CCI analysis v3.0) (blue) and HOAPS 4.0 (orange) datasets for the years 1987 until 1998. The time series of their monthly difference is given in the lower panel.

5.1.5.2.2 HOAPS vs. NOCS 2.0

There is an almost constant offset between HOAPS 4.x (SST CCI analysis v3.0) and NOCS 2.0 data in northern hemispheric and southern sub-/tropical oceans (Figure 5-7, bottom left panel). In the northern hemisphere, the differences are mostly negative, i.e., NOCS 2.0 has higher wind speeds. The global mean difference is about -0.48 m/s. This corresponds to a relative difference of 6.8% between the two datasets. In the southern sub-/tropics we found mainly variations of wind speed differences close to 0 m/s. The southern ocean is dominated by positive differences above 1 m/s, i.e., HOAPS 4.x (SST CCI analysis v3.0) shows larger values. We keep in mind here that NOCS 2.0 data bases on ship measurements. Therefore the NOCS 2.0 data is delivered with a quality flag. We see from the maps (light and dark grey shadings in Figure 5-7) that most of the southern hemispheric oceans are marked with partly unreliable values, especially the southern ocean around Antarctica. Due to the lack of observations used for NOCS 2.0 data, a larger discrepancy between HOAPS 4.x (SST CCI analysis v3.0) and NOCS 2.0 is expected.

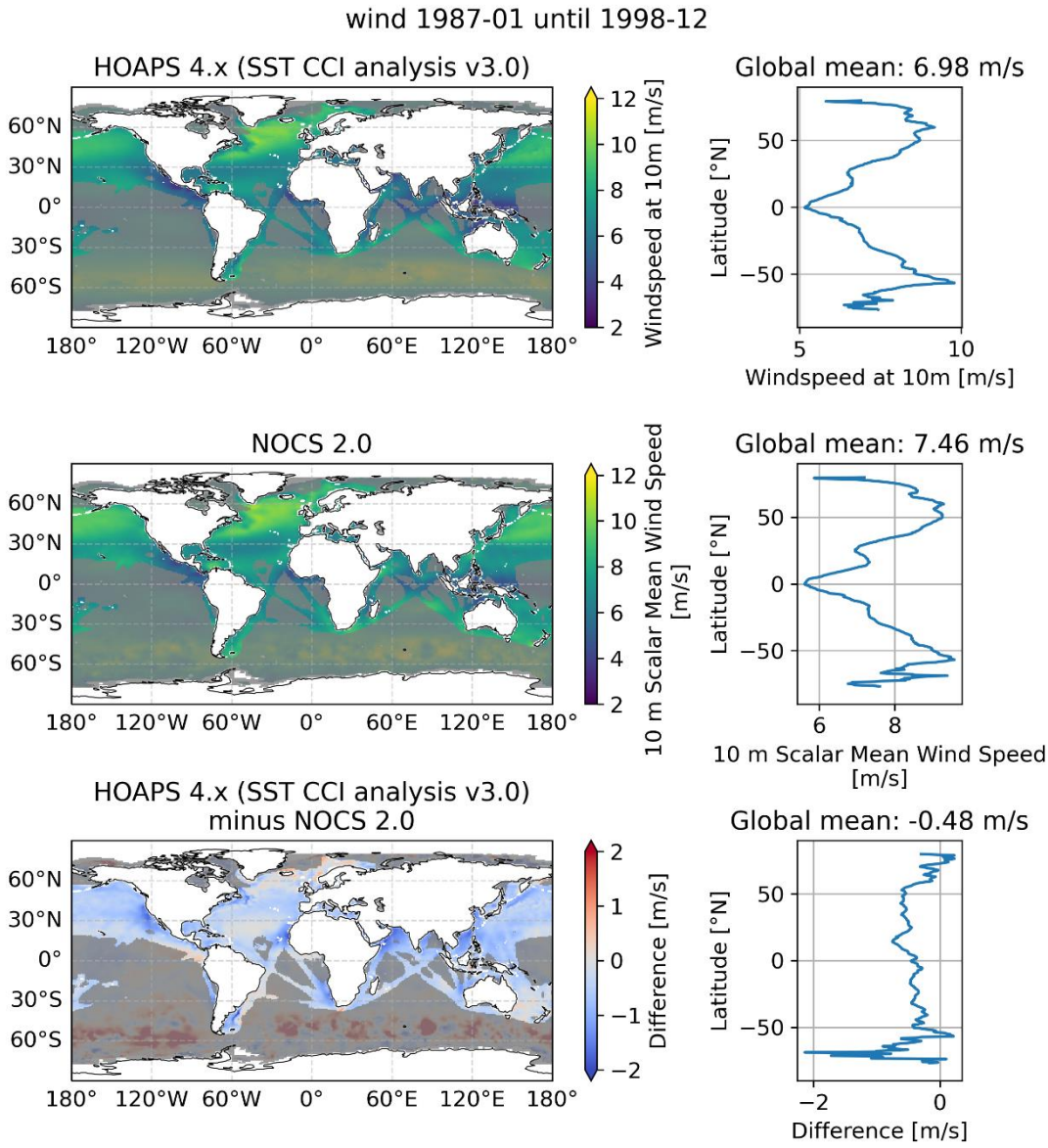

Figure 5-7: Mean wind speed fields of HOAPS 4.x (SST CCI analysis v3.0) and NOCS 2.0 for the years 1987 until 1998. The top row shows the spatial variations of the HOAPS 4.x (SST CCI analysis v3.0) data. The panels in the middle illustrate the NOCS 2.0 dataset. The bottom row shows the difference between both datasets. Respective two-dimensional fields are plotted on the left side. The right column shows the corresponding zonal means (global means in the titles). The grey shading marks areas of unreliable NOCS 2.0 data, i.e. less than 60% of all months from January 1987 until December 1998 are used for the average. Please note: Global and zonal means in the right column are based only on all grid cells/times for which high quality NOCS data is available. In case of global and zonal means, we do not filter for a minimum amount of available months.

We found similar features for the differences between HOAPS 4.0 and NOCS 2.0 data (respective figure is not shown here). As the differences between HOAPS 4.x (SST CCI analysis v3.0) and HOAPS 4.0 (Figure 5-5, bottom row) indicate, too, the global mean wind speed and global mean difference with respect to HOAPS 4.0 are of equal size as the afore-mentioned ones with respect to HOAPS 4.x (SST CCI analysis v3.0).

The wind speeds differences time series (Figure 5-8) reveal a mixed picture for global mean differences of both HOAPS 4.x (SST CCI analysis v3.0) vs. NOCS 2.0 and HOAPS 4.0 vs.

NOCS 2.0 data, with the values fluctuating in a similar range from -0.7 m/s up to -0.1 m/s. It is not obvious from the time series that one of the two HOAPS datasets is in general closer to the independent NOCS 2.0 dataset. The phases discussed above in the scope of the HOAPS-internal comparison can also be identified here, albeit less pronounced.

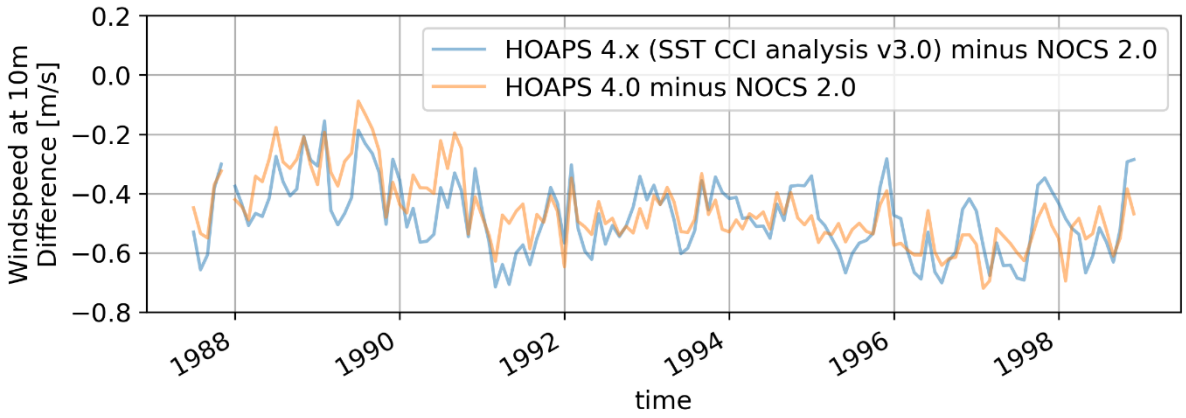

Figure 5-8: HOAPS minus NOCS 2.0 difference time series of global mean 10m-wind-speed. The figure shows the time series of monthly global mean differences for the parameter wind speed. The blue line illustrates the data for HOAPS 4.x (SST CCI analysis v3.0) minus NOCS 2.0 difference. The orange line displays the HOAPS 4.0 minus NOCS 2.0 data. Both time series cover the period 1987 until 1998. Please note: Both time series have been computed by using only grid cells that contain high quality NOCS data.

5.1.5.3 EVAPORATION AND LATENT HEAT FLUX

5.1.5.3.1 SST CCI analysis v3.0 vs. OISST

The HOAPS algorithm derives evaporation from the latent heat flux. The details on the computation of evaporation are given in the HOAPS 4.0 Algorithm Theoretical Baseline Document (Andersson et al., 2016) in section 3.3.3. The latent heat flux estimation uses the COARE bulk aerodynamic approach by Fairall et al. (1996, 2003) in an adapted COARE 2.6a (Bradley et al., 2000) version. The used COARE algorithm for HOAPS is equivalent to COARE 3.0 (Fairall et al., 2003). Besides air density, Dalton number and specific latent heat of evaporation, the main input parameters of this bulk approach are near HOAPS surface wind speed (see above) and the difference between the saturation specific humidity minus HOAPS near surface specific air humidity. As described in the HOAPS 4.0 ATBD (Andersson et al., 2016), the saturation specific humidity is calculated from SST using the Magnus formula, while HOAPS near-surface humidity is derived from the microwave observations directly, through a linear combination of per-channel brightness temperatures (independent of SST). We expect both parameters (evaporation and latent heat flux) will show changes with respect to the differing input SST data as SST enters the respective derivations through the saturation humidity, air density and wind speed (Anderson et al., 2011, 2016).

Both datasets, HOAPS 4.x (SST CCI analysis v3.0) and HOAPS 4.0 (OISST), show the typical spatial features for evaporation (Figure 5-9) / latent heat flux (Figure 5-10). These features are the maxima in the area of the sub-/tropical ocean gyres, decreasing evaporation towards the poles, the drop of the evaporation rate in the ITCZ, and higher evaporation/upward latent heat flux in the regions of warm western boundary currents. The global mean evaporation difference between both datasets is about 0.12 mm/d (3.6%). The higher evaporation in HOAPS 4.x corresponds to slightly higher SST in the SST CCI analysis v3.0 data.

The difference plot at the bottom of Figure 5-9 indicates generally higher values in HOAPS 4.x (SST CCI analysis v3.0) compared to HOAPS 4.0. Especially the western boundary currents in the Atlantic Ocean, the Indian and southern Pacific Ocean are regions with larger evaporation values in HOAPS 4.x (SST CCI analysis v3.0) compared to HOAPS 4.0. The North Atlantic

boundary current and the Agulhas current at the southern tip of Africa feature peak deviations among these and are also showing up clearly in the direct SST comparison (Figure 5-1, bottom left).

We also note, the drop of the ITCZ in the Pacific is more pronounced in HOAPS 4.x (SST CCI analysis v3.0) than it is in HOAPS 4.0. The same is valid for the upwelling regions near the coasts of North and South America, also in line with the SST comparison (Figure 5-1).

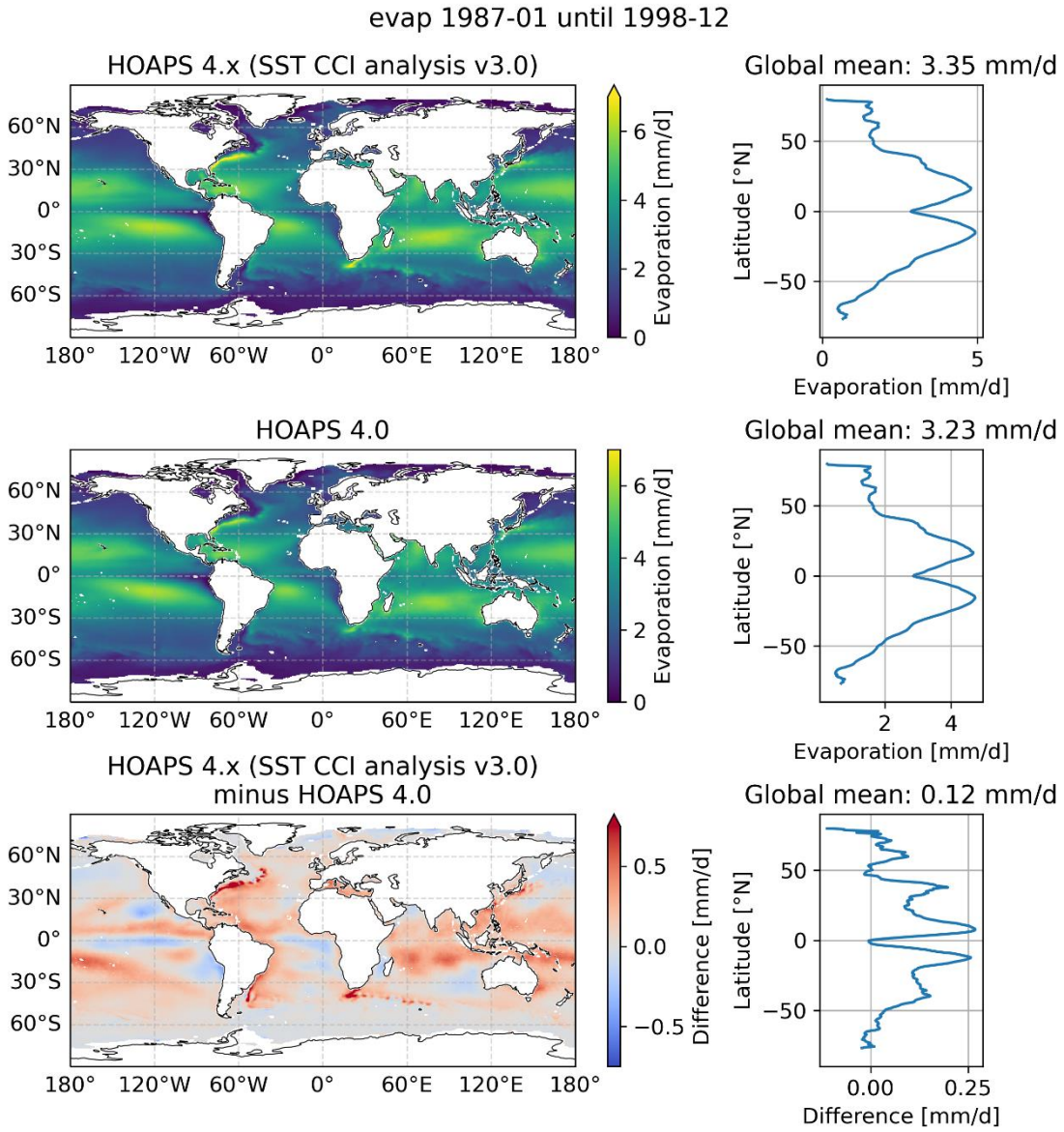

Figure 5-9: Mean evaporation for the years 1987 until 1998. The top row shows the spatial variations of the HOAPS 4.x (SST CCI analysis v3.0) data. The panels in the middle illustrate the HOAPS 4.0 dataset. The bottom row shows the difference between both datasets. Respective two-dimensional fields are plotted on the left side. The right column shows the corresponding zonal means (global means in the titles).

Corresponding illustrations for the latent heat flux are given in Figure 5-10. Since evaporation estimation depends on the latent heat flux, spatial features and zonal averages are similar. The latent heat flux' global mean difference (HOAPS 4.x (SST CCI analysis v3.0) minus HOAPS 4.0) between both datasets is 3.18 W/m^2. That is 3.4% of the global mean latent heat flux.

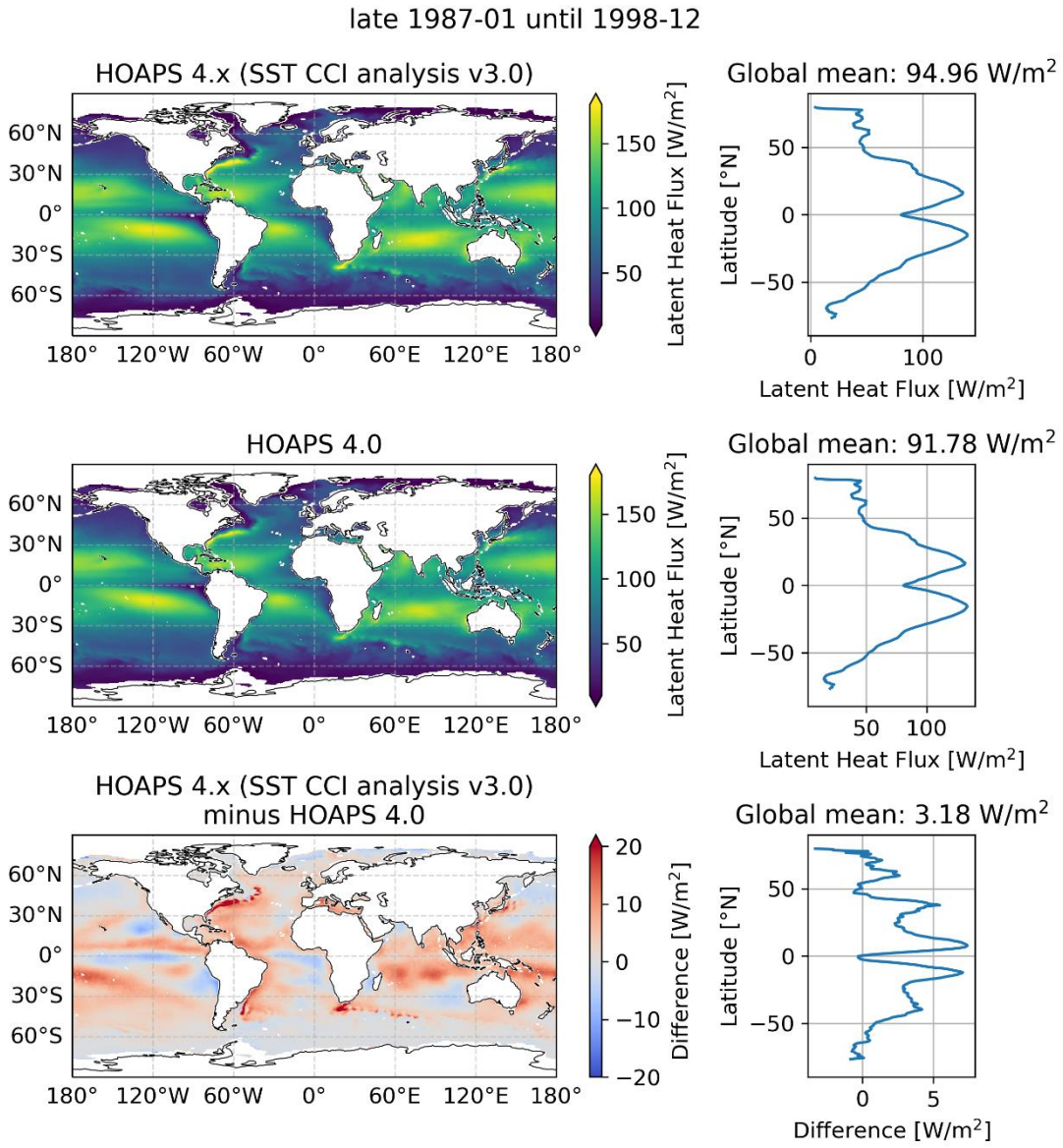

Figure 5-10: Mean latent heat flux for the years 1987 until 1998. The top row shows the spatial variations of the HOAPS 4.x (SST CCI analysis v3.0) data. The panels in the middle illustrate the HOAPS 4.0 dataset. The bottom row shows the difference between both datasets. Respective two-dimensional fields are plotted on the left side. The right column shows the corresponding zonal means (global means in the titles).

The time series for the HOAPS parameters evaporation (Figure 5-11) and latent heat flux (Figure 5-12) show a permanent offset between HOAPS 4.x (SST CCI analysis v3.0) and HOAPS 4.0 data. This offset is positive for the entire period 1987–1998. It varies from 0.01 mm/d up to about 0.20 mm/d around the global mean difference of 0.12 mm/d for the parameter evaporation. In case of the latent heat flux differences, the lower and upper limits as well as average difference are 0 W/m², 6 W/m² and 3.18 W/m².

There is no trend visible for the differences in this period. Consequently, the increase in evaporation (respective latent heat flux) due to the SST CCI analysis v3.0 could be seen as stable in time.

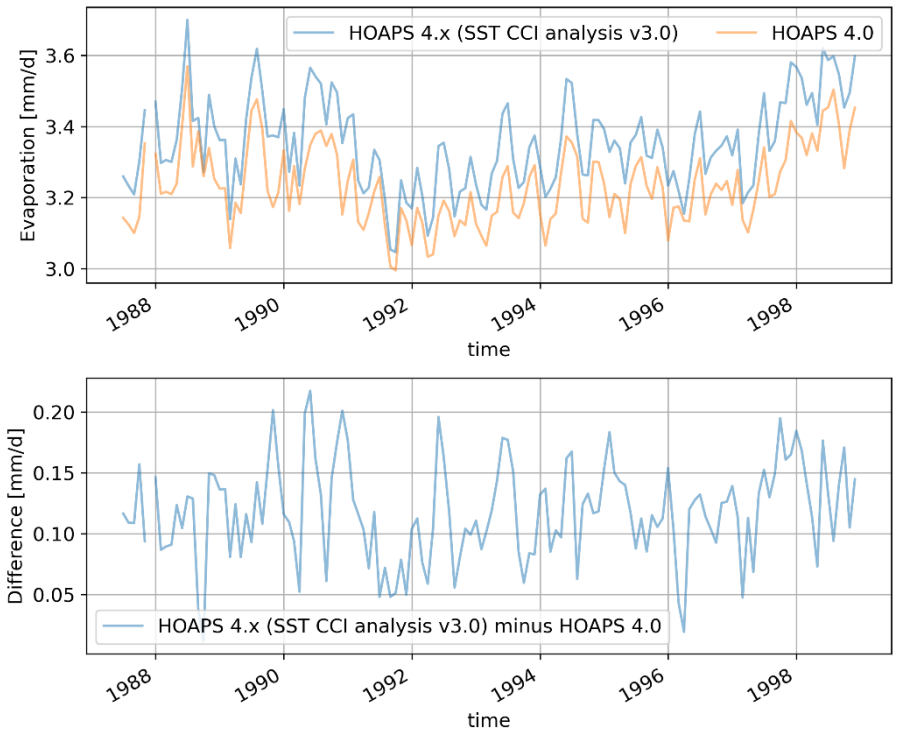

Figure 5-11: Monthly time series of evaporation. The upper panel shows the time series of monthly global means for HOAPS 4.x (SST CCI analysis v3.0) (blue) and HOAPS 4.0 (orange) datasets for the years 1987 until 1998. The time series of their monthly difference is given in the lower panel.

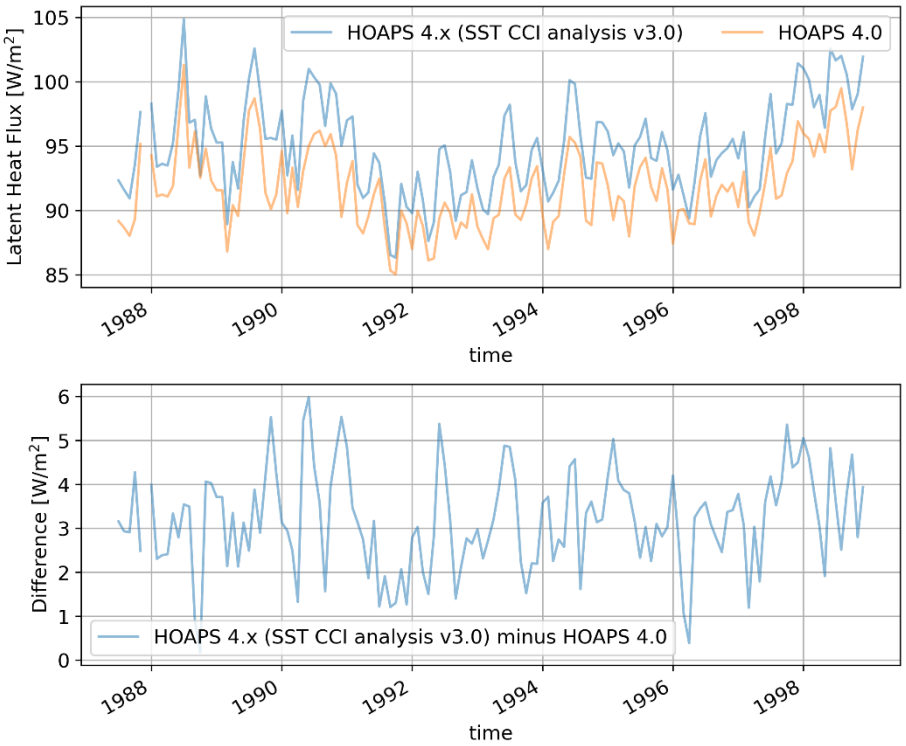

Figure 5-12: Monthly time series of latent heat fluxes. The upper panel shows the time series of monthly global means for HOAPS 4.x (SST CCI analysis v3.0) (blue) and HOAPS 4.0 (orange) datasets for the years 1987 until 1998. The time series of their monthly difference is given in the lower panel.

5.1.5.3.2 HOAPS vs. NOCS 2.0

Since the NOCS 2.0 dataset does not contain evaporation, we compare HOAPS 4.x (SST CCI analysis v3.0) and NOCS 2.0 in terms of latent heat flux here. The respective maps and zonal means are displayed in Figure 5-13. Similar large-scale features can be found in both datasets (see top and middle maps of Figure 5-13). As in previous comparisons to NOCS 2.0 (above), the global mean of 101.92 W/m^2 differs from the value given in Figure 5-10 since we applied the quality mask of the NOCS 2.0 dataset in order to find reliable data points.

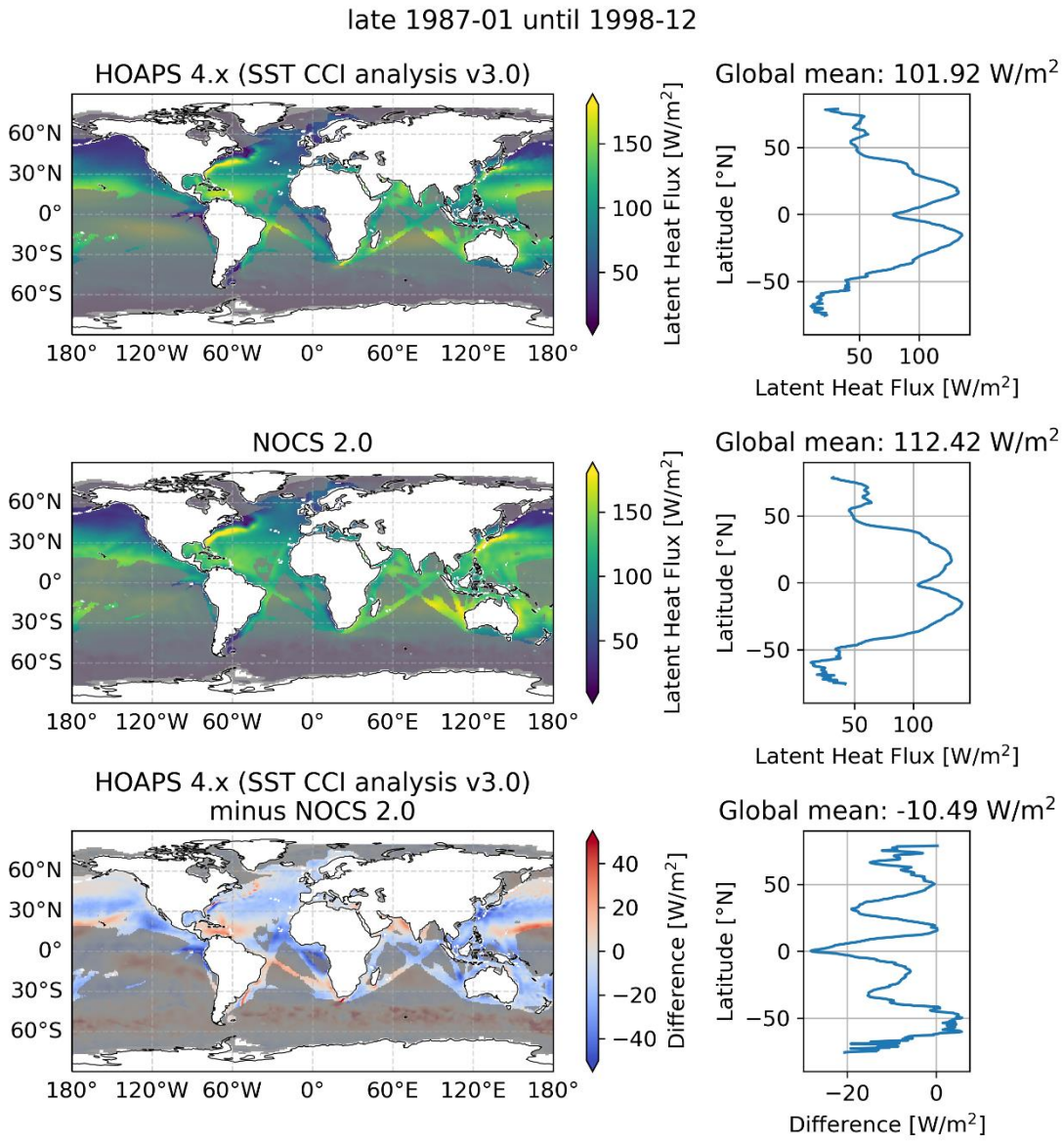

Figure 5-13: Mean latent heat fluxes from HOAPS 4.x (SST CCI analysis v3.0) and NOCS 2.0 for the years 1987 until 1998. The top row shows the spatial variations of the HOAPS 4.x (SST CCI analysis v3.0) data. The panels in the middle illustrate the NOCS 2.0 dataset. The bottom row shows the difference between both datasets. Respective two-dimensional fields are plotted on the left side. The right column shows the corresponding zonal means (global means in the titles). The grey shading marks areas of unreliable NOCS 2.0 data, i.e. less than 60% of all months from January 1987 until December 1998 are used for the average. Please note: Global and zonal means in the right column are based only on all grid cells/times for which high quality NOCS data is available. In case of global and zonal means, we do not filter for a minimum amount of available months.

HOAPS 4.x (SST CCI analysis v3.0) differs from NOCS 2.0 by -10.49 W/m^2 in the global mean. This difference is equivalent to a lack of 10.3% of the global mean latent heat flux in NOCS 2.0 compared to HOAPS 4.x (SST CCI analysis v3.0). Many local differences arise in the tropics and subtropics especially in the Atlantic and Pacific (Figure 5-13, bottom left). The zonal mean differences show three minima at about 30 °N/S and near the Equator. Two reliable maxima can be found at about 15 °N and in the northern mid-latitudes. Both maxima exhibit zonal differences near to zero, i.e. HOAPS 4.x (SST CCI analysis v3.0) and NOCS 2.0 do not differ for these latitude bands on a zonal scale. Both zonal maxima differ in their respective origin. The northern mid-latitude maximum results from an area where differences are close to zero (see Figure 5-13, bottom left panel). The other zonal maximum (near 30 °N) is a result of two dipole features. Higher NOCS 2.0 latent heat fluxes are situated in the eastern Atlantic/Pacific and smaller ones can be found in the western parts of both oceans. The zonal maximum at zero indicates that the poles cancel each other out.

Two separated features dominate the minima. The first one is located in the subtropical Atlantic. The second pattern can be found in the Pacific Ocean. Features of smaller latent heat flux in the HOAPS 4.x (SST CCI analysis v3.0) data for both locations cover both areas. These features are not present in the NOCS 2.0 data.

Over large parts of the global oceans, the difference between SST CCI analysis v3.0 and NOCS 2.0 are relatively constant, with NOCS 2.0 exceeding SST CCI analysis v3.0 slightly (Figure 5-3, bottom left panel). However, in key regions such as western boundary currents, the differences are shifted away from this large-scale mean. These more local features and the non-linearity of the HOAPS retrieval lead to more nuanced differences in latent heat flux (Figure 5-13, bottom left panel).

As before, with many features being the same as for the HOAPS 4.x / NOCS 2.0 comparison, we do not present a respective figure for comparing HOAPS 4.0 data with NOCS 2.0 here.

Now, we will take a closer look at the temporal evolution of global mean differences (Figure 5-14) between both HOAPS data sets and NOCS 2.0 respectively. Apart from April 1990, the differences with respect to HOAPS 4.x (SST CCI analysis v3.0) show higher (less negative) values than the HOAPS 4.0 minus NOCS 2.0 differences. I.e., the HOAPS 4.x (SST CCI analysis v3.0) latent heat flux is closer to the NOCS 2.0 dataset than the data from HOAPS 4.0. The means of both time series are -10.49 W/m^2 (HOAPS 4.x /SST CCI analysis v3.0) and -14.24 W/m^2 (HOAPS 4.0 / OISST), respectively, given their variability. Both times series do not show a clear trend. Thus, we expect HOAPS 4.x (SST CCI analysis v3.0) and HOAPS 4.0 datasets to be stable in time with respect to NOCS 2.0. A slight improvement in stability might be visible in HOAPS 4.x: in early 1992 the HOAPS 4.x bias is less negative than the bias for HOAPS 4.0, i.e., the bias for HOAPS 4.0 might exhibit a small break. A comparable feature is hardly visible in the lower panel of Figure 5-12 where both HOAPS versions are compared directly. It is noted that the availability of high quality NOCS data is biased towards the northern hemisphere and NOCS itself might have (small) stability issues. This requires more analysis.

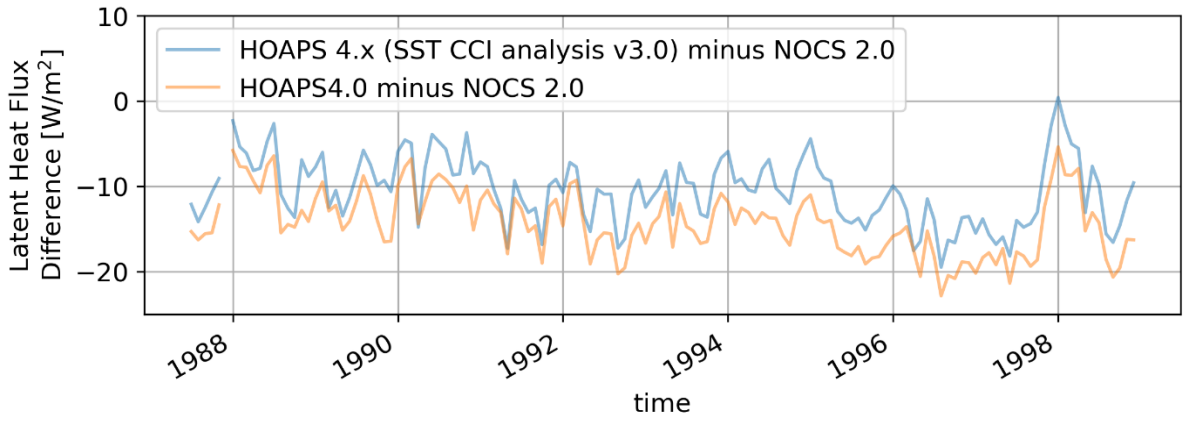

Figure 5-14: HOAPS minus NOCS 2.0 difference time series of global mean latent heat fluxes. The figure shows the time series of monthly global mean differences for the parameter latent heat flux. The blue line illustrates the data for HOAPS 4.x (SST CCI analysis v3.0) minus NOCS 2.0 difference. The orange line displays the HOAPS 4.0 minus NOCS 2.0 data. Both time series cover the period 1987 until 1998. Please note: Both time series have been computed by using only grid cells that contain high quality NOCS data.

5.1.6 CONCLUSIONS

In this study, we analysed the effects of using the ESA SST CCI Analysis v3.0 dataset in the production of the EUMETSAT CM SAF HOAPS dataset. We focussed on evaporation, latent heat flux and wind speed as subset of the eight EUMETSAT CM SAF HOAPS parameters. For these three HOAPS parameters, we described the features in the differences of temporal means (spatial fields) and spatial means (temporal evolution).

Here, we noticed the differences between the individual HOAPS parameters. The parameters evaporation and latent heat flux show clear spatial differences between SST CCI analysis v3.0 and OISST but with an offset being stable in time. Wind speed has spatial features that are not necessarily stable for the entire period. Such a variation requires further investigations.

Finally, we were able to reproduce a HOAPS 4 dataset using the ESA SST CCI Analysis v3.0 product. There are indications of improvements when using the SST CCI dataset. Such improvements have been found by comparing HOAPS with NOCS 2.0 data especially for the HOAPS parameter latent heat flux in terms of a reduced absolute difference between HOAPS 4.x and NOCS 2.0. We expect similar improvements for related parameters like evaporation. A full validation of this new HOAPS dataset has not yet been carried out.

5.1.7 REFERENCES

Andersson, A., Fennig, K., Schröder, M. (2011). Algorithm Theoretical Baseline Document – HOAPS release 3.2, Satellite Application Facility on Climate Monitoring.

Andersson, A., Fennig, K., Schröder, M., Graw, K. (2016). Algorithm Theoretical Baseline Document – HOAPS release 4.0, Satellite Application Facility on Climate Monitoring.

Andersson, A., Graw, K., Schröder, M., Fennig, K., Liman, J., Bakan, S., Hollmann, R., Klepp, C. (2017). Hamburg Ocean Atmosphere Parameters and Fluxes from Satellite Data – HOAPS 4.0, Satellite Application Facility on Climate Monitoring, DOI:10.5676/EUM_SAF_CM/HOAPS/V002, https://doi.org/10.5676/EUM_SAF_CM/HOAPS/V002.

Bradley, E. F., Fairall, C. W., Hare, J. E., and Grachev, A. A. (2000). An Old and Improved Bulk Algorithm for Air-sea Fluxes: COARE 2.6 A, in: Preprints, 14th Symp. on Boundary Layers and Turbulence, Aspen, CO, *Am. Meteorol. Soc.*, 294–296.

Berry, D. I., and Kent, E. C. (2009). A new air - sea interaction gridded dataset from ICOADS with uncertainty estimates, *Bulletin of the American Meteorological Society, 90*, 645–656. DOI: 10.1175/2008BAMS2639.1, https://doi.org/10.1175/2008BAMS2639.1.

Berry, D. I., and Kent, E. C. (2011). Air - sea fluxes from ICOADS: the construction of a new gridded dataset with uncertainty estimates, *International Journal of Climatology, 31*, 987–1001: DOI: 10.1002/joc.2059, https://doi.org/10.1002/joc.2059.

Fairall, C. W., Bradley, E. F., Rogers, D. P., Edson, J. B., and Young, G. S. (1996). Bulk Parameterization of Air-sea Fluxes for Tropical Ocean-Global Atmosphere Coupled Ocean-Atmosphere Response Experiment, *J. Geophys. Res., 101*, 3747–3764.

Fairall, C. W., Bradley, E. F., Hare, J. E., Grachev, A. A., and Edson, J. B., (2003). Bulk Parameterization of Air-Sea Fluxes: Updates and Verification for the COARE algorithm, *J. Climate, 16*, 571–591.

Masunaga, H., Schröder, M., Furuzawa, F. A, Kummerow, C., Rustemeier, E., and Schneider, U. (2019). Inter-product biases in global precipitation extremes, Environ. Res. Lett., 14(125016), https://doi.org/10.1088/1748-9326/ab5da9

Reynolds, R. W., Smith, T. M., Liu, C., Chelton, D. B., Casey, K. S., Schlax, M. G. (2007). Daily High-Resolution-Blended Analyses for Sea Surface Temperature, *J. Climate, 20*, 5473–5496, doi: http://dx.doi.org/10.1175/2007JCLI1824.1.

Reynolds, R. W. (2009). What's New in Version 2. OISST Webpage. http://www.ncdc.noaa.gov/sites/default/files/attachments/Reynolds2009_oisst_daily_v02r00_version2-features.pdf.

Robertson, F. R., Roberts, J. B., Bosilovich, M. G., Bentamy, A., Clayson, C. A., Fennig, K., Schröder, M., Tomita, H., Compo, G. P., Gutenstein, M., Hersbach, H., Kobayashi, C., Ricciardulli, L., Sardeshmukh, P., and Slivinski, L. C. (2020). Uncertainties in Ocean Latent Heat Flux Variations over Recent Decades in Satellite-Based Estimates and Reduced Observation Reanalyses, *J. Climate, 33(19)*, 8415–8437, https://doi.org/10.1175/JCLI-D-19-0954.1

Taylor, P.K., Josey, S., Berry, D. I., Kent, E. C. (2009). NOCS (National Oceanography Centre, Southampton) Flux Datasets: marine surface meteorology, freshwater and heat fluxes, NCAS British Atmospheric Data Centre, 2019. http://catalogue.ceda.ac.uk/uuid/23443335e20d25df00ab67880b10c31c

5.2 G. Bonino (CMCC): A deep machine learning approach to predict Sea Surface Temperature over the Mediterranean Sea

5.2.1 KEY MESSAGES

- ESA SST CCI Analysis product version 3 provides a spatial and temporal coverage of the sea surface temperature field that is essential for studies with the aim to improve SST predictability over the Mediterranean Sea.

5.2.2 SCIENTIFIC ANALYSIS

5.2.2.1 AIMS OF THE STUDY

The aim of the study is to build a deep machine learning architecture to predict Sea Surface Temperature over the Mediterranean Sea.

5.2.2.2 METHOD

We applied Long Short-Term Memory (LSTM) networks to predict Sea Surface Temperature (SST) time-series. LSTM networks are types of recurrent neural networks capable of learning order dependence in sequence prediction problems, and they have been widely applied in temperature forecasting problems (Haghbin et al. 2021, Tran et al. 2021, Guo et al. 2022). We defined the LSTM with 60 neurons in the first hidden layer and 7 neurons in the output layer for predicting SST. The model is a Multivariate and Multi-step LSTM model, which means that it predicts seven time-steps of SST into the future (i.e. 7 neurons in the output layer), and we used, as input times-series, SST (from ESA CCI SST Analysis product version 3), Sea Level Pressure (SLP), Geopotential Height (GEO), Wind Speed (WS) and Sensible Heat (SENS), Latent Heat (LAT), incoming solar radiation (INC) taken from ERA5 dataset (Hersbach et al., 2020), the months of the year (MM) at time-steps t-1,t-2,t-3,t-4,t5,t-6, t-7. As a first attempt, we are trying to predict SST over two target areas, the “Western Mediterranean” and the “Eastern Mediterranean” areas in Figure 5-15. ¾ of the dataset of ESA SST CCI Analysis product version 3 is used to train the model, the remaining part to test it.

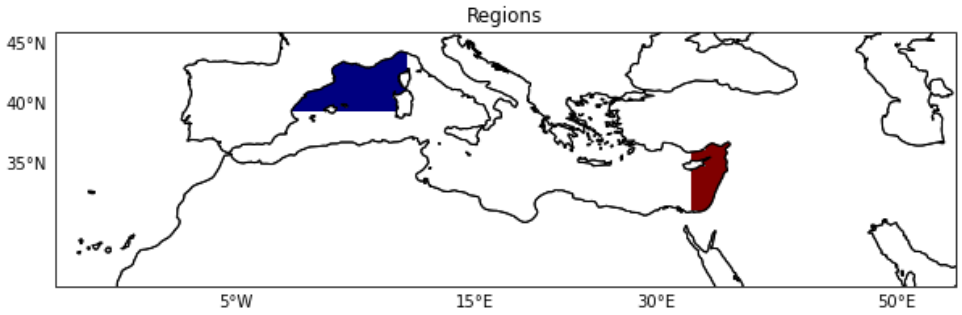

Figure 5-15. Boundaries of Western Mediterranean (blue) and Eastern Mediterranean (red) areas.

5.2.2.3 RESULTS

Figure 5-16 shows the LSTM network performance (LSTM) against a simple linear regression model (LIN) for the SST daily predictions in terms of Root Mean Square Error (RMSE) for the Western Mediterranean (Figure 5-16a) and for Eastern Mediterranean (Figure 5-16b) regions, covering the 2017-2021 period. We can appreciate that our model is skillful in predicting SST in both regions. It is very interesting that the LSTM model shows lower RMSE than the linear regression model for all the lead days in both regions. The results are promising. The objective is

to expand the prediction and the comparison to all the regions shown in Figure 5-15. Moreover, we tried to investigate the role of each driver in affecting prediction skill. We evaluated the daily prediction, randomly shuffling the values of the drivers, used as input in the test case, one at time (i.e. one experiment for each shuffled driver). The results are shown in Figure 5-17. The labels indicate, for each experiment, the driver that has been shuffled. The "true" label represents the background experiment reported in Figure 5-16. For both regions, the RMSE increases notably with respect to the background experiment when the incoming solar radiation is randomly modified. This preliminary result gives insight on the predictive power of the incoming solar radiation in driving SST variability. Further analyses are needed to properly evaluate its role. It is worth mentioning that the case in which the SST, as a driver input, is shuffled is not shown because the RMSE grows up to 5 Celsius, indicating that, as expected, the SST itself has the major predictive power.

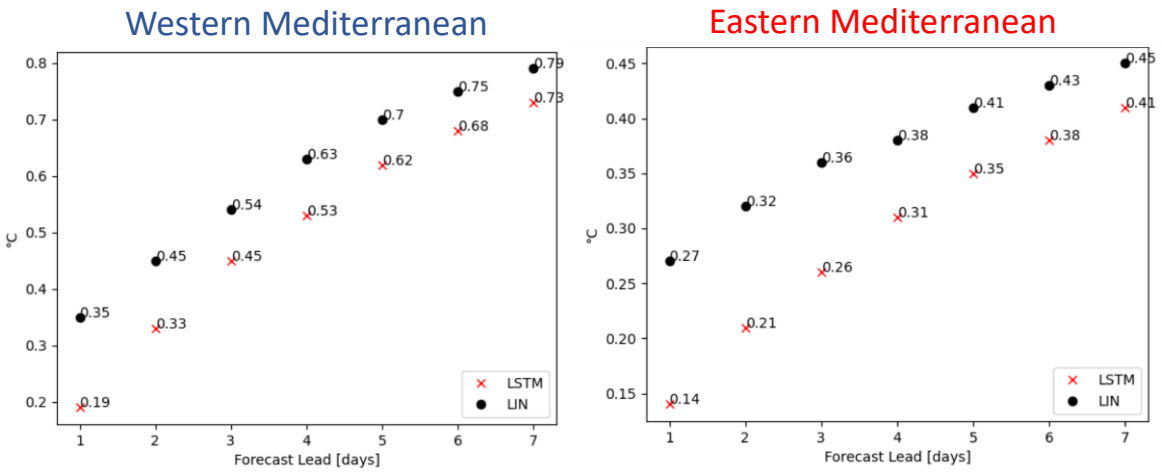

Figure 5-16. LSTM network performance (LSTM) against a linear regression model (LIN) for the SST daily predictions in terms of Root Mean Square Error (RMSE) for (a) Western Mediterranean, (b) Eastern Mediterranean regions.

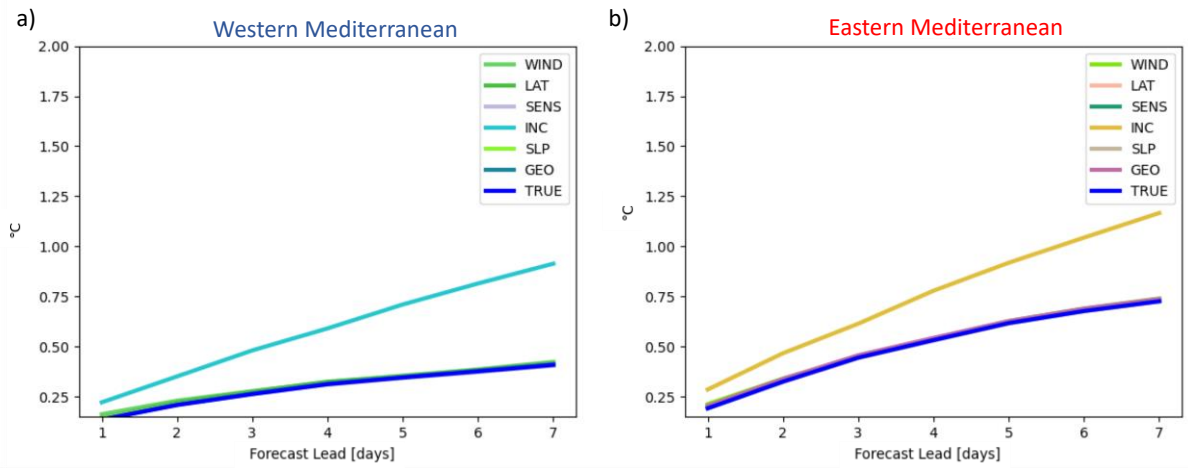

Figure 5-17. Root Mean Square Error (RMSE) of shuffled experiments for each day of forecast lead for (a) Western Mediterranean, (b) Eastern Mediterranean regions.

5.2.2.4 CONCLUSIONS

We do not assess the quality of the SST CCI product v3 directly, but the quality of the predictions is overall an indicator of the quality of the product. The preliminary work exposed in this report shows that the data looks promising to be used as train and test dataset for deep machine learning approach focused on predicting SST.

5.2.3 REFERENCES

Haghbin, M., Sharafati, A., Motta, D., Al-Ansari, N., & Noghani, M. H. M. (2021). Applications of soft computing models for predicting sea surface temperature: a comprehensive review and assessment. Progress in earth and planetary science, 8(1), 1-19.

Hersbach, H., Bell, B., Berrisford, P., Hirahara, S., Horányi, A., Muñoz-Sabater, J., Nicolas, J., Peubey, C., Radu, R., Schepers, D., et al.: The ERA5 global reanalysis, Quarterly Journal of the Royal Meteorological Society, 146, 1999–2049, 2020.

Guo, X., He, J., Wang, B., & Wu, J. (2022). Prediction of Sea Surface Temperature by Combining Interdimensional and Self-Attention with Neural Networks. Remote Sensing, 14(19), 4737.

Tran, T. T. K., Bateni, S. M., Ki, S. J., & Vosoughifar, H. (2021). A review of neural networks for air temperature forecasting. Water, 13(9), 1294

5.3 R. Quilestino-Olario, B.M. Concolis, D.P. Atup, B. Edullantes (Department of Biology and Environmental Science, University of the Philippines Cebu)

5.3.1 KEY MESSAGES

- The SST CCI analysis v3 dataset provides a balanced resolution wherein the 0.05-degree resolution can address the concerns of missing SST data of coarser SST datasets especially towards the coast. At the same time, it fits the recommended length (i.e., 30 years) needed to calculate the baseline climatology for MHW detection.
- A subset tool is requested for future downloads to aid researchers focusing on smaller boundaries in not downloading the whole 40-year global files.

5.3.2 SCIENTIFIC ANALYSIS

5.3.2.1 AIMS OF THE ANALYSIS

Marine heatwaves (MHWs) are the prolonged, discrete, anomalously warm water events (Hobday et al., 2016) which have been observed to exhibit an increasing trend in duration and frequency (Oliver et al., 2018) in line with the ongoing anthropogenic global warming (Laufkötter et al., 2020). Because of this, MHWs now pose more threats in causing adverse impacts on marine ecosystems both biologically (Smale et al., 2019) and socioeconomically (Smith et al., 2021). As an effort to monitor its extent of possible effects, detection and prediction now contributes a greater portion in the progress and advances in understanding MHWs (Benthuysen et al., 2020).

Relatively, the Philippines, as part of the center of global marine biodiversity and a fisheries-dependent nation (Carpenter & Springer, 2005), is vulnerable to the impacts of MHWs (Yao et

al., 2020). Yet, there is a current limitedness of the scientific understanding of MHWs in Philippine waters (Edullantes et al., 2022). To address this, the Survey of Heatwaves in the Philippine Seas (SHIPS) Project aims to detect MHWs within the marine biogeographic regions of the country.

Following the algorithm in Hobday et al. (2016) and Schlegel & Smit (2018), the usage of high-resolution sea surface temperature (SST) datasets is evident to produce the needed results. Preliminary detection is carried out using the Optimum Interpolation SST (OISST) of the National Centers for Environmental Information (NCEI)/National Oceanic and Atmospheric Administration (NOAA) (Reynolds et al., 2007). However, one of the noticeable results using the NOAA-OISST data is how some data is not reflected well within the narrower water bodies in the Philippines given the archipelagic setting. This “gappiness” in missing data is particularly noted near the coasts (Schlegel et al., 2019) and some previous studies (e.g., Shaltout, 2019) encountered this with the NOAA-OISST dataset as well.

Given the opportunity to initially explore the pre-release version of the SST CCI analysis v3 products, we would like to include this dataset in the comparison of SSTs among other SST products to check which can provide adequate information especially towards the coastline.

5.3.2.2 METHOD

This analysis uses the following SST datasets:

- The NOAA Optimum Interpolation SST (OISST) (Reynolds et al. 2007) which is produced using AVHRR and GTS that covers 01 September 1981 – 01 January 2023 over a 0.25° × 0.25° spatial resolution;
- The ESA SST CCI Analysis L4 product version 3.0 (Merchant et al., 2019) which is a satellite-only SST-depth analysis created by OSTIA system from SST CCI ATSR, SST CCI AVHRR, SST CCI AMSR and SST CCI SLSTR products. It has a 0.05° × 0.05° spatial resolution with daily files covering 01 January 1980 – 31 December 2021; and
- The NASA Jet Propulsion Laboratory Multiscale Ultrahigh Resolution (MUR) SST (Chin et al. 2017) created using AVHRR and MODIS (IR) with AMSR2 (MW) and iQUAM *in situ* data that is spatially 0.01° × 0.01° over a period from 01 June 2002 – 17 January 2023.

Data wrangling and visualization is done in the R environment (R Core Team, 2013), including the downloading of the NOAA-OISST and MURSST datasets through the Environmental Research Division's Data Access Program (ERDDAP) server accessible using the ‘rerddap’ package of R (Chamberlain et al., 2019). The SST CCI analysis v3 was downloaded using the provided link of the test data directory.

Due to memory limitations in the computer we are using, this analysis makes use of a single-day SST dataset, particularly on 31 December 2021, which is the last common day shared by the three SST products. The area focused is within a bounding box focused on the central Philippines with the geographic coordinates: y_{max} – 12° 11’ 9.33”, y_{min} – 8° 44’ 17.04”, x_{max} – 125° 52’ 21.83”, and x_{min} – 121° 37’ 16.59”. These coordinates were used to filter the SST CCI analysis v3 from its global data and for the subset downloading of the NOAA-OISST and MURSST data in R. For consistency, the SST values in the SST CCI analysis v3 are converted from Kelvin (K) to Celsius (°C) as the other two datasets are using this. Interpolation was also set to false for comparative purposes.

5.3.2.3 RESULTS

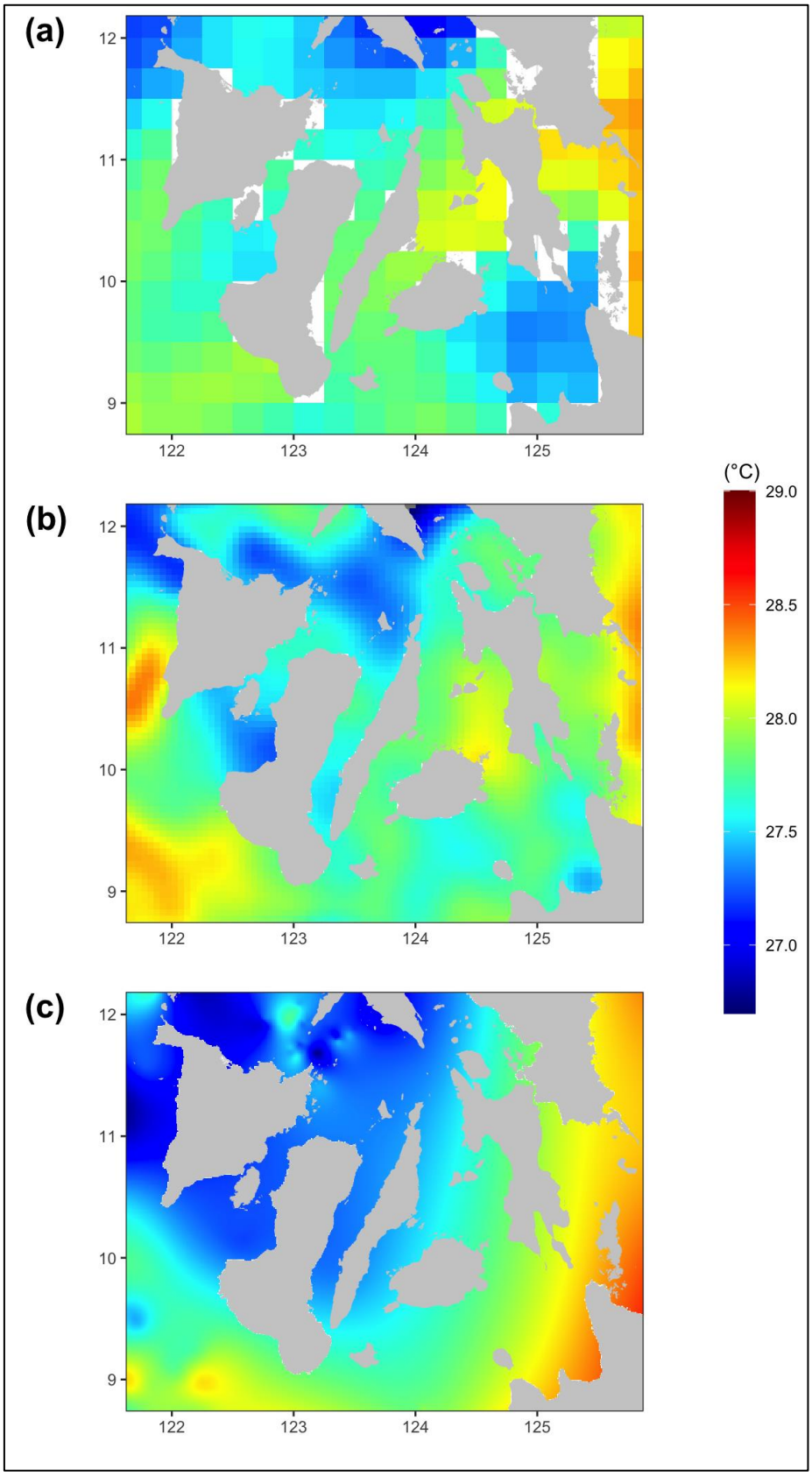

Figure 5-18. The SST values on 31 December 2021 in the central Philippines using the (a) NOAA-OISST, (b) SST CCI analysis v3, and (c) MURSST datasets.

As noticed, the NOAA-OISST output in Figure 5-18a displays the noted "gappiness" in most of the coasts of the islands within the central Philippines. Although already a high-resolution data, the 0.25° x 0.25° resolution might encounter some limitations in smaller water regions such as the narrow spaces between the islands of the Philippines. Within a smaller and "zoomed-in" boundary such as this (rather than global scale assessments), the produced output is somehow "coarser" than the other two datasets.

For the SST CCI analysis v3 output in Figure 5-18b, the issue on the missing data towards the coast is greatly resolved with minimal "white spaces" observed. The SST values also follow the pattern with the NOAA-OISST (Figure 5-18a) output where cooler values on 31 December 2021 is apparent on the northwestern parts of the map and the eastern portion reflects the warm values. Even though the squareness of pixels is still observable, the pixelization is lessened given that the SST CCI analysis v3's resolution is 5x finer (0.05° x 0.05°) than that of the NOAA-OISST's (0.25° x 0.25°).

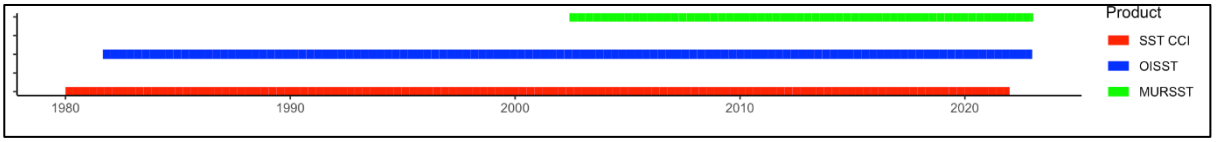

Figure 5-19. Visualization of the length of available data between the three SST products.

Lastly, the MURSST output in Figure 5-18c displays the most "fluid" SST data among the three. Given that the bounding area is small, the fineness of pixels can be attributed to the ultra-high resolution of 0.01° x 0.01° which is the smallest among the three. In terms of missing data, some minute coasts still reflect gaps but on a macro-scale are negligible at first glance. SST patterns are also similar but the coolness of the northwestern part and the warmth of the eastern portion of the map is quite more pronounced in Figure 5-18c. Certain warm areas in the western portion and cool areas in the southeastern portion for both Figure 5-18a and Figure 5-18b have also been oppositely reflected in Figure 5-18c.

Temporally, both the SST CCI analysis v3 and the NOAA-OISST provides the longest time frame of available data with around 40 years' worth of SST values. Although currently ending in 2021, the SST CCI analysis v3 provides information way back to 1980 which is not encompassed in the NOAA OISST. Additionally, scanning the segregated folder, the SST CCI analysis v3 even includes information up to 01 August 1979 which is really useful especially in analyzing historical conditions in the satellite area and comparing it to the current conditions in the post-2000s. Relatively new, the MURSST however provides the shortest length of around 20 years. In terms of MHW detection, it is recommended to define a baseline temperature climatology using 30 years of data (Hobday et al., 2016). In this sense, the SST CCI and the NOAA OISST provides a more apt dataset for the detection of MHWs. Although Schlegel et al. (2019) discusses MHW detection with sub-optimal data, the MURSST data's short length may be unable to reflect the majority of the daily anomaly at some areas, particularly in the nearshore zone (Danielson et al., 2021). This MURSST limitation places the SST CCI analysis v3 at an advantage and once it is updated to the 2022-2023 dataset, the SST CCI analysis v3 might prove more advantageous than the NOAA-OISST in terms of data time length.

5.3.3 CONCLUSIONS

The SST CCI analysis v3 can improve the detection of MHWs with a balanced resolution both in spatial and temporal aspects. Since many places in the world have archipelagic settings and coastline areas, this product can aid well in the analysis or regional assessments of MHWs where closer looks on such areas merit the need for a finer spatial resolution data with enough years that fit the recommended calculation of climatology.

5.3.4 REFERENCES

Benthuysen JA, Oliver EC, Chen K, Wernberg T. Advances in understanding marine heatwaves and their impacts. Frontiers in Marine Science. 2020:147.

Carpenter KE, Springer VG. The center of the center of marine shore fish biodiversity: the Philippine Islands. Environmental biology of fishes. 2005 Apr;72(4):467-80.

Chamberlain S, Tupper B, Mendelssohn R. Rerddap: General purpose client for 'ERDDAP' servers. R package version 0.4. 2019;2.

Chin TM, Vazquez-Cuervo J, Armstrong EM. A multi-scale high-resolution analysis of global sea surface temperature. Remote sensing of environment. 2017 Oct 1;200:154-69.

Danielson SL, Hennon TD, Monson D, Suryan RM, Campbell RW, Baird SJ, Holderied K, Weingartner T. A study of marine temperature variations in the northern Gulf of Alaska across years of marine heatwaves and cold spells. Exxon Valdez Oil Spill Trustee Council; 2021.

Edullantes B, Concolis BM, Quilestino-Olario R, Atup DP, Cortes A, Yñiguez AT. Marine Heatwaves and their Impacts: Research Perspectives in the Philippines. Philippine Journal of Science. 2022 Oct;151(5):1885-92.

Hobday AJ, Alexander LV, Perkins SE, Smale DA, Straub SC, Oliver EC, Benthuysen JA, Burrows MT, Donat MG, Feng M, Holbrook NJ. A hierarchical approach to defining marine heatwaves. Progress in Oceanography. 2016 Feb 1;141:227-38.

Laufkötter C, Zscheischler J, Frölicher TL. High-impact marine heatwaves attributable to human-induced global warming. Science. 2020 Sep 25;369(6511):1621-5.

Merchant CJ, Embury O, Bulgin CE, Block T, Corlett GK, Fiedler E, Good SA, Mittaz J, Rayner NA, Berry D, Eastwood S. Satellite-based time-series of sea-surface temperature since 1981 for climate applications. Scientific data. 2019 Oct 22;6(1):1-8.

Oliver EC, Donat MG, Burrows MT, Moore PJ, Smale DA, Alexander LV, Benthuysen JA, Feng M, Sen Gupta A, Hobday AJ, Holbrook NJ. Longer and more frequent marine heatwaves over the past century. Nature communications. 2018 Apr 10;9(1):1-2.

R Core Team. R: A language and environment for statistical computing. 2013

Reynolds RW, Smith TM, Liu C, Chelton DB, Casey KS, Schlax MG. Daily high-resolution-blended analyses for sea surface temperature. Journal of climate. 2007 Nov 15;20(22):5473-96.

Schlegel RW, Smit AJ. heatwaveR: A central algorithm for the detection of heatwaves and cold-spells. Journal of Open Source Software. 2018 Jul 31;3(27):821.

Schlegel RW, Oliver EC, Hobday AJ, Smit AJ. Detecting marine heatwaves with sub-optimal data. Frontiers in Marine Science. 2019 Nov 28;6:737.

Shaltout M. Recent sea surface temperature trends and future scenarios for the Red Sea. Oceanologia. 2019 Oct 1;61(4):484-504.

Smale DA, Wernberg T, Oliver EC, Thomsen M, Harvey BP, Straub SC, Burrows MT, Alexander LV, Benthuysen JA, Donat MG, Feng M. Marine heatwaves threaten global biodiversity and the provision of ecosystem services. Nature Climate Change. 2019 Apr;9(4):306-12.

Smith KE, Burrows MT, Hobday AJ, Sen Gupta A, Moore PJ, Thomsen M, Wernberg T, Smale DA. Socioeconomic impacts of marine heatwaves: Global issues and opportunities. Science. 2021 Oct 22;374(6566):eabj3593.

Yao Y, Wang J, Yin J, Zou X. Marine heatwaves in China's marginal seas and adjacent offshore waters: past, present, and future. Journal of Geophysical Research: Oceans. 2020 Mar;125(3):e2019JC015801.

5.4 Roshin. P. Raj (Nansen Environmental and Remote Sensing Center, and Bjerknes Center for Climate Research)

5.4.1 SCIENTIFIC ANALYSIS

5.4.1.1 AIMS OF THE STUDY

Atlantic Water (AW) transported to the Arctic Ocean from the northeast Atlantic via the Nordic Seas plays a major role in the local and global climate system. The poleward AW transport has been found to influence the sea ice cover and local climate in the Barents Sea (BS; Årthun et al., 2012; Øystein et al., 2020) and Svalbard (Walczowski and Piechura, 2011). Atmospheric teleconnection between the sea ice variability in the BS and extreme Indian monsoon rainfall is revealed recently (Chatterjee et al., 2021), thereby highlighting the possible remote impact of AW variability in the Nordic Seas and the Barents Sea. AW heat variability in the Nordic Seas has also been found to affect marine ecosystems (Hátún et al., 2009), and is also reflected in the continental climate of northwestern Europe (Årthun et al., 2017). Furthermore, it is also known that the gradual transformation of AW along its pathway in the Nordic Seas plays a major role in the formation of deep overflow waters (Eldevik et al., 2009), a main source of the North Atlantic Deep Water (Dickson and Brown, 1994). On its way into the Arctic from the Nordic Seas and the Barents Sea, the AW submerges and until recently was believed to play a minor role in the Arctic climate (Sirevaag and Fer, 2012; Rudels et al., 2013). Studies (e.g., Polyakov et al., 2017) show that the warm AW anomalies entering the Arctic via the Fram Strait (FS) are found to reach far into the Eurasian Basin in the Arctic, where they surface and release heat upward, resulting in reduced winter sea-ice formation, and thus impacting Arctic climate in a significant way. All of these studies underline the importance of monitoring the AW pathway and heat transport in the Nordic Seas. In the Barents Sea, the poleward Atlantic Water flow undergoes considerable modifications and eventually enters the Polar Basin through the St. Anna Trough (e.g., Schauer et al., 2002), thereby contributing to the renewal of the intermediate and deep water in the Arctic Ocean (Rudels et al. 1994; Jones et al. 1995; Rudels et al. 2000).

Investigation of the ‘Atlantification’ and the occurrence of ‘Marine heat waves’ in the Nordic Seas and the Barents Sea are two main recent topics of scientific research. Atlantification is a commonly used term for the increasing influence of Atlantic Water in the Arctic Ocean. Studies also projects a north eastward shift of “Atlantification” along the AW pathways in the future (Årthun et al., 2019). In short, as suggested by Asbjørnsen et al. (2020). The changes associated with the Arctic marine ecosystem have also been found to be associated with “Atlantification” (Ingvaldsen et al., 2021).

Marine heatwaves (MHW) are events of extreme sea surface temperatures (SST) and have become more frequent due to climate change (IPCC, 2021). These events have recently got much attention as they have high impacts on marine life, ecosystems, and fisheries. There are promising results in terms of predicting such extreme events (Jacox et al., 2022). Recently, such heatwaves have also been detected in the Arctic Ocean and the Barents Sea (Huang et al., 2021; Mohamed et al., 2022). However, we lack understanding of such extremes in our oceanic region, and they could potentially be more frequent in the future (Report by PlanMiljø, 2022). A contribution on MWH in the region is planned for the next Ocean Science Report (OSR8).

The main aim of this study is to investigate the interannual and decadal variability of the sea surface temperature in the Nordic Seas and the Barents Sea. A direct assessment of the Atlantification and MWH will be performed in the future.

5.4.1.2 METHOD

Simple statistical analysis such as time series analysis, climatological and composite analysis are used.

5.4.1.3 RESULTS

The Nordic Seas and the Barents Sea are buffer zones between the North Atlantic Ocean to the south and the Arctic Ocean to the North. The heat and salt from the north Atlantic are transported from the North Atlantic to the Nordic Seas and Barents Sea via the two branches of the Norwegian Atlantic Current (NwAC; Figure 5-20).

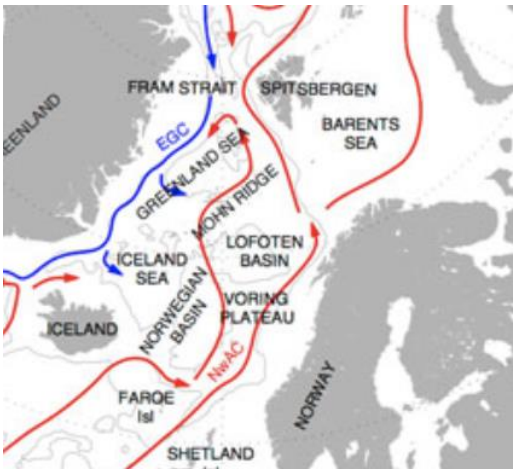

Figure 5-20. The circulation of the study region, Nordic Seas and the Barents Sea. The Nordic Seas is comprised of the Norwegian Sea (Norwegian Basin, Vøring Plateau, Lofoten Basin), The Iceland Sea and the Greenland Sea. The red and blue arrows respectively indicates the inflowing AW and outflowing polar waters.

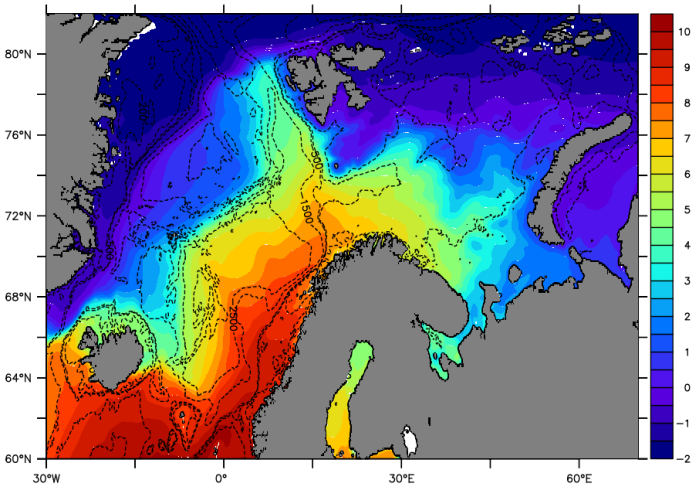

Figure 5-21. SST Climatology (1980-2021; ˚C) of the Nordic Seas and the Barents Sea. The black contours indicate the bathymetry of the region.

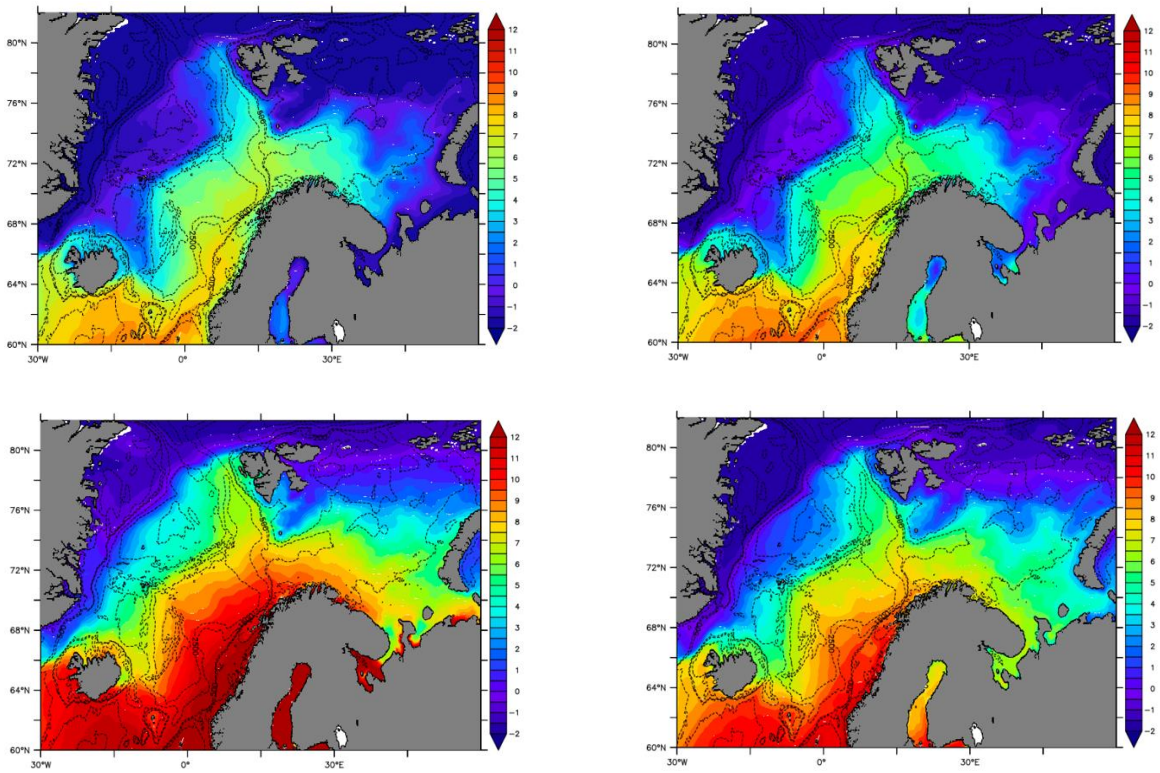

Figure 5-22. Monthly climatology (1980-2021) of the sea surface temperature (°C) in the Nordic Seas and the Barents Sea: (top left)-January; (top right)- May; (bottom left)-July; (bottom right)-October. The black contours indicate the bathymetry of the region.

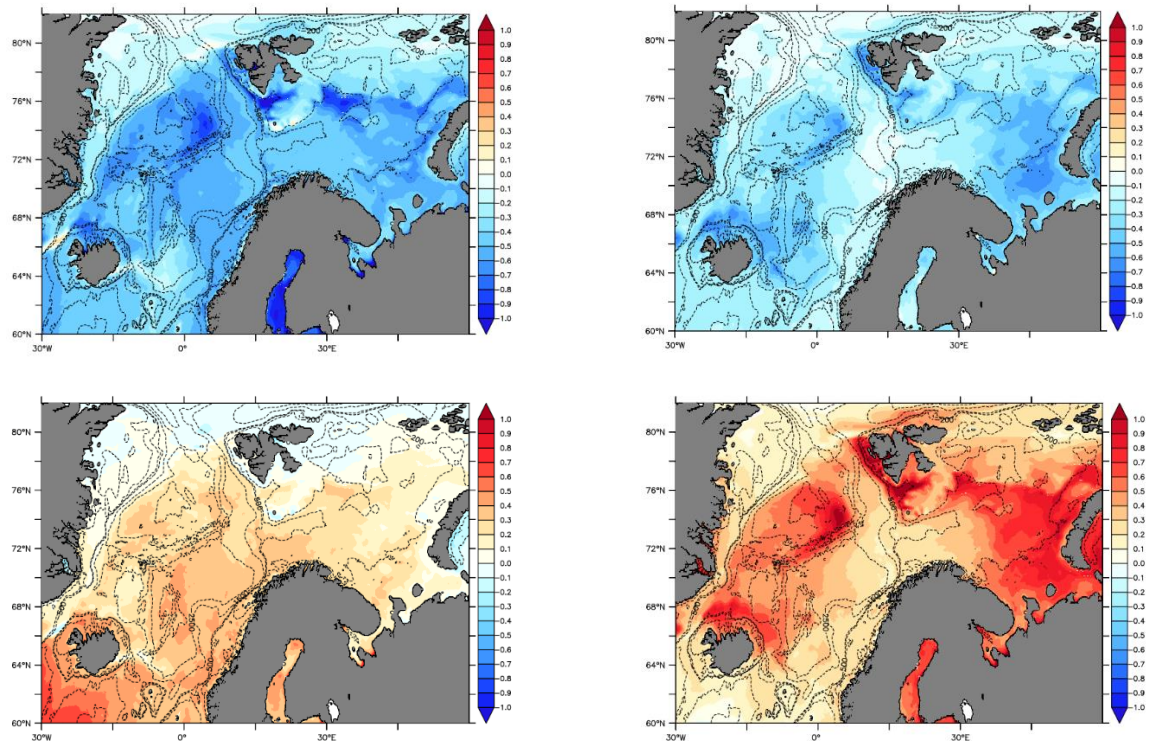

Figure 5-23. Composite 10-year mean of SST anomalies (°C) in the Nordic Seas and the Barents Sea: (top left)- 1980-1989; (top right)- 1990-1999; (bottom left)-2000-2009; (bottom right)-2010-2021. Anomalies are estimated w.r.t mean of the entire time series (1980-2021). The black contours indicate the bathymetry of the region.

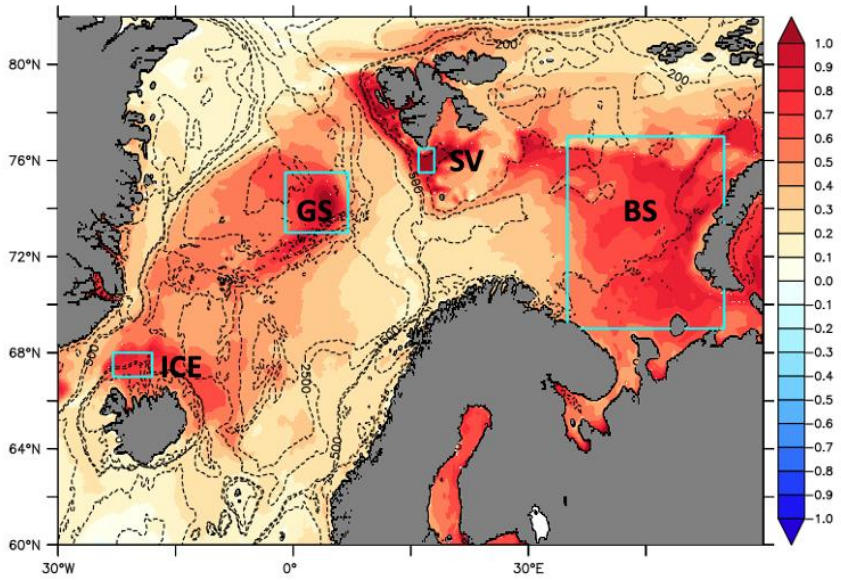

Figure 5-24. Composite mean (2010-2021) of SST anomalies (°C) in the Nordic Seas and the Barents Sea. Anomalies are estimated w.r.t mean of the entire time series (1980-2021). The black contours indicate the bathymetry of the region. The boxes shown in the figure indicates the regions selected for timeseries analysis.

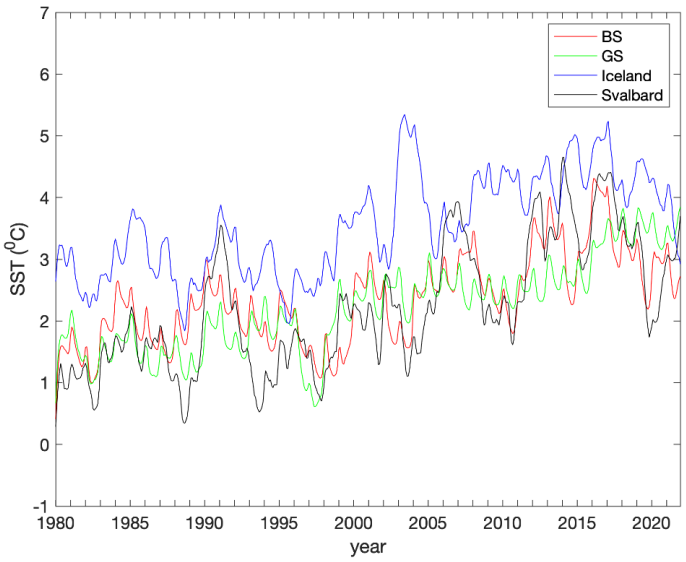

Figure 5-25. Interannual variability (12-month running mean) of SST in the 4 regions (Barents Sea box, Greenland Sea box, Iceland Sea box and Svalbard region), locations shown in Figure 5-24

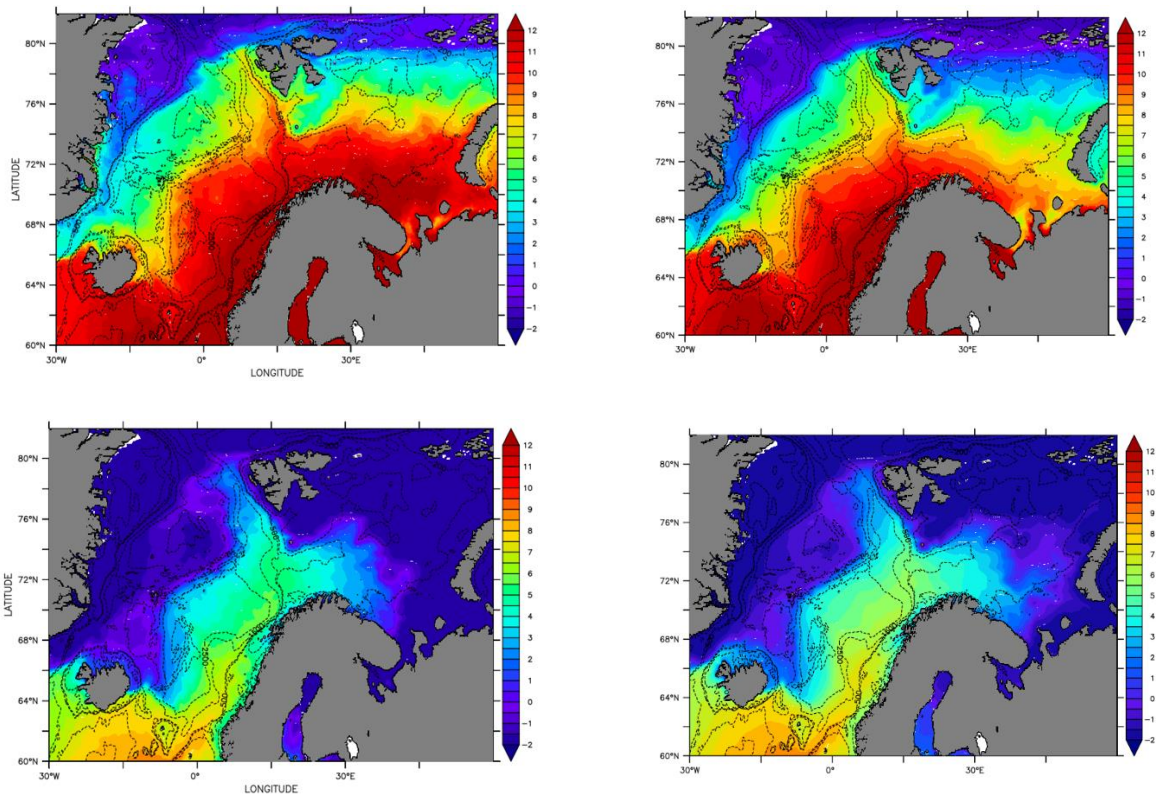

Figure 5-26. Monthly mean SST (°C) in the Nordic Seas and the Barents Sea: (top left)-August 2013; (bottom left)- April 1982 and its comparison to the respective monthly climatologies (1980-2021): (top right)-August; (bottom right)-April. August 2013 and April 1982 are the respective months during which the SST is the BS box (location in Figure 5-24) is the highest and the lowest. The black contours indicate the bathymetry of the region.

Figure 5-21 clearly portrays the signature of the inflowing AW in the eastern Nordic Seas and the Barents Sea. As the AW is transported within the region, it loses heat to the atmosphere and SST decreases. SST of the inflowing AW varies within the range of 3^{o}C -11^{o}C. The SST of the Polar waters near Greenland, originating from the Arctic are the lowest. The seasonal variability of SST in the study region is shown in Figure 5-22. During winter (example, January), the SST of the region is the lowest. The maximum SST is confined to the core of the barotropic slope current, the eastern branch of the NwAC. A very clear distinction of the Arctic front between the Greenland and Lofoten basin (Raj et al., 2019) is seen during winter and spring (example, May). Intrusion of Arctic waters into the eastern part of the Nordic Seas near the Iceland Sea is also seen. Note that while the SST is minimum in the Greenland Sea during winter, it is the lowest during Spring in the north-eastern Barents Sea. This is associated with the larger intrusion of AW in the region during winter associated with the stronger westerlies. The SST of the study region is maximum during summer and gradually decreases during Autumn. In general, the SST of the study region shows a continuous increase during the last 4 decades. The increase is the highest in 4 regions, eastern Barents Sea, near Svalbard, Greenland Sea and near Iceland. A major exception is in the region of the inflow of AW in the eastern Nordic Seas (Vøring Plateau, Lofoten Basin and Barents Sea Opening), where the SST during the 3rd decade (2000-2009) seems to be higher than the current decade (2010-2021). This indicates the increasing role of atmospheric impact on the SST of other regions in comparison to the inflowing AW.

Figure 5-25 shows an increasing trend in the SST of the 4 regions since 1997-1998 time-period. Notably there is a considerable drop in SST during the recent years (2019-2021) in the two regions (BS and Iceland). Even though the Svalbard region also witnessed a drop in the SST during 2019-2020, there has been an increase since. Unlike the other 3 regions, the GS region

does not portray the drop. SST of the BS is the found to be the highest during 2013 and 2016. The recent MHW observed in the Barents Sea is during 2016.

Figure 5-26 shows the SST during August 2013 and April 1982, when anomalously high and low SST are observed in the BS region. The comparison with the respective SST monthly climatology portrays the variability in SST provides a better picture of the reasons associated. During the anomalously positive event (August 2013), the SST of the eastern Barents Sea, especially the south-eastern part is found to show the largest variability. The colder Polar Waters in the northern part of the BS is also warmer than the climatology. In addition, the figure shows indications of warmer waters reaching the Fram Strait and the warming of the polar waters near Greenland. During April 1982 (anomalously cold event), in general there is a cooling in the BS region. The climatology map shows the intrusion of AW towards the eastern part of the BS, while the extend is limited during the anomalous event. Also, notable that the Return AW near the Fram Strait is slightly warmer during the event in comparison to the climatology. The SST variability during these anomalous events needs to be studied in detail.

5.4.1.4 CONCLUSIONS

In general, there is a gradual increase in SST of the Nordic Seas and the Barents Sea. A major exception is in the region of the inflow of AW in the eastern Nordic Seas which indicates the increasing role of atmospheric impact on the SST of the region in comparison to the inflowing AW.

5.5 J. Carton and T. Smith (Univ. Maryland and NOAA/NESDIS)

5.5.1 KEY MESSAGES

- CCIv3 has substantially reduced the cold bias in the eastern subtropical North Atlantic and Arabian Sea.
- CCIv3 still seems to have a hemispheric bias (cold North, warm south)
- CCIv3 still seems to have a western boundary current warm bias.

5.5.2 SCIENTIFIC ANALYSIS

Here we focus on the time mean of the three years of NOAA7: 1982-4, and treat IQUAM observations as ‘truth’. To check our results we also examine the time mean difference between CCIv3 and OISSTv2 (which is locked to the in-situ observations through its bias-correction scheme). The results are shown in Figure 5-27.

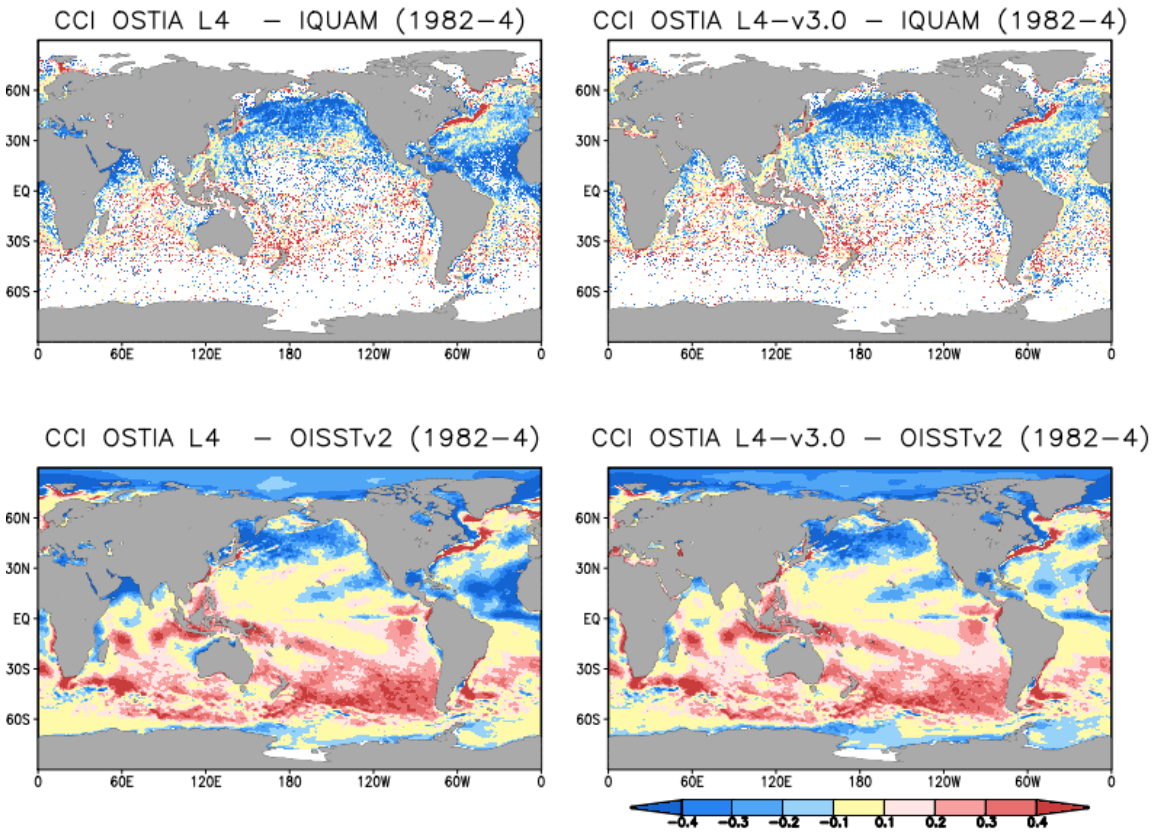

Figure 5-27. Comparison of CCI L4 SST estimates with in-situ observations and OISSTv2 during the three years 1982-1984. Lefthand column shows comparison using the regular CCI, while the righthand column shows comparison using this new CCI-v3. Here the in-situ observations are the IQUAM nighttime observations (highest quality, including ships). Comparison is carried out daily and summed.

5.5.2.1 AIMS OF THE STUDY

We examine time mean bias during 1982-1984 (NOAA7). We began by examining the time mean difference between CCI L4 and the IQUAM in-situ observations and found what looked like a pattern of O(0.2K) biases. We then wanted to find out if changes introduced in CCIv3 have eliminated the time-mean bias.

5.5.2.2 METHOD

The time mean differences are calculated by first interpolating the CCI L4 data and binning the observations onto a ¼-deg daily global grid. The differences are computed each day and then summed over the three year period. Thus, the collocations have a maximum spatial distance of 25 km and a maximum temporal distance of 1dy.

5.5.2.3 RESULTS

Results are included in 'scientific analysis'.

5.5.2.4 CONCLUSIONS

If we are correct then the CCI team may want to look for the sources of time mean 1) hemispheric bias, and 2) western boundary current bias for NOAA07. We've looked at CCI for

NOAA9 and NOAA11 and guess that these two missions also have hemispheric and western boundary current bias.

5.6 Luisa Lamas (Instituto Hidrográfico, Portugal)

5.6.1 KEY MESSAGES

- **ESA SST CCI Analysis product version 3.0** (SST CCI v3) was compared against SST in-situ data from 15 moored buoys across the Northeastern Atlantic.
- In general, the SST_{depth} data from **SST CCI v3** reproduced well the variability and magnitude of the SST measured at every buoys location, with root mean square errors spanning between 0.2 and 0.6°C for all buoys, but one.
- The analysis did not retrieve a clear relation between the accuracy for coastal, oceanic or islandic buoys. However, on average, the **SST CCI v3** product overestimated the SST on the islandic buoys (Azores and Madeira) and underestimated the SST for continental buoys.
- Generally, the **SST CCI v3** showed a seasonal pattern of cooling winters (negative mean differences) and warmer summers (positive mean differences).
- There was no clear relation between the RMSE and the location of the buoy, suggesting that the product is consistently accurate for coastal and open ocean.

5.6.2 SCIENTIFIC ANALYSIS

5.6.2.1 AIMS OF THE STUDY

Sea surface temperature (SST) is a key parameter that influences many environmental processes, including ocean dynamics, biology and climate. For instance, thermal gradients in the upper ocean are directly related to the heat budget between the ocean and the atmosphere, which plays a crucial role in global climate. Accurate knowledge of SST with respect to not only its variability, but also its short- and long-term trends is imperative for understanding the role of the ocean in a changing climate. A good assessment of SST across the Atlantic is essential to understanding the ocean's contribution to climate change and will contribute to the effectiveness of policy decisions. Although SST data are one of the oldest datasets available, mainly from research ships, drifting and moored buoys, represent sparse and sporadic data points. Satellite observations, however, can provide continuous, global coverage of ocean surface temperature, but still need to be calibrated and validated against in situ data.

Here, the European Space Agency's Sea Surface Temperature Climate Change Initiative (ESA SST CCI) Analysis Product Version 3.0 (hereinafter **SST CCI v3)** is compared against in-situ SST data collected by 15 moored buoys located in the eastern Atlantic. The main objective of this study is to validate **SST CCI v3** data and assess the product's utility for ocean and climate studies over the Portuguese marine waters, and in particular for shallower waters, where some of the coastal buoys are moored.

5.6.2.2 METHOD

Daily values of SST_{depth} from **SST CCI v3** were compared against in situ data acquired by 15 (fifteen) coastal buoys operated by the Hydrographic Institute (IH), the University of Azores (UA), Observatory for the Environment of the Azores (OAA) and the Ports Administration of the Madeira Autonomous Region (APRAM). Data is scattered across the Eastern North Atlantic, providing a significant coverage in an area with relatively scarce in-situ data (Figure 5-28).

SST CCI v3 consists of daily files of Satellite-only SST_{depth} analysis created by OSTIA system from SST CCI ATSR, SST CCI AVHRR, SST CCI AMSR and SST CCI SLSTR products, at 0.05 deg resolution, covering the 1980 – 2021 period.

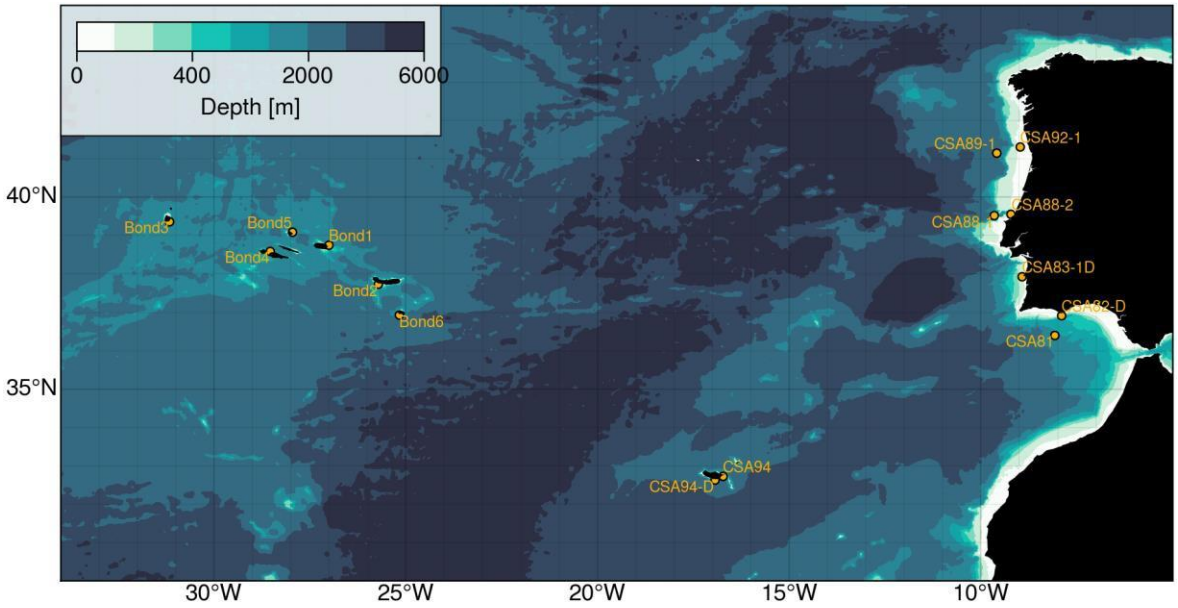

Figure 5-28. Portuguese marine waters showing the 15 coastal and oceanic moored buoys that collected the SST data used in this study.

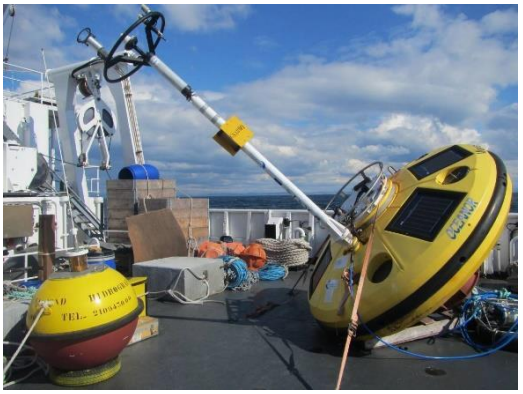

Figure 5-29. Oceanographic Datawell Waverider (left) and Meteo-oceanographic Oceanor Wavescan (right) buoys. © Instituto Hidrográfico

Observations were made by sensors attached to two types of buoys - Meteo-oceanographic Fugro Oceanor Wavescan (hereinafter FO) and Datawell Waverider (DW). Both types are equipped with a trans-receiver GPS (Global Positioning System). The FO buoys, equipped with Aanderaa 4050 temperature sensors, measure SST at approximately 1 m depth and ensure real-time access to the data through its INMARSAT-C satellite link communication system. Temperature is measured with a resolution of 0.001C and accuracy of +/- 0.03. The DW buoys are equipped with internal temperature sensors located at 0.7 m depth and have a HF link communication system installed (Figure 5-29), measuring temperature data with a resolution of 0.05C and expected accuracy of 0.2C. Information about the name, location, depth and start date of collecting temperature data is shown in Table 5-2.

Table 5-2. Position, depth, type and start date of SST measurements for each buoy. Shaded colors were added to mark different locations: red: Coastal Continental Portugal (PTC); green: Oceanic PTC; blue: Coastal Madeira (PTM); orange: Coastal Azores (PTA).

Station Name	Position (WGS 84)	Depth (m)	Buoy Type	Start Date	Match-ups N
CSA92-1	41°19.00'N 08°59.00'W	83	DW	1998	7174
CSA83-1D	37°55.27'N 08°55.73'W	97	DW	1988	8315
CSA82-D	36°54.28'N 07°53.90'W	93	DW	1986	8620
CSA89-1	41°08.92'N 09°34.90'W	1622	FO	2010	2174
CSA88-1	39°30.94'N 09°38.24'W	1850	FO	2009	2284
CSA88-2	39°33.61' N 09°12.60' W	80	FO	2010	2179
CSA81	36°23.90'N 08°04.10'W	1334	FO	2014	1883
CSA94-D	32°37.1'N 16°56.5'W	100	DW	1996	6776
CSA94	32°43.2'N 16°43.7'W	100	DW	2002	3950
Bond1	38° 45.04'N 27° 00.60'W	100	DW	2005	3709
Bond2	37° 43.89'N 25° 43.46'W	90	DW	2005	3509
Bond3	39° 21.86'N 31° 10.00'W	80	DW	2006	2633
Bond4	38° 35.26'N 28° 32.26'W	110	DW	2007	3918
Bond5	38° 05.21'N 27° 57.73'W	97	DW	2007	3997
Bond6	36°55.27'N 25°09.99'W	120	DW	2007	545

The DW SST data are acquired at a sample rate of 30 minutes, whereas the FO data are acquired at a sample rate of 1 hour. Upon reception, data follows a validation procedure at the contributing institutions, the IH, the UAC and the APRAM, process after which data are loaded into transactional local databases. For this study, the data were reprocessed following the QARTOD (Integrated Ocean Observing System, 2017) method for quality control, and were daily averaged to compare with the daily datasets of **SST CCI v3.**

SST_{depth} (20 cm) data points from the **SST CCI v3** database were extracted at each buoy location using the nearest neighbour method. The neighbouring 3x3 pixels were also extracted to analyse the uncertainties associated with point-to-pixel match-up and account for buoy displacement. The number of match-ups between the buoy data (from deployment to 31-12-2020) and the **SST CCI v3** data, N, is specified in Table 5-2.

Results from the years between each buoy deployment (all after 1981) and 2021, with sporadic gaps of in-situ data, are shown and discussed in the next section. Results will be analysed descriptively, qualitatively and quantitatively using determination coefficients (R^2), root mean square error (RMSE), and mean signed error (MSE) to assess the differences between both

datasets. Descriptive analysis also include the daily differences between both datasets (ΔT = **SST CCI v3** – in-situ SST).

The mentioned statistical parameters are calculated using the SST value at the nearest pixel and using the mean and median of surrounding 3 x 3 pixels. For readable purposes, this report will only show detailed results of three buoys, one for each section of the Portuguese EEZ: buoy CSA83-1D from Coastal Portugal Mainland, buoy Bond5 from Azores and buoy CSA94-D from Madeira. These buoys were selected based on the consistency of the record (in relation to gaps) and the overall number of match-ups.

5.6.2.3 RESULTS

The different match-up techniques used in this study (nearest, 3x3 mean and 3x3 median) resulted in differences lower than two orders of magnitude in relation to the statistical parameter computed and thus, for that reason, the analysis will be presented only for the nearest pixel method.

In general, the **SST CCI v3** represents well the variability and magnitude of the sea surface temperature measured at each buoy location, for both coastal and oceanic, located along Portugal mainland, Azores and Madeira islands (Figure 5-30). Time series analysis show the consistency of the **SST CCI v3** dataset, with no significant change in the mean differences magnitude over time. Moreover, the analysis also indicate that there is a seasonal variability of the differences, with generally the summers presenting positive anomaly (overestimation by the **SST CCI v3**) and winters with negative anomaly (underestimation by the **SST CCI v3**). The mean seasonal cycle (Figure 5-31) for each buoy, indicate that the **SST CCI v3** presents cooler winters and warmer summers for the PTC and PTA buoys and the opposite for PTM buoy. However, this result is not true for all buoys in the PTC, but is consistent for the PTA buoys. For most buoys, seasonal monthly differences were lower than 0.2°C.

Histograms using the entire match-up database are used to analyse the differences in the distribution of the **SST CCI v3** (Figure 5-32). Overall, the **SST CCI v3** data represented well the distribution of the SST for all buoys, showing bimodal distributions for the PTA and PTM buoys and unimodal distribution for the PTC buoys, as expected. The differences between in-situ and satellite-derived SST showed normal distribution centered near zero, indicative of close relation between both datasets. There is a slight difference between the ΔT distribution for the three buoys presented in Figure 5-31, showing a slight overestimation for the island buoys and underestimation for the continental buoys. Nonetheless, daily differences rarely exceeded 0.5°C.

Determination coefficients, which quantifies the relation between both datasets in terms of variability, were higher than 0.97 for the three buoys analysed in detail, indicating that the **SST CCI v3** reproduces well the observed in-situ SST (Figure 5-33). For these three buoys, the RMSE was lowest for the PTA buoy, with a value of 0.275°C, followed by the buoy from PTC, with a RMSE of 0.344°C and the highest value of RMSE, 0.368°C, was obtained for PTM buoy.

The average MSE was used qualitatively to analyse if there was, on average, a tendency for the **SST CCI v3** to underestimate or overestimate the in-situ SST. Concerning the three buoys analysed, the lowest MSE value was -0.009°C for the PTC buoy, which was also the only buoy showing negative MSE, denoting, on average, an underestimation. The other two buoys, located in the islands, showed positive MSE, 0.0.035°C and 0.065°C, respectively, indicating overestimation of the parameter. However, the magnitude of the MSE suggests that the average difference between both databases is orders of magnitude bellow the uncertainty of the measurement itself, and thus will not represent a measurement of accuracy of the data.

Figure 5-34 and Figure 5-35 summarize the statistical results obtained for all the buoys. Generally, the **SST CCI v3** reproduces well the SST measured in-situ by all the buoys, with R2 values higher than 0.96 and with an accuracy between 0.2°C (Oceanic PT buoy) and 0.6°C (PTA

buoy). A clear high value of RMSE and MSE was obtained for Bond4 buoy (PTA) which needs to be further analysed.

Overall, the **SST CCI v3** seems to underestimate (negative MSE) the temperature for the buoys in the PTC area and overestimate (positive MSE) for islandic buoys. Differences between both datasets rarely exceeded 0.5°C, but show consistent spatial (continental vs islandic) and seasonal (summer vs winter) differences. However, further analysis needs to be performed to assess the seasonal and spatial variability of the **SST CCI v3** product. The RMSE and MSE values for the coastal and oceanic buoys did not show a clear relation between the product accuracy and the fact that the buoy is located near the coast or offshore.

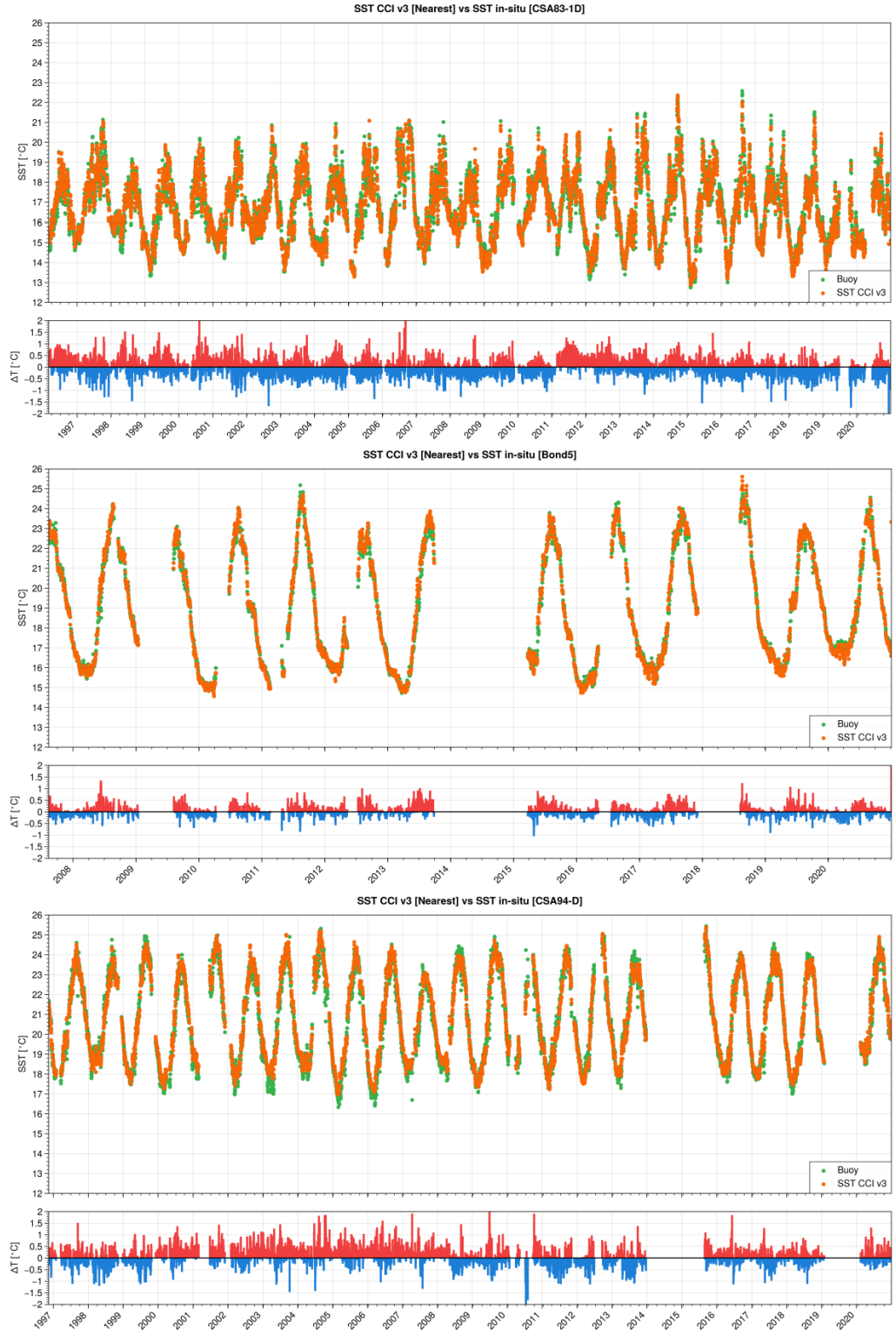

Figure 5-30. Daily SST timeseries (top panel) and difference ΔT (bottom panel) between SST CCI v3 (SSTdepth at nearest pixel; in orange) and in-situ SST (green) from (first row) CSA83-1D buoy; (second row) Bond5 buoy; (third row) CSA94-D buoy. Red (blue) represents positive (negative) values.

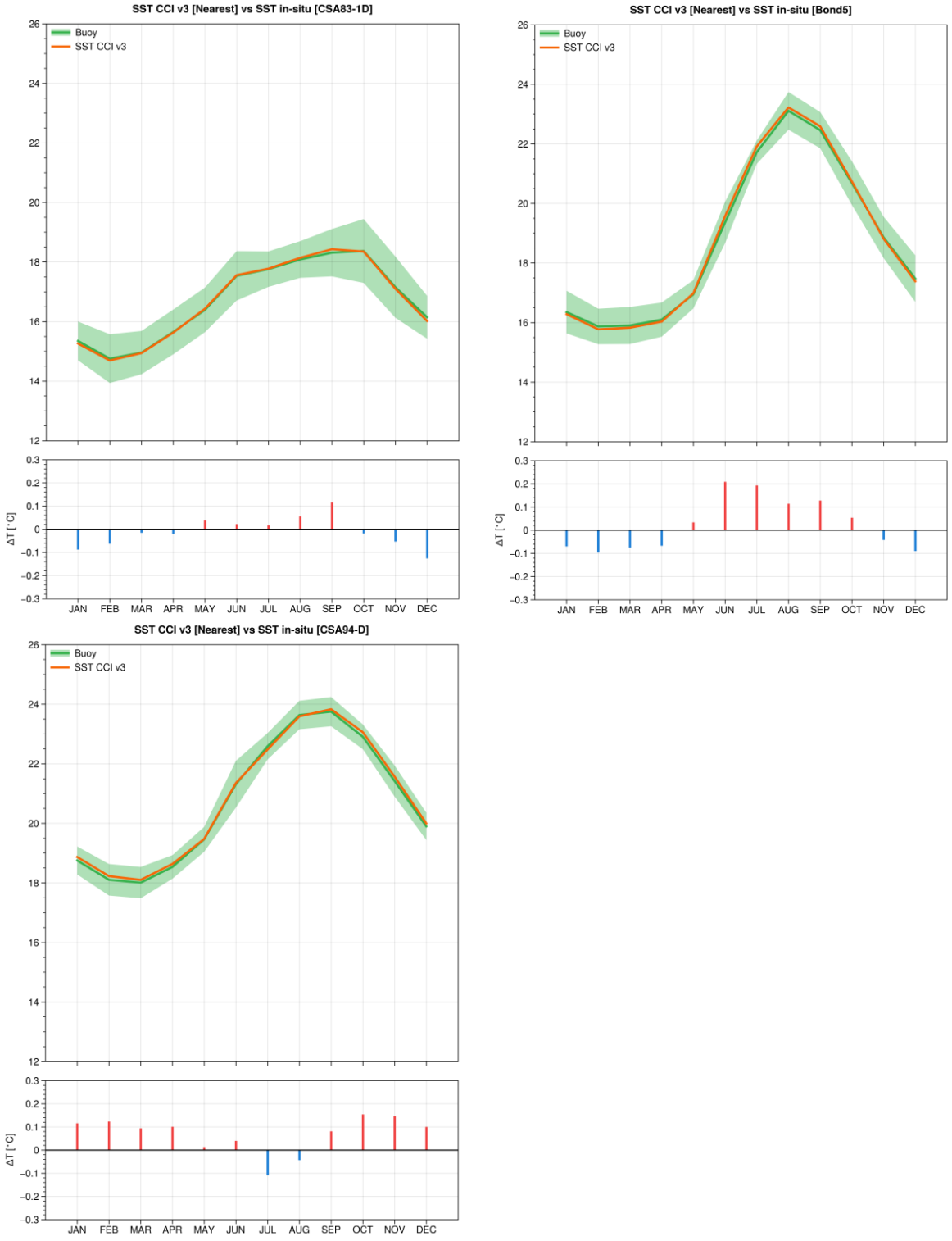

Figure 5-31. Seasonal cycle for SST (top) and difference ΔT (bottom) between SST CCI v3 (SST_{depth} at nearest pixel; in orange) and in-situ SST from CSA83-1D (top, left); CSA88-1 (top, right); Bond5 (bottom, left) and CSA94-D (bottom, right). Red (blue) represents positive (negative) values. Shaded green area represent the ± standard deviation.

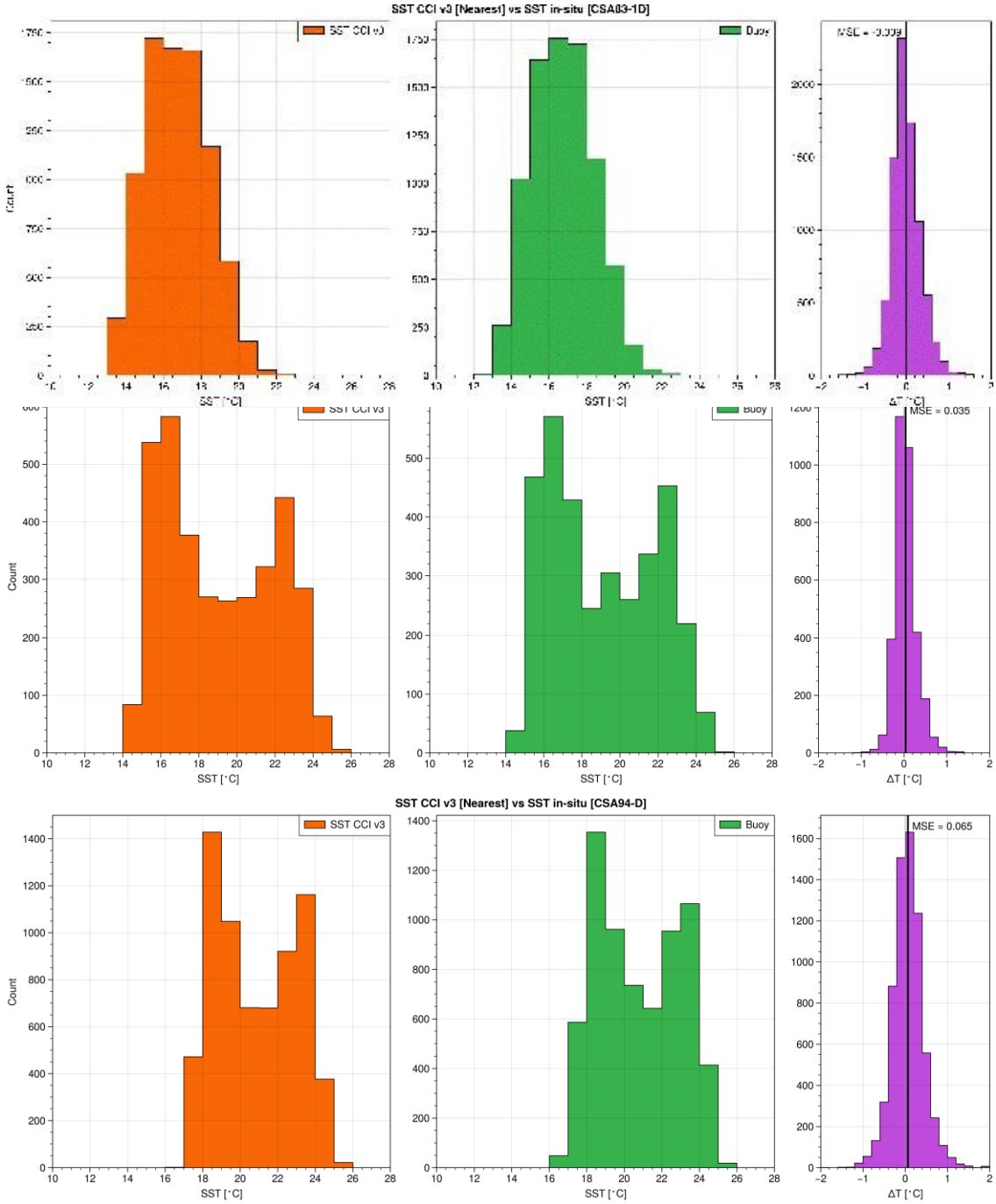

Figure 5-32. Histograms for match-up data from SST CCI v3 (left, orange) and SST buoy data (middle, green) and difference ΔT between SST CCI v3 and SST buoy data (right, purple). Top) CSA83-1D buoy; Middle) Bond5 buoy; Bottom) CSA94-D buoy.

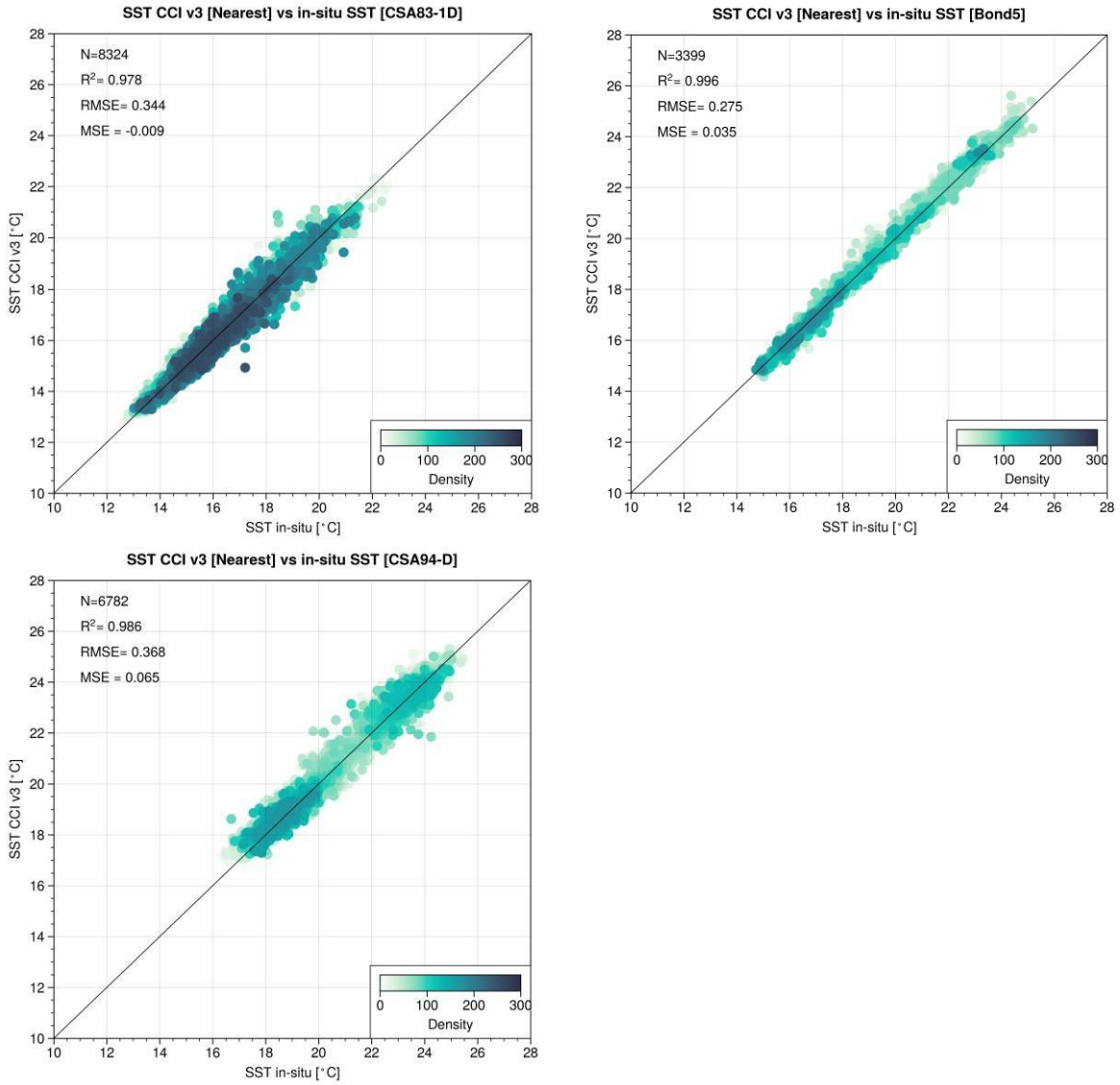

Figure 5-33. Dispersion plots with density and statistical parameters between SST CCI v3 against in-situ buoy data. N represents number of match-ups; R^2 is the coefficient of determination, RMSE the root mean square error and MSE the mean signed error. Top, left: CSA83-1D; Top, right: Bond5; Bottom, left: CSA94-D.

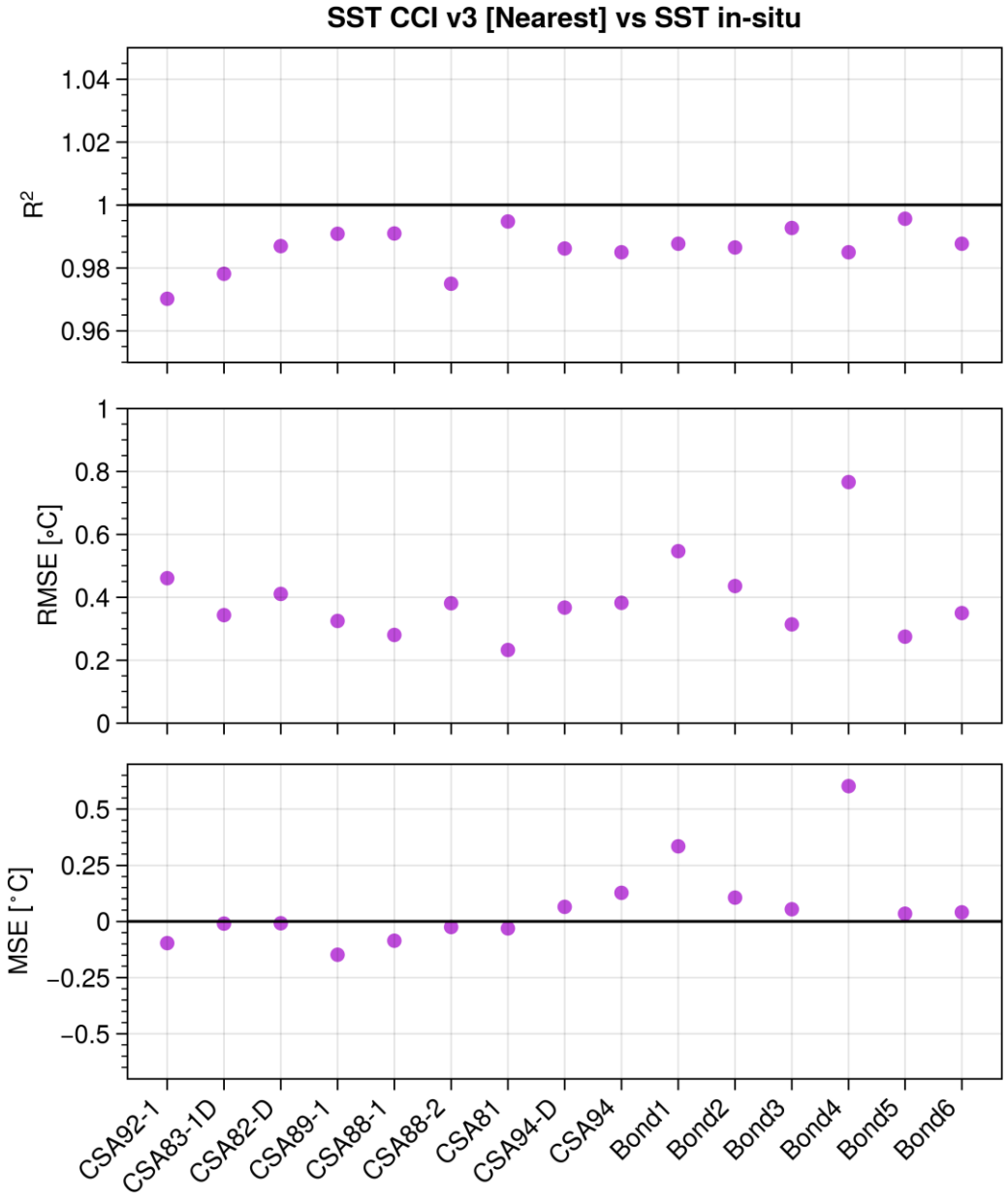

Figure 5-34. Average R2 (top), RMSE (middle) and MSE (bottom) represented for each buoy. Coastal PTC buoys: CSA92-1, CSA83-1D, CSA82-D; Oceanic PTC buoys: CSA89-1, CSA88-1, CSA88-2 and CSA81; PTM buoys: CSA94-D and CSA94; PTA: Bond1, Bond2, Bond3, Bond4, Bond5 and Bond6.

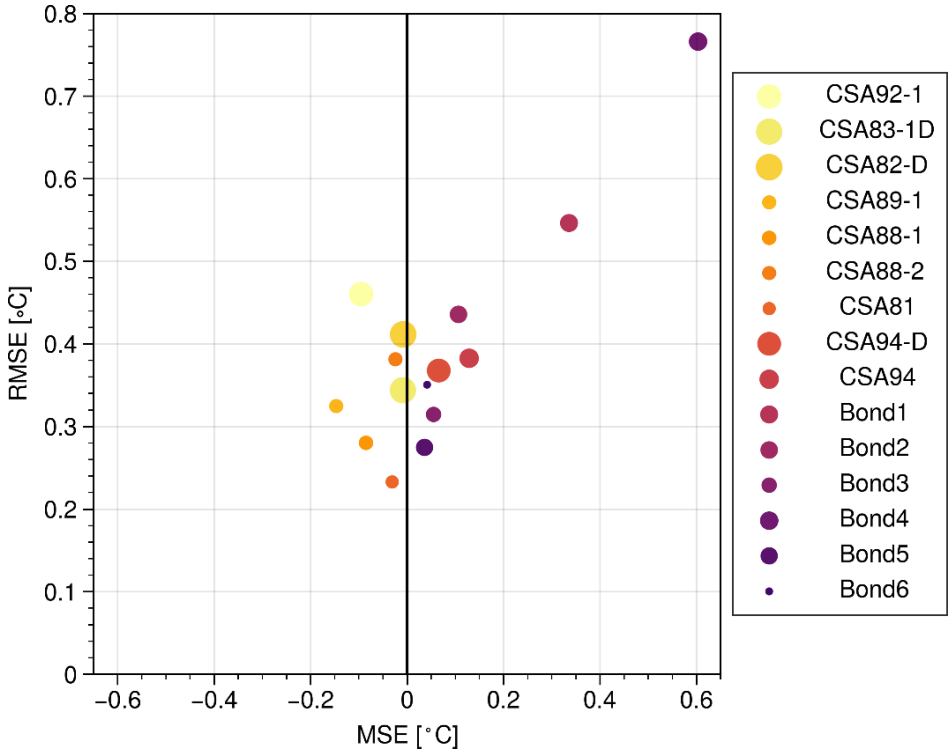

Figure 5-35. Dispersion plots of MSE vs RMSE for each buoy, coloured by buoy and sized by N (number of match-ups).

5.6.2.4 CONCLUSIONS

This report shows that the **SST CCI v3** product generally reproduces the spatial and seasonal variability of the in-situ surface temperature with an accuracy between 0.2 to 0.6°C at most of the buoys location. There is a consistent seasonal pattern of the differences between the **SST CCI v3** and in-situ SST, showing a tendency for overestimation during the summer and underestimation during the winter.

The mean differences also showed that the **SST CCI v3**, on average, underestimates the SST in the location of the continental buoys and overestimates in the islandic buoys locations. However, there was no clear relation between the RMSE and the location of the buoy, suggesting that the product is consistently accurate for coastal and open ocean.

Further analysis should be performed for inter-annual, seasonal and spatial variability.

6. FURTHER ISSUES AND RECOMMENDATIONS REPORTED BY REGISTERED USERS

6.1 Feedback on ease of use of the products and documentation

- Very easy to use.
- The SST CCI analysis v3 product is actually easy to use. R environment loads the .nc file easily and it can be prepared well due to the proper organization and stacking of data. Initially, we opt to test it in detecting MHW events. However, limitations in computer capacity inhibited us from processing since we cannot combine 40 years of data which is needed before we can filter for the Philippine seas boundary. But nevertheless, product- and documentation-wise, the SST CCI analysis v3 is easy to wrangle.
- The ESA SST CCI CCI Analysis product version 3 is easy to download and the documentation is complete.
- Daily global datasets are readily accessible and easy to work with. The processing and analysis of the data during this work was performed using Python 3.8 and no relevant problems were encountered.
- The documentation was clear and sufficient to understand the data and use it.
- More information on the uncertainty of each SST CCI v3 measurement would be beneficial for this analysis.

6.2 Recommendations

- Downloading the global dataset is easy to me (as I am sitting in Norway), however may not be easy for someone sitting in an African nation. Instead of downloading the global data, it may be helpful if one can select and download the data for their region of interest.
- A subset tool is requested for future downloads to aid researchers focusing on smaller boundaries in not downloading the whole 40-year global files. Aside from recommending updates to 2022 or 2023, we do hope that the SST CCI be also made available with data access forms or filters so that students like us with no high-powered computers can subset it before downloading.
- Continuous validation with in-situ data should be undertaken in order to improve the product by minimizing the bias and error from interpolations.

This Page Is Intentionally Blank